

The Role of Charge Localisation in Mass Spectrometry

KEVIN JOHN WELHAM

A Thesis submitted to the University of London in partial
fulfilment of the requirements for the Degree of
Doctor of Philosophy

January 1992

Department of Pharmaceutical Chemistry

The School of Pharmacy

University of London

ProQuest Number: U063188

All rights reserved

INFORMATION TO ALL USERS

The quality of this reproduction is dependent upon the quality of the copy submitted.

In the unlikely event that the author did not send a complete manuscript and there are missing pages, these will be noted. Also, if material had to be removed, a note will indicate the deletion.



ProQuest U063188

Published by ProQuest LLC (2017). Copyright of the Dissertation is held by the Author.

All rights reserved.

This work is protected against unauthorized copying under Title 17, United States Code
Microform Edition © ProQuest LLC.

ProQuest LLC.
789 East Eisenhower Parkway
P.O. Box 1346
Ann Arbor, MI 48106 – 1346

Abstract.

Ab-Initio molecular orbital calculations have been used to investigate the degree of charge localisation associated with the formation of ground state molecular radical cations upon electron impact for some simple amides, thio-amides, urea, thiourea, and their N-methyl substituted analogues, and guanidine. Some of the thio-amides which were not commercially available, were synthesised for the mass spectrometric studies.

Ionisation energies have been calculated from the molecular orbital energies, using Koopmans' Theorem, and related to the predicted site of charge location in the molecular radical cations. The molecular orbital data was also used to study the effect of N-methylation on ionisation energy. The results obtained were found to be in close agreement with results obtained from photoelectron spectroscopy and electron impact mass spectrometry.

Mulliken population analysis was used to obtain total atomic charges from the molecular orbital calculations so that the charge distributions in the neutral molecules and the radical cations could be compared. The molecular orbital calculations predict the major change in charge distribution to be equally shared between each nitrogen atom of urea, upon ionisation, with very little charge located on the oxygen; however for thiourea the change in charge distribution is largely located on the sulphur atom with very little change in the charge on either of the nitrogen atoms. These results are in agreement with previous predictions based on observed experimental data. The amides show more delocalisation with the charge more evenly distributed between nitrogen and oxygen, although N-methylation causes the charge to be preferentially located on nitrogen. The thio-amides show the charge preferentially located on sulphur throughout. Molecular orbital calculations have also been used to investigate the energetics of the major fragmentation reaction in some of these compounds in relation to the predicted site of charge location in both the ground state molecular radical cations, and the fragment ions. This study has enabled an attempt to be made at rationalising the observed electron impact mass spectra on the basis of the calculated change in charge distribution upon ionisation of the compounds studied.

Contents.

List of figures.	6
List of tables.	9
Acknowledgement.	13
1. Electron Impact Mass Spectrometry.	14
1.1. The Ionisation Process, Franck-Condon Factors.	14
1.2. Adiabatic and Vertical Ionisation Energy.	17
1.3. Ionisation Efficiency Curves.	18
1.3.1. Threshold Laws.	18
1.3.2. Autoionisation.	20
1.4. Determination of Ionisation Energies.	20
1.4.1. Optical Spectroscopy.	21
1.4.2. Threshold Experiments.	21
1.4.2.1. Photoionisation Thresholds.	21
1.4.2.2. Electron Impact Thresholds.	22
1.4.3. Electron Spectroscopy.	23
1.5. The Internal Energy distribution of the Molecular Ion.	24
1.5.1. The Energy Deposition Function.	24
1.5.2. The Thermal Energy Distribution.	31
1.6. Fragmentation and Appearance Energies.	32
1.7. The Quasi-Equilibrium Theory.	35
1.7.1. Introduction.	35
1.7.2. Basic Assumptions.	36
1.7.3. The Rate Expression.	37
1.7.4. Modified QET - The Phase Space Theory.	40
1.7.5. Recent Developments in Mass Spectrometry Theory.	40

1.7.6. Calculation of Mass Spectra.	41
1.7.7. Tests of the QET.	42
1.7.8. Applications of the QET.	45
1.8. Substituent Effects on Fragmentation Reactions.	47
1.9. Metastable Ions.	48
1.10. Charge Localisation.	50
1.11. References.	54
2. Molecular Quantum Mechanics.	61
2.1. General Introduction.	61
2.2. The Theoretical Background.	62
2.2.1. The Schrodinger Equation.	62
2.2.2. Separation of Nuclear motion : Potential Surfaces.	64
2.2.3. Atomic Units.	67
2.2.4. Molecular Orbital Theory.	68
2.2.5. Basis Set Expansions.	71
2.2.6. Variational Methods and Hartree-Fock Theory.	74
2.2.6.1. Closed-Shell Systems.	75
2.2.6.2. Open-Shell Systems.	78
2.2.6.3. Koopmans' Theorem and Ionisation Potentials.	80
2.2.7. Symmetry Properties.	81
2.2.8. Mulliken Population Analysis.	81
2.2.9. Multiple-Determinant Wavefunctions.	84
2.2.9.1. Full Configuration Interaction.	87
2.2.9.2. Limited Configuration Interaction.	89
2.2.9.3. Moller-Plesset Perturbation Theory.	93
2.3. References.	98

3. Chemical Calculations and Mass Spectrometry.	100
3.1. General Introduction.	100
3.3. References.	102
4. Experimental Methods.	103
4.1. Preparation of Materials.	103
4.2. Computer calculations.	103
4.2.1. General Introduction.	103
4.2.2. Molecular mechanics	104
4.2.3. Semi-Empirical Molecular Orbital Methods.	107
4.2.4. Ab-Initio Molecular Orbital Methods.	108
4.3. Calculation Methods.	110
4.4. Accuracy of the Methods.	111
4.5. Mass Spectrometry.	111
4.6. References.	112
5. Previous Work.	114
5.1. Introduction.	114
5.2. Mass Spectrometry.	114
5.2.1. Amides.	114
5.2.2. Thioamides.	118
5.2.3. Ureas.	118
5.2.4. Thioureas.	120
5.2.5. Ionisation energies and charge localisation.	121
5.2.6. Charge localisation concept.	123
5.3. Computer Calculations.	125
5.3.1. Amides and Thioamides.	125
5.3.2. Ureas and Thioureas.	128

5.3.3. Charge Distributions.	129
5.4. References.	134
6. Discussion of Present Work.	138
6.1. Introduction.	138
6.2. Amides and Thioamides.	139
6.2.1. Methanamides and thiomethanamides.	139
6.2.1.1. Mass Spectrometry.	163
6.2.2. Ethanamides and thioethanamides.	170
6.2.2.1. Mass Spectrometry.	185
6.2.3. Charge distribution and the interpretation of mass spectra.	192
6.3. Ureas, thioureas and guanidine.	202
6.3.1. Charge distribution and mass spectrometry.	223
6.4. The tetramethylurea radical cation.	225
6.5. Conclusions.	228
6.6. References.	232
Appendix i. Papers Published as a Co-Author by the Author of this Thesis.	235

List of Figures.

Figure 1.1	Schematic diagram of an electron impact ion source.	14
Figure 1.2	Schematic potential energy curves for a molecule and its ion in their electronic ground states.	16
Figure 1.3	Theoretical ionisation cross sections for electron impact.	19
Figure 1.4	Schematic diagram of a photoelectron spectrometer.	24
Figure 1.5	Hypothetical ion yield curves from monoenergetic electrons.	26
Figure 1.6	Internal energy distributions for propane.	28
Figure 1.7	Internal energy distribution of 1,2-diphenylethane.	29
Figure 1.8	Thermal energy distribution of propane molecular ion.	31
Figure 1.9	Schematic potential energy diagram of an ion.	37
Figure 1.10	Schematic diagram of isolated state decay.	43
Figure 1.11	Schematic $k(E)$ curve and internal energy distribution.	45
Figure 1.12	Typical metastable ion peak shapes.	49
Figure 2.1	Schematic sections of potential surfaces.	66
Figure 2.2	Electron configuration diagram.	70
Figure 2.3	Partitioning of full configuration interaction Hamiltonian.	89
Figure 2.4	Use of a window for designating substitutions to be made in limited configuration interaction.	91
Figure 4.1	Potential energy curve for stretching a chemical bond.	105
Figure 5.1	The α -cleavage reaction in simple primary amides.	115

Figure 5.2	70eV mass spectrum of butanamide.	116
Figure 5.3	70eV mass spectra of (a) N-butylethanamide and (b) N-butyl- ² H ₃ -ethanamide.	117
Figure 5.4	Proposed sites for ionisation of urea and thiourea.	122
Figure 6.1	Key to methanamides and thiomethanamides studied.	139
Figure 6.2	Change in calculated charge distribution on ionisation for the methanamides and thiomethanamides.	147
Figure 6.3	70eV mass spectra of (a) methanamide and (b) thiomethanamide.	164
Figure 6.4	70eV Mass spectra of (a) N-methylmethanamide and (b) N-methylthiomethanamide.	165
Figure 6.5	70eV Mass spectra of (a) N,N-dimethylmethanamide and (b) N,N-dimethylthiomethanamide.	166
Figure 6.6	Key to ethanamides and thioethanamides studied.	170
Figure 6.7	Change in calculated charge distributions on ionisation for the ethanamides and thioethanamides.	178
Figure 6.8	Change in calculated charge distributions on ionisation for the ethanamide tautomers.	184
Figure 6.9	70eV Mass spectra of (a) ethanamide and (b) thioethanamide	186
Figure 6.10	70eV Mass spectra of (a) N-methylethanamide and (b) N-methylthioethanamide.	187
Figure 6.11	70eV Mass spectra of (a) N,N-dimethylethanamide and (b) N,N-dimethylthioethanamide.	188
Figure 6.12	Fragmentation scheme for the ethanamides and thioethanamides.	189
Figure 6.13	C-N bond cleavage for the methanamides.	193
Figure 6.14	Key to the ureas studied.	202
Figure 6.15	Key to the thioureas studied.	203

Figure 6.16	Ab-initio calculated changes in charge distribution on ionisation for urea, thiourea and guanidine.	207
Figure 6.17	AMPAC calculated changes in charge distribution on ionisation for the ureas.	219
Figure 6.18	AMPAC calculated changes in charge distribution on ionisation for the thioureas.	220
Figure 6.19	Molecular ion representations for urea and thiourea.	223
Figure 6.20	AMPAC calculated structures for the tetramethylurea radical cation.	226

List of Tables.

Table 5.1	The ratio $A^+/(M-A)^+$ from the N-methylureas.	119
Table 6.1	Ab-initio calculated parameters for methanamide and its radical cations.	140
Table 6.2	Ab-Initio calculated parameters for N-methylmethanamide and its radical cations.	141
Table 6.3	Ab-initio calculated parameters for N,N-dimethyl methanamide and its radical cations.	142
Table 6.4	Ab-initio calculated parameters for thiomethanamide and its radical cations.	143
Table 6.5	Ab-initio calculated parameters for N-methylthiomethanamide and its radical cations.	144
Table 6.6	Ab-initio calculated parameters for N,N-dimethyl thiomethanamide and its radical cations.	145
Table 6.7	Calculated ionisation energies for the neutral methanamides and thiomethanamides.	148
Table 6.8	Mulliken symmetry symbols.	150
Table 6.9	Comparison of calculated ionisation energies with those measured from PES and EIMS.	151
Table 6.10	MP3/6-31G [*] //3-21G [*] ab-initio results for methanamide and it's radical cation.	156
Table 6.11	MP3/6-31G [*] //3-21G [*] ab-initio results for thiomethanamide and it's radical cation.	157
Table 6.12	Ab-initio calculated parameters for ethanal and it's radical cation.	159

Table 6.13	Ab-initio calculated parameters for ethenol and its radical cation.	160
Table 6.14	Calculated energy differences for ethanal and ethenol tautomers.	161
Table 6.15	Ab-initio parameters for methanimide and its radical cation.	162
Table 6.16	Calculated energy differences for methanamide and methanimide tautomers.	163
Table 6.17	Fragment ion accurate mass data for methanamides and thiomethanamides.	167
Table 6.18	8eV mass Spectra of the methanamides and thiomethanamides.	168
Table 6.19	Ab-initio calculated parameters for ethanamide and its radical cations.	171
Table 6.20	Ab-initio calculated parameters for N-methylethanamide and its radical cation.	172
Table 6.21	Ab-initio calculated parameters for N,N-dimethyl ethanamide and its radical cation.	173
Table 6.22	Ab-initio calculated parameters for thioethanamide and its radical cations.	174
Table 6.23	Ab-initio calculated parameters for N-methyl thioethanamide and its radical cation.	175
Table 6.24	Ab-initio calculated parameters for N,N-dimethyl thioethanamide and its radical cation.	176
Table 6.25	Calculated ionisation energies for the neutral ethanamides and thioethanamides.	177
Table 6.26	Comparison of calculated ionisation energies with those measured by PES and MS.	179

Table 6.27	Ab-initio calculated parameters for the ethanimide tautomer and its radical cation.	181
Table 6.28	Ab-initio calculated parameters for the ethenolamine tautomer and its radical cation.	182
Table 6.29	Calculated Hartree-Fock energies for ethanamide and its tautomers.	183
Table 6.30	Energy differences between ethanamide and its tautomers.	183
Table 6.31	Orbital energies and ionisation energies for ethanamide and its tautomers.	185
Table 6.32	8eV mass spectral data for ethanamides and thioethanamides.	190
Table 6.33	Changes in charge distributions on ionisation for the methanamides.	194
Table 6.34	Fragment ion intensities and charge distributions for the methanamides.	194
Table 6.35	8eV fragment ion intensities for the methanamides.	195
Table 6.36	Changes in charge distributions on ionisation for the thiomethanamides.	196
Table 6.37	Fragment ion intensities and charge distributions for the thiomethanamides.	196
Table 6.38	Charge distributions for the methanamide and thiomethanamide radical cations.	197
Table 6.39	Charge distributions and ion intensities for the methanamides and thiomethanamides.	198
Table 6.40	Charge distributions for the ethanamide and thioethanamide radical cations.	199
Table 6.41	Charge distributions and ion intensities for the ethanamides and thioethanamides.	200
Table 6.42	Ab-initio calculated parameters for urea and its radical cation.	204

Table 6.43	Ab-initio calculated parameters for thiourea and its radical cation.	205
Table 6.44	Ab-initio calculated parameters for guanidine and its radical cation.	206
Table 6.45	Semi-empirical MO calculated parameters for urea and its radical cation.	209
Table 6.46	Semi-empirical MO calculated parameters for N-methylurea and its radical cation.	210
Table 6.47	Semi-empirical MO calculated parameters for N,N-dimethylurea and its radical cation.	211
Table 6.48	Semi-empirical MO calculated parameters for N,N,N'-trimethylurea and its radical cation.	212
Table 6.49	Semi-empirical MO calculated parameters for N,N,N,N'-tetramethylurea and its radical cation.	213
Table 6.50	Semi-empirical MO calculated parameters for thiourea and its radical cation.	214
Table 6.51	Semi-empirical MO calculated parameters for N-methylthiourea and its radical cation.	215
Table 6.52	Semi-empirical MO calculated parameters for N,N-dimethylthiourea and its radical cation.	216
Table 6.53	Semi-empirical MO calculated parameters for N,N,N'-trimethylthiourea and its radical cation.	217
Table 6.54	Semi-empirical MO calculated parameters for N,N,N,N'-tetramethylthiourea and its radical cation.	218
Table 6.55	Calculated and measured ionisation energies for the ureas and thioureas.	222
Table 6.56	Ion intensity and charge distribution ratios for the C-N bond cleavage reaction in the ureas.	224

Acknowledgement

I wish to record my sincere thanks to my supervisor Dr. M.A. Baldwin for providing me with the opportunity to carry out research in mass spectrometry and for his support and encouragement throughout the course of this work. His patience when progress was slow was much appreciated.

Thanks are also due to all the other students and staff of the mass spectrometry laboratory for providing the enjoyable and stimulating atmosphere in which this work was carried out.

The help and advice from Dr. D.G. Peacock on obtaining access to the CRAY computer was invaluable and both he and Mr. C.H. James are also thanked for stimulating discussions on all aspects of computing.

Special thanks are also due to Prof. Allan Maccoll for kindly and diligently proof reading the entire manuscript and, lastly but by no means least I wish to thank Professors W.A. Gibbons and A.T. Florence for their patience and understanding during the completion of this thesis.

1. Electron Impact Mass Spectrometry.

1.1 The Ionisation Process, Franck-Condon Factors

Electron Impact, (EI), is still the most common technique currently in use, within mass spectrometry, for the production of positive ions. A small amount of the substance to be examined is introduced, as a vapour, into the ion source at the operating pressure (ca. 10^{-6} torr). The vapour passes through an inlet into the ionisation chamber (Figure 1.1), where it is bombarded with a beam of electrons accelerated from a hot filament. The energy of the electron beam can be varied from 0 to 100 eV.

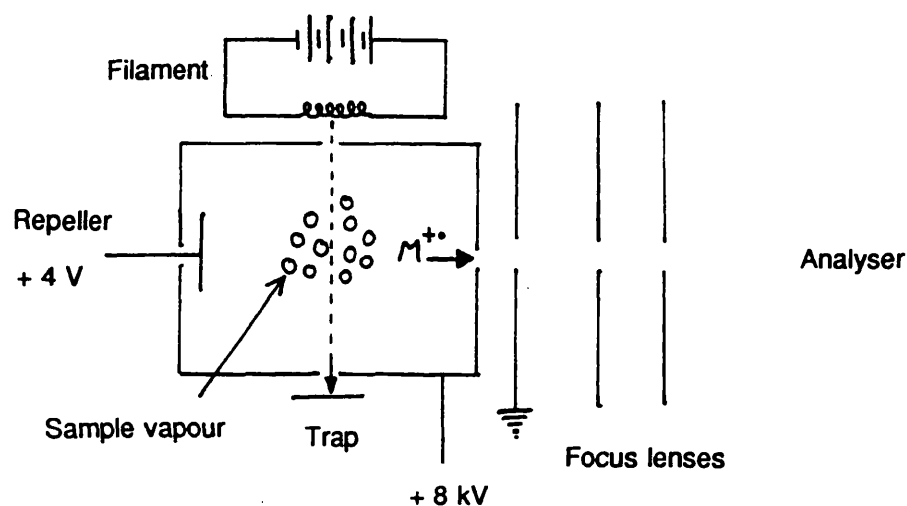


Figure 1.1. Schematic of an electron impact ion source

The ionisation energies, (IE's), of most organic molecules fall in the range 7-13 eV ($1\text{eV} = 96\text{ kJ mol}^{-1}$); consequently energy in excess of the ionisation energy may be imparted to the ion formed. If the electron is removed from the highest occupied molecular orbital, (HOMO), of the molecule the minimum energy necessary for this process is termed the first ionisation energy, (IE) of the molecule and the reaction is represented as follows:



The M^+ symbolism denotes that the molecular ion thus formed is both a positive ion and a

radical. This follows because organic molecules are almost without exception even-electron species where all electrons are paired. The alternative process, electron capture by a molecule of vapour to give a negative ion radical;



is usually less probable under the conditions used.

Removal of an electron from lower lying molecular orbitals of the neutral molecule requires the supply of more energy from the ionisation process. A recent book by Mark provides a good review of electron impact processes ¹, while more general coverage of the fundamental aspects of mass spectrometry are given in a book by Levsen ². The heat of formation of the ion $M^{\cdot +}$ (at 0 K) is given by equation [1.3] below.

$$\Delta H_f (M^{\cdot +}) = \Delta H_f (M) + IE (M) \quad [1.3]$$

This equation assumes that the heat capacities of the ion and the neutral are identical, this is often very nearly the case. The heats of formation of the neutral species are generally known from thermochemical measurements and have been tabulated ^{3,4}. The removal of an electron occurs within about 10^{-16} s, (at 50eV an electron has a velocity of $4.2 \cdot 10^{10} \text{ ms}^{-1}$ and will traverse a molecule with a diameter of a few angstroms in about 10^{-16} s ⁵). This is about two orders of magnitude faster than a molecular vibration (10^{-13} s to 10^{-14} s), thus the ionisation takes place at an effectively constant internuclear distance. This is the Franck-Condon Principle. The ionisation process can be most conveniently discussed for a diatomic molecule in the first instance. Figure 1.2. shows schematically the potential energy curves for the ground electronic states of the ion and the neutral molecule. In Figure 1.2a. the potential energy curve of the ion has a minimum at an internuclear distance only slightly greater than that for the neutral molecule.

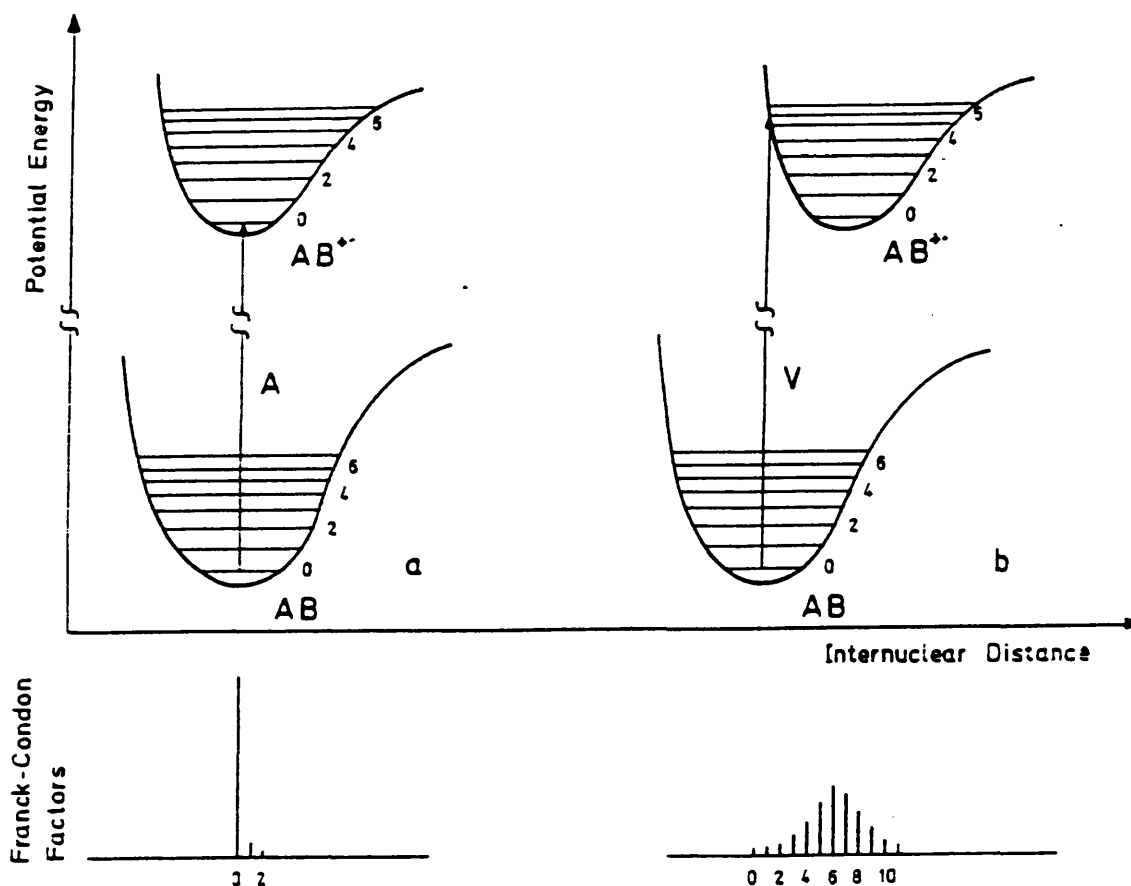


Figure 1.2. Schematic potential energy curves for a molecule and its ion in their electronic ground states assuming (a) small and (b) large bond length changes after ionisation (A = adiabatic ionisation energy, V = vertical ionisation energy). The distribution of Franck-Condon factors for various transitions is shown schematically in the lower part of the figure.

This holds approximately if a non-bonding electron is removed in the ionisation process; whilst in Figure 1.2b. the minimum of the first ionized state is shifted considerably to larger internuclear distances (as expected if a bonding electron were removed). In principle electronic transitions are possible from the ground vibrational level ($v = 0$) of the molecule to the various vibrational levels ($v' = 0, 1, 2, 3, \dots$) of, for instance, the first ionized electronic state, and the relative transition probabilities may be represented to a good approximation by the squares of

the normalized vibrational overlap integrals, also called Franck-Condon factors.

These relative transition probabilities can be readily calculated for smaller molecules ⁶. It follows from the Franck-Condon principle that the relative transition probabilities (Franck-Condon factors) depend strongly on changes in the internuclear distance after ionisation, as also illustrated in Figure 1.2., where the Franck-Condon factors for the transitions to the various vibrational levels in the ionized state are represented as bars. Such a graph of the distribution of Franck-Condon factors is known as a Franck-Condon envelope. In reality the Franck-Condon progressions are much more sensitive to changes in internuclear distance than is shown in the schematic Figure 1.2.

1.2 Adiabatic and Vertical Ionisation Energy

The energy difference between the ground vibrational levels ($v' = v = 0$) of the lowest electronic states of a molecular ion and the corresponding neutral molecule is defined as the adiabatic ionisation energy (A in Figure 1.2a). In contrast, the vertical ionisation energy of a diatomic molecule corresponds to the transition from the ground state of the molecule to the state of the ion for which the Franck-Condon factor is largest ⁷ (V in Figure 1.2b). In some instances the vertical and the adiabatic ionisation energy may be identical (see Figure 1.2a.). However, the simple potential energy diagram represented in Figure 1.2. for a diatomic molecule is no longer applicable when polyatomic molecules are considered. It has been pointed out by Vestal ⁸ that for such polyatomic molecules the vertical ionisation energy in this form may be less well defined. According to molecular quantum mechanics the vertical ionisation energy for a polyatomic molecule is the energy required to remove an electron while holding the nuclei fixed in their positions. This vertical ionisation energy approximates closely to the maximum of the Franck-Condon envelope.

For thermochemical calculations, e.g. for the determination of the heat of formation of an ion according to Eq.[1.3], it is the adiabatic ionisation energy which is required. However, it can clearly be seen from Figure 1.2b. that the determination of the adiabatic ionisation energy may be difficult with photoionisation and especially so with electron impact techniques if a bonding

electron (e.g. in alkanes) is removed during the ionisation process, since the Franck-Condon factor for the adiabatic transition is considerably smaller than when a non-bonding electron is removed. Vestal⁸ has pointed out that the adiabatic transition cannot be zero and may in fact be as large as other transitions, however because of the very rapid increase in the density of states with energy the probability for an adiabatic transition may be several orders of magnitude smaller than the maximum transition probability. Under these circumstances it becomes difficult if not impossible to determine the adiabatic ionisation energy using photoionisation or electron impact methods and in some cases, such as in methane, the improbability of the adiabatic transition occurring is the main reason for not determining the adiabatic ionisation energy. If however a non-bonding electron is removed during the ionisation process (e.g. from a heteroatom), the Franck-Condon factor for the adiabatic transition is very large compared to other transitions to neighbouring vibrational levels.

1.3 Ionisation Efficiency Curves

1.3.1 Threshold Laws

The ionisation efficiency curves represent the relationship between the intensity of an ion signal (e.g. the molecular ion) and the energy of the impacting particle. A simple relationship between the ionisation cross section, σ , and the energy of the impacting particle for a transition to a given electronic, vibrational, and rotational state has been presented by Wigner⁹ and Geltman¹⁰.

$$\sigma (E) = A (E - E_0)^{n-1} \quad [1 . 4]$$

where E_0 is the threshold energy, n is the number of electrons ejected from the collision complex, and A is a constant. A linear threshold law is found for single ionisation of an atom, (no vibrational or rotational excitation), by electron impact (Figure 1.3a). The break in the curve indicates transitions to the first excited electronic state. A quadratic law is expected for double ionisation by electron impact as illustrated in Figure 1.3b. Whereas a linear threshold law was

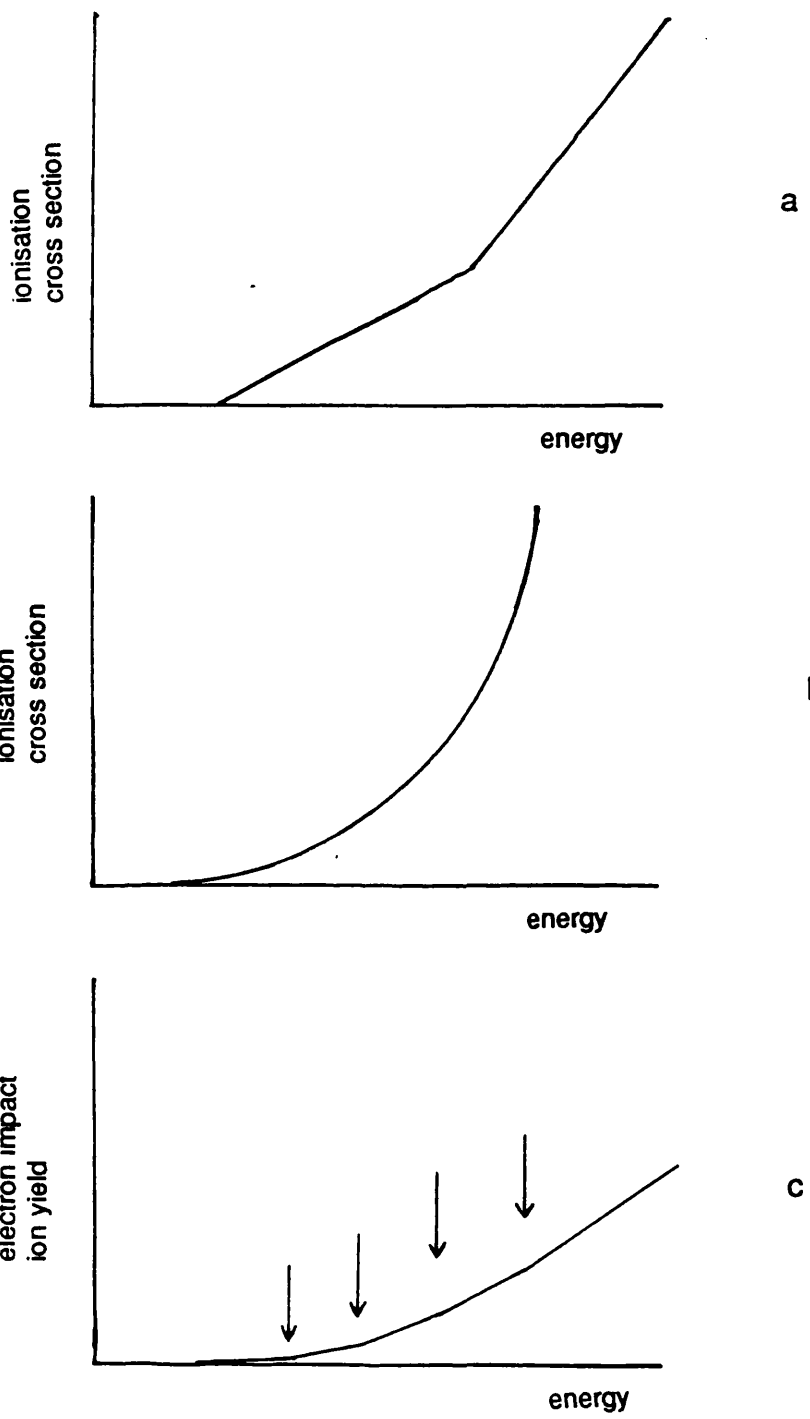


Figure 1.3. Theoretical ionisation cross sections for electron impact (a) single ionisation of an atom (no vibrational states), (b) double ionisation of an atom, and (c) for a polyatomic molecule.

assumed for a single ionisation of an atom, in the case of polyatomic molecules undergoing electron impact ionisation it is expected that the ionisation efficiency curve will consist of a series of straight line segments. The onset of each new segment represents transitions to a new vibrational level, the slope of each segment increases successively in accord with the increasing Franck-Condon factors (Figure 1.3c.). The observation of straight line segments in the ionisation efficiency curve of polyatomic molecules has been claimed in some instances, although their existence has not been unambiguously confirmed ¹¹. The ionisation efficiency curve for photoionisation of molecules appears to be a step function with the height of each individual step being proportional to the Franck-Condon factor of the corresponding transition.

1.3.2 Autoionisation

The shape of the ionisation cross section curve may be further complicated by the occurrence of autoionisation. If a molecule is excited by the impinging electron (or photon) to a superexcited neutral state lying above the lowest ionic state (and possibly above several excited ionic states) then this excited state of the molecule can undergo radiationless decay either, by formation of an ion and an electron of the same total energy by autoionisation, or by ion pair formation, or by pre-dissociation into neutral fragments. The superexcited state of the molecule may be due to electronic or vibrational excitation ¹². Autoionisation usually occurs by Rydberg levels of the molecule converging to excited states of the ion, making it difficult to detect the steps of an excited state due to direct ionisation ¹². Autoionisation is a resonance process which may complicate the interpretation of both photoionisation and electron impact ionisation cross section measurements.

1.4 Determination of Ionisation Energies

The problem of accurate ionisation energy measurements has been thoroughly discussed in several articles ^{11,13,14}. Three principle methods are currently used for experimentally determining ionisation energies of organic molecules ¹¹.

- (1) Optical spectroscopy.

(2) Threshold experiments.

(3) Electron spectroscopy.

1.4.1 Optical Spectroscopy

Spectroscopic techniques applied to ionisation energy measurements of smaller molecules have supplied the most accurate data. The adiabatic ionisation energy is determined by finding the convergence limit of a Rydberg series, this allows an energy resolution of 10^{-4} nm (= 0.1 meV) to be achieved although most ionisation energies are reported with a resolution of 10^{-2} nm (= 10 meV) ¹¹.

1.4.2 Threshold Experiments

The threshold laws for electron impact and photoionisation measurements have been discussed in Section 1.3.

1.4.2.1 Photoionisation Thresholds

Even for large organic molecules the photoionisation threshold curve has a reasonably sharp onset, most probably corresponding to the adiabatic threshold, for those molecules where a non-bonding electron is removed in the ionisation process. If, however, a bonding electron is removed during ionisation (e.g. in alkanes) the photoionisation threshold curve has a very gradual onset and it is not apparent whether the onset point includes the 0-0 transition corresponding to the adiabatic ionisation energy or not ¹¹. Another uncertainty in the determination of adiabatic ionisation energies is due to the possible presence of hot bands which may be responsible for the gradual onset of the photoionisation curves of the higher alkanes. For aliphatic hydrocarbons, including methane, the adiabatic ionisation energies are not yet firmly established; however in many other cases adiabatic ionisation energies can be determined which agree with spectroscopic data to within 5-10 meV.

1.4.2.2 Electron Impact Thresholds

The use of electron impact techniques suffers from two major disadvantages: 1) the linear threshold law makes it more difficult to determine the true onset of the ionisation cross section curve; 2) conventional electron beams have a large energy spread due to the Boltzmann distribution of the electrons coming from the hot filament, the potential drop across the filament, the field penetration, and the surface adsorption. This second shortcoming can be overcome to a large extent by using an electron monochromator^{15,16} (double hemispherical sector) and a calibration gas. Despite the unfavourable threshold behaviour and the tacit assumption that the threshold behaviour of the calibration gas is similar to that of the compound under study, ionisation energies in agreement with experimental photoionisation thresholds to within 30 meV have been reported with this technique. Quasi-monoenergetic ions can be obtained with the RPD (Retarding Potential Difference)^{17,18} and the EDD (energy distribution difference)¹⁹ techniques, in which a small portion of the broad electron energy distribution is selected by measuring the difference in ion currents at nominal electron energies E and $E + dE$. The equipment to produce monoenergetic or quasi-monoenergetic electrons is not available in most laboratories, therefore polyenergetic electron impact techniques are commonly used to determine ionisation energies. In these cases both a calibration gas and a variety of different extrapolation methods are used to correct for the broad electron energy distribution, (semilog plot²⁰, extrapolated voltage difference²¹, energy compensation²², critical slope²³, and second derivative²⁴). These methods have been described in detail by Kiser¹⁴. The various extrapolation methods have been tested for reliability, both experimentally and theoretically, by Occolowitz and co-workers²⁵. Model ionisation efficiency curves were used to show that the critical slope method should give the most reliable values; this conclusion was supported by their experimental results which showed that the ionisation energies obtained by the critical slope method were close to published photoionisation data. In general the accuracy of the various extrapolation methods ranges from 0.1 to 0.5 eV.

1.4.3 Electron Spectroscopy

Electron spectroscopy provides a range of accurate methods for ionisation energy measurements, the most important of which is the photoelectron spectroscopy technique²⁶⁻²⁹. Photoelectron spectroscopy has two variations, the first and still most widely applied version uses photons of constant energy to achieve ionisation, generally the He I resonance line at 21.22 eV or the He II line at 40.81 eV are used. The energy distribution of the ejected electrons reflects the distribution of accessible energy levels of the neutral target molecule according to Equation [1.5].

$$E_{ion} = h\nu - E_{electron} \quad [1.5]$$

Several different types of analyzers have been employed for the energy analysis of the ejected electrons, the most efficient being the 127 degree electrostatic sector analyzer. The contact potential contribution necessitates calibration of the energy scale with gases of known ionisation energies. In the resonance ionisation technique, also called threshold or zero kinetic energy photoelectron spectroscopy³⁰⁻³⁴, the photon energy is varied and only those photoelectrons with zero kinetic energy are detected. The photon energy therefore corresponds directly to the energy of the transition to an accessible ionic state, without interference from autoionisation. The zero energy electrons can be detected by two different methods, the first of which accelerates all the electrons through a known potential drop and then selects those whose energy corresponds exactly to the potential drop itself using a 127 degree electrostatic analyzer. In the second method,^{33,34} Figure 1.4, the electrons are accelerated by a small uniform electric field toward a set of collimating holes. The majority of hot electrons are emitted with a significant velocity component perpendicular to the applied field and will follow trajectories such as b in Figure 1.4., they will therefore not be detected. However, zero kinetic energy electrons will have no perpendicular velocity component (trajectory a) and will thus be detected.

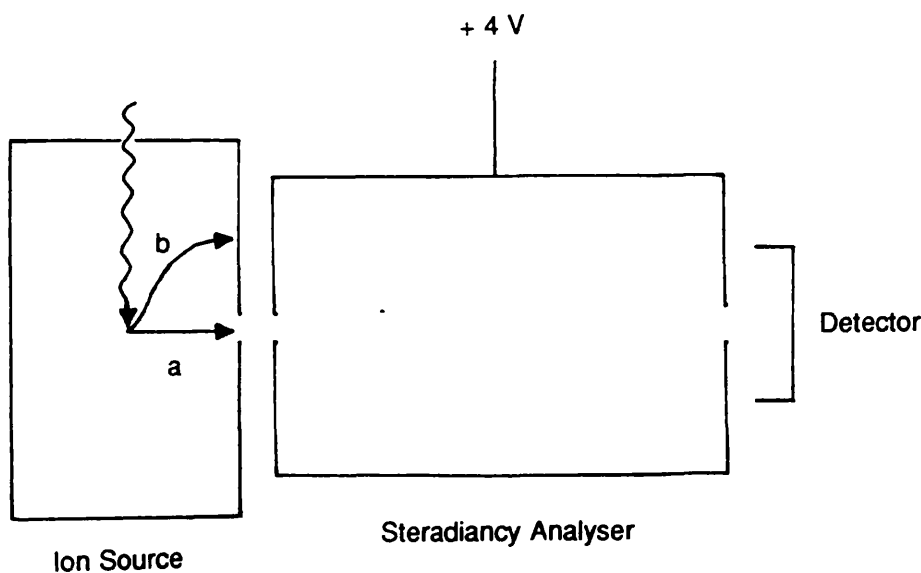


Figure 1.4. Schematic arrangement of a photoelectron spectrometer for the detection of zero kinetic energy electrons ³³.

In a photoelectron spectrum the ejected electrons arise from allowed electronic transitions to all vibrational levels which are Franck-Condon accessible. Assuming that the photoionisation law is a step function which is flat from the ionisation threshold energy up to the photon source line energy, which is not exactly the case as discussed below, the energy of the electrons ejected from a given electronic state will have a distribution determined by the Franck-Condon factors. In principle, therefore, with sufficient energy resolution, a "bar-graph" of experimental Franck-Condon factors can be obtained. This considerably simplifies the detection of the 0-0 transition and thus the adiabatic ionisation energy. The accuracy of ionisation energy measurements by photoelectron spectroscopy is approaching 2 meV in favourable cases, but is more typically of the order of one or several hundredths of an eV.

1.5 The Internal Energy Distribution of the Molecular Ion

1.5.1 The Energy Deposition Function

As has already been briefly mentioned (Section 1.1.), ionisation of a molecule by electron

impact will generally lead to excitation energy being imparted to the molecular ion during the ionisation process, if the energy of the impinging electron is higher than the ionisation energy of the molecule (as is generally the case). This excitation energy is in addition to the thermal energy present in the molecule before ionisation. The probability of depositing a given energy, E , into the molecular ion as a function of the energy, V , of the impinging electron is expressed by the energy deposition function, $P(E, V)$. The energy deposition function depends on both the probability distribution $Y(E)$ for electronic transitions from the ground state of the molecule to the different vibrational levels of the various electronic states of the ion, as described by the Franck-Condon factors, and on the threshold behaviour. This can be described as the variation in the probability of transferring an energy $E + I$, where I is the adiabatic ionisation energy, to the molecular ion as a function of the energy, V , of the impinging electron, expressed as a function of the energy difference, $f(V - E - I)$ ⁸. The energy deposition function can then be expressed as follows:

$$P(E, V) = f(V - E - I) Y(E) \quad [1.6]$$

Knowledge of the energy deposition function is of great importance for understanding the fragmentation of an ion as described by the Quasi-Equilibrium Theory, (QET), discussed later in Section 1.7. A reliable experimental determination of the energy deposition function is difficult. However, it has been shown, originally by Morrison³⁵ and later by Chupka et al.³⁶⁻³⁹, that the energy distribution within the molecular ions is given by the first derivative of the total ionisation efficiency for photoionisation and by the second derivative of the total ionisation efficiency for electron impact ionisation; provided that the Geltman threshold laws are valid. This is illustrated in Figure 1.5. Neglecting vibrational and rotational excitation Figure 1.5. assumes that, upon ionisation, transitions to the ground electronic state or one of two excited states are possible with relative probabilities of 1:2:1, and that the transition probabilities are the same for photoionisation and electron impact. Three groups of ions, with internal energies of zero, E_1 , and E_2 respectively, are formed leading to three straight line segments in the total

ionisation efficiency curve for electron impact (Figure 1.5a.). The successive slope increase corresponds to the relative population of the three states.

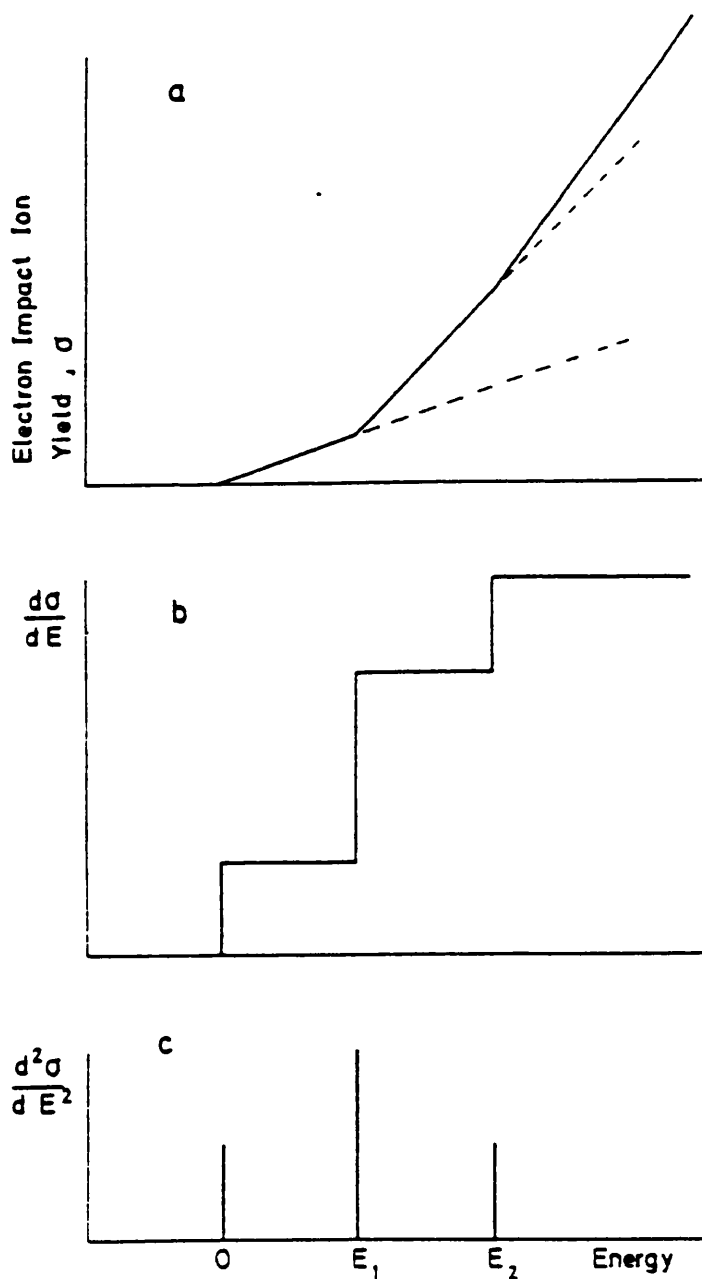


Figure 1.5. Hypothetical ion yield curves obtained with monoenergetic electrons (a) assuming the validity of Geltman's law¹⁰. Transitions to the ground or one of two excited electronic states are assumed to be possible with relative probabilities 1:2:1. The second derivative of this curve (c) represents the internal energy distribution of the ions.

Similarly the total ionisation efficiency curve for photoionisation (Figure 1.5b.) shows three steps, the heights of which again represent the relative transition probabilities to the three electronic states. It can now be seen that the first derivative of the electron impact cross section curve (Fig.1.5a.) is the curve of Figure 1.5b., the photoionisation cross section curve, and finally that the second derivative of Fig.1.5a., or first derivative of Fig.1.5b, is the curve of Fig.1.5c. which shows three peaks at the energies I , $I + E_1$, and $I + E_2$ representing the energy distribution of the molecular ions. Figure 1.5c. is identical to the photoelectron spectrum of the molecule under study if the Geltman threshold law is valid over the whole energy range. In reality the derivative methods only provide a rough approximation to the energy distribution because the threshold laws are only approximate. Considerable deviations are expected from the theoretical behaviour particularly at higher energies. Substantial autoionisation may also occur, especially under electron impact conditions, so that it is not known whether any structure observed in the second derivative curve of the total ionisation efficiency for electron impact is due to an excited state or to autoionisation. The energy distribution derived by this procedure is necessarily a poorer approximation for electron impact than for photoionisation, particularly if polyenergetic electrons are used.

Although the energy distributions obtained from the second derivative method are only a rough approximation to the real situation, they do at least give some indication of the range of energies transferred to the molecular ion upon electron impact ionisation. The second derivative of the total ionisation cross section for electron impact, (EI), of propane as a function of the energy of the ions is shown in Figure 1.6a.³⁶ The figure suggests that most propane molecular ions have internal energies in the range of 0-6 eV, however, the energy distribution curve shows little structure. The first derivative of the photoionisation cross section of propane from 11 to 14 eV (corresponding to 0-3 eV internal energy) is shown in Figure 1.6b³⁸, in contrast to the electron impact curve there is a pronounced minimum at 13 eV (≈ 2 eV internal energy). Photoelectron spectroscopy provides the most direct information on the energy deposition function, at least for photoionisation. The photoelectron spectrum directly represents the energy distribution for photoionisation provided that the photoionisation threshold law is a

step function up to the photon source energy (21.22 eV). However, the photoelectron spectrum must be corrected for the energy-dependent transmission function of the electron energy analyzer before it can be used to estimate the energy deposition function.

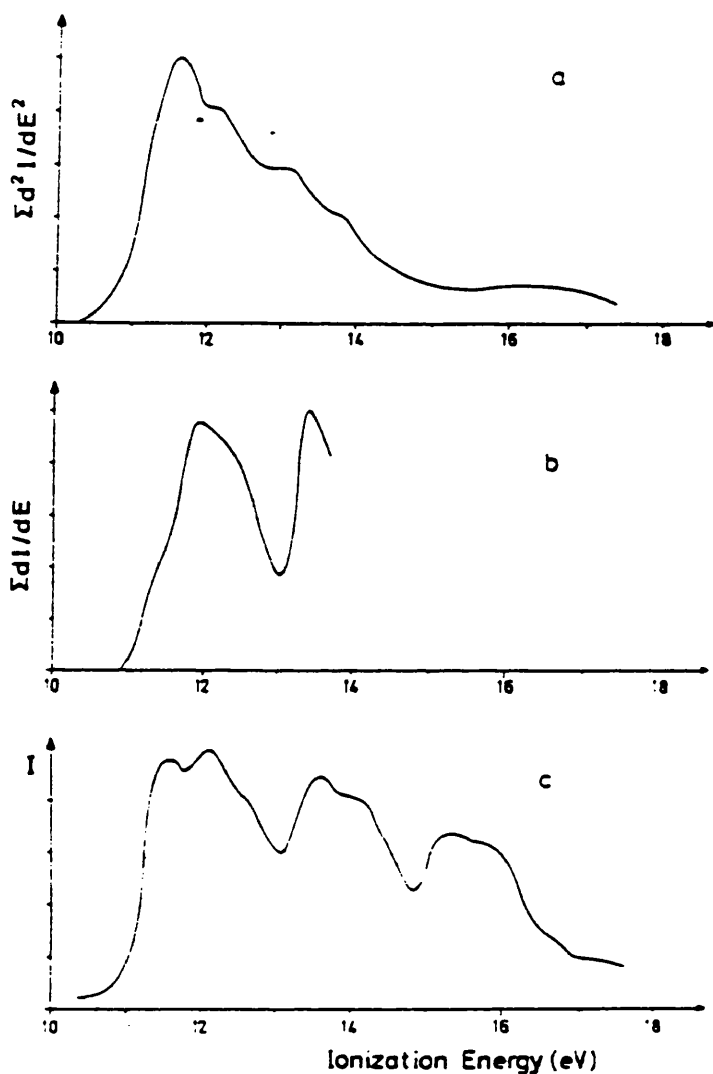


Figure 1.6. Internal energy distribution curve for propane obtained by (a) electron impact ³⁶, (b) photoionisation ³⁸ and (c) photoelectron spectroscopy⁴¹.

Direct equation of the photoelectron spectrum with the energy deposition function is however not generally possible because the relative intensities of transitions to various electronic states, i.e. the heights of the peaks in the photoelectron spectrum, are dependent on the photon

source energy ⁴⁰. Therefore photoelectron spectra only provide a reliable estimate of the photoionisation deposition function for the particular photon energy used (e.g. 21.22 eV), although, as mentioned above, it is advantageous that the photoelectron technique suffers far less from autoionisation than do photoionisation and electron impact yield measurements. The photoelectron spectrum of propane, Figure 1.6c ⁴¹, shows two distinct minima; in contrast to Figure 1.6a. There is a good correspondence between the energy distribution derived from the photoionisation efficiency curve (Figure 1.6b) and the photoelectron spectrum (Figure 1.6c) within the comparable energy range. The electron impact energy deposition function is of more interest to organic mass spectrometrists than that for photoionisation, but, as discussed above, the second derivative method does not give reliable information on this function. The suggestion that the photoelectron spectrum may be used as a crude approximation after electron impact is therefore of interest, and approximate energy distributions of 1,2-diphenylethane molecular ions produced by electron impact have been derived from modified photoelectron spectra using the EI threshold law, thermal energy convolution and empirical observation of ion abundances ⁴².

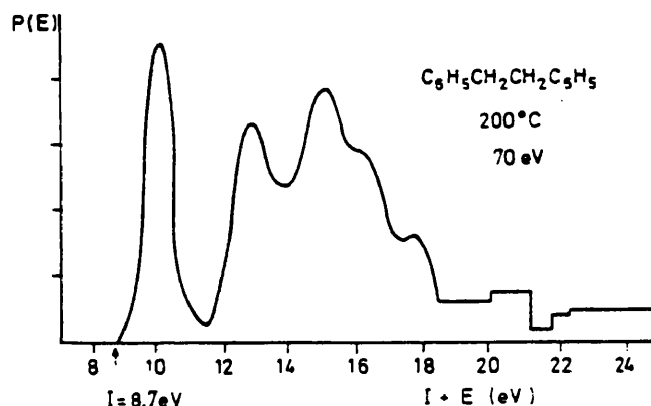


Figure 1.7. Internal energy distribution of 1,2-diphenylethane molecular ions formed by 70 eV energy electron impact. the curve has been obtained from the corresponding photoelectron spectrum which has been convoluted with the thermal energy distribution and adjusted to reflect the ion abundances in the 70 eV mass spectrum ⁴².

The energy distribution function for 1,2-diphenylethane derived by this method is illustrated in Figure 1.7, and shows a pronounced minimum at 11 eV. The existence of this minimum in the internal energy distribution of 1,2-diphenylethane is corroborated by a strong temperature dependence of the metastable ion for benzyl ion formation, the appearance energy for which almost coincides with the location of the minimum in $P(E)$ ⁴². At present it is not completely clear whether and to what extent the energy distribution in an ion after EI can be related to the suitably modified photoelectron spectrum of that compound, and arguments for ^{8,42,43} and against ^{44,45,46} this methodology have been raised.

Although the same types of ionisation processes may occur in electron and photon impact, optically forbidden transitions may occur under EI conditions leading to the population of additional ionic states, and as has already been pointed out, the relative transition probabilities, i.e. the peak heights, of the photoelectron spectrum are energy dependent and will be different for 20 and 70 eV.

It has been suggested by Meisels et al. ⁴⁴ that more reliable energy deposition functions may be obtained by folding the energy loss function into photoelectron spectra, where the energy loss functions are calculated from the Bethe-Born theory of collisions, using experimentally determined photoionisation cross sections; energy deposition functions for methane, ethane and ethylene were reported.

In summary, reliable electron impact deposition functions are not as yet available. Previous results and comparison with photoelectron spectroscopy clearly show that the majority of ions formed after 70 eV electron impact have a range of internal energies of 0-10 eV, while only a small fraction of molecular ions will be formed with energies in excess of 10 eV. This explains why the pattern of EI mass spectra changes very little at energies above 20 eV. There is also some strong indication that this energy distribution shows pronounced minima, with many compounds, in correspondence with those observed in photoelectron spectroscopy; although a quantitative correspondence between the photoelectron spectra, modified for a linear threshold law and thermal energy, and the unknown electron impact energy distribution cannot generally be expected.

1.5.2 The Thermal Energy Distribution

The experimentally determined energy distribution, i.e. using the first or second derivative methods, contains both the energy imparted to the molecular ion during the ionisation process, E_{dep} ; described by the energy deposition function, and the thermal energy, E_{th} , present in the molecule before ionisation. The probability that a molecule at a temperature, T , has an energy in the range E to $E + dE$ is given by:⁸

$$P_{\text{th}}(E) dE = \frac{\rho(E) \exp(-E/kT)}{\int_0^{\infty} \rho(E) \exp(-E/kT) dE} \quad [1.7]$$

where k is the Boltzmann constant and $\rho(E) dE$ is the number of states of the molecule with energy between E and $E + dE$. The thermal energy distribution of propane calculated by Erhardt and Osberghaus⁴⁷ is shown in Figure 1.8, and shows that even for a small molecule the average thermal energy, which is already 0.2 eV at 100 deg. centigrade, rises to more than 1 eV at 1000 deg. centigrade.

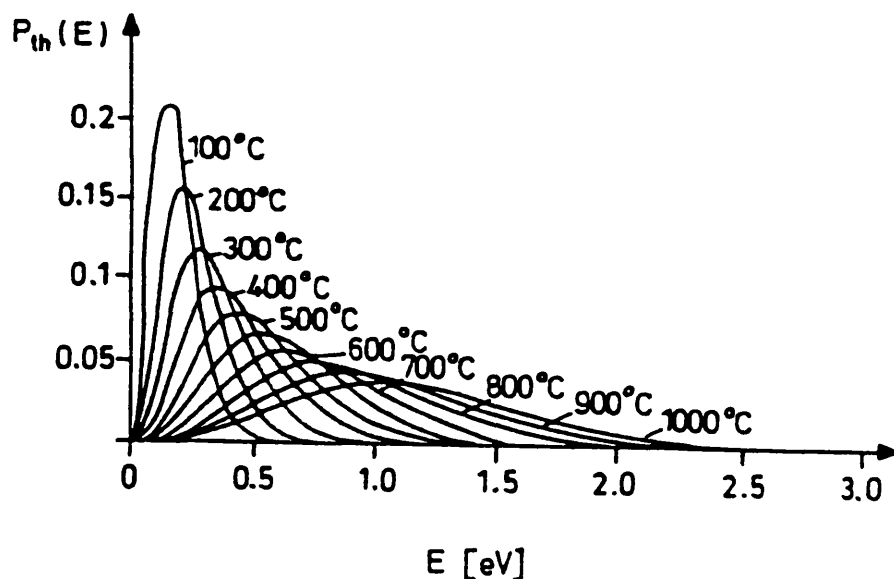


Figure 1.8. Thermal energy distribution of the propane molecular ion⁴⁷.

Electron impact ionisation sources are typically operated at 150 to 250 deg. centigrade. The maximum of the thermal energy distribution is shifted to even higher energies with increasing molecular weight ⁴⁸.

$$P(E) = \int_0^E P_{th}(E - E_{dep}) P_{dep}(E_{dep}) dE \quad [1.8]$$

If during the ionisation process an energy, E_{dep} , is transferred to the molecular ion, then, at a total internal energy, E , the fraction $E - E_{dep}$ represents the thermal energy. The total internal energy distribution, $P(E)$, can be obtained by convoluting the thermal energy distribution function, $P_{th}(E - E_{dep})$, and the energy deposition function, $P_{dep}(E_{dep})$.

1.6 Fragmentation and Appearance Energies

The excess energy remaining in the molecular ion (M^+), after ionisation, may then lead to one (or possibly more) bond(s) breaking and the molecular ion dissociating into fragments. Depending on their energy content, molecular ions may remain as such or dissociate into fragment ions by elimination of a radical



or by loss of an even-electron molecule



In either event the species $B \cdot$ and D are thereafter ignored by the mass spectrometer since they are not charged species and are not analyzed. Depending on their internal energies the ions A^+ and $C^+ \cdot$ may also fragment further. The minimum energy required to form a given ion and its accompanying fragments from a molecule is the appearance energy (AE). This assumes that the ground state species are involved in the fragmentation reaction, however

either the ion or the neutral or both species may be formed with excess vibrational energy resulting in a high experimental value for the appearance energy. Appearance energy measurements are of great importance in the determination of activation energies and ionic heats of formation, and the accuracy of the measurements is governed by the same factors as have already been discussed for ionisation energy measurements. The accuracy of appearance energy measurements is lower than that for ionisation energy measurements due to the more gradual increase of the ionisation efficiency curve at onset. Reproducibilities ranging from 0.01 to 0.1 eV can be achieved using monoenergetic electron or photon techniques as discussed in Section 1.4. However, as with ionisation energies, most appearance energies have been determined using polyenergetic ions and one of the extrapolation methods previously mentioned (Section 1.4.). With these techniques the accuracy ranges from 0.1 eV to 0.5 eV in an unpredictable manner.

The difference between appearance and ionisation energies, $AE - IE$, is taken to define the critical energy, E_c , of the reaction, however, this difference is often too high due to the kinetic shift. The critical energy, E_c , of a reaction is the difference between the zero-point energy of the reactant and the zero-point energy of the "transition state", i.e. the minimum energy for the reaction to occur. The critical energy refers strictly to rotational ground states, that is, rotational temperatures of absolute zero and is not equivalent to the activation energy obtained from Arrhenius plots (for systems under conditions of thermal equilibrium and to which Maxwell-Boltzmann statistics may be applied). Activation energies from Arrhenius plots concern the average energies of reactants and transition states ⁴⁹.

The kinetic shift is the excess energy required to drive the fragmentation fast enough for the ion to decompose in the ion source i.e. within 10^{-6} s, and the existence of a kinetic shift, first discussed in detail by Chupka ⁵⁰, is a direct consequence of the quasi-equilibrium theory (QET). If an ion is formed in the ion source of a conventional magnetic sector instrument, an energy E_s in excess of the activation energy, E_0 , is necessary to obtain a rate of 10^6 s⁻¹ which corresponds to the maximum ion lifetime in the source. This is the most probable rate leading to decomposition after 10^{-6} s, however, considerably smaller rates ($= 10^4$ s⁻¹) also contribute

albeit with low probability to this decomposition time and this is of importance for threshold measurements. From Figure 1.11. it can be seen that the kinetic shift will be larger the shallower the rise of k with E . The kinetic shift will be larger with bigger molecules, higher critical energies and "tighter" transition states. The excess energies required to obtain rate constants of 10^5 , 10^6 , and 10^7 s^{-1} have been calculated by Vestal⁸ for a variety of decomposition processes. The results indicate that the kinetic shift is negligible for most fragmentation processes, but can reach considerable values for reaction processes having high critical energies i.e. for the loss of hydrogen from the benzene ion a kinetic shift of the order of 1.5 eV may be expected. In order that kinetic shifts may be detected experimentally it is desirable to study ions of considerably longer lifetimes than are usually available in conventional mass spectrometers. The ion cyclotron resonance technique has been used by Gross⁵¹ to study the appearance energy of ions with an average lifetime of 10^{-2} s, and with the recent commercial availability of quadrupole ion traps and fourier transform mass spectrometers it is possible to study ions which are trapped for seconds and more accurate appearance potentials should be more easily measurable. Time-dependent breakdown graphs have also been used by Lifshitz et al⁵² to give reliable information on kinetic shifts by determining the normalised second derivative electron impact efficiency curves as functions of time using the method of ion trapping in the space charge of a pulsed electron impact source. The determination of appearance potentials is further complicated by the occurrence of a competitive shift^{42,53-55}, this occurs if two k versus E curves intersect, and results in the observed appearance energies being too high. Another complicating factor in the measurement of appearance energies is the thermal shift. This effect is due to the thermal energy present in a molecule prior to ionisation and as a result less energy is required to produce the ion at threshold. Under normal electron impact conditions where a hot ion source is used ($\approx 200^\circ\text{C}$), the average thermal energy for large organic molecules may reach considerable values (up to 0.8 eV has been calculated for 1,2-diphenylethane⁴²). The thermal shift increases with increasing molecular size due to the larger number of degrees of freedom over which the thermal energy can be distributed. Calculated thermal shifts have generally been in very good

agreement with experimental values, demonstrating that the thermal energy plays a full role in the dissociation of the molecular ion, as predicted by the QET. The thermal shift leads to lower apparent appearance energies and therefore partially offsets the kinetic shift.

1.7 Quasi-Equilibrium Theory

1.7.1 Introduction

There is considerable similarity between the fragmentation of large organic ions produced by electron impact in the mass spectrometer and the fragmentation processes associated with the thermal decomposition of organic molecules. Evidence for this similarity comes from the large number of observations indicating that ions undergo bond ruptures at weak bonds, elimination of molecular species such as H_2 , H_2O , CH_4 , and molecular rearrangements; all of which are known to occur preferentially in thermal reactions. Additionally, fragmentation threshold measurements on the ions indicate that in most cases the preferred processes are those which have the lowest energy requirement. In thermal decompositions the molecules are continuously energized and deactivated by collisions with the buffer gas and the resultant energy distribution can be described by a temperature. In contrast, the ions produced by electron impact in a conventional mass spectrometer are each energized by a single electron impact and are assumed to undergo no subsequent collisions prior to detection. Each ion is therefore formed with a specific amount of internal energy and angular momentum, both of which are independently conserved in all subsequent dissociations. Transitions to various electronic, vibrational, and rotational states of the ion are possible during the ionisation process, this leads to a collection of ions having a distribution of internal energies which will be quite different from the thermal distribution, and which will differ with electron energy and with the nature of the molecular species. The decomposition of diatomic ions can, for the most part, be explained by examination of the potential curves for the various accessible electronic states of the ions; and is generally well understood in terms of a simple spontaneous dissociation model. However, there are many observations (e.g. the presence of metastable ions, the small kinetic energy

released on fragmentation) which indicate that this simple model is not valid for polyatomic ions. The implication from the observations is that fragmentation does not immediately follow ionisation, but rather that it is slow enough to allow the transfer of energy into the various degrees of freedom involved in the observed dissociation. These observations inspired Rosenstock and co-workers⁵⁶, in 1952, to develop a statistical theory, called Quasi-Equilibrium Theory, to explain the electron impact induced fragmentation of polyatomic ions in a mass spectrometer.

1.7.2 Basic Assumptions

The Quasi-Equilibrium Theory (QET) is based on the following assumptions^{8,56,57,58}:

1. The time required for dissociation of the initial molecular ion is long compared with the time of interaction leading to its formation and excitation. Ionisation occurs within roughly 10^{-16} s, however, the shortest conceivable dissociation time is of the order of a single vibrational period ($= 10^{-14}$ s). The QET assumes that dissociation only occurs after at least several vibrations so that the molecular ion has lost all "memory" of how and where the ionisation occurred, i.e. the rate of decomposition is independent of the ionisation mode.
2. The rate of dissociation is slow compared to the rate of redistribution of the initial excitation energy over all degrees of freedom. Possible mechanisms for this energy redistribution are via radiationless transitions such as vibronic relaxation and vibrational relaxation.
3. The fragmentation products are formed by a series of competing and consecutive unimolecular reactions.
4. Ions generated in a mass spectrometer represent isolated systems in a state of "internal equilibrium". Isolated systems can be treated as microcanonical ensembles in which all systems within an energy interval between E and $E + dE$ of the phase space are distributed uniformly over all states within this interval. Such an ensemble is in statistical equilibrium⁵⁹. The rates for unimolecular decomposition can thus be calculated using the Absolute

Reaction Rate Theory modified to apply to such non-thermal situations, i.e. by integrating microcanonical rate expressions over the excitation energy distributions. It follows from 4. that the rate for a particular process is a function of the excitation energy only and tends to a limiting value at high internal energies.

1.7.3 The Rate Expression

The aim of any kinetic theory is to calculate the rate of reaction, and the Absolute Rate Theory of Eyring⁶⁰ was applied to isolated systems to develop a rate expression for QET by Rosenstock et al.⁵⁶.

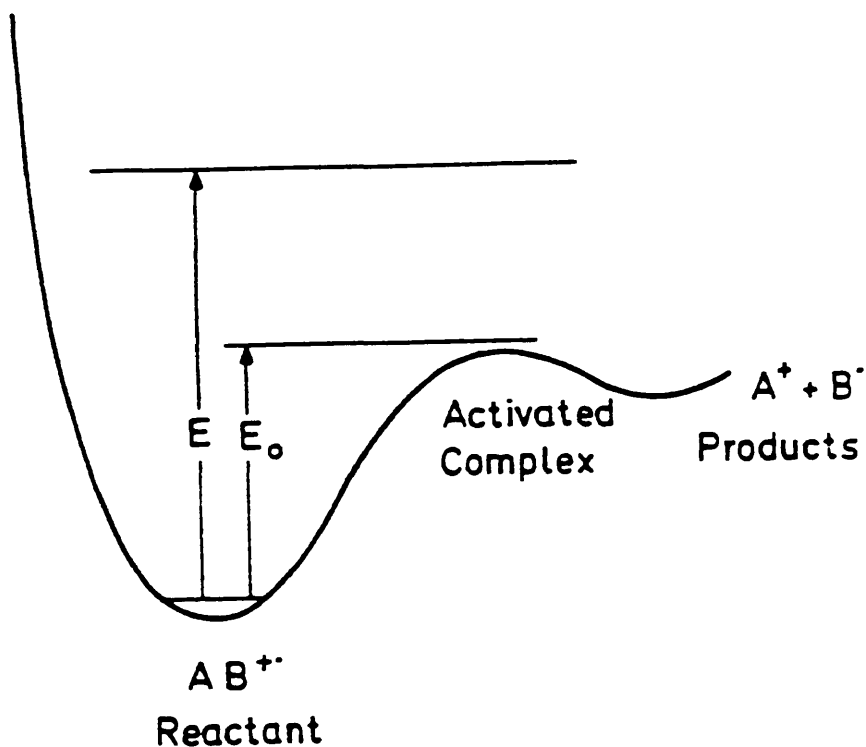


Figure 1.9. Schematic potential energy diagram of an ion.

Figure 1.9. shows schematically the model used in this treatment, where a slice through a potential surface is shown. The dissociation is described, in this model, as a motion along a reaction coordinate separable from all other internal coordinates by a critical "activated complex" or "transition state" configuration.

Decomposition occurs if a sufficient amount of energy has accumulated in the reaction coordinate to overcome the energy barrier (critical energy, E_c) of the "transition state". The dissociation is treated semi-classically and quantum mechanical reflection and tunnelling at the barrier are neglected.

The rate expression derived for QET is given below in Eq.[1.11],

$$k = \sigma \nu \left[\frac{(E - E_0)}{E} \right]^{N-1} \quad [1.11]$$

where k_i is the unimolecular rate constant for the i th reaction, σ is the symmetry factor, that is, the number of identical reactions which lead to the formation of a given ion. The factor ν is a structural parameter which contains the products of the moments of inertia and the vibrational frequencies of the reactant ion and the transition state, E and E_0 are the total energy of the reactant, and the critical energy of the fragmentation reaction under consideration respectively and N is the number of harmonic oscillators in the molecule.

An equivalent equation for thermal reactions was obtained by Marcus and Rice⁶¹, using a different approach consisting of a reformulation of the Rice-Ramsperger-Kassel theory, now termed RRKM theory⁶¹⁻⁶³. Calculation of the rate constant for a given fragmentation reaction requires a knowledge of the configuration of the molecular ion and the transition state, the vibrational and rotational frequencies in both the molecular ion and the transition state, the symmetry factor and the critical energy. Most QET calculations are based on the assumption that the structure of the molecular ion is very similar to that of the neutral molecule, however, much less is known about the transition state structure and this is the most severe handicap in QET calculations. The geometry of the transition state is usually termed as either "loose" (no rotations are stopped) or "tight" (one or more internal rotations are stopped), hence the transition state of a direct bond cleavage is classified as "loose" and that of a rearrangement reaction as "tight". Vibrational and rotational frequencies can be obtained from high level molecular orbital calculations for small organic ions, or by photoelectron spectroscopy however,

there is still a problem assigning these frequencies in the transition state, where some fitting to experimental data is nearly always required. One of the original aims of the QET was the calculation of complete mass spectra, which on comparison with experimentally obtained spectra would allow the validity of the theory to be tested. This has been done for a variety of polyatomic ions but is not a very rigorous test because the spectra rarely agree. The differences arise from the difficulty in selecting the correct fragmentation scheme from a number of possibilities and also from problems in determining the critical energy for each step in the fragmentation scheme, and in the lack of precision with which the energy distribution in the molecular ions is known. There are also problems in the basic theory such as with the expressions used to estimate the number of quantum states, several of which have been proposed. The importance of the QET lies in the fact that it offers a theoretical concept for understanding the fragmentation of gaseous ions allowing a number of phenomena in organic mass spectrometry, such as kinetic shifts, isotope effects, and the dependence of the fragment intensities on the internal energy and lifetime to be predicted and explained. A good introduction to the application of transition state theory to unimolecular reactions, with several examples from mass spectrometry has been published ⁶⁴.

More recently, improved theories have been proposed such as modified QET or Phase Space Theory (discussed in section 1.7.4. below) and a quantum theory of unimolecular reactions has been formulated by Pritchard ⁶⁵, which treats the unimolecular reaction as a perturbation of the process of molecular relaxation. In this treatment the unimolecular dissociation process is treated as a queuing problem with three steps: 1) the collisional activation of ordinary molecules into the reactive energy range. 2) the randomisation process(es) by which these molecules assemble this energy into a form of motion which will lead to reaction; and 3) the reaction process itself in which a molecule is transformed into fragments. This yields a result essentially equivalent to that described by Forst in 1972 ⁶⁶, there is also an equivalent formulation of this approach by Troe ⁶⁷ and an attempt has been made to link the two formulations and establish the connections between them ⁶⁸.

1.7.4 Modified QET - Phase Space Theory

According to the principle of microscopic reversibility a transition state can be reached either by decomposition of the reactant ion or by recombination of the ionic and neutral products with the rates for the forward and backward reactions being equal. Using this principle it was first shown by Klots⁶⁹⁻⁷¹ that it is possible to avoid the problem of defining an unknown transition state configuration by instead calculating the cross section for the formation of a collision complex from the separated fragments. The thermodynamic properties of the fragments are amenable to experimental observation and another important advantage of this treatment is that the total angular momentum is conserved in contrast to the original formulation of the QET. This theory, known as Phase Space Theory⁵⁸, rests on the basic assumption of the QET: the rate of dissociation is slow relative to the rate of redistribution of internal energy.

A disadvantage of this theory is that good collision cross section data are required for the calculations and these are rarely available. The Langevin collision model has been applied to the calculation of these cross sections⁷²⁻⁷⁴, although this has limited applicability since the Langevin model cannot be applied to molecules which have a permanent dipole moment. Several rate expressions based on modified QET or phase space theory, have been developed^{75,76}. The Phase Space Theory assumes "loose" transition states in all cases and it has been pointed out that the rate constants calculated by this theory represent upper limits⁷⁶, so that in general the calculated rate constants are too high if "tight" transition states are involved.

1.7.5 Recent Developments in Mass Spectrometry Theory

Despite its simplicity the QET does provide a sound conceptual framework for the study of the processes occurring in mass spectrometry. However, it is also true that it occasionally breaks down in its standard formulation. Various aspects of this problem have been discussed in several recent reviews^{63,64,77-81}. When the QET fails it is necessary to identify which of the conditions is breaking down, because it is sometimes possible, once the origin of the failure is understood, to develop a more adequate statistical treatment. The original transition state

theory consisted of replacing the study of an entire potential energy surface by the consideration of just a single point on it. The great simplicity of this description can be retained at the cost of introducing several energy-dependent (and angular momentum dependent) generalized transition states. In general, each measurable property of a chemical reaction (energy-threshold, reaction rate and energy partitioning) is under the control of a particular bottleneck. In addition to the familiar potential energy barriers and orbiting complexes, regions of strong non-adiabatic interaction and sharp bends in the reaction path are likely to induce a bottleneck effect. An alternative way of improving upon the simple transition state theory without undertaking unduly complicated calculations is to use the statistical adiabatic channel theory developed by Quack and Troe⁸². This is not much harder than variational transition state theory and it provides an appealing picture of a unimolecular reaction. It reduces to RRKM/QET and phase space theories in special limiting cases. As emphasized by Mies and Krauss⁸³, quantum effects can lead to non-exponential decay, i.e. to a breakdown of the concept of the rate constant. In addition, branching ratios are not always correctly calculated by the RRKM/QET equations. However, great care has to be taken before declaring a particular reaction to be inherently non-statistical. Although some features of some particular reactions appear to be at odds with the basic RRKM/QET equations, it may be possible to take advantage of the state of microcanonical equilibrium to derive an extended statistical theory of wider applicability.

1.7.6 Calculation of Mass Spectra

As has already been mentioned, the QET has been used to calculate mass spectra for comparison with experimentally measured spectra. These calculations are usually carried out in three steps:

1. the rate constant, $k(E)$, is determined for each fragmentation;
2. a breakdown graph is constructed from the individual rate constants;
3. convolution of the breakdown graph with the internal energy distribution yields the mass spectrum.

The complete fragmentation path, i.e. the breakdown scheme, of the molecule must be known in order to carry out these calculations and there are various methods available for obtaining this information:

1. Energetic considerations
2. Isotopic labelling
3. Metastable transitions
4. The dependence of the spectrum on electron energy
5. High resolution data
6. Direct experimental determination of the breakdown graphs.

Of these methods, isotopic labelling and metastable transitions give the most valuable information on the breakdown scheme, although not every fragmentation reaction gives rise to a metastable peak. The breakdown graph represents the relative intensity ratio of the molecular and all fragment ions as a function of the internal energy of the molecular ion, i.e. the graph shows the extent to which the intensity of the molecular ion is decreasing and the fragment ions are forming with increasing excitation energy within 10^{-5} seconds. Once the rate constants are known the intensity of the molecular and fragment ions are calculated using the rate equations for unimolecular decomposition⁸⁴ for both consecutive and competing reactions. The mass spectrometric time scale can be readily calculated for a given accelerating voltage, instrument geometry and ion mass and finally convolution of the breakdown graph with the internal energy distribution leads to the mass spectrum.

1.7.7 Tests of the QET

Numerous experiments have been devised to test the basic assumptions of the QET since its introduction in 1952, including studies on the energy randomisation hypothesis, isolated electronic states and ion lifetimes. These tests have also been used to check the quantitative agreement between QET calculations and experimental data. The energy randomisation hypothesis has been supported by field ionisation kinetic measurements which demonstrate⁸⁵

that many unimolecular decompositions reach their maximum intensity after about 10 picoseconds, indicating that the large majority of ions seem to decompose after complete energy randomisation in agreement with the QET assumption. However, rate constants for radiationless transitions need not be fast as demonstrated for a variety of neutral systems. Rate constants of the order of several times 10^8 seconds⁻¹ have been reported for vibronic relaxation, throwing some suspicion on the energy randomisation assumption^{86,87}. Isolated electronic states have been invoked in the past to rationalise observed phenomena, however, most of these phenomena have now been rationalized without the intervention of such states.

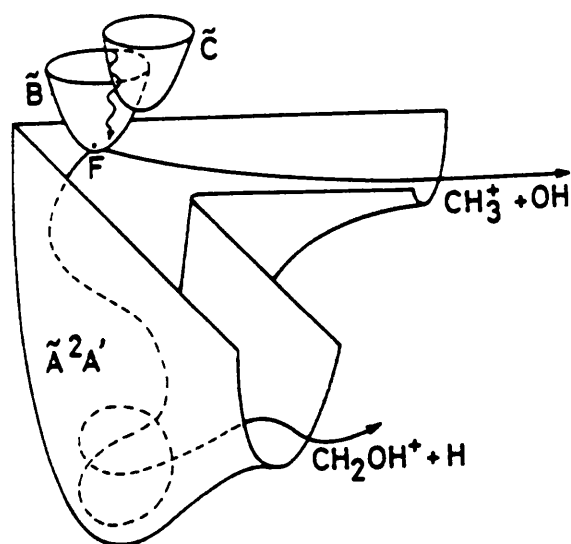


Figure 1.10. Isolated state decay corresponds to a branching in the reactive flux between the statistical and non-statistical paths.

It has also been pointed out by Rosenstock⁸⁸, that although the original formulation of the QET did assume internal conversion of all ions to the electronic ground state; this is not a central assumption and that if isolated electronic states are present in a molecular ion then each state can be described separately by the QET. The example of methanol molecular ions does constitute an example where the QET cannot explain the formation of the methyl cation

adequately. The explanation of this was only unravelled in 1982 by J.C. Lorquet and co-workers⁸⁹. The dissociation mechanism in this case is bimodal with most of the ions being produced by a statistical QET mechanism except for the formation of CH_3^+ ions. These result from a branching in the reaction path brought about by an avoided crossing between two potential energy surfaces. One of the reactive paths gives rise to the QET component, whereas the other leads directly to the $\text{CH}_3^+ + \text{OH}$ dissociation asymptote (Figure 1.10.). The CH_3^+ ions are produced by a fast, diatomic-like, non-statistical mechanism which escapes energy redistribution. "Isolated state decay" corresponds then to dissociation of the non-randomized fraction of the population, and not to isolation, i.e. to lack of radiationless transitions to the lower electronic states. Ion lifetime measurements have demonstrated that a continuum of rate constants exists and that there must be a continuous distribution of energies, however, the limited reproducibility of ion lifetime measurements means that this can only be regarded as a qualitative test of the QET. Most of the time the experimental evidence is in favour of the statistical theory of unimolecular decomposition i.e. the QET. Photoion-photoelectron coincidence (PIPECO) measurements have revealed that for most molecules the ion yield curves are smooth functions of energy alone and this constitutes convincing support for the validity of the basic assumption of the QET, i.e. That the molecular ion has reached a state of microcanonical equilibrium.

Other experiments which have furnished evidence in favour of the validity of the basis of the QET include, the calculation of mass spectra, the experimental determination of breakdown curves by electron impact, photoionisation, charge exchange and photoion- photoelectron coincidence measurements, determination of the rate constants and measurements of the kinetic energy release distribution.

Agreement between experiment and results of QET calculations is generally good provided that an adequate mathematical treatment of QET is used.

1.7.8 Applications of the QET

The QET has been applied to many aspects of the fragmentation behaviour of organic ions and

has had considerable success in explaining and predicting many observed phenomena. The discussion of k versus E curves has been shown to be particularly useful in interpreting the relative abundances of molecular and fragment ions as a function of the internal energy, the ion lifetime, the transition state configuration and a variety of other parameters ^{8,90,91}. Theoretical calculations and experimental evidence have demonstrated that, the rate constant, k , for a particular decomposition process, rises rapidly with energy near the threshold then levels off at higher energies before eventually reaching a constant value.

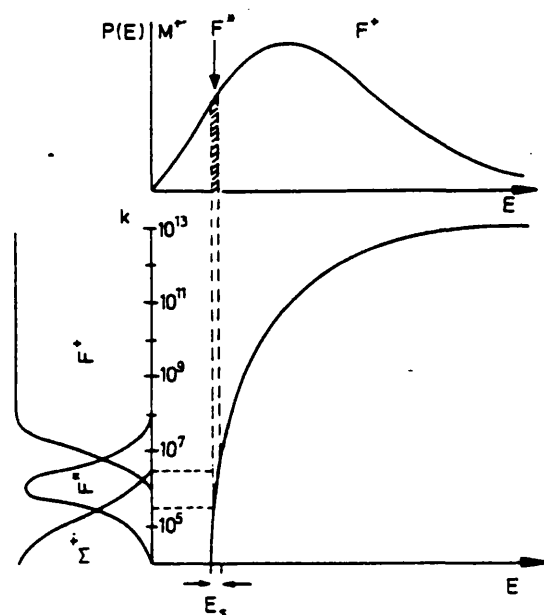


Figure 1.11. Schematic $k(E)$ curve (lower part) and internal energy distribution (upper part). The energy range contributing to the molecular ion (M^+), the metastable ion (F^+), and the normal fragment (F^+) are indicated.

This is as expected because the shortest physically meaningful decomposition time for an excited organic ion is of the order of one vibrational period (10^{-13} to 10^{-14} s), and therefore the maximum rate constant for a simple direct bond cleavage is of the order of $= 10^{14} \text{ s}^{-1}$. The intensity of a fragment depends on both the $k(E)$ function and the energy distribution, $P(E)$, and

both functions are illustrated in Figure 1.11., along with the intensities of the molecular ion, the metastable ion and the normal fragment ion as a function of the rate constant.

The definitions of the molecular ion, the fragment ion and the metastable ion are based on a time scale, but a range of rate constants contributes (with varying weight) to a given decomposition time, hence the ranges of rate constants giving rise to the different types of ions are not sharp, but overlap somewhat as shown in Figure 1.11. Metastable ions decompose predominantly, but not exclusively, with rate constants in the range $5 \cdot 10^5$ to $5 \cdot 10^6 \text{ s}^{-1}$ as indicated by horizontal dashed lines in Figure 1.11. The ratios of the appropriate areas of the $P(E)$ function for the molecular ion, the metastable ion, and the normal fragment ion are approximately proportional to the abundance ratios for the corresponding ion types. It is also apparent from Figure 1.11. that the greater the difference between the appearance energy and the ionisation energy, $(AE - IE)$, the greater the intensity of the molecular ion will be. The steeper the slope of the $k(E)$ curve the smaller the abundance of the metastable ion for that particular decomposition will be. Only a narrow range of energies contributes to the metastable ion and therefore its abundance is also a sensitive function of the energy distribution of the molecular ion, especially as pronounced maxima and minima in the $P(E)$ function are observed at low energies with many compounds. The shape of the $k(E)$ curve is predominantly determined by two factors: the geometry of the transition state and the critical energy of the process under study. The QET has also been applied to the study of the internal energy and ion lifetime dependence of competing rearrangement reactions and direct bond cleavages where the critical energy and the geometry of the transition state will be different in each case^{92,93,94}, and to studies on atom "scrambling" where some or all of the atoms take part in atom exchange reactions in the ion prior to decomposition⁹⁵⁻⁹⁸. The distribution of internal energy between fragments has been studied by looking at the internal energy of product ions⁵³ and a degree of freedom effect has been observed^{99,100} which has been rationalised using QET calculations and photoelectron spectra to determine $P(E)$ ¹⁰¹. Kinetic isotope effects are also observed in the mass spectrometric study of isotopically labelled compounds, although they are only significant in the case of deuterium labelling.

1.8 Substituent Effects on Fragmentation Reactions

The ionisation energies of a homologous series of a monofunctional compound, RX, are a linear function of the polar substituent constant, σ^+ , or the inductive substituent constant, σ^{+102} , of the alkyl group R. In the case of the thiols (X = SH), electron releasing alkyl groups bonded to the sulphur atom of the thiol facilitate electron removal and thereby lower the ionisation energy. The linear correlation holds even for the simplest thiol in the series, H₂S. The equations obtained for the correlation lines enable the ionisation energies of molecules in a homologous series to be calculated with high accuracy even if experimental data is not available. Correlation lines have been obtained for a variety of different functional groups including alcohols ¹⁰³, halides ¹⁰⁴, carboxylic acids ¹⁰⁵, amines ¹⁰⁶, nitriles ¹⁰⁷, ethers ¹⁰⁸, thioethers ¹⁰⁹, ketones ¹¹⁰, alkynes ¹¹¹, alkenes ¹¹² and others ¹¹³⁻¹¹⁵. In monosubstituted aromatic compounds a linear correlation between the ionisation energy and Brown's σ^+ constant is observed, with electron withdrawing substituents increasing the ionisation energy and electron donating substituents decreasing the ionisation energy. For disubstituted aromatic compounds the effects of the substituents are additive but not in a linear manner and both empirical and theoretical equations have been derived for calculating the ionisation energies of such disubstituted compounds from the individual σ^+ constants of both substituents ^{116,117}. Linear correlations have also been observed between the appearance energies and Hammett's σ ¹¹⁸ and Brown's σ^+ ¹¹⁹ constants in several series of substituted compounds although the correlation is not as good as that for ionisation energies, i.e. there is more scatter in the appearance energy values. The dependence of the appearance potential on the σ or σ^+ values reflects the influence of the substituent on the ionisation energy, the critical energy and to a lesser extent on the kinetic shift. An electron donating substituent leads in most cases to an increase in AE - IE and thus to an increased critical energy, although several instances are known where the opposite behaviour is observed ^{42,120} and there is no theoretical concept to explain these opposite effects of the substituent on the critical energy. Substituent effects on fragment ion abundances have been studied by several workers using a variety of ionisation techniques and the literature on this work has been reviewed ¹²¹⁻¹²³. No simple relationship

seems to exist, and the fragment abundances are controlled by several factors which can be explained within the framework of the QET, such as the rate constant, $k(E)$, of the process under study, the rate constants of competing reactions and secondary decompositions. Substituent effects on the kinetic energy release upon metastable decomposition have also been reported in some instances such as the loss of NO^\cdot from substituted nitrobenzenes ¹²⁴.

1.9 Metastable Ions

Ions which undergo unimolecular decomposition outside the ion source of a mass spectrometer are termed "metastable ions". If the decompositions occur within the field free regions of a magnetic sector type instrument they give rise to metastable peaks. Since the first correct interpretation of the origin of metastable peaks, by Hipple and Condon in 1945 ¹²⁵, it has been shown that a wealth of information for fundamental studies, the elucidation of reaction mechanisms and ion structure assignments can be extracted from them. Metastable ions have been extensively studied by Beynon and co-workers ¹²⁶⁻¹²⁸, and therefore this section will just give a brief summary. Metastable ions have lifetimes in the range 10^{-6} to 10^{-5} s depending on the geometry of the instrument being used (see Figure 1.11.), and as a result of the well defined lifetime window they have a rather narrow range of internal energies (about 0.1 to 1.0 eV above threshold). The existence of metastable ions can be predicted directly from the QET: After primary excitation, rapid radiationless transitions give rise to highly vibrationally excited ground state ions with a distribution of internal energies and thus a distribution of rate constants for fragmentation including those which predominantly lead to fragmentation in the metastable time range. There are two additional sources for metastable decompositions ¹²⁷:

- 1) Crossings of potential energy surfaces may lead to symmetry-forbidden predissociation which is slow enough to be detected within the metastable ion lifetime window.
- 2) Metastable decompositions may also be due to tunnelling through the dissociation barrier. Decomposing ions release part of their excess internal energy as kinetic energy, T , leading to a range of translational energies in the ion beam. Metastable ions formed outside the ion source have large translational energies as a result of the accelerating potential applied to all the ions in the

mass spectrometer. This results in an amplification of the translational energy spread caused by ion decomposition which for metastable ions means that the kinetic energy released is readily detected as peak broadening. This energy spread is not amplified for fragment ions formed in the ion source as a result of their low translational energies and is hence not detected as peak broadening. Small average T-values lead to narrow, gaussian shaped peaks due to the non-fixed energy in the transition state being the main source of the kinetic energy release.

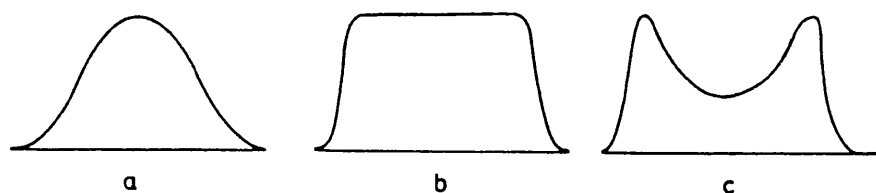


Figure 1.12. Typical peak shapes of metastable ions observed in magnetic sector instruments: a) gaussian, b) flat-topped, c) dish-shaped.

This non-fixed energy is statistically partitioned on fragmentation thus explaining the gaussian peak shape. Larger T-values lead to flat-topped or dish-shaped peaks ¹²⁶ (see Figure 1.12.). The minimum observed in the centre of dish-shaped peaks results from discrimination of ions with a maximum velocity component in the collector slit direction by the finite slit length (see reference 126 for a full discussion) and is most pronounced for short slits and long ion paths from the point of decomposition to the collector. Depending on the point of decomposition and the geometry of the mass spectrometer, the metastable peaks may be studied and recorded by scanning either the magnetic field strength, the electric sector potential, or the accelerating potential or combinations of these.

1.10 Charge Localisation

The QET gives a theoretical approach to the understanding of the complex spectra produced

by organic molecules undergoing mass spectrometric study, however many workers have adopted a more empirical approach with considerable success. This empirical approach is based on the concept of the charges produced by ionisation of a neutral molecule being located at specific favoured sites in the resulting ions ^{129,130}. The most favoured radical and charge sites in the molecular ion are assumed to arise from removal of the lowest energy electron in the molecule in the ionisation process. Relative energy requirements are similar to those for electronic transitions affecting ultraviolet spectra, hence favourability for ionisation generally follows the pattern of $\sigma < \pi < n$ -electrons. The localized charge may then be responsible for initiating reactions by attraction of an electron pair leading to bond cleavage and fragmentation. These reactions parallel other chemical reactions, particularly those in processes such as photolysis and pyrolysis. McLafferty ¹²⁹ has used a knowledge of the factors influencing chemical reactions, in conjunction with the reasonable supposition that the major fragment peaks observed in a mass spectrum should correspond to the most stable ion products of the kinetically and thermodynamically most favoured fragmentation pathways, to provide an insight into many of the characteristic features observed in mass spectra. He cites four aspects of fragmentation as being of particular importance:-

1. **Product Stability.** Ions which are stabilised by resonance or by inductive effects will have enhanced rates of formation and a reduced rate of decomposition. In consequence the fragment peak is relatively intense in the mass spectrum which is produced as a result of a series of competing and consecutive reactions.
2. **Bond Labilities.** Generally the labilities of bonds in ions parallel those in the molecules from which they are formed, and the weaker bonds are preferentially broken.
3. **Steric Factors.** These can affect the competition between unimolecular reaction pathways in several ways but the most significant of these relates rearrangement reactions where the transition state configuration has strict steric requirements. These reactions tend to be slow and hence they are

suppressed by competition with faster simple cleavage reactions. Steric factors can also influence product stability.

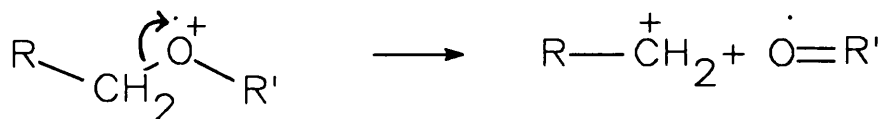
4. **Charge Competition in Ion Decompositions.** In odd-electron (OE) ions the fragmentation may occur as a result of radical initiation or charge initiation leading to two types of fragmentation which are summarised below:

Radical: The radical electron is donated together with another electron from another bond resulting in formation of a double or triple bond in place of a single or double bond, with the loss of a radical. A rearrangement could also occur with the formation of a new bond to a more distant atom with the expulsion of a neutral molecule. e.g.



(fish-hook arrows signify movement of single electrons)

Cation: An electron pair is transferred to the initial charge site thereby moving the site of the charge and resulting in the elimination of a radical containing the original charge site. Alternatively a new bond to a rearranging group or atom is formed with cleavage of a bond to the charge site resulting in elimination of a neutral molecule. e.g.



(double headed arrows signify movement of pairs of electrons)

The considerations which govern retention versus migration of the charge in OE^+ decompositions were first described by Stevenson in 1951¹³¹ and are known as Stevenson's Rule. This was re-formulated by Audier in 1969¹³² and states that: In the dissociation of an ion the positive charge will remain on the fragment of lower ionisation energy. Steric effects seem to have little effect on the operation of this rule. In even-electron (EE^+) ions the closest parallels to Stevenson's Rule which are applicable are due to Field (1972) and Bowen et al. (1978). They point out the energetic favourability of forming neutrals with low proton affinities. Even-electron ions have no unpaired electrons and hence cannot undergo the radical fragmentations outlined above.

Using this approach based on the principles outlined above, the mass spectra of many classes of compound have been rationalised. Further evidence for the validity of the charge localisation concept has come from the effect of substitution at the predicted charge site on measured ionisation energies^{133,134}, and more recently from molecular orbital calculations^{135,136}. The validity of the charge localisation concept has repeatedly been criticized¹³⁷⁻¹³⁹, particularly with reference to calculated charge distributions, although attempts to find experimental evidence against the concept have not proved successful. The concept and role of charge localisation was re-investigated by Williams and Beynon¹⁴⁰, who emphasize that the important factor is the localized radical site rather than the charge. The experimental evidence seems to indicate that partial localisation of the unpaired electron density in certain orbitals does not cause the dissociation, but rather it reduces the critical energy for the cleavage of certain bonds and thus increases the rate constant for the reaction. Therefore the concept of charge localisation whilst not being explicitly accounted for within the QET, is not in contradiction with the theory either. In spite of its successes the ability of the QET to deal with more complex molecules, particularly those containing several functional groups was questioned¹⁴¹ and organic mass spectrometrists generally adopted the charge (or radical) site localisation scheme for rationalising mass spectra. Several calculations were carried out using a modified version of the classical approximation¹⁴²⁻¹⁴⁴ in which the total number of oscillators was replaced by an effective number which increases linearly with rising electron energy; giving a rate equation of

the general form shown in [1.12] below. The same equation is used for direct bond cleavages and rearrangement reactions and despite some arbitrary assumptions and a poor approximation used for the density of states the agreement between calculated and experimental data was surprisingly good. These results need to be treated with some caution in view of the arbitrary choice of the parameters, however, they seem to support the premise that the QET can be used to explain the fragmentation behaviour of complex organic molecules with partial or predominant charge localisation.

$$k = \nu \left[\frac{(E - E_0)}{E} \right]^{(N-1)x} \quad [1.12]$$

where $x = 0.2 + 0.03(E - E_0)$.

These approaches to rationalising mass spectra will be discussed in more detail later in this work.

1.11. References

1. T.D. Mark, in *Electron-Molecule Interactions and Their Applications*, Vol.1, (L.G. Christophorou, Ed.), Academic Press, Orlando, 1984.
2. K. Levsen, *Fundamental Aspects of Organic Mass Spectrometry*, Verlag. Chemie, 1978.
3. D.R. Stull, E.F. Westrum and G.C. Sinke, *The Chemical Thermodynamics of Organic Compounds*, Wiley, New York, 1969.
4. H.M. Rosenstock, K. Draxl, B.W. Steiner, and J.T. Herron, *J. Phys. Chem. Ref. Data*, Vol. 6, 1977.
5. J.H. Beynon, R.A. Saunders, and A.E. Williams, *The Mass Spectra of Organic Molecules*, Elsevier, New York, 1968.
6. H.M. Rosenstock and R. Botter, *Recent Developments in Mass Spectrometry*, Proceedings of Int. Conf. on Mass Spectrometry, Kyoto, Japan, University Press, Baltimore, 1970.
7. F.H. Field and J.L. Franklin, *Electron Impact Phenomena*, Academic Press, New York, 1957.
8. M.L. Vestal, in *Fundamental Processes in Radiation Chemistry*, (P. Ausloos, Ed.), Interscience Publisher, New York, 1968.
9. E.P. Wigner, *Phys. Rev.*, **73**, 1002 (1948).
10. S. Geltman, *Phys. Rev.*, **102**, 171 (1956).
11. H.M. Rosenstock, *Int. J. Mass Spectrom. Ion Phys.*, **20**, 139 (1976).
12. W.A. Chupka, in *Ion-Molecule Reactions*, (J.L. Franklin, Ed.), Butterworths, London, 1972.
13. J.H. Beynon, R.G. Cooks, K.R. Jennings, and A.J. Ferrer-Correia, *Int. J. Mass Spectrom. Ion Phys.*, **18**, 87 (1975).
14. R.W. Kiser, *Introduction to Mass Spectrometry*, Prentice-Hall,
15. J.A. Simpson, and C.E. Kuyatt, *Rev. Sci. Instrum.*, **34**, 265 (1963).

16. K. Maeda, G.P. Semeluk, and F.P. Lossing, *Int. J. Mass Spectrom. Ion Phys.*, **1**, 395 (1968).
17. R.E. Fox, W.M. Hickam, T. Kjeldaas, Jr., and D.J. Grove, *Phys. Rev.*, **84**, 859 (1951).
18. R.E. Fox, W.M. Hickam, D.J. Grove, and T. Kjeldaas, Jr., *Rev. Sci. Instrum.*, **26**, 1101 (1955).
19. R.E. Winters, J.H. Collins, and W.L. Courchene, *J. Chem. Phys.*, **45**, 1931 (1966).
20. F.P. Lossing, A.W. Tickner, and W.A. Bryce, *J. Chem. Phys.*, **19**, 1254 (1951).
21. J.W. Warren, *Nature*, **165**, 810 (1950).
22. R.W. Kiser, and E.J. Gallegos, *J. Phys. Chem.*, **66**, 947 (1962).
23. R.E. Honig, *J. Chem. Phys.*, **16**, 105 (1948).
24. J.D. Morrison, *J. Chem. Phys.*, **21**, 1767 (1953).
25. J.L. Occolowitz, B.J. Cerimele, and P. Brown, *Org. Mass Spectrom.*, **8**, 61 (1974).
26. F.I. Vilesov, B.L. Kurbatov, and A.N. Terenin, *Dokl. Akad. Nauk. SSSR*, **138**, 1329 (1961).
27. D.W. Turner, and M.I. Al-Jobory, *J. Chem. Phys.*, **37**, 3007 (1962).
28. D.W. Turner, C. Baker, A.D. Baker, and C.R. Brundle, *Molecular Photoelectron Spectroscopy*, Wiley-Interscience, New York, 1970.
29. J.H.D. Eland, *Photoelectron Spectroscopy*, Butterworths, London, 1974.
30. D. Villarejo, R.R. Herm, and M.G. Inghram, *J. Chem. Phys.*, **46**, 4995 (1967).
31. D. Villarejo, *J. Chem. Phys.*, **48**, 4014 (1968).
32. W.B. Peatman, T.B. Borne, and E.W. Schlag, *Chem. Phys. Lett.*, **3**, 492 (1969).
33. T. Baer, W.B. Peatman, and E.W. Schlag, *Chem. Phys. Lett.*, **4**, 243 (1969).
34. R. Spohr, P.M. Guyon, W.A. Chupka, and J. Berkowitz, *Rev. Sci. Instrum.*, **42**, 1872 (1971).
35. J.D. Morrison, *J. Appl. Phys.*, **28**, 1409 (1957).
36. W.A. Chupka, and M. Kaminsky, *J. Chem. Phys.*, **35**, 1991 (1961).
37. W.A. Chupka, *J. Chem. Phys.*, **30**, 191 (1959).
38. W.A. Chupka, and J. Berkowitz, *J. Chem. Phys.*, **47**, 2921 (1967).

39. K.M.A. Refaey, and W.A. Chupka, *J. Chem. Phys.*, **48**, 5205 (1968).
40. W.C. Price, A.W. Potts, and D.G. Streets, in *Electron Spectroscopy*, (D.A. Shirley, Ed.), North-Holland, Amsterdam, 1972.
41. B. Brehm, J.H.D. Eland, R. Frey, and H. Schulte, *Int. J. Mass Spectrom. Ion Phys.*, **21**, 373 (1976).
42. F.W. McLafferty, T. Wachs, C. Lifshitz, G. Innorta, and P. Irving, *J. Amer. Chem. Soc.*, **92**, 6867 (1970).
43. H.M. Rosenstock, and M. Krauss, *Advan. Mass Spectrometry*, **2**, 251 (1963).
44. G.G. Meisels, C.T. Chen, B.G. Giessner, and R.H. Emmel, *J. Chem. Phys.*, **56**, 793 (1972).
45. G. Innorta, S. Torrioni, and S. Pignataro, *Org. Mass Spectrom.*, **6**, 113 (1972).
46. B.N. McMaster, in *Mass Spectrometry Vol.3*, (R.A.W. Johnstone, Ed.), The Chemical Society, London, 1975.
47. H. Ehrhardt, and O. Osberghaus, *Z. Naturforsch.*, **15a**, 575 (1960).
48. B. Steiner, C.F. Giese, and M.G. Inghram, *J. Chem. Phys.*, **34**, 189 (1961).
49. A. Maccoll, *Org. Mass Spectrom.*, **15**, 109 (1980).
50. W.A. Chupka, *J. Chem. Phys.*, **30**, 191 (1959).
51. M.L. Gross, *Org. Mass Spectrom.*, **6**, 827 (1972).
52. C. Lifshitz, M. Weiss, and S. Landau-Gefen, *Proceedings of the 25th Conference of the American Society for Mass Spectrometry*, Washington, 1977, p. 512.
53. D.J. McAdoo, P.F. Bente, M.L. Gross, and F.W. McLafferty, *Org. Mass Spectrom.*, **9**, 525 (1974).
54. C. Lifshitz and F.A. Long, *J. Chem. Phys.*, **41**, 2468 (1964).
55. I. Howe, in *Mass Spectrometry, Vol.2*, (D.H. Williams, Ed.), The Chemical Society, London, 1973.
56. H.M. Rosenstock, M.B. Wallenstein, A.L. Wahrhaftig, and H. Eyring, *Proc. Nat. Acad. Sci.*, **38**, 667 (1952).

57. H.M. Rosenstock, in *Advances in Mass Spectrometry*, Vol.4, The Institute of Petroleum, London, 1968.
58. C. Lifshitz, in *Advances in Mass Spectrometry*, Vol.7, Heyden, London, 1977.
59. R.C. Tolman, *The Principles of Statistical Mechanics*, Oxford University Press, London, 1938.
60. S. Glasstone, K.J. Laidler, and H. Eyring, *Theory of Rate Processes*, McGraw-Hill, New York, 1941.
61. R.A. Marcus and O.K. Rice, *J. Phys. and Colloid Chem.*, **55**, 894 (1951).
62. R.A. Marcus, *J. Chem. Phys.*, **20**, 359 (1952).
63. W. Forst, *Theory of Unimolecular Reactions*, Academic Press, New York, 1973.
64. J.H. Beynon and J.R. Gilbert, *Application of Transition State Theory to Unimolecular Reactions*, Wiley, New York, 1984.
65. H.O. Pritchard, *The Quantum Theory of Unimolecular Reactions*, Cambridge University Press, Cambridge, 1984.
66. W. Forst, *J. Phys. Chem.*, **76**, 342-8 (1972).
67. J. Troe, *J. Chem. Phys.*, **66**, 4745-57; 4758-75 (1977).
68. N.S. Snider, *J. Chem. Phys.*, **77**, 789-97 (1982).
69. C.E. Klots, *Adv. Mass Spectrom.*, **6**, 969 (1973).
70. C.E. Klots, *Chem. Phys. Lett.*, **38**, 61 (1976).
71. C.E. Klots, *J. Chem. Phys.*, **64**, 4269 (1976).
72. P. Langevin, *Ann. Chim. Phys., Ser. 7*, 317 (1903).
73. P. Langevin, *Ann. Chim. Phys.*, **5**, 245 (1905).
74. T.A. Lehman and M.M. Bursley, Wiley-Interscience, New York, 1976, p.132.
75. W.J. Chesnavich and M.T. Bowers, *J. Chem. Phys.*, **66**, 2306 (1977).
76. W.J. Chesnavich and M.T. Bowers, *J. Amer. Chem. Soc.*, **99**, 1705 (1977).
77. *Gas Phase Ion Chemistry*, (M.T. Bowers, Ed.), Academic Press, New York, 1979.
78. C. Lifshitz, *Adv. Mass Spectrom.*, **7A**, 3 (1978).
79. J.C. Lorquet, *Org. Mass Spectrom.*, **16**, 469 (1981).

80. C. Lifshitz, *J. Phys. Chem.*, **87**, 2304 (1983).
81. P.J. Derrick and K.F. Donchi, in *Comprehensive Chemical Kinetics*, Vol.24, (C.H. Bamford and C.F.H. Tipper, Eds.), Elsevier, Amsterdam, 1983.
82. M. Quack and J. Troe, *Ber. Bunsenges. Phys. Chem.*, **78**, 240 (1974); J. Troe, *J. Chem. Phys.*, **75**, 226 (1981).
83. F.H. Mies and M. Krauss, *J. Chem. Phys.*, **45**, 4455 (1966).
84. A.A. Frost and R.G. Pearson, *Kinetics and Mechanism*, 2nd Ed., Wiley, New York, 1961.
85. K. Levsen and H.D. Beckey, *Int. J. Mass Spectrom. Ion Phys.*, **9**, 63 (1972).
86. M.H. Hui and S.A. Rice, *J. Chem. Phys.*, **61**, 833 (1974).
87. C.-S. Huang and E.C. Lim, *J. Chem. Phys.*, **62**, 3826 (1975).
88. H.M. Rosenstock, J.T. Larkins, and J.A. Walker, *Int. J. Mass Spectrom. Ion Phys.*, **11**, 309 (1973).
89. C. Galloy, C. Lecomte, and J.C. Lorquet, *J. Chem. Phys.*, **77**, 4522 (1982)
90. R.G. Cooks, I. Howe, and D.H. Williams, *Org. Mass Spectrom.*, **2**, 137 (1969).
91. D.H. Williams and I. Howe, *Principles of Organic Mass Spectrometry*, McGraw-Hill, London, 1972.
92. D.H. Williams and R.G. Cooks, *Chem. Commun.*, 254 (1968).
93. K.B. Tomer, J. Turk, and R.H. Shapiro, *Org. Mass Spectrom.*, **6**, 235 (1972).
94. J.R. Dias and C. Djerassi, *Org. Mass Spectrom.*, **6**, 385 (1972).
95. K. Levsen, F.W. McLafferty, and D.M. Jerina, *J. Amer. Chem. Soc.*, **95**, 6332 (1973).
96. K. Levsen and H.D. Beckey, *Int. J. Mass Spectrom. Ion Phys.*, **14**, 45 (1974).
97. H. Budzikiewicz and R. Stolze, *Monath.*, **108**, 869 (1977).
98. R.P. Morgan, P.J. Derrick, and A.G. Harrison, *J. Amer. Chem. Soc.*, **94**, 4189 (1977).
99. F.W. McLafferty and W.T. Pike, *J. Amer. Chem. Soc.*, **89**, 5951 (1967); *ibid*, 5953.
100. R.G. Cooks and D.H. Williams, *Chem. Commun.*, 627 (1968).
101. P.F. Bente, F.W. McLafferty, D.J. McAdoo, and C. Lifshitz, *J. Phys. Chem.*, **79**, 713 (1975).

102. R.W. Taft and I.C. Lewis, *Tetrahedron*, **5**, 210 (1959).
103. L.S. Levitt and B.W. Levitt, *Tetrahedron*, **27**, 3777 (1971).
104. L.S. Levitt and B.W. Levitt, *Tetrahedron*, **29**, 941 (1973).
105. B.W. Levitt and L.S. Levitt, *Chem. and Ind.*, 990 (1970).
106. B.W. Levitt and L.S. Levitt, *Israel J. Chem.*, **9**, 71 (1971).
107. B.W. Levitt, H.F. Widing, and L.S. Levitt, *Chem. and Ind.*, 793 (1973).
108. B.W. Levitt and L.S. Levitt, *Experientia*, **26**, 1183 (1970).
109. B.W. Levitt and L.S. Levitt, *Israel J. Chem.*, **9**, 711 (1971).
110. B.W. Levitt and L.S. Levitt, *Chem. and Ind.*, 724 (1972).
111. L.S. Levitt, *Chem. and Ind.*, 637 (1973).
112. L.S. Levitt, B.W. Levitt, and C. Parkanyi, *Tetrahedron*, **28**, 3369 (1972).
113. L.S. Levitt and B.W. Levitt, *Chem. and Ind.*, 132 (1973).
114. H.F. Widing and L.S. Levitt, *Tetrahedron*, **30**, 611 (1974).
115. A. Streitweiser, *Prog. Phys. Org. Chem.*, **1**, 1 (1963).
116. F. Benoit, *Org. Mass Spectrom.*, **9**, 626 (1974).
117. J.M. Behan, R.A.W. Johnstone, and T.W. Bentley, *Org. Mass Spectrom.*, **11**, 207 (1976).
118. L.P. Hammett, *Physical Organic Chemistry*, McGraw-Hill, New York, 1940, Chapter VII.
119. H.C. Brown and Y. Okamoto, *J. Amer. Chem. Soc.*, **80**, 4979 (1958).
120. P. Brown, *Org. Mass Spectrom.*, **4**, 519 (1970).
121. M.M. Bursey, *Org. Mass Spectrom.*, **1**, 31 (1968).
122. M.M. Bursey, in *Advances in Linear Free Energy Relationships*, (J. Shorter, Ed.), Plenum, 1972.
123. T.W. Bentley and R.A.W. Johnstone, in *Advances in Physical Organic Chemistry*, Vol.8, (V. Gold, Ed.), Academic Press, 1970.
124. J.H. Beynon, M. Bertrand, and R.G. Cooks, *J. Amer. Chem. Soc.*, **95**, 1739 (1973).
125. J.A. Hipple and E.U. Condon, *Phys. Rev.*, **68**, 54 (1945).

126. R.G. Cooks, J.H. Beynon, R.M. Caprioli, and G.R. Lester, *Metastable Ions*, Elsevier, 1973.
127. R.G. Cooks and J.H. Beynon, in *Mass Spectrometry, International Review of Science, Phys. Chem. Series II, Vol.5*, Butterworths, London, 1975, Chapter 5.
128. J.H. Beynon and R.G. Cooks, *Int. J. Mass Spectrom. Ion Phys.*, **19**, 107 (1976).
129. F.W. McLafferty, *Interpretation of Mass Spectra*, 3rd Edition, University Science Books, 1980.
130. F.W. McLafferty, *Chem. Commun.*, 78 (1966).
131. D.P. Stevenson, *Disc. Faraday Soc.*, **10**, 35 (1951).
132. H.E. Audier, *Org. Mass Spectrom.*, **2**, 283 (1969).
133. M.A. Baldwin, A.G. Loudon, A. Maccoll, and K.S. Webb, *Org. Mass Spectrom.*, **11**, 1181 (1976).
134. M.A. Baldwin, A.G. Loudon, K.S. Webb, and P.C. Cardnell, *Org. Mass Spectrom.*, **12**, 279 (1977).
135. M.A. Baldwin and K.J. Welham, *Rapid Commun. Mass Spectrom.*, **1**, 13 (1987).
136. M.A. Baldwin and K.J. Welham, *Org. Mass Spectrom.*, **23**, 425 (1988).
137. T.W. Bentley, R.A.W. Johnstone, and F.A. Mellon, *J. Chem. Soc. (B)*, 1800 (1971).
138. C. Krier, J.C. Lorquet, and A. Berlingin, *Org. Mass Spectrom.*, **8**, 387 (1974).
139. F.W. McLafferty, in *Recent Developments in Mass Spectrometry*, (K. Ogata and T. Hayakawa, Eds.), University Park Press, Baltimore, 1970. p.70.
140. D.H. Williams and J.H. Beynon, *Org. Mass Spectrom.*, **11**, 103 (1976).
141. G. Spiteller and M. Spiteller-Friedmann, *Justus Liebigs Ann. Chem.*, **690**, 1 (1965).
142. A.N.H. Yeo and D.H. Williams, *J. Amer. Chem. Soc.*, **92**, 3984 (1970).
143. A.N.H. Yeo and D.H. Williams, *Org. Mass Spectrom.*, **5**, 135 (1971).
144. R. Heller, P. Krenmayr, and K. Varmuza, *Org. Mass Spectrom.*, **9**, 1134 (1974).

2. Molecular Quantum Mechanics.

2.1 General Introduction

The quantum theory of matter came into being as a result of the failure of classical physics to provide adequate explanations for several observations in different areas of physics and chemistry. Planck was the first to suggest that energy was quantised when he proposed a radical solution to the black-body radiation problem. The quantum hypothesis soon gained in stature and scope by solving several other outstanding problems. In 1913 Bohr arbitrarily welded Planck's quantum hypothesis to classical mechanics and although his calculation was not what we would today call quantum mechanical, it was the first synthesis of quantum theory and mechanics.

The first successful proposal about how to do quantum mechanical calculations was due to Heisenberg (1926), who put forward the scheme known as 'matrix mechanics'. In the same year Schrodinger put forward his rival theory of 'wave mechanics'. The two theories appeared to be quite different at first, however it was not long before Schrodinger himself was able to show that the two approaches were mathematically equivalent. Each has its advantages for different types of problem, but Schrodinger's formulation is conceptually simpler and has become more widely adopted. The time independent Schrodinger equation is given in [2.1] below. Most of quantum mechanics is concerned with finding solutions of this deceptively simple equation.

$$\hat{H}\Psi = E\Psi \quad [2.1]$$

The key to theoretical chemistry is molecular quantum mechanics. This is the branch of science relating molecular properties to the motion and interactions of electrons and nuclei. Soon after its formulation in 1925¹, it became clear that solution of the Schrodinger differential equation could, in principle, lead to direct quantitative prediction of most, if not all, chemical phenomena using only the values of a small number of physical constants (Planck's constant, the velocity

of light, and the masses and charges of electrons and nuclei). Such a procedure constitutes an ab-initio approach to chemistry, independent of any experiment other than determination of the constants. It was also recognised early on that solution of the Schrodinger equation was a formidable if not completely impossible mathematical problem for any but the simplest of systems.

The underlying physical laws necessary for the mathematical theory of a large part of physics and the whole of chemistry are thus completely known, and the difficulty is only that the exact application of these laws leads to equations much too complicated to be soluble².

P.A.M. Dirac 1902-1984

In practice the Schrodinger equation has to be replaced by approximate mathematical models for which the possibility of solution exists. The development of powerful digital computers has led to significant progress in recent years, both in the development of ever more sophisticated approximate quantum mechanical models and in the application of these models to problems of chemical significance.

2.2 The Theoretical Background

2.2.1 The Schrodinger Equation

From quantum mechanics¹, the energy and many properties of a stationary state of a molecule can be obtained by solution of the Schrodinger partial differential equation,

$$\hat{H}\Psi = E\Psi \quad [2.1]$$

Here \hat{H} is the Hamiltonian, a differential operator representing the total energy. E is the numerical value of the energy of the state, that is, the energy relative to a state in which the constituent particles (nuclei and electrons) are infinitely separated and at rest. Ψ is the

wavefunction, it depends on the cartesian coordinates of all the particles (which may take any value from $-\infty$ to $+\infty$) and also on the spin coordinates (which may take only a finite number of values corresponding to spin angular momentum coordinates in a particular direction). The square of the wavefunction, Ψ^2 (or $|\Psi|^2$ if Ψ is complex), is interpreted as a measure of the probability distribution of the particles within the molecule.

The Hamiltonian \hat{H} , like the energy in classical mechanics is the sum of kinetic and potential parts,

$$\hat{H} = \hat{T} + \hat{V} \quad [2.2]$$

The kinetic energy operator T is the sum of differential operators,

$$\hat{T} = - \frac{\hbar^2}{8 \pi^2} \sum_i \frac{1}{m_i} \left(\frac{d^2}{dx^2} + \frac{d^2}{dy^2} + \frac{d^2}{dz^2} \right) \quad [2.3]$$

The sum is over all particles i (nuclei + electrons) and m_i is the mass of particle i, \hbar is Planck's constant. The potential energy operator is the coulomb interaction,

$$\hat{V} = \sum_i \sum_j \left(\frac{e_i e_j}{r_{ij}} \right) \quad [2.4]$$

where the sum is over distinct pairs of particles (i,j) with electric charges e_i, e_j separated by a distance r_{ij} . For electrons, $e_i = -e$, while for a nucleus with atomic number Z_i , $e_i = +Z_i e$.

The Hamiltonian described above is nonrelativistic. It ceases to be appropriate as the velocities of the particles approach the speed of light³. Certain small magnetic effects, for example, spin-orbit coupling, spin-spin interactions, and so forth are also omitted in this Hamiltonian; these are usually of minor significance in discussions of chemical energies.

One other restriction has to be imposed on the wavefunctions. The only solutions of [2.1] that are physically acceptable are those with appropriate symmetry under interchange of identical particles. For boson particles, the wavefunction is unchanged, that is, symmetric, under such interchange. For fermion particles, the wavefunction must be multiplied by -1, that is, antisymmetric. Electrons are fermions, so that Ψ must be antisymmetric with respect to interchange of the coordinates of any pair of electrons. This is termed the antisymmetry

principle. The Schrodinger equation for any molecule will have many solutions, corresponding to different stationary states. The state with the lowest energy is the ground state and most of the techniques and applications described here are concerned with the ground states of the molecules and radical cations studied.

2.2.2 Separation of Nuclear Motion : Potential Surfaces

The first major step in simplifying the general molecular problem in quantum mechanics is the separation of the nuclear and electronic motions. This is possible because the nuclear masses are much greater than those of the electrons, and, therefore, nuclei move much more slowly. As a consequence, the electrons in a molecule adjust their distribution to changing nuclear positions rapidly. This makes it a reasonable approximation to suppose that the electron distribution depends only on the instantaneous positions of the nuclei and not on their velocities. In other words the quantum mechanical problem of fixed nuclei may first be solved, leading to an effective electronic energy $E_{\text{eff}}(R)$ which depends on the relative nuclear coordinates, denoted by R . This effective energy is then used as a potential energy for a subsequent study of the nuclear motion. $E_{\text{eff}}(R)$ will depend on all of the relative nuclear coordinates. For a diatomic molecule, only the internuclear distance, R , is required and $E_{\text{eff}}(R)$ is the potential curve for the molecule. For a polyatomic system, more relative coordinates are needed, and $E_{\text{eff}}(R)$ is termed the potential surface for the molecule. This separation of the general problem into two parts is often called the adiabatic or Born-Oppenheimer approximation. It was first quantitatively examined by Born and Oppenheimer⁴, who showed that it was valid, provided that the ratio of electron to nuclear mass was sufficiently small. The Born-Oppenheimer approximation may be formulated quantitatively by writing the Schrodinger equation for electrons in the field of fixed nuclei,

$$\hat{H}^{\text{elec}} \Psi^{\text{elec}}(r, R) = E^{\text{eff}}(R) \Psi^{\text{elec}}(r, R) \quad [2.5]$$

Here, Ψ_{elec} is the electronic wavefunction which depends on the electronic coordinates, r , as

well as on the nuclear coordinates, R. The Hamiltonian \hat{H}_{elec} which corresponds to the motions of electrons only in the field of fixed nuclei is,

$$\hat{H}^{\text{elec}} = \hat{T}^{\text{elec}} + \hat{V} \quad [2.6]$$

where \hat{T}_{elec} is the electronic kinetic energy,

$$\hat{T}^{\text{elec}} = - \left(\frac{\hbar^2}{8\pi^2 m} \right) \sum_{\text{electrons}} \left(\frac{d^2}{dx^2} + \frac{d^2}{dy^2} + \frac{d^2}{dz^2} \right) \quad [2.7]$$

and \hat{V} is the coulomb potential energy,

$$\hat{V} = - \sum_{\text{electrons}} \sum_{\text{nuclei}} \frac{Z_s e^2}{r_{is}} + \sum_{\text{electrons}} \sum_{i < j} \frac{e^2}{r_{ij}} + \sum_{\text{nuclei}} \sum_{s < t} \frac{Z_s Z_t e^2}{R_{st}} \quad [2.8]$$

The first part of [2.8] corresponds to electron-nuclear attraction, the second part to electron-electron repulsion, and the third to nuclear-nuclear repulsion. The last is independent of the electronic coordinates and is a constant contribution to the energy for any particular nuclear configuration.

The main task of theoretical studies of electronic structure is to solve, at least approximately, the electronic Schrodinger equation [2.5], and hence find the effective nuclear potential function $E_{\text{eff}}(R)$. From here on, the superscripts in [2.5] are omitted; and it is assumed that the Hamiltonian, \hat{H} , wavefunction, Ψ , and the energy, E , refer to electronic motion only, each quantity being implicitly a function of the relative nuclear coordinates, R.

The potential surface, $E(R)$, is fundamental to the quantitative description of chemical structures and reaction processes. If we deal with the lowest-energy solution of the electronic Schrodinger equation, $E(R)$ is the ground-state potential energy surface. When explored as a function of R, it will generate a number of local minima, as illustrated in Figure 2.1a.

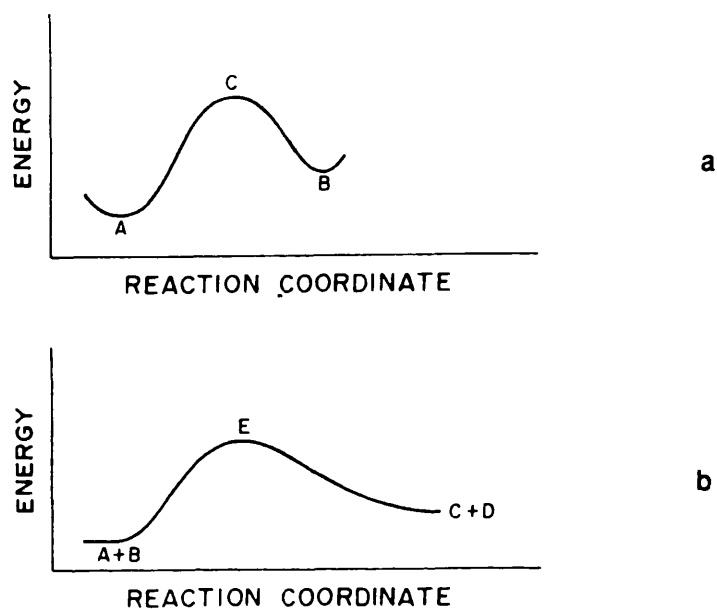


Figure 2.1. Schematic sections of potential surfaces

These minima correspond to equilibrium structures, that is; the geometry corresponding to a minimum of $E(R)$ is the geometry a molecule would have if all the nuclei were stationary. In practice this is never the case and finite nuclear motion occurs because of zero-point vibration, even at low temperatures. Nevertheless, the equilibrium geometry corresponding to the potential minimum is usually a good approximation to the averaged structure. If there are several distinct potential minima, the molecule has a number of isomeric forms, and the theory can be used to explore their structures and relative energies. The potential surface may also contain saddle points, that is, stationary points where there are one or more orthogonal directions in which the energy is at a maximum.

In mathematical terms, the second derivative matrix of E with respect to nuclear coordinates has one or more negative eigenvalues at such a point. A saddle point with one negative eigenvalue frequently corresponds to a transition structure for a chemical reaction. This is defined as the point of lowest maximum energy on a valley connecting to minima on the potential surface. Transition structures also exist for reactions involving separated species as

shown in Figure 2.1b which illustrates a section of a potential surface for a bimolecular reaction

$A + B \rightarrow C + D$ with an intermediate transition structure (E).

2.2.3 Atomic units

At this point it is useful to adopt new units which eliminate the fundamental physical constants from the electronic Schrodinger equation [2.5]. This involves introduction of the Bohr radius, a_0 , defined by [2.9].

$$a_0 = \frac{h^2}{(4\pi^2 m e^2)} \quad [2.9]$$

This is the atomic unit of length (the bohr). New coordinates (x',y',z') may now be introduced:

$$x' = \frac{x}{a_0} \quad [2.10]$$

In a similar way, a new atomic unit of energy is introduced, E_H , which is the coulomb repulsion between two electrons separated by 1 bohr:

$$E_H = \frac{e^2}{a_0} \quad [2.11]$$

This unit is termed the Hartree and new energies (E') are given by

$$E' = \frac{E}{E_H} \quad [2.12]$$

If [2.10] and [2.12] are substituted into the Schrodinger equation [2.5], we have,

$$\hat{H}' \Psi' = E' \Psi' \quad [2.13]$$

where the Hamiltonian, \hat{H}' , in atomic units, is

$$\hat{H}' = -\frac{1}{2} \sum_i^{\text{electrons}} \left(\frac{d^2}{dx_i^2} + \frac{d^2}{dy_i^2} + \frac{d^2}{dz_i^2} \right) - \sum_i^{\text{electrons}} \sum_s^{\text{nuclei}} \left(\frac{Z_s}{r_{is}} \right) + \sum_{i < j}^{\text{electrons}} \left(\frac{1}{r_{ij}} \right) + \sum_{s < t}^{\text{nuclei}} \left(\frac{Z_s Z_t}{R_{st}} \right) \quad [2.14]$$

Throughout the rest of this work, atomic units are assumed and the primes in all equations have been dropped.

2.2.4 Molecular Orbital Theory

Molecular orbital theory is an approach to molecular quantum mechanics which uses one-electron functions or orbitals to approximate the full wavefunction. A molecular orbital, $\Psi(x, y, z)$, is a function of the cartesian coordinates x, y, z of a single electron. Its square, Ψ^2 (or square modulus $|\Psi|^2$ if Ψ is complex), is interpreted as the probability distribution of the electron in space. To describe the distribution of an electron completely, the dependence on the spin coordinates, ξ , also has to be included. This coordinate takes on one of two possible values ($+1/2, -1/2$), and measures the spin angular momentum component along the z axis in units of $\hbar/2\pi$. For spin aligned along the positive z axis, the spin wavefunction is written $\alpha(\xi)$. Thus,

$$\alpha\left(+\frac{1}{2}\right) = 1 \qquad \alpha\left(-\frac{1}{2}\right) = 0 \qquad [2.15]$$

Similarly for spin along the negative z axis, the spin wavefunction is $\beta(\xi)$, so that

$$\beta\left(+\frac{1}{2}\right) = 0 \qquad \beta\left(-\frac{1}{2}\right) = 1 \qquad [2.16]$$

The complete wavefunction for a single electron is the product of a molecular orbital and a spin function, $\Psi(x, y, z)\alpha(\xi)$ or $\Psi(x, y, z)\beta(\xi)$. It is termed a spin orbital, $\chi(x, y, z, \xi)$.

It might appear that the simplest type of wavefunction appropriate for the description of an n-electron system would be in the form of a product of spin orbitals,

$$\Psi_{product} = \chi(1) \chi(2) \dots \chi(n) \quad [2.17]$$

where $\chi_i(i)$ is written for $\chi_i(x_i, y_i, z_i, \xi_i)$, the spin orbital of electron i. However such a wavefunction is not acceptable, as it does not have the property of antisymmetry. If the coordinates of electrons i and j are interchanged in this wavefunction, the product ... $\chi_i(i)$... $\chi_j(j)$... becomes ... $\chi_j(i)$... $\chi_i(i)$... which is not equivalent to multiplying by -1. To ensure antisymmetry, the spin orbitals may be arranged in a determinantal wavefunction.

$$\Psi_{determinant} = \begin{vmatrix} \chi_1(1) & \chi_2(1) & \dots & \chi_n(1) \\ \chi_1(2) & \chi_2(2) & \dots & \chi_n(2) \\ \vdots & \vdots & \vdots & \vdots \\ \chi_1(n) & \chi_2(n) & \dots & \chi_n(n) \end{vmatrix} \quad [2.18]$$

Here the elements of the first row of the determinant contain assignments of electron 1 to all the spin orbitals $\chi_1, \chi_2, \dots, \chi_n$, the second row contains all possible assignments of electron 2, and so forth. The determinantal wavefunction [2.18] does have the property of antisymmetry, this is guaranteed because interchange of the coordinates of electrons i and j is equivalent to interchange of rows i and j in the determinant, which does have the effect of changing the sign⁵. On expansion the determinant becomes a sum of products of spin orbitals,

$$\Psi_{determinant} = \sum_P (-1)^P \hat{P} [\chi_1(1) \chi_2(2) \dots \chi_n(n)] \quad [2.19]$$

where P is a permutation operator, changing the coordinates 1,2,...,n according to any of the n! possible permutations among the n electrons. (-1) is +1 or -1 for even and odd permutations respectively. The wavefunction [2.19] is sometimes called an antisymmetrized product function. In building up a determinantal wavefunction, the usual practice is to choose a set of molecular

orbitals, $\Psi_1, \Psi_2, \Psi_3, \dots$, and then to assign electrons of α or β spin to these orbitals. Since each orbital is later associated with an energy, this assignment of electrons is often represented by an electron configuration diagram such as shown in Figure 2.2. The electrons are represented by arrows, (\uparrow for α , \downarrow for β), orbitals of lowest energy being at the bottom of the diagram. It is not possible for a molecular orbital to be occupied by two electrons of the same spin. This is the Pauli exclusion principle⁶, which follows because the determinantal wavefunction [2.18] vanishes if two columns are identical⁵. Hence orbitals may be classified as doubly occupied (Ψ_1, Ψ_2 in Figure 2.2a), singly occupied (Ψ_3) or empty (Ψ_4). Most molecules have an even number of electrons in their ground (lowest-energy) states and may be represented by closed-shell wavefunctions with orbitals either doubly occupied or empty.

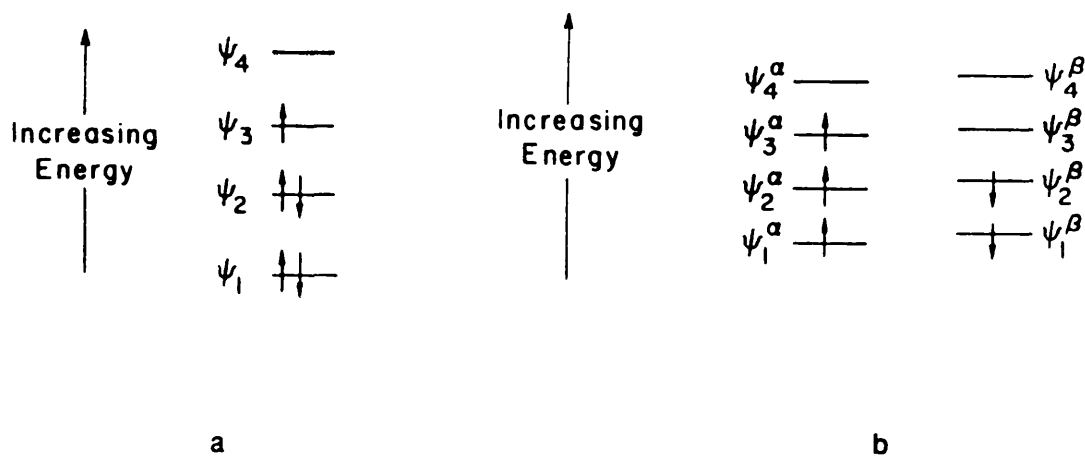


Figure 2.2. Electron configuration diagram

Some further properties of molecular orbital wavefunctions are worth noting. It is possible to force the orbitals to be orthogonal to each other, that is,

$$S_{ij} = \int \Psi_i^* \Psi_j \, dx \, dy \, dz = 0 \quad \text{for } i \neq j \quad [2.20]$$

(The asterisk denotes complex conjugation.) This can be accomplished without changing the value of the whole wavefunction by mixing columns of the determinant⁵. Orthogonal orbitals are used throughout this work. The spin functions, α and β , are orthogonal by integration over spin space (actually summation over the two possible values of ξ):

$$\sum_{\xi} \alpha(\xi) \beta(\xi) = \alpha\left(+\frac{1}{2}\right) \beta\left(+\frac{1}{2}\right) + \alpha\left(-\frac{1}{2}\right) \beta\left(-\frac{1}{2}\right) = 0 \quad [2.21]$$

Molecular orbitals may be normalized, that is,

$$S_{ii} = \int \Psi_i^* \Psi_i \, dx \, dy \, dz = 1 \quad [2.22]$$

by multiplication of the individual Ψ_i by a constant. Normalisation corresponds to the requirement that the probability of finding an electron anywhere in space is unity. Given [2.22], the determinantal wavefunction [2.18 or 2.19] may be normalized by multiplication by a factor of $(n!)^{-1/2}$, that is,

$$\int \dots \int \Psi^* \Psi \, d\tau_1 \, d\tau_2 \, \dots \, d\tau_n = 1 \quad [2.23]$$

Integration in [2.23] is over all coordinates (cartesian and spin) of all electrons.

With these features it is now possible to write down a full many-electron molecular orbital wavefunction for the closed-shell ground state of a molecule with n (even) electrons, doubly occupying $n/2$ orbitals:

$$\Psi = (n!)^{-\frac{1}{2}} \begin{vmatrix} \Psi_1(1) \alpha(1) & \Psi_1(1) \beta(1) & \dots & \dots & \Psi_{\frac{n}{2}}(1) \beta(1) \\ \Psi_1(2) \alpha(2) & \Psi_1(2) \beta(2) & \dots & \dots & \Psi_{\frac{n}{2}}(2) \beta(2) \\ & \vdots & \vdots & \vdots & \vdots \\ \Psi_1(n) \alpha(n) & \Psi_1(n) \beta(n) & \dots & \dots & \Psi_{\frac{n}{2}}(n) \beta(n) \end{vmatrix} \quad [2.24]$$

This determinant [2.24] is often called a Slater determinant⁷.

2.2.5 Basis Set Expansions

Many electron wavefunctions are constructed from molecular orbitals in the form of a single determinant, however in practical applications of the theory a further restriction is imposed. This restriction requires that the molecular orbitals be expressed as linear combinations of a finite set of N prescribed one-electron functions known as basis functions. If the basis functions are $\phi_1, \phi_2, \dots, \phi_N$, then an individual orbital Ψ_i can be written

$$\Psi_i = \sum c_{\mu i} \phi_{\mu} \quad [2.25]$$

where $c_{\mu i}$ are the molecular orbital expansion coefficients (The convention of using Roman subscripts for molecular orbitals and Greek subscripts for basis sets has been followed in all of this work). These coefficients provide the orbital description with some flexibility, but do not allow for complete freedom unless the ϕ_{μ} define a complete set. However, the problem of finding the orbitals has been reduced from finding complete descriptions of the three dimensional function Ψ_i to finding only a finite set of linear coefficients for each orbital. In simple qualitative versions of molecular orbital theory, atomic orbitals of constituent atoms are used as the basis functions. Such treatments are often described as linear combinations of atomic orbital (LCAO) theories. However, the mathematical treatment is more general, and any set of appropriately defined functions may be used for a basis expansion.

A basis set that is well defined for any nuclear configuration and therefore useful for a theoretical model is conveniently defined by a particular set of basis functions associated with each nucleus and depending only on the nuclear charge. Such functions may have the symmetry properties of atomic orbitals and may be classified as s, p, d, f, ... types according to their angular properties.

$$\begin{aligned} \phi_{1s} &= \left(\frac{\zeta_1^3}{\pi}\right)^{\frac{1}{2}} \exp(-\zeta_1 r) \\ \phi_{2s} &= \left(\frac{\zeta_2^5}{96\pi}\right)^{\frac{1}{2}} r \exp\left(-\frac{\zeta_2 r}{2}\right) \\ \phi_{2px} &= \left(\frac{\zeta_2^5}{32\pi}\right)^{\frac{1}{2}} x \exp\left(-\frac{\zeta_2 r}{2}\right) \end{aligned} \quad [2.26]$$

Two types of atomic basis functions have received widespread use. Slater-type atomic orbitals (STO's) have exponential radial parts and are labelled like hydrogen atomic orbitals, 1s, 2s, 2p_x,... , they have the normalized form given in equation 2.26 above, where ζ_1 and ζ_2 are constants determining the size of the orbitals. STO's provide reasonable representations of atomic orbitals with standard values of ζ recommended by Slater⁸. Unfortunately they are not suited to numerical work, their integrals are very computer intensive to evaluate, and their use in practical molecular orbital calculations has been limited.

The second type of basis function consists of gaussian-type atomic functions. These are powers of x, y, z multiplied by $\exp(-\alpha r^2)$, α being a constant determining the size, that is the radial extent, of the function. The first ten such functions in normalized form are given in [2.27];

$$\begin{aligned}
 g_s(\alpha, r) &= \left(\frac{2\alpha}{\pi}\right)^{\frac{3}{4}} \exp(-\alpha r^2) \\
 g_x(\alpha, r) &= \left(\frac{128\alpha^5}{\pi^3}\right)^{\frac{1}{4}} x \exp(-\alpha r^2) \\
 g_y(\alpha, r) &= \left(\frac{128\alpha^5}{\pi^3}\right)^{\frac{1}{4}} y \exp(-\alpha r^2) \\
 g_z(\alpha, r) &= \left(\frac{128\alpha^5}{\pi^3}\right)^{\frac{1}{4}} z \exp(-\alpha r^2) \\
 g_{xx}(\alpha, r) &= \left(\frac{2048\alpha^7}{9\pi^3}\right)^{\frac{1}{4}} x^2 \exp(-\alpha r^2) \\
 g_{yy}(\alpha, r) &= \left(\frac{2048\alpha^7}{9\pi^3}\right)^{\frac{1}{4}} y^2 \exp(-\alpha r^2) \\
 g_{zz}(\alpha, r) &= \left(\frac{2048\alpha^7}{9\pi^3}\right)^{\frac{1}{4}} z^2 \exp(-\alpha r^2) \\
 g_{xy}(\alpha, r) &= \left(\frac{2048\alpha^7}{9\pi^3}\right)^{\frac{1}{4}} xy \exp(-\alpha r^2) \\
 g_{yz}(\alpha, r) &= \left(\frac{2048\alpha^7}{9\pi^3}\right)^{\frac{1}{4}} yz \exp(-\alpha r^2) \\
 g_{xz}(\alpha, r) &= \left(\frac{2048\alpha^7}{9\pi^3}\right)^{\frac{1}{4}} xz \exp(-\alpha r^2)
 \end{aligned}
 \tag{2.27}$$

The gaussian functions g_s , g_x , g_y , and g_z have the angular symmetry of the s- and three p-type atomic orbitals. The six second order functions g_{xx} , g_{yy} , g_{zz} , g_{xy} , g_{xz} , and g_{yz} do not all have the angular symmetry of atomic orbitals, however they may be combined to give a set of five

d-type atomic functions, that is g_{xy} , g_{xz} , g_{yz} and the two further functions

$$\begin{aligned} g_{3zz-rr} &= \frac{1}{2} (2g_{zz} - g_{xx} - g_{yy}) \\ g_{xx-yy} &= \left(\frac{3}{4}\right)^{\frac{1}{2}} (g_{xx} - g_{yy}) \end{aligned} \quad [2.28]$$

A sixth linear combination yields an s-type function,

$$g_{rr} = 5^{-\frac{1}{2}} (g_{xx} + g_{yy} + g_{zz}) \quad [2.29]$$

In a similar manner the ten third-order gaussian functions may be combined into a set of seven f-type atomic functions and a further set of three p-type functions.

Gaussian type functions were introduced into molecular orbital calculations by Boys⁹. They are less satisfactory than STO's as representations of atomic orbitals, particularly because they do not have a cusp at the origin and therefore do not adequately describe the wavefunction at the nucleus. Nevertheless, they have the important advantage that all integrals in the computations can be explicitly evaluated without recourse to numerical integration.

A third possibility is to use linear combinations of gaussian functions as basis functions. For example, an s-type basis function ϕ_{μ} may be expanded in terms of s-type gaussians,

$$\phi_{\mu} = \sum_s d_{\mu s} g_s \quad [2.30]$$

Where the coefficients $d_{\mu s}$ are fixed. Basis functions of this type are called contracted gaussians, the individual g_s being termed primitive gaussians.

2.2.6 Variational methods and Hartree-Fock theory

A determinantal wavefunction may be constructed from molecular orbitals, which may in turn be expanded in terms of a set of basis functions; a method for fixing the expansion coefficients

is provided by Hartree-Fock theory.

Hartree-Fock theory is based on the variational method in quantum mechanics¹⁰. If ϕ is any antisymmetric normalized function of the electronic coordinates, then an expectation value of the energy corresponding to this function can be obtained from the integral

$$E' = \int \phi^* \hat{H} \phi d\tau \quad [2.31]$$

where integration is over the coordinates of all electrons. The asterisk again denotes complex conjugation. If ϕ happens to be the exact wavefunction, Ψ , for the electronic ground state, it will satisfy the Schrodinger equation [2.1] and, since Ψ is normalized, E' will be the exact energy E ,

$$E' = E \int \Psi^* \Psi d\tau = E \quad [2.32]$$

However if ϕ is any other normalized antisymmetric function, it can be shown that E' is greater than E ,

$$E' = \int \phi^* \hat{H} \phi d\tau > E \quad [2.33]$$

It follows from this that if ϕ is the antisymmetric molecular orbital function [2.24], the energy E' calculated from [2.31] will be too high. The variational method may be applied to determine optimal orbitals in single determinant wavefunctions. A basis set for orbital expansion is selected, and the coefficients $c_{\mu i}$ (as in Eq.2.25) may then be adjusted to minimize the expectation value of the energy E' . The resulting value of E' will then be as close as is possible to the exact energy E within the limitations imposed by: (a) the single determinant wavefunction, and (b) the particular basis set employed. Hence, the best single determinant wavefunction, in an energy sense, is found by minimizing E' with respect to the coefficients $c_{\mu i}$. This implies the variational equations

$$\frac{dE'}{dc_{\mu i}} = 0 \quad (\text{all } \mu, i) \quad [2.34]$$

These equations will first be dealt with for closed-shell systems.

2.2.6.1 Closed-Shell Systems

The variational condition [2.34] leads to a set of algebraic Roothan-Hall equations $c_{\mu i}$. They were derived independently for the closed-shell wavefunction [2.24] by Roothan¹¹ and by Hall¹² and are given below

$$\sum_{\nu=1}^N (F_{\mu\nu} - \epsilon_i S_{\mu\nu}) c_{\nu i} = 0 \quad \mu = 1, 2, \dots, N \quad [2.35]$$

with the normalisation conditions

$$\sum_{\mu=1}^N \sum_{\nu=1}^N c_{\mu i}^* S_{\mu\nu} c_{\nu i} = 1 \quad [2.36]$$

Where, ϵ_i is the one-electron energy of molecular orbital Ψ_i , $S_{\mu\nu}$ are the elements of an $N \times N$ matrix termed the overlap matrix,

$$S_{\mu\nu} = \int \phi_{\mu}^*(1) \phi_{\nu}(1) dx_1 dy_1 dz_1 \quad [2.37]$$

and $F_{\mu\nu}$ are the elements of another $N \times N$ matrix, the Fock matrix,

$$F_{\mu\nu} = H_{\mu\nu}^{core} + \sum_{\lambda=1}^N \sum_{\sigma=1}^N P_{\lambda\sigma} [(\mu\nu/\lambda\sigma) - \frac{1}{2} (\mu\lambda/\nu\sigma)] \quad [2.38]$$

In this expression, $H_{\mu\nu}^{core}$ is a matrix representing the energy of a single electron in a field of

"bare" nuclei. Its elements are,

$$H_{\mu\nu}^{core} = \int \phi_{\mu}^* (1) \hat{H}^{core} (1) \phi_{\nu} (1) dx_1 dy_1 dz_1, \quad [2.39]$$

$$\hat{H}^{core} (1) = -\frac{1}{2} \left(\frac{\delta^2}{\delta x_1^2} + \frac{\delta^2}{\delta y_1^2} + \frac{\delta^2}{\delta z_1^2} \right) - \sum_{A=1}^M \frac{Z_A}{r_{1A}}$$

Here Z_A is the atomic number of atom A, and the summation is carried out over all atoms. The quantities $(\mu\nu/\lambda\sigma)$ appearing in [2.38] are two-electron repulsion integrals:

$$(\mu\nu/\lambda\sigma) = \iint \phi_{\mu}^* (1) \phi_{\nu} (1) \left(\frac{1}{r_{12}} \right) \phi_{\lambda}^* (2) \phi_{\sigma} (2) dx_1 dy_1 dz_1 dx_2 dy_2 dz_2 \quad [2.40]$$

they are multiplied by the elements of the one-electron density matrix, $P_{\lambda\sigma}$

$$P_{\lambda\sigma} = 2 \sum_{i=1}^{occ} c_{\lambda i}^* c_{\sigma i} \quad [2.41]$$

The summation is over occupied molecular orbitals only. The factor of two indicates that two electrons occupy each molecular orbital, and the asterisk denotes complex conjugation (required if the molecular orbitals are not real functions). The electronic energy E^{ee} is now given by [2.42],

$$E^{ee} = \frac{1}{2} \sum_{\mu=1}^N \sum_{\nu=1}^N P_{\mu\nu} (F_{\mu\nu} + H_{\mu\nu}^{core}) \quad [2.42]$$

which, when added to [2.43], accounting for the internuclear repulsion,

$$E^{nr} = \sum_{A<B}^M \sum \frac{Z_A Z_B}{R_{AB}} \quad [2.43]$$

(where Z_A and Z_B are the atomic numbers for atoms A and B, and R_{AB} is their separation) yields an expression for the total energy. The Roothan-Hall equations [2.35] are not linear since the Fock matrix $F_{\mu\nu}$ itself depends on the molecular orbital coefficients, $c_{\mu i}$, through the density matrix expression [2.41]. Solution necessarily involves an iterative process and since the resulting molecular orbitals are derived from their own effective potential, the technique is frequently called self-consistent field (SCF) theory.

2.2.6.2 Open-Shell Systems

For open-shell systems, in which electrons are not completely assigned to orbitals in pairs, the Roothan-Hall equations need some modification. This applies, for example, to doublet free radicals or triplet states, for which one component will have an excess of α electrons. Simple molecular orbital theory can be extended to open-shell systems in two possible ways. The first is described as spin-restricted Hartree-Fock (RHF) theory¹³, and in this approach a single set of molecular orbitals is used, some being doubly occupied and some being singly occupied with an electron of α spin. This is the case illustrated for a five-electron doublet state in Figure 2.2a. The spin orbitals used in the determinant are then $(\Psi_1\alpha)(\Psi_1\beta)(\Psi_2\alpha)(\Psi_2\beta)(\Psi_3\alpha)$. The coefficients $c_{\mu i}$ are still defined by the expansion [2.25] and their optimum values are still obtained from the variational conditions [2.34]. However, details are more complicated since different conditions apply to singly- and doubly-occupied orbitals¹³.

The second type of molecular orbital theory in common use for open-shell systems is spin-unrestricted Hartree-Fock (UHF) theory¹⁴. In this approach, different spatial orbitals are assigned to α and β electrons, and thus there are two distinct sets of molecular orbitals Ψ_i^α and Ψ_i^β ($i= 1, \dots, N$). The electron configuration for a five electron doublet may be written as $(\Psi_1^\alpha\alpha)(\Psi_1^\beta\beta)(\Psi_2^\alpha\alpha)(\Psi_2^\beta\beta)(\Psi_3^\alpha\alpha)$ and is illustrated in Figure 2.2b. It should be noted that the previously doubly-occupied orbital Ψ_1 is now replaced by two distinct orbitals, Ψ_1^α and Ψ_1^β . Since the RHF function is a special case of the UHF function, it follows from the variational principle that the optimized UHF energy must be below the optimized RHF value. On the other hand, UHF functions have the disadvantage that they are not true eigenfunctions of the total

spin operator, unlike exact wavefunctions which necessarily are. Thus, UHF wavefunctions which are designed for doublet states (as in the example shown in Figure 2.2b) are contaminated by functions corresponding to states of higher spin multiplicity, such as quartets. In UHF theory, the two sets of molecular orbitals are defined by two sets of coefficients,

$$\Psi_i^\alpha = \sum_{\mu=1}^N c_{\mu i}^\alpha \phi_\mu \quad ; \quad \Psi_i^\beta = \sum_{\mu=1}^N c_{\mu i}^\beta \phi_\mu \quad [2.44]$$

These coefficients are varied independently, leading to the UHF generalisation of the Roothan-Hall equations¹⁴,

$$\begin{aligned} \sum_{\nu=1}^N (F_{\mu\nu}^\alpha - e_i^\alpha S_{\mu\nu}) c_{\mu\nu}^\alpha &= 0 \\ \sum_{\nu=1}^N (F_{\mu\nu}^\beta - e_i^\beta S_{\mu\nu}) c_{\mu\nu}^\beta &= 0 \quad \mu = 1, 2, \dots, N \end{aligned} \quad [2.45]$$

Here, the two Fock matrices are defined by

$$\begin{aligned} F_{\mu\nu}^\alpha &= H_{\mu\nu}^{core} + \sum_{\lambda=1}^N \sum_{\sigma=1}^N [(P_{\lambda\sigma}^\alpha + P_{\lambda\sigma}^\beta) (\mu\nu/\lambda\sigma) - P_{\lambda\sigma}^\alpha (\mu\lambda/\nu\sigma)] \\ F_{\mu\nu}^\beta &= H_{\mu\nu}^{core} + \sum_{\lambda=1}^N \sum_{\sigma=1}^N [(P_{\lambda\sigma}^\alpha + P_{\lambda\sigma}^\beta) (\mu\nu/\lambda\sigma) - P_{\lambda\sigma}^\beta (\mu\lambda/\nu\sigma)] \end{aligned} \quad [2.46]$$

The density matrix is also separated into two parts,

$$P_{\mu\nu}^\alpha = \sum_{i=1}^{\alpha occ} c_{\mu i}^{\alpha*} c_{\nu i}^\alpha \quad ; \quad P_{\mu\nu}^\beta = \sum_{i=1}^{\beta occ} c_{\mu i}^{\beta*} c_{\nu i}^\beta \quad [2.47]$$

The integrals $S_{\mu\nu}$, $H_{\mu\nu}^{core}$ and $(\mu\nu/\lambda\sigma)$ appearing in the UHF equations are the same as those already defined in the Roothan-Hall procedure for closed-shell systems.

2.2.6.3 Koopmans' Theorem and Ionisation Potentials

An important theorem due to Koopmans^{15,16} states that the eigenfunctions of the Fock operator for a closed-shell determinant, that is, $(\Psi_1)^2 (\Psi_2)^2 \dots (\Psi_w)^2 \dots (\Psi_{n/2})^2$, are also appropriate for a determinant in which one electron has been removed from Ψ_w , that is, $(\Psi_1)^2 (\Psi_2)^2 \dots (\Psi_w) \dots (\Psi_{n/2})^2$. Furthermore, the energy difference between the original species and its ionized form is equal to the corresponding eigenvalue, ϵ_w . The significance of Koopmans' theorem is that of all the possible transformed sets of molecular orbitals, each giving the same total determinantal wavefunction, the original set, that is, those corresponding to the closed-shell determinant, is most appropriate for the description of the ionized species.

The Fock eigenvalues ϵ_w , provide approximate values for the negatives of the ionisation potentials of the closed-shell molecule if Koopmans' theorem is applied. However, it should be noted that the Koopmans' wavefunction for the ionized species, with all orbitals identical to those in the parent, is not the full RHF wavefunction for the open-shell configuration $(\Psi_1)^2 (\Psi_2)^2 \dots (\Psi_w) \dots (\Psi_{n/2})^2$. The energy of the ionized species can be further lowered if the RHF wavefunction is completely redetermined, this allows the remaining orbitals to "relax" following the ionisation process. It follows that Koopmans' ionisation potentials, ϵ_w , are always numerically larger than those resulting from application of RHF theory separately to the parent and the ionized species. However, the correlation energy correction is normally greater in the unionized molecule because there are more electrons, this means that relaxation and correlation corrections go in opposite directions, sometimes leading to good agreement between ϵ_w and experimentally observed ionisation potentials.

Koopmans' theorem also applies to spin-unrestricted (UHF) Hartree-Fock wavefunctions of the type considered in Section 2.2.6.2. Thus, for a radical with one extra α electron, the highest eigenvalue of the UHF α Fock matrix is an approximation to the radical ionisation energy to give a singlet cation. The theorem may not be generally used, however, for the spin-restricted (RHF) open-shell case.

2.2.7 Symmetry Properties

In molecules for which the nuclear framework has elements of symmetry, the molecular orbitals belong to irreducible representations of the corresponding point group, and can be classified accordingly. For example, in an LCAO treatment of the hydrogen molecule, the lowest (unnormalized) molecular orbital is $1s_a + 1s_b$, where $1s_a$ and $1s_b$ are the atomic orbitals. This orbital may be labelled as σ_g , where σ indicates axial symmetry and the g subscript indicates that the orbital is unchanged under inversion. Similarly a higher energy orbital (unoccupied in the molecular ground state) is $1s_a - 1s_b$ and may be labelled σ_u , the u subscript indicating change of sign under inversion. Full details of the notation and possible symmetries of molecular orbitals can be found elsewhere¹⁷. A common practice is to label molecular orbitals by the irreducible representation¹⁷, preceded by an integer giving the energy ordering within that symmetry. Thus, the electronic configuration of the water molecule (which belongs to the C_{2v} point group) is given as

$$(1a_1)^2 (2a_1)^2 (3a_1)^2 (1b_2)^2 (1b_1)^2 \quad [2.48]$$

The notation here indicates that the occupied orbitals include three totally symmetric orbitals ($1a_1$, $2a_1$, $3a_1$), and one orbital with a node in the molecular plane ($1b_1$), and one with a node perpendicular to the molecular plane ($1b_2$).

2.2.8 Mulliken Population Analysis

The electron density function or electron probability distribution function, $p(r)$, is a three-dimensional function defined such that $p(r)dr$ is the probability of finding an electron in a small volume element, dr , at some point in space, r . Normalisation requires that

$$\int p(r) dr = n \quad [2.49]$$

where n is the total number of electrons. For a single determinant wavefunction in which the orbitals are expanded in terms of a set of N basis functions, ϕ_u , $p(r)$ is given by,

$$p(r) = \sum_{\mu}^N \sum_{\nu}^N P_{\mu\nu} \phi_{\mu} \phi_{\nu} \quad [2.50]$$

where $P_{\mu\nu}$ are the elements of the density matrix [2.41]. It is desirable to allocate the electrons in some fractional manner among the various parts of the molecule (atoms, bonds, etc.). For example, it may be useful to define a total electronic charge on a particular atom in a molecule in order that quantitative meaning may be given to such concepts as electron withdrawing or donating ability. Suggestions about how to do this, starting from the density matrix were made by Mulliken¹⁸, and collectively they now constitute the topic of Mulliken population analysis. Integration of [2.50] gives

$$\int p(r) dr = \sum_{\mu}^N \sum_{\nu}^N P_{\mu\nu} S_{\mu\nu} = n \quad [2.51]$$

where $S_{\mu\nu}$ is the overlap matrix over basis functions [2.37]. The total electron count n is thus composed of individual terms $P_{\mu\nu} S_{\mu\nu}$. Given that the basis functions are normalized, that is, $S_{\mu\mu} = 1$, the diagonal terms in [2.51] are just $P_{\mu\mu}$, each of which represents the number of electrons directly associated with a particular basis function ϕ_{μ} . This is termed the net population of ϕ_{μ} . The off-diagonal components of [2.51] occur in pairs, $P_{\mu\nu} S_{\mu\nu}$ and $P_{\nu\mu} S_{\nu\mu}$, of equal magnitude. Their sum,

$$Q_{\mu\nu} = 2P_{\mu\nu} S_{\mu\nu} \quad (\mu \neq \nu) \quad [2.52]$$

is referred to as an overlap population and is associated with two basis functions ϕ_{μ} , ϕ_{ν} , which may be on the same atom or on two different atoms. The total electronic charge is now apportioned in two parts, the first associated with individual basis functions, the second with pairs of basis functions:

$$\sum_{\mu}^N P_{\mu\mu} + \sum_{\mu < \nu}^N Q_{\mu\nu} = n \quad [2.53]$$

Such a representation of the electron distribution is not always convenient, and it is sometimes desirable to partition the total charge among only the individual basis functions. This may be accomplished in many ways, one such is to divide the overlap populations, $Q_{\mu\nu}$, equally between the basis functions ϕ_μ , ϕ_ν , adding half to each of the net populations $P_{\mu\mu}$ and $P_{\nu\nu}$. This gives a gross population for ϕ_μ , defined as

$$q_\mu = P_{\mu\mu} + \sum_{\nu \neq \mu} P_{\mu\nu} S_{\mu\nu} \quad [2.54]$$

The sum of the gross populations for all N basis functions, ϕ_μ , is, of course, equal to the total electron count,

$$\sum_{\mu}^N q_\mu = n \quad [2.55]$$

This particular partitioning scheme is just one of many possibilities and the choice of division of the overlap populations $Q_{\mu\nu}$ into equal contributions from ϕ_μ and ϕ_ν is completely arbitrary. The gross basis function populations may be used to define gross atomic populations according to [2.56]

$$q_A = \sum_{\mu}^A q_\mu \quad [2.56]$$

Here the summation is carried out for all functions ϕ_μ on a particular atom A . Assuming all basis functions to be atom-centred, it follows that the sum of gross atomic populations is equal to the total electron count. Finally, a total atomic charge on A may be defined as $Z_A - q_A$, where Z_A is the atomic number of atom A . The sum of charges must be 0 for a neutral molecule, +1 for a singly charged cation and so forth. A total overlap population, q_{AB} , between two atoms A and B may be defined in a similar manner,

$$q_{AB} = \sum_{\mu}^A \sum_{\nu}^B Q_{\mu\nu} \quad [2.57]$$

Here summation is carried out for all μ on atom A and all ν on atom B. Total overlap populations provide quantitative information on the binding between atoms. A large positive value of q_{AB} indicates a significant electron population in the region between A and B, at the expense of density in the immediate vicinity of the individual atomic centres, and is a feature generally associated with strong bonding. Conversely, a significant negative value of q_{AB} implies that electrons have been displaced away from the interatomic region, indicating an antibonding interaction.

Although Mulliken populations often provide valuable information on electron distributions in molecules, they must be used with some caution. As mentioned above, the partitioning of $Q_{\mu\nu}$ into individual orbital contributions is arbitrary, and also, quantities such as gross atomic and total overlap populations are strongly dependent on the particular basis set employed. Several other methods for producing population analyses have been developed¹⁹⁻²², although it is fair to say that the Mulliken scheme is still the most widely used.

2.2.9 Multiple-Determinant Wavefunctions

Much effort has been put into the development of the theory of single-determinant wavefunctions and the associated computer programs, and most of the work described in this thesis has been carried out within the framework of Hartree-Fock theory. This effort has been justified by the adequacy of the Hartree-Fock descriptions of the ground states of most molecules, however, it is recognised that exact wavefunctions cannot generally be expressed as single determinants and that there was a need for further refinements of the theory to eliminate errors implicit in the Hartree-Fock approximation.

In this section, two of the methods which address this problem will be briefly outlined. Both use a linear combination of Slater determinants, each of which represents an individual electron configuration. Such a wavefunction is said to invoke configuration interaction. The primary deficiency of Hartree-Fock theory is the inadequate treatment of the correlation between motions of electrons, in particular, single-determinant wavefunctions take no account of correlation between electrons with opposite spin. Correlation of the motions of electrons with

the same spin is partially, but not completely, accounted for by virtue of the determinantal form of the wavefunction. These limitations lead to calculated (Hartree-Fock) energies that are above the exact values. By convention, the difference between the Hartree-Fock and exact (nonrelativistic) energies is the correlation energy,

$$E_{(exact)} = E_{(Hartree-Fock)} + E_{(correlation)} \quad [2.58]$$

The neglect of correlation between electrons of opposite spin leads to a number of qualitative deficiencies in the description of electronic structure. One important consequence is that closed-shell Hartree-Fock functions often do not dissociate correctly when nuclei are moved to infinite separation. Also the best single-determinant wavefunction may not always have the full symmetry of the exact wavefunction and this can lead to problems, for example, in the handling of degeneracy of states. Even at the level of the best single-determinant, the degeneracy of some states is incorrectly handled, and it is not until configuration interaction is introduced that a proper description results.

Many other deficiencies of Hartree-Fock calculations have come to light in applying the theory. For example, it is well known that bond dissociation energies are seriously underestimated if correlation between the bonding pair of electrons is not adequately accounted for. Thus, applications to the energies of transition structures, which often involve the partial breaking of bonds, may be suspect if single-determinant wavefunctions are used. Even the properties of "normal" molecules are sometimes subject to considerable errors because of restrictions inherent in the Hartree-Fock approximation. While equilibrium geometries are usually given well at the single-determinant level, many examples of significant deviations between Hartree-Fock calculated and experimental bond lengths are now well documented. Calculated molecular vibration frequencies, providing a measure of the shape of the potential surface in the vicinity of the equilibrium structure, have also been shown to be sensitive to the level of treatment given to correlation effects. The requirements for a satisfactory model chemistry play an important role in the selection of methods used in the study of electron correlation. The first

requirement is that the method should be well defined and applicable in a continuous manner to any number of electrons and any arrangement of nuclei. This implies that the choice of determinants or electron configurations must be made without appeal to special symmetry features; calculated properties of unsymmetrical structures must be continuous with those for symmetrical arrangements to which they are closely related. The restriction also requires care in the elimination of electron configurations that are presumed to make only small contributions to the total wavefunction, they can only be neglected if their contribution is so small that it falls below an acceptable round-off level. A second requirement is that, whatever method of configuration interaction is employed, it must not lead to such a rapid increase in required computation with molecular size as to preclude its use in systems of chemical interest. A third requirement for a satisfactory model is size consistency. This means that the method must give additive results when applied to an assembly of isolated molecules, unless this is true, comparison of properties of molecules of different size will not lead to quantitatively meaningful results. Size-consistency is not easy to achieve and it plays a major role in the selection of appropriate methods for calculating the correlation energy. A fourth desirable model feature is that the calculated electronic energy be variational, that is, it should correspond to an upper bound to the energy that would derive from exact solution of the Schrodinger equation. This will be true if the energy is calculated as an expectation value of the Hamiltonian according to the variational theorem (Section 1.2.6). The advantage of variational methods is that they provide a criterion by which to judge the quality of the theoretical model.

Most Hartree-Fock methods satisfy all these four model requirements. So that, if the basis functions are specified for each atom according only to its atomic number, and if they are centred only at the nuclear positions, the resulting energy surface is usually well-defined and variational, at least for electronic ground states. Hartree-Fock models are also generally size-consistent and, given present computer technology, may be applied to a variety of chemical systems. Practical models incorporating electron correlation do not usually satisfy all four requirements !! Calculations beyond the Hartree-Fock level first require the selection of the determinants (or electron configurations) which are allowed to participate in the

multiple-determinant wavefunction, and then determination of the appropriate linear coefficients. These tasks must be performed in ways that satisfy the model requirements as closely as possible. A number of methods will now be outlined, beginning with full configuration interaction, which is perfect in principle but usually unachievable in practice, that is, it fails the second requirement, and continuing with other schemes that are practical, but which only satisfy the other requirements to a limited degree.

2.2.9.1 Full Configuration Interaction

If a system containing n electrons described by a basis set of N functions, ϕ_μ , is considered, there will be $2N$ spin orbital basis functions of the type ϕ_μ^α and ϕ_μ^β , which in turn may be linearly combined into $2N$ spin orbitals χ_i . If the Hartree-Fock problem using these basis functions has been solved and the single determinant wavefunction Ψ_0 has been obtained,

$$\Psi_0 = (n!)^{-\frac{1}{2}} |\chi_1 \chi_2 \dots \chi_n| \quad [2.59]$$

(The determinant [2.24] has been specified in abbreviated form.) The spin orbitals used in this determinant, $\chi_1, \chi_2, \dots, \chi_n$, are a subset of the total set determined in the variational procedure, the unused spin orbitals correspond to unoccupied or virtual spin orbitals χ_a ($a = n+1, n+2, \dots, 2N$). Occupied orbitals will henceforth be denoted by subscripts i, j, k, \dots and virtual ones by a, b, c, \dots . Determinantal wavefunctions may now be constructed by replacing one or more of the occupied spin orbitals χ_i, χ_j, \dots in [2.59] by virtual spin orbitals χ_a, χ_b, \dots . These determinants with $s > 0$ will be denoted as Ψ_s , and may be further classified into single-substitution functions, Ψ_i^a in which χ_i is replaced by χ_a , double-substitution functions, Ψ_{ij}^{ab} in which χ_i is replaced by χ_a and χ_j by χ_b , triple-substitution functions, and so forth. The general substitution determinant may be written, $\Psi_{ijk\dots}^{abc\dots}$, with the restrictions $i < j < k < \dots$ and $a < b < c < \dots$ to avoid repeating any configuration. This series of substituted determinants goes all the way to n -substituted terms in which all occupied spin orbitals are replaced by virtual spin orbitals.

In the full configuration method, a trial wavefunction is used,

$$\Psi = a_0 \Psi_0 + \sum_{s>0} a_s \Psi_s \quad [2.60]$$

where the summation $\sum_{s>0}$ is over all substituted determinants. The unknown coefficients, a_s , are then determined by the linear variational method, leading to Eq.[2.61],

$$\sum_s (H_{st} - E_i \delta_{st}) a_{si} = 0 \quad t = 0, 1, 2, \dots \quad [2.61]$$

Where, H_{st} is a configurational matrix element,

$$H_{st} = \int \dots \int \Psi_s H \Psi_t \, d\tau_1 \, d\tau_2 \dots d\tau_n \quad [2.62]$$

and E_i is an energy. The lowest root E of Eq.[2.61] leads to the energy of the electronic ground state. Eq.[2.61] bears some similarity to the Roothan-Hall equations [2.35], however, because the determinantal wavefunctions Ψ_s are mutually orthogonal, the overlap matrix S in Eq.[2.35] is replaced by a simple delta function.

The full configuration interaction method represents the most complete treatment possible within the limitations imposed by the basis set. The difference between the Hartree-Fock energy with a given basis set and the full CI energy is the correlation energy within the basis. As the basis set becomes more complete, that is, as $N \rightarrow \infty$, the result of a full configuration interaction treatment will approach the exact solution of the nonrelativistic Schrodinger equation. The full CI method is well-defined, size-consistent, and variational, however it is not practical except for very small systems because of the very large number of substituted determinants, the total number of which in Eq.[2.60] is $(2N!)/[n!(2N - n)!]$.

Before considering practical correlation methods, it is useful to examine the general form of the full Hamiltonian matrix, H_{st} . This is illustrated in Figure 2.4, where rows and columns have been arranged starting with Ψ_0 , the Hartree-Fock function, and proceeding through single, double,

triple substitutions and so forth. It follows from Eq.[2.62] that the element in the upper left-hand corner, designated H_{00} , is the Hartree-Fock energy. Certain blocks of elements in the first row (H_{0s}) or first column (H_{s0}) vanish. If s is a single substitution, H_{0s} vanishes by Brillouin's theorem²³. If s is a substitution which is triple or higher, H_{0s} again vanishes, due to the fact that the Hamiltonian contains only one and two-electron terms. It is only the double substitutions which lead to nonvanishing terms, H_{0s} , and as a result, the simplest correlation models account only for determinants formed from Ψ_0 by double substitutions.

	Single Substitutions	Double Substitutions	Triple and Higher Substitutions
H_{00}	0	H_{0s}	0
Single Substitutions	0		
Double Substitutions	H_{s0}		
Triple and Higher Substitutions	0		

Figure 2.3 Partitioning of full configuration interaction Hamiltonian showing zero sections.

2.2.9.2 Limited configuration interaction

The most straightforward way of limiting the length of the CI expansion [2.60] is to truncate the series at a given level of substitution. If no substitutions are permitted, $\Psi = \Psi_0$, corresponding to the Hartree-Fock solution. Inclusion of single substitution functions only, termed Configuration Interaction, Singles or CIS normally leads to no improvement relative to the Hartree-Fock wavefunction or energy.

$$\Psi_{CIS} = a_0 \Psi_0 + \sum_i^{\text{occ}} \sum_a^{\text{virt}} a_i^a \Psi_i^a \quad [2.63]$$

Generally, the simplest procedure to have any effect on the calculated energy is limited to double substitutions only, and is termed Configuration Interaction, Doubles or CID,

$$\Psi_{CID} = a_0 \Psi_0 + \sum_{i < j}^{occ} \sum_{a < b}^{virt} a_{ij}^{ab} \Psi_{ij}^{ab} \quad [2.64]$$

This is an important practical procedure. Its execution requires evaluation of the matrix elements H_{0s} and H_{st} , Eq.[2.62], for double substitutions, and solution of Eq.[2.61]. Two major computational tasks are involved. The first is a transformation of two-electron integrals ($\mu\nu/\lambda\sigma$) over basis functions, Eq.[2.40], into corresponding integrals with the Hartree-Fock spin orbitals χ_i replacing the basis functions ϕ_μ . The second is the determination of the lowest (or lowest few) energy solutions of Eq.[2.61] and the associated wavefunction coefficients. These tasks are both computationally significant and considerable effort has been put into the development of efficient algorithms.

At a slightly higher level of theory, both single and double substitutions can be included in the configuration interaction treatment. The model is termed Configuration Interaction, Singles and Doubles, or CISD and the trial wavefunction is given by Eq.[2.65].

Here all coefficients are varied to minimize the expectation value of the energy. Although the single substitutions do not contribute by themselves in (CIS), they do contribute to the wavefunction, Eq.[2.65], since there are nonzero matrix elements of the Hamiltonian between singly- and doubly-substituted determinants. However, since the participation is indirect, the energy lowering due to inclusion of single substitutions is considerably less than that for doubles.

$$\Psi_{CISD} = a_0 \Psi_0 + \sum_i^{occ} \sum_a^{virt} a_i^a \Psi_i^a + \sum_{i < j}^{occ} \sum_{a < b}^{virt} a_{ij}^{ab} \Psi_{ij}^{ab} \quad [2.65]$$

The computational task in CID or CISD calculations can be reduced by limiting the set of spin orbitals that are involved in the single or double substitutions. This is most conveniently done

in terms of a window (Figure 2.4, left) in which only a set of high-energy occupied and low-energy virtual spin orbitals is used. There are two special cases of the use of windows in CI which are worthy of special mention.

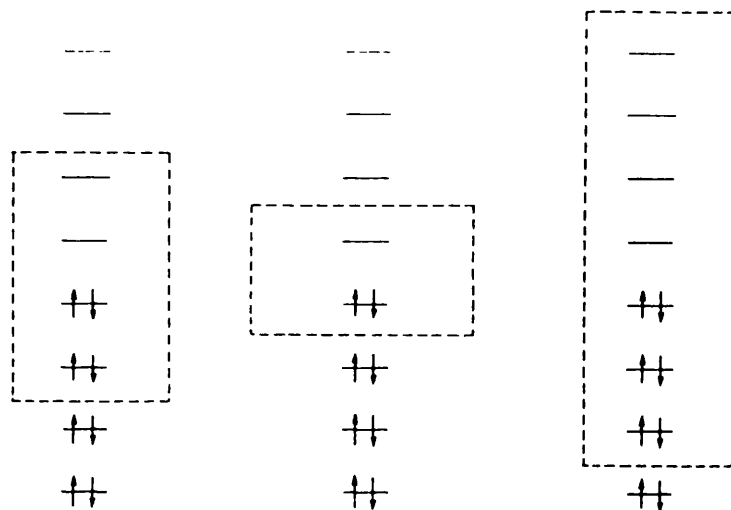


Figure 2.4. Use of a window for designating substitutions to be considered in limited configuration interaction.

The first is the use of the smallest possible size of window for a closed-shell calculation (Figure 2.4, middle). This consists of the highest-occupied molecular orbital (HOMO) and the lowest-unoccupied molecular orbital (LUMO). Within this window, there is the Hartree-Fock configuration, $\dots(\Psi_i\alpha)(\Psi_j\beta)$, four singly-substituted configurations, $\dots(\Psi_i\alpha)(\Psi_a\alpha)$, $\dots(\Psi_i\alpha)(\Psi_a\beta)$, $\dots(\Psi_a\alpha)(\Psi_j\beta)$, $\dots(\Psi_j\beta)(\Psi_a\beta)$, and one doubly-substituted configuration, $\dots(\Psi_a\alpha)(\Psi_a\beta)$. Of these six determinants, the two with both α or both β electrons do not mix with Ψ_0 and represent two of the components of the triplet state wavefunctions for the configuration $\dots(\Psi_i)(\Psi_a)$. Solution of Eq.[2.61] for the remaining four determinants leads to a third component of the triplet wavefunction, and three solutions corresponding to the ground and two low-lying

singlet states. The triplet wavefunction is

$$(2n)^{-\frac{1}{2}} \{ |\dots (\Psi_i \alpha) (\Psi_a \beta) \rangle - |\dots (\Psi_a \alpha) (\Psi_i \beta) \rangle \} \quad [2.66]$$

and the three singlet wavefunctions are appropriate linear combinations of the three functions [2.67]:

$$(2n)^{-\frac{1}{2}} \left\{ \begin{aligned} & n^{-\frac{1}{2}} |\dots (\Psi_i \alpha) (\Psi_i \beta) \rangle \\ & |\dots (\Psi_i \alpha) (\Psi_a \beta) \rangle + |\dots (\Psi_a \alpha) (\Psi_i \beta) \rangle \\ & n^{-\frac{1}{2}} |\dots (\Psi_a \alpha) (\Psi_a \beta) \rangle \end{aligned} \right\} \quad [2.67]$$

This technique, which because of its simplicity has received considerable application in studies involving the elucidation of reaction transition structures²⁴ is sometimes referred to as 3 x 3 configuration interaction.

A second useful type of window constraint is the frozen-core approximation (Figure 2.4, right). In this method, all virtual spin orbitals are included in the window, but those occupied spin orbitals which correspond principally to inner-shell electrons are omitted. For each first-row element, that is, lithium to neon, in a molecule, a single molecular orbital is eliminated; for each second-row atom, that is, sodium to argon, four orbitals are eliminated, and so forth. The contributions from the inner-shell electrons to the total correlation energy are not particularly small, but appear to be relatively constant from one molecular environment to another. As a result the shapes of potential surfaces are little affected by omission of these contributions. These limited configuration interaction methods satisfy some of the general conditions discussed earlier (Section 2.2.9), they are well defined in the general form, although use of a window may lead to difficulties. With the HOMO-LUMO window, for example, the method is ill defined if either the highest-occupied or lowest-unoccupied molecular orbitals belong to a degenerate set. The solution of Eq.[2.61] is practical for reasonably large n and N . The methods are variational, since the energy is calculated as an expectation value. The most

serious deficiency of the CID and CISD limited configuration interaction methods is that they fail to satisfy the size-consistency condition. Serious attempts have been made to obtain corrections to the CID and CISD methods, the most commonly used of which is due to Langhoff and Davidson²⁵, who proposed the approximate formula

$$\Delta E_{\text{correction}} = (1 - a_0^2) \Delta E_{\text{CISD}} \quad [2.68]$$

where ΔE_{CISD} is the correlation energy at the CISD level and a_0 is the coefficient of the Hartree-Fock function in the CISD expansion. This corrects a major part of the discrepancy, however there are difficulties about this formula which include: (a) the total energy is still not precisely size-consistent and (b) a correction is incorrectly applied to a two-electron system, when CISD is equivalent to full configuration interaction.

2.2.9.3 Moller-Plesset Perturbation Theory

The perturbation theory of Moller and Plesset²⁶, closely related to many-body perturbation theory, is an alternative approach to the correlation problem. Within a given basis set, its aim is still to find the lowest eigenvalue and corresponding eigenvector of the full Hamiltonian matrix illustrated in Figure 2.2. However, the approach is not to truncate the matrix as in limited CI, but rather to treat it as the sum of two parts, the second being a perturbation on the first. Moller-Plesset models are formulated by first introducing a generalized electronic Hamiltonian, \hat{H}_λ , according to

$$\hat{H}_\lambda = \hat{H}_0 + \lambda \hat{V} \quad [2.69]$$

Where, \hat{H}_0 is an operator such that the matrix with elements

$$\int \dots \int \Psi_s \hat{H}_0 \Psi_t \, d\tau_1 \, d\tau_2 \dots d\tau_n \quad [2.70]$$

is diagonal. The perturbation is defined by

$$\lambda \hat{V} = \lambda (\hat{H} - \hat{H}_0) \quad [2.71]$$

where \hat{H} is the correct Hamiltonian and λ is a dimensionless parameter. Clearly \hat{H}_λ coincides with \hat{H}_0 if $\lambda = 0$, and with \hat{H} if $\lambda = 1$. In Moller-Plesset theory, the zero-order Hamiltonian, \hat{H}_0 , is taken to be the sum of the one-electron Fock operators. The eigenvalue, E_s , corresponding to a particular determinant, Ψ_s , is the sum of the one-electron energies, ϵ_i , for the spin orbitals which are occupied in Ψ_s . Ψ_λ and E_λ , the exact or full CI (within a given basis set) ground-state wavefunction and energy for a system described by the Hamiltonian \hat{H}_λ , may now be expanded in powers of λ according to Rayleigh-Schrodinger perturbation theory²⁷,

$$\begin{aligned} \Psi_\lambda &= \Psi^{(0)} + \lambda \Psi^{(1)} + \lambda^2 \Psi^{(2)} + \dots \\ E_\lambda &= E^{(0)} + \lambda E^{(1)} + \lambda^2 E^{(2)} + \dots \end{aligned} \quad [2.72]$$

Practical correlation methods may now be formulated by setting the parameter $\lambda = 1$, and by truncation of the series in Eq.[2.72] to various orders. The methods are referred to by the highest-order energy term allowed, that is, truncation after second order as MP2, after third-order as MP3 and so forth.

The leading terms in expansions [2.72] are:

$$\Psi^{(0)} = \Psi_0 \quad [2.73]$$

$$E^{(0)} = \sum_I^{\text{occ}} \epsilon_i \quad [2.74]$$

$$E^{(0)} + E^{(1)} = \int \dots \int \Psi_0 \hat{H} \Psi_0 \, d\tau_1 \, d\tau_2 \dots d\tau_n \quad [2.75]$$

where Ψ_0 is the Hartree-Fock wavefunction and ϵ_i are the one-electron energies defined by Eq.[2.35]. The Moller-Plesset energy to first-order is thus the Hartree-Fock energy. The first-order contribution to the wavefunction is

$$\Psi^{(1)} = \sum_{s>0} (E_0 - E_s)^{-1} V_{s0} \Psi_s \quad [2.76]$$

where V_{s0} are matrix elements involving the perturbation operator, \hat{V} ,

$$\int \dots \int \Psi_s \hat{V} \Psi_0 \, d\tau_1 \, d\tau_2 \dots d\tau_n \quad [2.77]$$

It follows that the first order contribution to the coefficient a_s in Eq.[2.61] is given by

$$a_s^{(1)} = (E_0 - E_s)^{-1} V_{s0} \quad [2.78]$$

As noted previously (Figure 2.3), V_{s0} vanishes unless s corresponds to a double substitution, so that only such substitutions contribute to the first-order wavefunction.

The second-order contribution to the Moller-Plesset energy is

$$E^{(2)} = - \sum_s^D (E_0 - E_s)^{-1} |V_{s0}|^2 \quad [2.79]$$

where Σ^D indicates that summation is to be carried out over all double substitutions. This probably represents the simplest approximate expression for the correlation energy. If Ψ_s is the double substitution $ij \rightarrow ab$, the explicit expression for V_{s0} is

$$V_{s0} = (ij | | ab) \quad [2.80]$$

where $(ij | | ab)$ is a two-electron integral over spin orbitals, defined by

$$(ij | | ab) = \iint \chi_i^*(1) \chi_j^*(2) \left(\frac{1}{r_{12}} \right) [\chi_a(1) \chi_b(2) - \chi_b(2) \chi_a(1)] \, d\tau_1 \, d\tau_2 \quad [2.81]$$

Here integration is over all coordinates (cartesian and spin) for both electrons. The final formula for the second order contribution to the energy then becomes

$$E^{(2)} = - \sum_{i < j}^{occ} \sum_{a < b}^{virt} (\epsilon_a + \epsilon_b - \epsilon_i - \epsilon_j)^{-1} | (ij | | ab) |^2 \quad [2.82]$$

One important point is that, unlike the simple CID and CISD configuration interaction schemes, MP2 requires only a partial transformation of the two-electron integrals of Eq.[2.40] into a spin orbital basis. The third-order contribution to the Moller-Plesset energy also follows directly from Rayleigh-Schrodinger theory and is

$$E^{(3)} = \sum_s^D \sum_t^D (E_0 - E_s)^{-1} (E_0 - E_t)^{-1} V_{0s} (V_{st} - V_{00} \delta_{st}) V_{t0} \quad [2.83]$$

where the summations are again carried out over double substitutions only. The matrix elements V_{st} between different double substitutions require a full integral transformation or other techniques of comparable complexity²⁸. At the fourth-order level of theory, single, triple, and quadruple substitutions also contribute, since they have nonzero Hamiltonian matrix elements with the double substitutions. The triple substitutions are the most difficult computationally, and some calculations have been carried out using only singles, doubles, and quadruples; this partial fourth-order level of theory is termed MP4SDQ.

MP2, MP3, and MP4 energy expressions again satisfy some, but not all, of the model conditions discussed earlier. They are well defined and they can be quite widely applied. In this last respect the computational labour for MP2 is dominated by the partial transformation of two-electron integrals which can be accomplished in $O(nN^4)$ steps. For the MP3 energy, evaluation of Eq.[2.83] requires $O(n^2N^4)$ steps, comparable to the labour involved in one iteration of a CID calculation. At the MP4 level, evaluation of the triple contribution requires $O(n^3N^4)$ steps²⁹. MP2, MP3, and MP4 energies do satisfy the size-consistency requirement, as do Moller-Plesset energy expansions terminated at any order. This follows since full CI is

size consistent with the Hamiltonian \hat{H}_λ for any value of λ ; hence, individual terms in Eq.[2.80] must be size consistent. In this respect the perturbation expressions are more satisfactory than the CID or CISD methods for determining correlation energies. However, perturbation theory results, terminated at any order, are no longer variational, since they are not derived as expectation values of the Hamiltonian.

2.3. References

1. (a) E. Schrodinger, *Ann. Physik*, **79**, 361 (1926).

General texts include:

- (b) P.W. Atkins, *Molecular Quantum Mechanics*, 2nd ed., Oxford University Press, Oxford, 1983;
 - (c) W.J. Hehre, L. Radom, P.v.R. Schleyer, and J.A.Pople, *Ab-Initio Molecular Orbital Theory*, Wiley-Interscience, New York, 1986.
2. P.A.M. Dirac, *Proc. Roy. Soc. (London)*, **123**, 714 (1929).
 3. (a) K.S. Pitzer, *Accounts Chem. Res.*, **12**, 271 (1979);
(b) P. Pyykko and J.P. Desclaux, *ibid.*, **12**, 276 (1979).
 4. M. Born and J.R. Oppenheimer, *Ann. Physik*, **84**, 457 (1927).
 5. For a brief review of the properties of determinants, see:
I.N. Levine, *Quantum Chemistry*, 3rd ed., pp 178-183, Allyn and Bacon, Boston, 1983.
 6. W. Pauli, *Z. Physik*, **31**, 765 (1925).
 7. J.C. Slater, *Phys. Rev.*, **34**, 1293 (1929); **35**, 509 (1930).
 8. J.C. Slater, *Phys. Rev.*, **36**, 57 (1930).
 9. (a) S.F. Boys, *Proc. Roy. Soc. (London)*, **A200**, 542 (1950);
(b) I. Shavitt in *Methods in Computational Physics*, vol.2, Wiley, New York, 1962, p. 1.
 10. For a discussion, see reference 5, pp. 172-192.
 11. C.C.J. Roothaan, *Rev. Mod. Phys.*, **23**, 69 (1951).
 12. G.G. Hall, *Proc. Roy. Soc. (London)*, **A205**, 541 (1951).
 13. (a) C.C.J. Roothaan, *Rev. Mod. Phys.*, **32**, 179 (1960);
(b) J.S. Binkley, J.A. Pople, and P.A. Dobosh, *Mol. Phys.*, **28**, 1423 (1974).
 14. J.A. Pople and R.K. Nesbet, *J. Chem. Phys.*, **22**, 571 (1954).

15. T.A. Koopmans, *Physica*, **1**, 104 (1933).
16. F.L. Pilar, *Elementary Quantum Chemistry*, McGraw-Hill, New York, 1968, p.350.
17. F.A. Cotton, *Chemical Applications of Group Theory*, 2nd ed., Wiley-Interscience, New York, 1971.
18. R.S. Mulliken, *J. Chem. Phys.*, **23**, 1833, 1841, 2338, 2343 (1955).
19. E.R. Davidson, *J. Chem. Phys.*, **46**, 3320 (1967).
20. K.R. Roby, *Molecular Physics*, **27**, 81 (1974).
21. R. Heinzmann and R. Ahlrichs, *Theor. Chim. Acta (Berl)*, **42**, 33 (1976).
22. A.E. Reed and F. Weinhold, *J. Chem. Phys.*, **78**, 4066 (1983).
23. L. Brillouin, *Actualities Sci. Ind.*, **71**, 159 (1934).
24. For a discussion on the use of 3×3 CI, see:
 - (a) L. Salem and C. Rowland, *Angew. Chem., Int. Ed. Engl.*, **11**, 92 (1972); applications include:
 - (b) W.J. Hehre, L. Salem, and M.R. Willcott, *J. Am. Chem. Soc.*, **96**, 4328 (1974);
 - (c) R.E. Townshend, G. Ramunni, G. Segal, W.J. Hehre, and L. Salem, *ibid.*, **98**, 2190 (1976).
25.
 - (a) S.R. Langhoff and E.R. Davidson, *Int. J. Quantum Chem.*, **8**, 61 (1974);
 - (b) J.A. Pople, R. Seeger, and R. Krishnan, *ibid.*, **Symp. 11**, 149 (1977).
26. C. Moller and M.S. Plesset, *Phys. Rev.*, **46**, 618 (1934).
27. For a discussion, see reference 5, p. 193 ff.
28. J.A. Pople, J.S. Binkley, and R. Seeger, *Int. J. Quantum Chem.*, **Symp. 10**, 1 (1976).
29.
 - (a) J.A. Pople, R. Krishnan, H.B. Schlegel, and J.S. Binkley, *Int. J. Quantum Chem.*, **14**, 545 (1978);
 - (b) R. Krishnan, M.J. Frisch, and J.A. Pople, *J. Chem. Phys.*, **72**, 4244 (1980);
 - (c) M.J. Frisch, R. Krishnan, and J.A. Pople, *Chem. Phys. Lett.*, **75**, 66 (1980).

3. Chemical Calculations and Mass Spectrometry.

3.1 General Introduction

Ab-Initio molecular orbital theory has now become a practical tool, not only for chemists, but for mass spectrometrists in particular. Efficient programs, such as Pople's GAUSSIAN 82¹, coupled either with increasingly powerful main-frame computers or with their cost effective minicomputer counterparts, allow the simultaneous investigation of the energies, structures and electronic distributions of molecules. Most small molecules, particularly those with classical structures, can be quite routinely calculated to any desired level of accuracy. Negatively charged ions require the use of basis sets augmented with diffuse functions, but positive ions can be treated at standard theoretical levels which work well for their neutral counterparts. Larger basis sets including d-type polarisation functions on first row elements, as well as electron correlation corrections are needed for non-classical ions, delocalized systems, and to determine the energy differences between open and closed shell species. There are several texts of accumulated experience which can be used as guides to the use of the available programs²⁻⁴. Gas phase ion chemists and calculational chemists have a natural, symbiotic relationship. Computations assist in elucidating the structures of ions and in understanding their behaviour by determining potential energy surfaces. Energies are currently the only calibration points between theory and experiment, although experimental methods to elucidate the structures of ions are being developed. Many species are generated in the gas phase in excited states and calculations are often necessary to help clarify observed experimental results. Although calculations have, to date, been used more often to underpin experimental observations, several research groups are now using computational chemistry as a primary research tool and predicting novel chemistry for a variety of ionic species. Ionic species are just as easy to calculate as their neutral counterparts and the information obtained through calculations or through mass spectrometry is likely to be of more general significance. The generalisation is often made that compared with their neutral counterparts, ions have larger interatomic distances and flatter potential energy surfaces⁵. As molecular size increases, so

the overall effect of removing or adding one electron should become less significant and therefore principles and concepts of chemical reactivity and bonding elucidated through mass spectrometry are unlikely to be peculiar to gaseous ions.

One very good reason for making measurements on ions rather than neutral molecules is the exact control possible over the motion of ions by the use of electric and magnetic fields, so that, translational spectroscopy, for example, is an easy experiment with ions. Other advantages to working with ions are that the ionisation process, corresponding to the energisation or activation of a neutral and the subsequent unimolecular reaction can be clearly distinguished from each other and studied separately.

Also the ionisation can be finely controlled, so that ions with selected discrete energies are accessible to study. Finally, there are no "side-reactions" in mass spectrometry, at least not under unimolecular reaction conditions, and in principle all the competing and parallel reactions of an ion can be distinguished and measured. This can provide a complete view of the chemistry of the ion under study, although can be difficult to achieve in practice.

The literature contains many examples of the collaboration between computational chemists and mass spectrometrists, both in the use of computational chemistry to predict stable species which have then been searched for and identified by mass spectrometry and in the use of computational chemistry in helping to elucidate the reaction pathway for ion fragmentations which are observed mass spectrometrically.

3.3 References

1. J.S. Binkley, R.A. Whiteside, K. Ragavachari, R. Seeger, D.J. DeFrees, M.J. Frisch, J.A. Pople and L.R. Kahn, GAUSSIAN82, Release A, Carnegie-Mellon University, Pittsburgh, 1982.
2. T. Clark, A Handbook of Computational Chemistry, Wiley-Interscience, New York, 1985.
3. J.J.P. Stewart, *J. Computer Aided Molecular Design*, 4(1), 1-105 (1990).
4. W.J. Hehre, L. Radom, P.v.R. Schleyer and J.A. Pople, *Ab-Initio Molecular Orbital Theory*, Wiley-Interscience, New York, 1986.
5. (a) P.J. Derrick and K.F. Donchi, in *Comprehensive Chemical Kinetics*, Vol. 24, (C.H. Bamford and C.F.H. Tipper, Eds.), Elsevier, Amsterdam, 1983.
(b) W. Forst, *Theory of Unimolecular Reactions*, Academic Press, New York, 1973.

4. Experimental Methods

4.1. Preparation of Materials

The thioamides were prepared from their corresponding amides by the method of Lawesson et al., this involves the addition of 0.0005 moles of Lawesson's reagent to 0.001 moles of the amide in 10 ml anhydrous tetrahydrofuran (THF). The reaction mixture was then left at room temperature for 5-10 mins with stirring ^{1,2}. This method allowed yields of >75% for the thioamides to be achieved. The thioamide products were purified by column chromatography using silica gel with petroleum ether/ acetone (50/50) as solvent. The purity was checked by thin layer chromatography (TLC) and by mass spectrometry. All other chemicals used were obtained from Sigma Chemical company and were used as purchased with no further purification.

4.2. Computer Calculations

All ab-initio molecular orbital calculations were carried out with full geometry optimisation using the Gaussian-82 suite of programs by Pople et al. ³, running on a Cray-1S computer at the University of London Computer Centre. Preliminary modelling of some of the larger molecules was performed on a Silicon Graphics IRIS 4D/20 personal workstation using the commercial version (Polygen Corp.)⁴ of Karplus' macromolecular mechanics modelling program CHARMM⁵. The larger methylated ureas and thioureas were calculated on the Silicon Graphics IRIS 4D/20 workstation using the semi-empirical molecular orbital package, AMPAC ⁶.

4.2.1 General Introduction

Chemical calculations that can predict the structures, energies and other properties of known or unknown molecules have often been heralded as important new tools in chemical research. The main objection to their use has been that the results may not be very reliable. Whilst this was certainly true a few years ago, the strengths and weaknesses of the common methods are now well known so that reliable estimates of their probable accuracies can be made. In some

cases, rare at present but becoming more common, the results of calculations may be more reliable than those from experiments. To achieve this sort of performance with calculations requires an enormous investment in computer time but the results which can be obtained can make this a worthwhile exercise. What other method can give the molecular structure, heat of formation, dipole moment, ionisation energies, charge densities, bond orders, spin densities, and so on in one experiment? Two recent books give insights into the practical use of these computational chemistry software packages ^{7,8}, describing the strengths and weaknesses of the standard packages and giving advice on getting started. This section briefly describes some of the major program packages currently available, which have become today's standard methods for chemical purposes. They are not perfect, but they have achieved a reliability that makes them a valuable addition to the range of tools available in chemical research and, perhaps more importantly, they have extended the range of possible research subjects by removing the limit that only compounds that can be made can be studied.

4.2.2 Molecular Mechanics

Molecular mechanics, or force field, calculations are based on a simple classical-mechanical model of molecular structure. The model nature of these calculations needs to be emphasized since there is very little significance in the parameters and energies in molecular mechanics calculations. This was shown in early force fields, which often gave similar results, but for completely different reasons. However, modern molecular mechanics programs can be considered to have achieved chemical accuracy, at least for certain types of molecule. The molecular mechanics method has recently been comprehensively reviewed by Burkert and Allinger ⁹, so only the principles of the method will be outlined here.

Molecular mechanics treats the molecule as an array of atoms governed by a set of classical-mechanical potential functions. This can be illustrated by considering the bond-stretching term in a molecule, where the potential at any given interatomic distance is given by a Morse curve as shown in Figure 4.1. The energy minimum occurs at the equilibrium bond length r , however, the expression for a Morse curve is complicated and would require

too much computer time, much more than other types of potential function, to evaluate. This is not a critical problem as the vast majority of molecules have bond lengths within a limited range (for bonds of a given type), symbolized by the shaded part Hooke's Law, gives a good fit to the realistic energy profile as shown by the dashed curve.

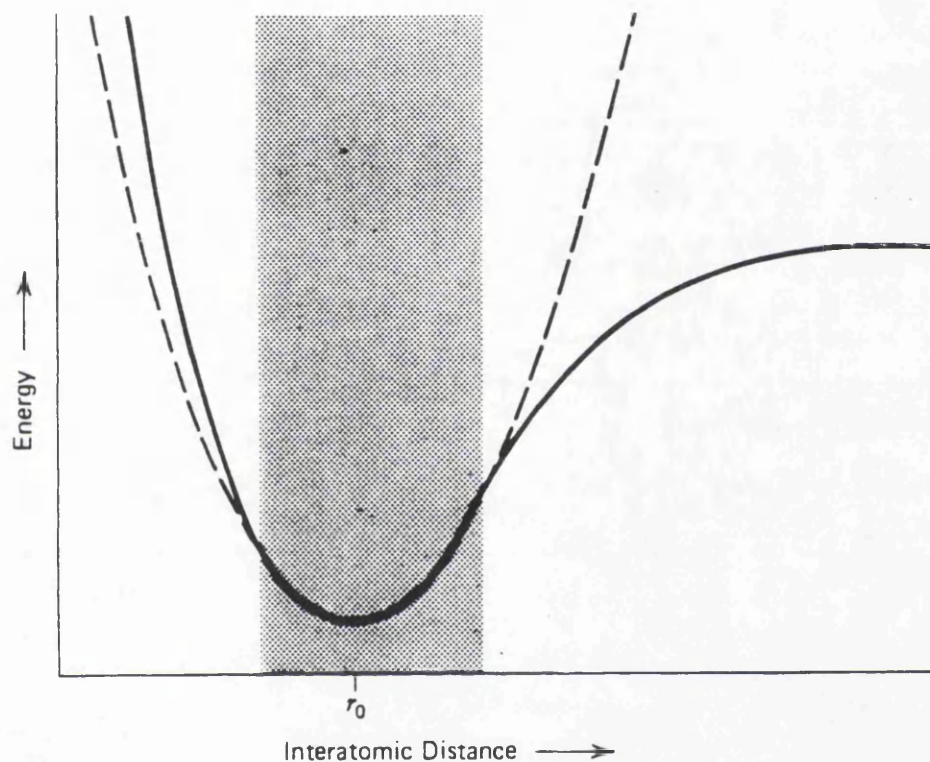


Figure 4.1. The potential energy curve for stretching a chemical bond. The dashed curve represents a simple Hooke's Law potential-function.

The Hooke's Law expression,

$$V = \frac{k(r-r_0)^2}{2} \quad [4.1]$$

where V is the potential energy and k is a constant, is simple to calculate and gives very fast execution of the program, so it is commonly used in many force fields. Problems may arise for molecules with long bonds that lie outside the shaded region, these are commonly caused by

steric effects and the situation is improved by adding a term proportional to $(r - r_0)^3$ to the expression given above. Molecular mechanics builds a molecular force field by adding other potential functions to that for bond stretching, such as angle bending, and both one- and two-fold torsion potentials. These combinations of potential functions are sometimes known as a valence force field because they account for the properties normally attributed to chemical bonds. For high quality quantitative calculations, steric interactions must be accounted for by including so-called Van der Waals functions. Each of these types of potential function is assumed to be transferable from molecule to molecule, so that, a given type of bond, for example, is assumed to have the same characteristics in any molecule in which it occurs. The success of molecular mechanics calculations indicates that this must frequently be a good approximation however a force field parametrized for classical species could not be used to predict the structure of non-classical ions, for example. The force field defines the mechanical model used to represent the molecule and the purpose of the programs is to find the optimum structure and energy based on this model. The model nature of the calculation requires that bonds be defined in the input and the model corresponds strictly to the classical valence bond picture of chemical bonding, carbon for instance has three different types of force field to describe sp^3 , sp^2 , and sp types of bonding. The starting geometry is then used to calculate bond lengths, bond angles and torsion angles, these values are in turn used in the potential expressions to calculate an initial steric energy. This steric energy is specific to the force field and does not correspond to any classical definition of strain energy, although it is related to the heat of formation by a simple expression. The structure is then optimized by using Newton-Raphson optimisation procedures which rely on analytically evaluating second derivatives of the molecular energy with respect to the geometrical parameters. Since all other factors remain constant throughout the optimisation of a structure it is sufficient to find a minimum with respect to the steric energy. Once the optimisation has converged the optimum geometry may be used to calculate other properties such as the dipole moment, moment of inertia and heat of formation. Widely used programs of this type include Allinger's MM series, of which MMP2 is the latest version and, for larger biochemical systems, Karplus CHARMM

program which was used for some of the preliminary calculations reported in this work.

4.2.3 Semi-Empirical Molecular Orbital Methods

Semi-Empirical molecular orbital calculations use sets of parameters to approximate the one-centre electron repulsion integrals instead of analytically evaluating them. These parameters along with the constants used to approximate the resonance integrals allow the results to be fitted as closely as possible to experimental data. The underlying molecular orbital theory is as described in Chapter 3. and relies heavily on the LCAO approach, as do most programs used in this type of work. The two most popular programs of this type in use today are probably MINDO/3 and MNDO, these have now been incorporated into a single package (MOPAC) and more recently have also included the use of the AM1 hamiltonian. These programs were developed by M.J.S. Dewar and his group specifically for applications in organic research and the aim was to produce an "MO-spectrometer" that should eventually be able to give chemically accurate results on large molecules at a reasonable cost in computing time. The original semi-empirical methods were developed by Pople and co-workers to reproduce the electronic properties of molecules rather than the molecular geometries. MINDO/3 is the last in a series of modified INDO (Intermediate Neglect of Differential Overlap) methods and was the first easy to use program package with automatic geometry optimisation to be made available to a wide range of non-specialist research groups. MINDO/3 has often been heavily criticized, especially by Pople and co-workers, who rejected parametrized INDO procedures in favour of ab-initio calculations, however it was a major instrument in introducing the concept of structure and energy calculations to organic chemical research. MNDO is an independent method based on the NDDO (Neglect of Diatomic Differential Overlap) approximation which has advantages for molecules in which lone pair-lone pair interactions may be important. The directionality of the electron-electron repulsion terms in the NDDO approximation is important in this respect and this helps to avoid some of the systematic MINDO/3 errors in such molecules.

The advantage of MINDO/3 and MNDO over ab-initio calculations is that not only are they

much faster but also the neglect of large numbers of integrals saves a lot of the core and disk space requirements in comparison with those for an equivalent ab-initio job. As a result much larger molecules can be calculated by semi-empirical methods than can be handled at even the simplest ab-initio level. The approximations inherent to the neglect of differential overlap (NDO) methods naturally cause a loss of accuracy but this can largely be compensated for by the parametrisation. As in molecular mechanics methods (Section 4.2.) the parametrisation cannot be better than the available experimental data, so the results for the less common elements such as beryllium and lithium cannot be expected to be as reliable as those for hydrocarbons. Another problem with the parametrisation of SCF methods like MINDO/3 and MNDO to fit experimental data is that the experimental data includes electron correlation which is not included at the SCF level of theory. Configuration interaction calculations are available in both MINDO/3 and MNDO but this results in the correlation being accounted for twice: once explicitly and once indirectly via the parametrisation. Results from these calculations are only meaningful when compared with each other and not as absolute values for, for instance, heats of formation. See reference 1 for a discussion on the performance of these programs and an assessment of their relative strengths and weaknesses.

4.2.4 Ab-Initio Molecular Orbital Methods

The term ab-initio implies a rigorous, nonparametrized molecular orbital treatment derived from first principles. This is not completely true because there are number of simplifying assumptions in ab-initio theory (see Chapter 3), but the calculations are more complete and therefore more expensive than those of the semi-empirical methods discussed above. It is possible to obtain chemical accuracy via ab-initio calculations, but the cost in computer time is enormous, and only small systems can be treated this accurately at present. In practice most calculations are performed at lower levels of theory than can be considered definitive, and the shortcomings are taken into account. The first stage in most ab-initio calculations is a single determinant LCAO-SCF calculation, as outlined in Chapter 3. In contrast to the NDO methods, however, there are many possible choices of atomic orbitals (the basis set). The GAUSSIAN series of

programs deals exclusively with Gaussian-type orbitals and includes several optional basis sets of varying size. The GAUSSIAN series of programs developed by Pople and co-workers are widely used and the GAUSSIAN-82³ program was used for most of the calculations reported later in this work. One of the main advantages of using such a widely distributed program system is that the methods and basis sets used become standard and a direct comparison with literature data is often possible. An ab-initio calculation is in many ways similar to the corresponding MNDO or MINDO/3 job. First the optimum geometry is obtained by minimisation techniques, of which three different ones are available in GAUSSIAN-82. Having reached the minimum energy structure the program then performs a Mulliken population analysis to obtain overlap populations and atomic charges and so forth, although these can be misleading in large-basis-set ab-initio calculations. This gives a wavefunction and a molecular structure at the single-determinant level and the program can be terminated here, alternatively the next step may be to apply some sort of electron correlation correction to the SCF energy. The GAUSSIAN programs provide a choice of methods for this correction with Moller-Plesset perturbation theory and configuration interaction methods available. GAUSSIAN-82 is made up of a series of "links", each of which is a separate program on some computers. Each link performs its own specific task within the overall calculation and communicates with the other links via a series of disk files. The links are grouped together in overlays of which there are twelve in the current version of GAUSSIAN-82, these overlays are simply sets of links, grouped together for convenience, which use a common set of control options.

There are several good bibliographies of ab-initio calculations including the series by Richards et al.¹⁰ and the recent compilation by Ohno and Morokuma¹¹, which both list the published calculations by molecular formula. The GAUSSIAN programs and the methods and basis sets available in them have recently been described by Hehre et al.⁸ and the Carnegie-Mellon Quantum Chemistry Archive¹² is a valuable source of data for calculations performed with the GAUSSIAN series of programs.

4.3 Calculation methods

All Ab-Initio data was obtained by using the standard 3-21G^{*} basis set and the Unrestricted Hartree-Fock (UHF) formalism was used throughout these calculations. Full geometry optimisation was carried out on all neutral molecules and radical cations studied and charge distributions were determined from Mulliken population analysis of the calculated molecular orbitals. Radical cations were studied at two different geometries, (i) corresponding to the same geometry as the neutral molecule which represents the situation immediately after ionisation and before any structural changes have occurred to reduce the energy of the system; and (ii) corresponding to the fully optimised geometry of the radical cation after allowing for electron and nuclear reorganisation to reduce the energy. The 3-21G^{*} level of theory allows the participation of d-symmetry functions in the bonding of all second row atoms but these particular functions are not included for first row heavy atoms. Initial geometry optimisations were carried out without symmetry constraints so that the molecular structure was not constrained to remain in the same symmetry point group as that for the initial starting structure. Subsequent calculations based on the geometries obtained from the initial calculations used symmetry constraints and the structures obtained were characterised by explicit evaluation of the second derivative eigenvalues to ensure that minima had been obtained. The use of symmetry constraints at this stage allows the computer to use symmetry relationships to reduce the amount of calculation necessary and therefore the geometry optimisation is performed more rapidly. By precluding the use of symmetry constraints in the preliminary calculations it was intended to allow more structures to be considered by keeping constraints imposed to a minimum. The charge distributions were determined from Mulliken population analysis, which was then used to calculate the total atomic charges. Mulliken analysis divides the electron density calculated for the overlap integrals equally between the two atoms concerned in order to facilitate the determination of total atomic charges. The version of the GAUSSIAN program used (GAUSSIAN-82) only computes the Mulliken population analysis on the uncorrelated wavefunction, therefore even when electron correlation was used, it only applies to the energies and ordering of the orbitals and not to the calculated atomic charges.

4.4. Accuracy of the methods

The semi-empirical methods are limited in accuracy by the quality of the data used to parametrise the methods. This means that the accuracy will differ for various compounds, although it is anticipated that any errors in the calculated results presented here will be less than $\pm 0.03 \text{ \AA}$ on bond lengths and less than $\pm 3^\circ$ on bond angles with respect to experimentally determined geometries. The accuracy of the charge distribution data is not known, since there is no easy way of comparing the calculated data with experimentally determined values. The limitations of the Mulliken method of calculating total atomic charges are discussed later, however it is anticipated that the errors in these calculations will cancel out in a comparative study of this kind. The bulk of the calculations reported in this study were carried out using the ab-initio program GAUSSIAN-82, this does not therefore suffer from any problems with parametrisation, however several assumptions have to be made in order that the problems become practical.

4.5. Mass Spectrometry

Mass spectrometry was performed on a VG-Analytical ZAB-2F double focusing mass spectrometer. A standard VG electron impact ion source was used for the 70eV spectra and for measurement of ionisation and appearance energies. High resolution accurate mass measurements were obtained at a mass resolving power of 7500 to check formula assignments for significant fragment ions.

4.6 References

1. S. Scheibye, B.S. Pedersen, and S.-O. Lawesson, *Bull. Soc. Chim. Belg.*, Vol.87, 3, 229-238 (1978).
2. B. Yde, N.M. Yousif, U. Pedersen, I. Thomsen, and S.-O. Lawesson, *Tetrahedron*, Vol.40, 11, 2047-2052 (1984).
3. J.S. Binkley, R.A. Whiteside, K. Raghavachari, R. Seeger, D.J. DeFrees, H.B. Schlegel, M.J.Frisch, J.A. Pople, and L.R. Kahn, GAUSSIAN82 Release A, Carnegie-Mellon University, Pittsburgh, 1982.
4. QUANTA Software Ver. 3.0, Reference Manual, Polygen Corporation, 1986, 1987, 1988, 1990.
5. B.R. Brooks, R.E. Bruccoleri, B.D. Olafson, D.J. States, S. Swaminathan and M. Karplus, *J. Computational Chemistry*, 4(3), 187-217 (1983).
6. J.J.P. Stewart, *J. Computer-Aided Mol. Design*, Special Issue, 4(1), 1-104 (1990).
7. T. Clark, *A Handbook of Computational Chemistry*, Wiley-Interscience, New York, 1985.
8. W.J. Hehre, L. Radom, P.v.R. Schleyer, and J.A. Pople, *Ab-Initio Molecular Orbital Theory*, Wiley-Interscience, New York, 1986.
9. U. Burkert and N.L. Allinger, "Molecular Mechanics," ACS Monograph 177, American Chemical Society, Washington, D.C., 1982.
10. W.G. Richards, T.E.H. Walker, and R.K. Hinkley, *A Bibliography of Ab-Initio Molecular Wave Functions*, Oxford University Press, Oxford, 1971; W.G. Richards, T.E.H. Walker, L. Farnell, and P.R. Scott, *ibid.*, supplement for 1970-3, 1974; W.G. Richards, P.R. Scott, E.A. Colbourn, and A.F. Marchington, *ibid.*, supplement for 1974-7, 1978; W.G. Richards, P.R. Scott, V. Sackwild, and S.A. Robins, *ibid.*, supplement for 1978-80, 1981.
11. K. Ohno and K. Morokuma, *Quantum Chemistry Literature Data Base*, Elsevier, Amsterdam, 1982; THEOCHEM, 1982, 8; 1983, 15, special issues.

12. R.A. Whiteside, M.J. Frisch, J.S. Binkley, D.J. DeFrees, H.B. Schlegel, K. Raghavachari, and J.A. Pople, *Carnegie-Mellon Quantum Chemistry Archive, 2nd Ed.*, Carnegie-Mellon University, Pittsburgh, 1981.

5. Previous Work.

5.1 Introduction

The work presented in this thesis concerns the role played by charge localisation in determining the observed mass spectra of organic compounds under electron impact conditions and with particular reference to some simple amides, ureas and their thio- analogues. This chapter will review the work that has gone before in this area with a view to preparing the ground for a later discussion of the present work.

5.2 Mass Spectrometry

5.2.1 Amides

The mass spectra of a wide variety of aliphatic amides were determined by Gilpin in 1959 ¹, and since then many mass spectrometry texts have included a section on the mass spectrometry of amides ²⁻⁶. The mass spectra of aliphatic amides show the operation of fragmentation processes which are characteristic of both aliphatic carbonyl compounds and amines ^{2,3}.

Molecular ions are generally observed in amide mass spectra although the intensity of the molecular ion may vary from a minimum of $\approx 0.5\%$ of the base peak for some amides, to being the base peak in the spectra of the simple amides studied in the present work. The most important fragmentation for the smaller, simple primary amides arises from α -cleavage, resulting in an ion of mass 44. The charge-localisation theory has been extensively used to rationalise the spectra of amides, with the ionisation being visualized as occurring by removal of one of the lone-pair electrons from oxygen or nitrogen as shown in Figure 5.1. The α -cleavage reaction may occur at either side of the carbonyl group and the abundances of the fragment ions thus formed can vary a great deal, although aliphatic amides generally produce only small peaks in their mass spectra corresponding to loss of NR_2^- . Usually cleavage between the alkyl chain and the carbonyl function is more important and $(\text{M} - \text{CONR}_2)^+$ ions are observed, although these ions may be the result of a consecutive reaction from the

$(M - NR_2)^+$ ions as illustrated in Eq.[5.1] below, since a heterolytic bond cleavage would be required for their direct formation. The moieties $CONR^+$ also appear as charged species at the appropriate m/z values.

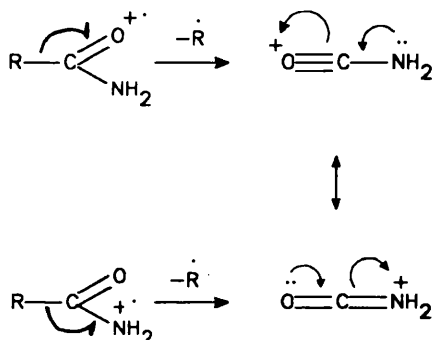


Figure 5.1. The α -cleavage reaction in simple primary amides giving rise to the resonance stabilized ion at m/z 44.

As may be anticipated by analogy to carbonyl compounds, simple β -fission does not occur, but evidence for γ -cleavage is found in the spectra of many longer chain amides¹, and is thought to occur by formation of a four membered ring.

As in other carbonyl compounds, as soon as a three (or greater) carbon chain is present, the process of β -cleavage with transfer of a γ -hydrogen atom (the McLafferty rearrangement) predominates. The resulting ion of mass 59 is the most abundant one in the spectra of all such primary amides so far investigated. This reaction is illustrated in Figure 5.2. for butanamide.

The mass spectra of N-alkyl and N,N-dialkyl amides show the sequential α - and C-N-cleavage with hydrogen rearrangement reaction which is a characteristic feature of the spectra of N-alkyl and N,N-dialkyl amines and is illustrated in Figure 5.3. for N-butylethanamide. In the absence of any α -substitution adjacent to the nitrogen, ions of mass 30 are formed by this fragmentation, deuterium labelling of the ethanamide-methyl group causes this peak to be shifted to mass 31 indicating that the transferred hydrogen originates from the acetyl group.

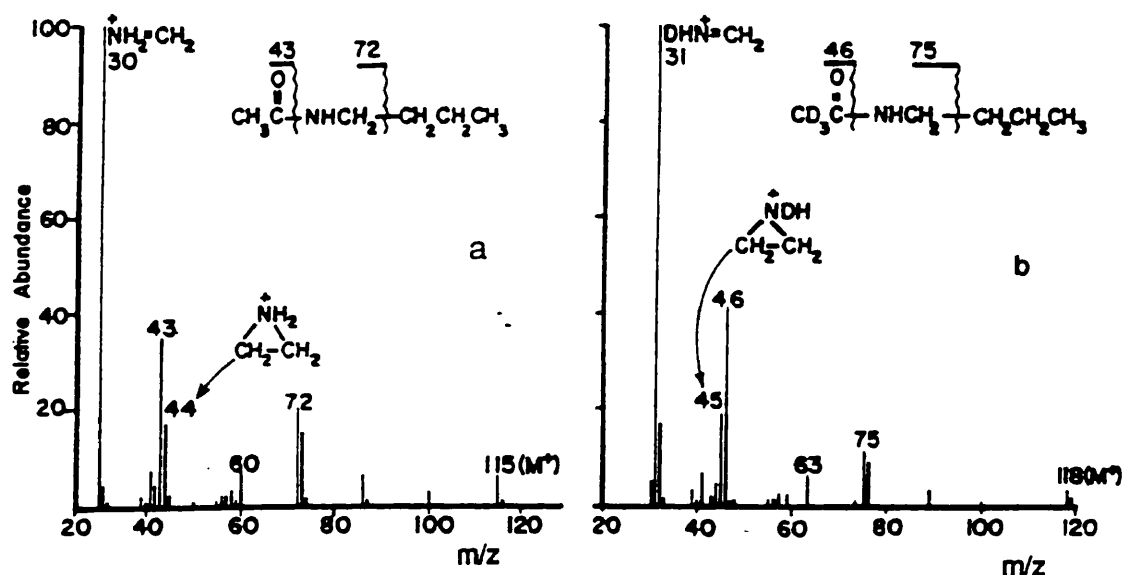


Figure 5.3. 70eV mass spectra of (a) N-butylethanamide and (b) N-butyl- $^2\text{H}_3$ -ethanamide showing characteristic fragmentation⁸.

The sequential β - and C-N-cleavage with hydrogen rearrangement reaction, seen in amines, is also observed in the spectra of amides, yielding ions of mass 44. The shift of this peak to mass 45 in the spectrum of N-butyl- $^2\text{H}_3$ -ethanamide (Figure 5.3b.) is consistent with the formation of a three-membered ring making the reaction energetically favourable and the reaction has been rationalised as being initiated by the electron-deficient nitrogen, using the charge-radical site localisation theory as discussed in section 2.10.² The predominant processes in the spectra of N,N-dialkyl amides are those discussed above for N-alkyl amides. The fragmentations of the N-alkyl and N,N-dialkyl amides have also been taken to reflect the strong reaction- initiating tendency of nitrogen³. Cleavage of the C-N amide bond, to give the alkanoyl ion RCO^+ , is greatly reduced compared with cleavage of the corresponding C-O bond in esters; and the normally unfavourable C-N bond cleavage with charge retention on nitrogen has been found to increase substantially on going from N-alkyl to N,N-dialkyl amides. Some amides, diethylethanamide for example, undergo direct ketene loss, paralleling the behaviour of unsaturated ethanoates and this reaction can provide a very characteristic peak in the spectra of N-aryl amides. Charge migration away from the amide function is only significant if

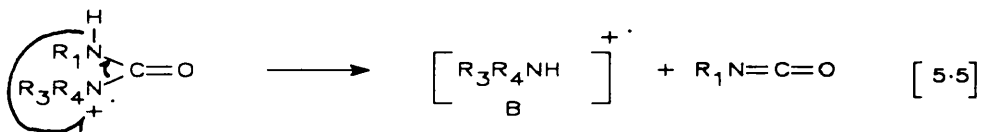
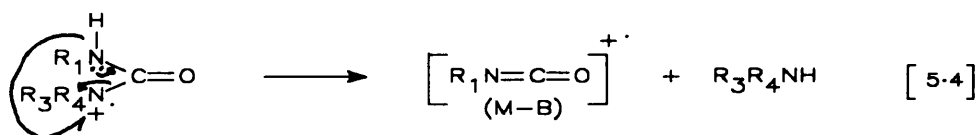
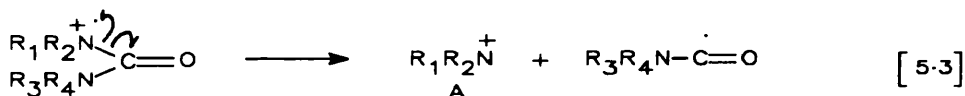
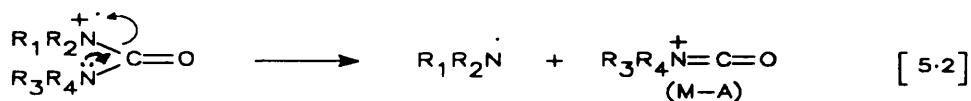
the resulting $(M-RCONHR)^{+\cdot}$ ion is substantially stabilized and the R groups are small. The tendency for charge retention in the amide function is much greater than for the corresponding esters due to the substantially reduced ionisation energies of the amides; however ethanamides of more complex molecules, such as steroids, usually exhibit characteristic $(M-CH_3CONH_2)^{+\cdot}$ peaks.

5.2.2 Thioamides

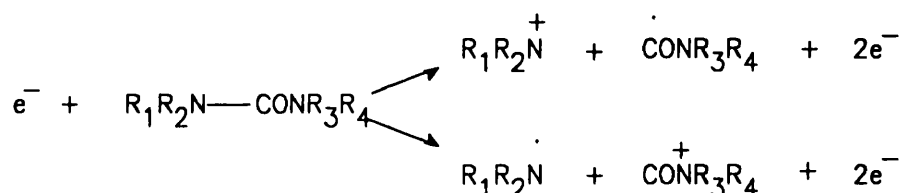
Very few references to the mass spectrometry of thioamides have been found and the only systematic work seems to be the studies of Maccoll and Baldwin and co-workers on the ionisation energies and fragmentation of some thioacetanilides ⁹⁻¹⁰.

5.2.3 Ureas

The electron impact mass spectra of urea and some of its substituted analogues were reported in a series of papers by Baldwin and co-workers from 1968-77 ¹¹⁻¹³. These authors stated that the mass spectra of urea and its N-methyl derivatives could be rationalised on the basis of four main processes, which together with the molecular ion were able to account for $\approx 70\%$ of the observed total ion current above and including m/z 15. These four processes are illustrated in equations [5.2] to [5.5] shown below.



The observation of the appropriate metastable peaks in the spectra of N-methyl, N,N-dimethyl, N,N'-dimethyl, and trimethylurea was used to confirm that type B fragmentation was produced by electron impact and not by pyrolysis of the molecules. It was also noted that for trimethyl and tetramethyl ureas the ion at m/z 44 could be formed from the (M-A) type ion, which can be written $\text{Me}_2\text{N}^+\text{CO}$, as well as directly from the molecular ion. This loss of carbon monoxide being akin to that previously reported for the isocyanates¹⁴. These A-type processes are bond cleavage reactions of the bonds α - to the carbonyl function and the authors found it instructive to consider the distribution of charge between the two fragments arising from the bond cleavage reaction:



[5.6]

The ratios they obtained for the N-methylated ureas are reproduced in table 5.1 and although care is needed in their interpretation, it is possible for loss of CO from (M-A) to give the A-type ion which would lead to an increase in the ratio, the observed variations can still be rationalised on the basis of the increasing stability of the ions $\text{Me}_2\text{N}^+ > \text{MeNH}^+ > \text{NH}_2^+$ and $\text{Me}_2\text{N}^+\text{CO} > \text{MeN}^+\text{HCO} > \text{H}_2\text{N}^+\text{CO}$.

Table 5.1.

The ratio $\text{A}^+ / (\text{M-A})^+$ from the N-methyl ureas

$\text{A}^+ / (\text{M-A})^+$	NH_2CO	MeNHCO	Me_2NCO
NH_2	0.30	0.50	0.30
MeNH	3.10	2.00	0.35
Me_2N	7.20	5.00	0.30

It should be emphasised here that this simple treatment takes no account of any sequential reactions causing further fragmentation of any of the ions considered, and that this may cause the ratios to differ substantially. This type of analysis may be better performed on low energy, low temperature spectra where there is less energy available for sequential reactions to occur. The B-type fragmentation is a 1-3 hydrogen transfer from nitrogen to nitrogen and when a similar charge distribution exercise is carried out the results show no obvious trends.

Arylureas and other N-alkylated ureas were also studied by Baldwin and co-workers and the fragmentation of these compounds was rationalized using the same basic reactions as described above (Equations [5.2] to [5.5]), along with some more reactions involving rupture of the C-C or C-N bonds.

5.2.4 Thioureas

The fragmentation patterns of some substituted thioureas were presented and discussed by the same authors ¹⁵, after preliminary reports had indicated major differences between their spectra and those of the corresponding ureas. In particular they noted large ions corresponding to $(M-SH)^+$ and $(M-H_2S)^+$ in the spectra of the thioureas whereas the analogous $(M-OH)^+$ and $(M-H_2O)^+$ ions were virtually absent in the spectra of the ureas. Reports on the pyrolysis products of thioureas under similar conditions in the mass spectrometer indicated that pyrolysis lead not only to the production of the corresponding isothiocyanate and amine, but also to the loss of hydrogen sulphide ¹⁶⁻¹⁷. Re-investigation of the mass spectra of the alkyl thioureas at lower source temperatures revealed that the $(M-H_2S)^+$ ions were formed by pyrolysis with subsequent ionisation ¹⁵, however the $(M-SH)^+$ ions were genuine electron impact fragments with metastable ions for the reaction $(M)^+ \rightarrow (M-SH)^+$ being observed in most cases studied. Also the intensity of the $(M-SH)^+$ ions relative to the molecular ion was found to be reasonably constant with variations in the source temperature. The most important fragmentation in the thioureas, as in the ureas, was found to be cleavage α to the central thiocarbonyl function, the A-type fragmentations illustrated in equations [5.2] and [5.3] above for the ureas. The ions produced by these α -cleavage processes carry a large proportion of the total ion current in the

spectra of both ureas and thioureas, however this proportion is lower for some of the thioureas than for the corresponding ureas. This difference is accounted for by the presence of other fragmentation routes in the thioureas whose equivalents are not present in the ureas. The first of these is the loss of the sulphhydryl radical, or in the case of tetramethyl thiourea the loss of the methyl sulphhydryl radical. The absence of the $(M-SH)^+$ ion in the spectrum of tetramethyl thiourea and its prominence in the spectrum of N-methyl thiourea suggests that a hydrogen on one of the nitrogens is involved, although whether this is a stepwise or concerted process is not as yet clear. Care is needed in the interpretation of the presence of methyl sulphhydryl and sulphhydryl cations in the spectra of these compounds since metastable peaks are observed indicating that these peaks arise from further fragmentation of the $(M-A)^+$ ions. Another major difference between the methyl ureas and the methyl thioureas is that the latter show $(M-43)^+$ and $(M-29)^+$ ions of reasonable intensity. These ions are thought to be formed by transfer of a methyl hydrogen to the sulphur atom in thioureas. Studies were also carried out on ethyl, butyl and aryl thioureas and the authors concluded that the differences in the fragmentations of the thioureas as compared to the ureas could be rationalised on the basis of a difference in charge location in the two groups. The charge was predicted to be on the nitrogen atom in the ureas and on the sulphur atom in the thioureas.

5.2.5 Ionisation energies and Charge Localisation

During the course of the electron impact studies on ureas and thioureas mentioned above, Baldwin et al. also published the ionisation energies of the same compounds and their N-methylated analogues. They interpreted the results as indicating that the ground state of the molecular ion for thioureas was best represented by (I), whereas for the ureas the results supported representation (II) see Figure 5.4. These conclusions were arrived at by considering the effect of N-methylation on the ionisation energies of each set of compounds¹⁸. For the ureas the effect of N-methylation was to increase the range of the ionisation energies measured for the series urea to tetramethyl urea and the effect was considered to be first-order, the spread of ionisation energies being 1.53 eV for the ureas.

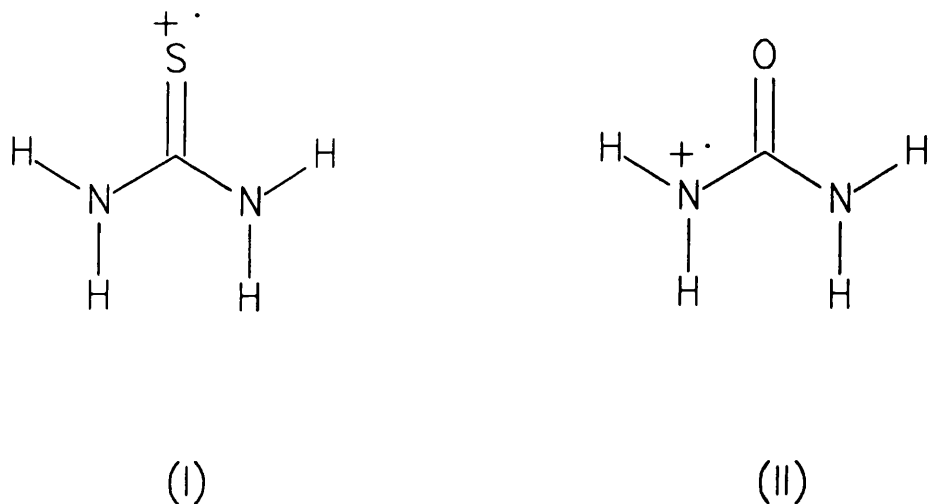


Figure 5.4. Proposed sites for ionisation of urea and thiourea.

In the case of the thioureas, the spread of the ionisation energies was only 0.55 eV, and the effect of N-methylation was considered to be second-order. Also the order of the NN- and NN'-dimethylated compounds was found to be reversed in the ureas as compared to the order found for the thioureas. In representation (II) where the charge is located on the nitrogen, the effect of N-methylation would be first-order since the methylation is occurring on the charge-bearing atom and NN-methylation should have an appreciably larger effect than NN'-methylation. In representation (I) where the charge is located on the sulphur atom, the effect of N-methylation would be second-order since the methylation is no longer occurring at the charge site. Also it was noted that for a second-order effect the result of NN-methylation should not differ significantly from that for NN'-methylation. These conclusions were supported by their observations for the ureas and thioureas and led to the general conclusion that the localisation of the charge in certain molecular ions was not only a useful concept but one that could be justified by energetic considerations.

Later work on the photoelectron spectra of the methanamides, ethanamides and their N-methylated analogues indicated that there are two molecular orbitals very close in energy, one of which is the highest occupied molecular orbital (HOMO) ¹⁹. Under these conditions it

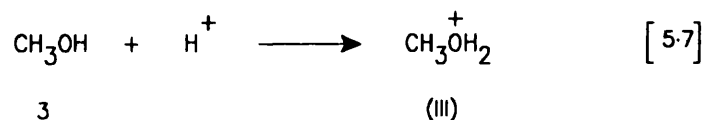
would seem that electron impact ionisation does not give the ionisation energy of the HOMO but a value which is a weighted average of the ionisation energies of all the orbitals concerned²⁰. The electron impact mass spectra, photoelectron spectra and photoionisation spectra²¹ of a range of amides, thioamides, ureas, thioureas and their methylated analogues as well as some related compounds were compared and discussed in relation to the charge localisation concept and additivity rules for the prediction of ionisation energies were examined²⁰. It was concluded that the additivity rules seemed to have some application and could be used to examine the nature of the HOMO in simple molecules.

5.2.6 The Charge Localisation Concept

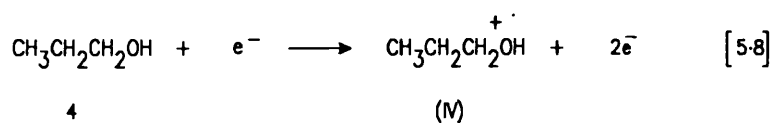
Since its introduction by McLafferty²², the concept of charge localisation (see section 2.10.) has been widely used to rationalise observed mass spectra and has been popularised by a number of texts (2-4). However, as has already been stated (see section 2.10.), its validity has been repeatedly questioned²³⁻²⁵. Bentley and Johnstone have adopted the view that the charge localisation approach is a convenient device for collating varied results but that it has no predictive capability²³. They base their criticisms on a discussion of the changes in electronic structure which will occur shortly, (within a few vibrations), after ionisation of a molecule and before the molecular ion formed can fragment. They also criticize the concept of localized orbitals from which electrons may be removed on the grounds that most of the orbitals will be delocalized and removal of electrons from delocalized orbitals will lead to delocalized charges. This criticism is backed to some extent by the calculated charge distributions for some neutrals and radical cations of Lorquet and co-workers²⁴ who have also criticized the charge localisation concept on these grounds.

The strengths and weaknesses of the charge localisation approach were reviewed in some detail by Williams and Beynon in 1976²⁶. These authors considered charge distributions in both molecules and ions and after examining the evidence from such isoelectronic species as $(\text{NH}_2)^{\cdot}$, $(\text{CH}_2)^{\cdot-}$, $(\text{H}_2\text{O})^{\cdot+}$; and $(\text{NH}_4)^+$ and $(\text{CH}_4)^{\cdot+}$ they concluded that the charge would be at least partially delocalized by bond polarisation and hyperconjugation. Further, they inferred,

from the similarity in chemical properties of the isoelectronic species above, that it is the electron distribution that determines the chemical properties and that the sign of or the presence of a charge is only of marginal importance. Evidence from semi-empirical molecular orbital calculations of the charge distribution in neutral and ionized ethylamine was also cited which again indicated significant delocalisation of the charge over at least a portion of the molecular structure (24). However the authors did stress the difficulties associated with attempting to calculate charge distributions in this way, and also mentioned further problems in that the structure of the reacting ion should not be assumed to resemble the structure of the neutral molecule from which it was formed. Another problem is that the approximation, so useful in ground state chemistry, that electronic effects cannot be transferred far in unsaturated systems, becomes untenable in odd electron structures. In the view of these authors the above difficulties prevent clear-cut evidence supporting the case for or against charge localisation. They do make the point, however, that there is not a great deal of contention regarding the localisation of charge in even electron ions, e.g. 3 → (III), is essentially universally accepted, although the delocalizing effects mentioned above will be operative in this case as well.



Structures of radical-cations are often drawn depicting removal of one electron from an essentially localized lone-pair orbital thus producing a species in which the charge and unpaired electron density are sited at one atom, e.g. 4 → (IV).



In this picture the nett positive charge is regarded as residing in the heteroatom nucleus and the unpaired electron density in an orbital largely localized on the same heteroatom (in this case oxygen). As has been mentioned above for the ethylamine radical cation, the calculated charge distribution shows partial delocalisation of the charge away from the heteroatom

although a large proportion of the charge is retained on the heteroatom containing portion of the ion. The delocalisation fits with that expected from polarisation of the bonds from atoms directly attached to the proposed charge site, and therefore the picture given in (IV) above may still be useful if not entirely accurate. Williams and Beynon conclude by arguing that it is the radical site which is of primary importance and that the name "charge localisation" is perhaps unfortunate. They go on to consider the evidence for and against radical site localisation and to consider whether localized radical sites could trigger chemical reactions. On balance the evidence from a range of techniques indicates that localized unpaired electron density is possible, and is a useful concept in free radical reactions for example. By considering the bond weakening effect of a localized radical site and the effect on the appearance energy of the fragment ion produced by substitution in a series of related molecules, the authors conclude that the bond weakening effect of localized radical sites may be used to account for observed effects. The overall conclusion from their work was that the "charge-radical localisation" concept as used in mass spectrometry (and other areas of organic chemistry) is a model for which there is some experimental evidence, and if used with caution serves a useful purpose until an alternative and better model becomes available.

5.3 Computer Calculations

5.3.1 Amides and Thioamides

The simple amides have been the subject of many quantum chemical investigations primarily as model systems for peptides. Ottersen and co-workers published a series of papers on the x-ray crystallography of methanamide and ethanamide which were compared with ab-initio molecular orbital calculations on those molecules and N-methylmethanamide²⁷⁻²⁹. These results were used to study the differences in C-N and C-O bond lengths found for these compounds. The ab-initio calculations were used to see if the experimentally observed differences were reflected by the theoretical results, and also to study the effect of substitution on the electron population of the N-C=O fragment²⁹. One of the major sources of interest in

the amides is the modelling of hydrogen bonds between amide functions in peptides which play an important role in stabilizing peptide conformations. Fully optimized structures for methanamide, ethanamide, and their mono-N-methylated analogues were published in 1979 by Fogarasi and co-workers in an attempt to clarify uncertainties in the previously reported structures³⁰. Despite detailed studies by both microwave spectroscopy^{31,32} and electron diffraction³³ on methanamide, the microwave geometries differed considerably in C=O and C-N bond lengths as well as on the question of planarity in these molecules. Ottersen's previous studies had assumed planarity and performed partial geometry optimisation. By considering the out-of-plane force constant matrices for the compounds studied, Fogarasi et al. found all four of the amides to be planar. They also looked briefly at cis-trans isomerism around the amide C-N bond, finding the trans isomer of N-methyl methanamide to be 8.36 kJ mol^{-1} more stable than the corresponding cis isomer. They assumed that the situation in N-methyl ethanamide would be similar. Semi-empirical calculations by Kolaskar³⁴ and Ramachandran et al.³⁵ produced non-planar structures for all amides from methanamide to N-methyl ethanamide using the CNDO/2 method, while simultaneous calculations using the INDO method produced planar structures. Nalewajski reported a slightly non-planar structure for methanamide using a version of the MINDO/2 method and complete geometry optimisation³⁶, however Fogarasi et al.³⁰ repeated this calculation using the original MINDO/2 (37) and obtained a planar geometry. One possible explanation for this would be incomplete optimisation in Nalewajski's calculations caused by an extremely shallow potential along one or several coordinates, this is especially problematic if cartesian coordinates are used because they do not directly show the force acting along the critical coordinates. The paper by Fogarasi et al. also comments on the sensitivity of the conformation around a nitrogen atom to the basis set used in the calculations. Their calculations were performed using a 4-21 Gaussian basis set which is similar to the common 4-31G basis set³⁸ with a slight reduction. However, it should be noted that Christensen et al. obtained a slightly non-planar conformation for methanamide using a large spd basis set³⁹. Fogarasi et al. conclude that their work predicts a planar geometry but that it cannot definitely rule out a non-planar equilibrium structure. They then went on to examine

the accuracy of their calculated geometries in comparison with other calculated structures and with experimental data and concluded that the calculation of fully optimized geometries by ab-initio techniques was feasible for fairly large molecules. A detailed evaluation of the MINDO/3 semi-empirical method was carried out on methanamide, N-methyl methanamide and ethanamide by Defina and Andrews ⁴⁰. The results were compared with previous ab-initio studies and with experimental data to assess the accuracy of the MINDO/3 method. Also included in the study were some ureas and heterocycles which were all related to similar structures in biological systems, the authors concluded that MINDO/3 provided a good description of the geometries and electronic properties of the heteroatomic molecules studied and that the method had wide applicability to biological systems. A series of papers on ab-initio studies of amides was published by Radom and Riggs ⁴¹⁻⁴⁶. These authors used the standard STO-3G minimal basis set and the 4-31G split-valence basis set, to study the structures of some simple amides and to emphasise the conformational aspects of the structures obtained. These results in general supported the conclusions from the previous study of Fogarasi et al. ³⁰, and extended to a discussion of the most stable conformations of the simple amides studied and to the barriers to rotation for the methyl groups in the N-methyl analogues. The barriers to rotation for the N-methyl in the amides studied were all between 0 and 2.6 kJ mol⁻¹, much smaller than the 10.0 kJ mol⁻¹ for methyl groups attached to a nitrogen atom having a formal double bond, as opposed to the partial double bond in the amides. A further study on the rotational barriers of methyl groups in N-methyl ethanamide and N,N-dimethyl ethanamide was carried out using the PCILO quantum chemical method by Remko et al. ⁴⁷, as part of a study on hydrogen bond interactions of the peptidic bond with water, methanol and phenol. Several semi-empirical studies on thioamides have been performed with a particular view to investigating the relationship between the electronic structure and the reactivity of these compounds. A series of papers has been published by Guimon, Gonbeau and Pfister-Guillouzo et al. on the electronic structure of thiocarbonyl compounds ⁴⁸⁻⁵². In particular a generalized study relating the photoelectron spectra of a series of thiocarbonyl compounds to their CNDO/2 calculated properties, indicated that in all compounds the lowest ionisation potential was

associated with a non-bonding orbital mostly localized on the sulphur atom⁵². The energy of the bonding π and σ orbitals was also found to be very sensitive to the nature of the substituents on the thiocarbonyl group. The effect of N-methylation was found to be a lowering of the ionisation potential for the asymmetric π orbital largely located on nitrogen bringing it closer to, but not lower than, the energy of the non-bonding sulphur orbital. Two papers utilising Huckel Molecular Orbitals (HMO) in order to correlate the electronic structure of some thioamides with their reactivity and with their UV and IR spectra have been published by A.O. Fulea and C. Fulea^{53,54}. These papers considered protonated as well as non-protonated structures. In the non-protonated thioamides the UV spectra showed two maxima, the first at a wavelength around 360 nm which was associated with an $n \rightarrow \pi^*$ transition, and a second more intense band at 260-270 nm, associated with a $\pi \rightarrow \pi^*$ transition. No references to calculations on radical cations or on other ionic species of the thioamides have been found.

5.3.2 Ureas and Thioureas

A thorough and extensive ab-initio study of urea was published by Elbert and Davidson in 1974⁵⁵ using configuration interaction to go beyond the Hartree-Fock level of theory. The paper was mainly concerned with providing an unambiguous theoretical analysis of the nature of the lowest lying excited states of urea, including values for many of the parameters describing the charge distributions, which are of interest for comparison with high resolution spectral data for emission from the triplet states. Several semi-empirical calculations were also carried out for comparison with the elaborate ab-initio treatment, including Huckel, extended Huckel and CNDO/2 treatments. Two methods of population analysis were also utilised, the Mulliken method⁵⁶ using nonorthogonal atomic orbitals for which there is no bound on orbital occupancy and a method based on Lowdin orthogonalized atomic orbitals⁵⁷ for which the overlap population is zero and the occupancy always lies between 0.0 and 2.0. CNDO/2 calculations for the methyl and NN'-dimethyl urea molecules have been carried out by some Russian workers⁵⁸. These calculations were compared with an earlier calculation on

the urea molecule in an attempt to determine the effect of methyl substitution on the electronic structure and properties of the amides. In these calculations the geometry was selected on the assumption that the bond lengths were equal to the sum of the atomic radii and that the valence angles reflected the hybridisation of the atoms in the molecules. The results were used to discuss the changes in charge distribution and their effects on the molecular structures. The paper concluded that the behaviour of the ureas investigated broadly reflected their resonance structures, the high mobility of the π -electrons, and their ability to localize electron density within the amine or carbonyl regions of the molecules. The paper also indicated that methyl substitution leads to redistribution of the entire electron density within the amide molecule due to the flexibility of its π -electron system. The charge on the oxygen atom was found to be reduced which implies a reduction in the basic properties of the amide. Also no linear relationship was found between the number of methyl groups and the changes in the atomic charges or the bond energies.

No references to calculations specifically on thioureas have been found although there have been some calculations on organic sulphur compounds comparing them with the corresponding oxygen compounds ⁵⁹.

5.3.3 Charge Distributions and Mass Spectrometry

Charge distributions are one of the products of molecular orbital calculations on systems under study, although they are often not the reason for carrying out the calculations. As has been mentioned above, despite the number of MO calculations on various amide and urea systems, there have been no previous references to calculations for the radical cations of these molecules. However several other molecules and their ionic counterparts have been studied and there have been a few previous attempts to rationalize mass spectra on the basis of the calculated charge distribution in the radical cations. Among these studies the work of Lorquet and co-workers on ethylamine has already been mentioned, with their conclusion that the charge in the radical cation was substantially delocalized. Other molecular orbital studies on charge distributions and their relationship to the observed mass spectra include a series of

papers by Hirota and co-workers on the fragmentation of higher normal alkanes⁶⁰⁻⁶⁵. In these papers the mass spectra of higher normal alkanes, tridecane and hexadecane among others, were measured over a wide range of ion source temperatures and ionizing voltage. The intensity of the C3 and C4 fragments was observed to decrease with decreasing temperature and ionizing voltage and this finding was explained by assuming that the fragmentations could be classified into two processes; a fast process and a slow process. Further, it was assumed that the MO calculated charge distributions could be applied to the fast process while the statistical theory applied to the slow process^{64,65}. This reasoning implies non-ergodic behaviour for the superexcited hydrocarbon molecular ions fragmenting via the "fast-process", since they are assumed to be fragmenting before the excess internal energy can be randomized. Hirota's MO theory assumed that the charge density at each bond of a highly excited molecular ion, produced by electron bombardment, is equal to the electron density at the bond in the highest occupied molecular orbital of the neutral molecule. The electron distribution in the neutral molecule was calculated using the linear combination of bonding orbitals (LCBO) approximation of Huckel's method, with the CH₃ and CH₂ groups being regarded as united "atoms". This method is a very crude approximation but was shown to be sufficient in the case of normal octane⁶⁵, for estimating the relative electron density of its skeletal bonds. The authors concluded that their data was in good agreement with predictions from the MO theory, particularly at reduced source temperature and low ionizing voltage. This was stated to be because the "slow-process" is virtually eliminated under these conditions, due to the ion being sufficiently excited to undergo rapid bond cleavage but no further fragmentation. It was also stated that too low an ionizing energy would probably lead to large numbers of ordinary excited ions undergoing slow decomposition and that the lower limit for the ionizing voltage was in keeping with papers by Platzman⁶⁶ and by Hatano and Shida⁶⁷ who have quantitatively estimated the fractions of ions and excited species produced from super-excited species⁶⁶. Hirota et al. claim that criticisms of their MO method for rationalising fragmentation from radical cations can now be explained and that the use of higher levels of MO theory to calculate the electron density will allow the range of compounds studied to

include branched chain alkanes. Finally they comment on the applicability of the MO method to compounds containing "lone-pair" electrons such as ketones and amines⁶⁸. From studies on propylamine they found that the discrepancy between theory and experiment increased as the ionizing voltage was lowered, in contrast to the situation for the alkanes. They explain this as being due to an increase in the abundance of the ordinary excited ion with excess energy as the ionizing voltage decreases. This increase in the fraction of excited ions fragmenting via the "slow-process" leads to a corresponding increase in the fragment ions observed for this process, relative to those formed via the "fast-process" from the highly excited species and since the electron density is greatest at the lone-pair of the highly excited species, scission of the C-C bonds is relatively more difficult (this is discussed in more detail in Ref. (65)). A similar double fragmentation scheme has been independently proposed by Miyazaki from studies on the gamma-ray radiolysis of butane⁶⁹, where a fast fragmentation process with a rate constant of the order of 10^{12} sec^{-1} was assumed in order to rationalize some of the observed fragmentation. Since the fragmentation caused by gamma-rays is now ascribed mainly to the effect of slow secondary electrons (delta-electrons), Hirota et al. used a similar fast process in their interpretation of mass spectra. The papers by Hirota and co-workers are interesting in that they are the only group who have calculated charge distributions and related them to mass spectrometric fragmentation reactions to have also considered the kinetics of the reactions. The consideration of the kinetics is rudimentary and appears to be included because it helps to explain the observed results and there is no detailed analysis. However the papers raise an important point, because the kinetics of the fragmentation reactions are generally ignored when charge distributions are calculated. In fact there is usually only a limited attempt to involve the thermodynamic behaviour of the ions as well, and it must not be forgotten that the charge site alone, assuming that one exists, cannot be responsible for causing fragmentation reactions. A further study by Loew et al. used an Iterative Extended Huckel Theory (IEHT) method and Mulliken population analysis to calculate values for bond densities and net atomic charges for the neutral molecule and the corresponding positive ion of the steroid hormone estrone⁷⁰. They concluded that the calculated net charges appeared to be unrelated to fragmentation

processes, but that calculated bond densities of the ground state molecular ion of estrone did allow prediction of the gross features of the fragmentation. They also speculated that bond densities calculated for the excited states of the molecular ion of estrone might provide a basis for finer distinction between sites of initial bond cleavage, information which is crucial to rationalisation of subsequent fragmentation of the molecular ion. Very recently Hrusak and co-workers have published several papers describing the results of a semi-empirical molecular orbital study of fragmentations in mass spectrometry⁷¹⁻⁷⁴. These authors have also considered that the changes in electron densities and in geometrical parameters produced on ionisation of a molecule may play a major role in determining the subsequent fragmentation of the ion. Many of the results which they describe parallel those described in this thesis and the use of semi-empirical molecular orbital methods seems to produce the same conclusions as the results of the ab-initio investigation described here. The systems studied by Hrusak et al. include a range of substituted acetyl compounds including acetamides where direct comparison with the data in this thesis is possible. The results of such a comparison indicate that the MNDO semi-empirical method provides good geometries and charge distributions for both neutral molecules and their radical cations. The latter could not be assumed *a priori* due to the parametrization of the MNDO method on the ground state experimental data from neutral molecules. The ab-initio method was used in this study in order to avoid the possibility of the semi-empirical methods giving spurious information for the radical cation systems under study due to their parametrization using experimental data for ground state neutral molecules. The work of Hrusak *et al*, however, appears to show that this may not be an important factor at least for systems with 'classical' structures. Hrusak and co-workers considered the atomic charges and how the calculated charges could be used to obtain a measure of the polarity of the bonds between pairs of atoms in the ion structures. They then related the calculated bond polarity to the fragmentation observed in EI mass spectrometry. These workers also tried to relate the calculated bond polarity to the length of the bond calculated by the MNDO method, however, despite some correlations being observed this approach is fraught with difficulty and was abandoned in this study due to the fact that most of the bond lengths calculated for the

neutral structures show increases on ionisation. This is not entirely unexpected since the removal of an electron from the system leads to an electronic reorganisation and a small increase in the bond lengths calculated for the radical cation over those calculated for the neutral molecule. Many of the earlier studies mentioned above also made use of semi-empirical methods of varying degrees of sophistication and were generally related to one or two distinct structures. This made a definitive conclusions difficult to reach because each method used was parametrized differently and to a greater or lesser degree of accuracy which was dependent upon the quality of the experimental data used. It has been stated previously that radical cations are characterised by flatter potential energy surfaces and increased bond lengths⁷⁵, relative to the corresponding neutral molecules, the calculations carried out in this study are in agreement with this.

5.4 References

1. J.A. Gilpin, *Analytical Chemistry*, **31**, 935-9 (1959).
2. J.H. Beynon, *Mass Spectrometry and its application to Organic Chemistry*, Elsevier, Amsterdam, 1960.
3. K. Biemann, *Mass Spectrometry, Organic Chemical Applications*, McGraw Hill, New York, 1962.
4. H. Budzikiewicz, C. Djerassi and D.H. Williams, *Mass Spectrometry of Organic Compounds*, Holden-Day, San Francisco, 1967.
5. J.H. Beynon, R.A. Saunders and A.E. Williams, *The Mass Spectra of Organic Molecules*, Elsevier, New York, 1968.
6. F.W. McLafferty, *The Interpretation of Mass Spectra*, 3rd Edn., University Science Books, 1980.
7. R.A.W. Johnstone, *Mass Spectrometry for Organic Chemists*, Cambridge University Press, London, 1972.
8. M.E. Rose and R.A.W. Johnstone, *Mass Spectrometry for Chemists and Biochemists*, Cambridge University Press, Cambridge, 1982.
9. M.A. Baldwin, P.C. Cardnell, A.G. Loudon, A. Maccoll, and K.S. Webb, *Advances in Mass Spectrometry*, Vol. 5, Institute of Petroleum, 666-669,
10. M.A. Baldwin, A.G. Loudon, A. Maccoll, and K.S. Webb, *Org. Mass Spectrom.*, **11**, 1181 (1976).
11. M.A. Baldwin, A. Kirzien-Konasiewicz, A.G. Loudon, A. MacColl, and D. Smith, *Chemical Communications*, 574 (1966).
12. M.A. Baldwin, A. Kirzien-Konasiewicz, A.G. Loudon, A. MacColl, and D. Smith, *J. Chem. Soc. (B)*, 34-40 (1968).
13. M.A. Baldwin, A.G. Loudon, A. Maccoll, and D. Smith, *Chemical Communications*, 350 (1967).
14. J.M. Ruth and R.J. Philippe, *Analyt. Chem.*, **38**, 720 (1966).

15. M.A. Baldwin, A.M. Kirkien, A.G. Loudon, and A. Maccoll, *Org. Mass Spectrom.*, **4**, 81-88 (1970).
16. H. Binder, *Monatsh. Chem.*, **98**, 431 (1967).
17. R.H. Shapiro, J.W. Serum, and A.M. Duffield, *J. Org. Chem.*, **33**, 243 (1968).
18. M.A. Baldwin, A. Maccoll, A. Kirkien-Konasiewicz, and B. Saville, *Chemistry and Industry*, 286-287, 1966.
19. G.W. Mines and H.W. Thompson, *Spectrochimica Acta*, **31A**, 137-142 (1975).
20. M.A. Baldwin, A.G. Loudon, K.S. Webb, and P.C. Cardnell, *Org. Mass Spectrom.*, **12**, 279-282 (1977).
21. K. Watanabe and J.R. Mottl, *J. Chem. Phys.*, **26**, 1773 (1957).
22. F.W. McLafferty, *Chem. Commun.*, **78** (1966).
23. T.W. Bentley, R.A.W. Johnstone, and F.A. Mellon, *J. Chem. Soc. (B)*, 1800 (1971).
24. C. Krier, J.C. Lorquet, and A. Berlingin, *Org. Mass Spectrom.*, **8**, 387 (1974).
25. F.W. McLafferty, in *Recent Developments in Mass Spectrometry*, (K. Ogata and T. Hayakawa, Eds.), University Park Press, Baltimore, p70, 1970.
26. D.H. Williams and J.H. Beynon, *Org. Mass Spectrom.*, **11**, 103 (1976).
27. T. Ottersen, H.H. Jensen, R. Johansen, and E. Wisloff-Nilssen, *J. Mol. Struct.*, **30**, 379 (1976).
28. T. Ottersen, *J. Mol. Struct.*, **26**, 365 (1975).
29. T. Ottersen, *Acta Chemica Scandinavica A*, **29**, 939-944 (1975).
30. G. Fogarasi, P. Pulay, F. Torok, and J.E. Boggs, *J. Mol. Struct.*, **57**, 259-270 (1979).
31. C.C. Costain and J.M. Dowling, *J. Chem. Phys.*, **32**, 158 (1960).
32. E. Hirota, R. Sugisaki, C.J. Neilsen, and G.O. Sorensen, *J. Mol. Struct.*, **49**, 251 (1974).
33. M. Kitano and K. Kuchitsu, *Bull. Chem. Soc. Japan*, **47**, 67-72 (1974).
34. A.S. Kolaskar, A.V. Lakshminarayanan, K.P. Sarathy, and V. Sasisekhran, *Biopolymers*, **14**, 1081 (1975).

35. G.N. Ramachandran, A.V. Lakshminarayanan, and A.S. Kolaskar, *Biochim. Biophys. Acta*, **303**, 8 (1973).
36. R.F. Nalewajski, *Z. Naturforsch., Teil A*, **32**, 276 (1977).
37. N. Bodor, M.J.S. Dewar, A. Harget, and E. Haselbach, *J. Amer. Chem. Soc.*, **92**, 3854 (1970).
38. R. Ditchfield, W.J. Hehre, and J.A. Pople, *J. Chem. Phys.*, **54**, 724 (1971).
39. D.H. Christensen, R.N. Kortzeborn, B. Bak, and J.J. Led, *J. Chem. Phys.*, **53**, 3912 (1970).
40. J.A. Defina and P.R. Andrews, *Int. J. Quant. Chem.*, **18**, 797-810 (1980).
41. N.R. Carlsen, L. Radom, N.V. Riggs, and W.R. Rodwell, *J. Amer. Chem. Soc.*, **101**, 2234 (1979).
42. L. Radom and N.V. Riggs, *Aust. J. Chem.*, **33**, 249 (1980).
43. L. Radom and N.V. Riggs, *Aust. J. Chem.*, **33**, 1635 (1980).
44. L. Radom and N.V. Riggs, *Aust. J. Chem.*, **33**, 2337 (1980).
45. L. Radom and N.V. Riggs, *Aust. J. Chem.*, **34**, 7 (1981).
46. L. Radom and N.V. Riggs, *Aust. J. Chem.*, **35**, 1071 (1982).
47. M. Remko, I. Sekerka, and V. Frecer, *Coll. Czech. Chem. Commun.*, **48**, 3214 (1983).
48. C. Guimon, D. Gonbeau and G. Pfister-Guillouzo, *J. Mol. Struct.*, **16**, 271 (1973).
49. U. Berg and J. Sandstrom, *Acta Chem. Scand.*, **20**, 689 (1966).
50. C. Guimon, D. Gonbeau and G. Pfister-Guillouzo, *Tetrahedron*, **29**, 3399 (1973).
51. M. Arbelot, C. Guimon, D. Gonbeau and G. Pfister-Guillouzo, *J. Mol. Struct.*, **20**, 487 (1974).
52. C. Guimon, D. Gonbeau and G. Pfister-Guillouzo, *J. Electron Spectrosc. Relat. Phenom.*, **4**, 49 (1974).
53. F. Comea, C. Fulea and A.O. Fulea, *Rev. Roumaine Chim.*, **18**, 111 (1973).
54. A.O Fulea and C. Fulea, *Rev. Roumaine Chim.*, **22**, 1513 (1977).
55. K. Elbert and E.R. Davidson, *Int. J. Quant. Chem.*, **8**, 857 (1974).
56. R.S. Mulliken, *J. Chem. Phys.*, **23**, 1833, 1841, 2338, 2343 (1955).

57. P.-O. Lowdin, *J. Chem. Phys.*, **18**, 365 (1950).
58. D.G. Medikhanov, V.P. Korobochkin, and A.A. Shchepetkin, (Inst. Metall., Sverdlovsk, USSR). Deposited document, 1982.
59. T. Matsushita, Y. Osamura, N. Misawa, K. Nishimoto, and Y. Tsuno, *Bull. Chem. Soc. Japan*, **52**, 2521 (1979).
60. K. Hatada and K. Hirota, *Bull. Chem. Soc. Japan*, **38**, 599 (1965).
61. K. Hirota, Y. Niwa and I. Fujita, *J. Phys. Chem.*, **73**, 464 (1969).
62. K. Hirota, I. Fujita, M. Yamamoto, and Y. Niwa, *J. Phys. Chem.*, **74**, 410 (1970).
63. K. Hirota, Y. Niwa, and I. Fujita, *Z. Physik. Chem. (N.F.)*, **67**, 244 (1969).
64. K. Fueki and K. Hirota, *Nippon Kagaku Zasshi*, **80**, 1202 (1959).
65. K. Hirota and Y. Niwa, *J. Phys. Chem.*, **72**, 5 (1968).
66. R. Platzmann, Proc. of the third Intern. Congr. of Radiation Res., 1966, G. Silini Ed., North Holland Publ. Co., Amsterdam, 1967, p20.
67. Y. Hatano and Shida, *Bull. Chem. Soc. Japan*, **41**, 1126 (1968).
68. T. Miyazaki, *J. Phys. Chem.*, **71**, 4148 (1967).
69. K. Hirota and M. Itoh, *Bull. Chem. Soc. Japan*, **39**, 1406 (1966).
70. G. Loew, M. Chadwick and D. Smith, *Org. Mass Spectrom.*, **7**, 1241 (1973).
71. J. Hrusak and M. Tkaczyk, *Org. Mass Spectrom.*, **24**, 989 (1989).
72. M. Tkaczyk and J. Hrusak, Symposium on Quantum Chemistry, High Tatra, Czech., October 1988, abstract p50.
73. J. Hrusak and M. Tkaczyk, *Rapid Commun. in Mass Spectrom.*, **4**, 178-180 (1990).
74. J. Hrusak and M. Tkaczyk, *Org. Mass Spectrom.*, **25**, 214 (1990).
75. P.J. Derrick and K.F. Donchi, in *Comprehensive Chemical Kinetics*, Vol 24, (C.H. Bamford and C.F.H. Tipper Eds.), Elsevier, Amsterdam, 1983.

6. Results and Discussion.

6.1 Introduction

The results from the ab-initio molecular orbital calculations on a series of simple amides, ureas and their thio- analogues are presented and discussed in this chapter. The calculations were performed using the GAUSSIAN-82 program of Pople et al.¹, running on a Cray-1S computer; and later on a Cray XMP/28 computer at the University of London Computer Centre, as detailed in chapter 4. For some of the larger urea and thiourea systems the semi-empirical molecular orbital program AMPAC was used on a Silicon Graphics Iris workstation because the structures were becoming too large for a full ab-initio study to be performed. The calculated charge distributions were determined for both the neutral molecules and their corresponding radical cations, with a view to studying the concept of charge localisation in the radical cations. This data is then compared with mass spectrometric data on these compounds to see if observed differences in their fragmentation behaviour could be rationalized on the basis of charge localisation within the ionic species. The concept of charge localisation has been useful in mass spectrometry in rationalizing fragmentation mechanisms but it has not met with universal support.

More than twenty years ago the ionisation energies (IE's) of urea and thiourea and their N-methylated analogues were measured², these results showed that methylation at a nitrogen reduced the IE of urea much more than it did for thiourea, and that dimethylation at a single nitrogen affected the IE of urea more than N,N'-dimethylation. These observations led to the conclusion that the charge was located on a nitrogen atom in the urea radical cations but on the sulphur atom in thiourea and that this was consistent with observed differences in the fragmentation behaviour of these compounds, in particular the observation of ions due to [M-SH]⁺ from the thioureas with no corresponding ions being observed from the ureas. Later measurements on some related amides appeared to confirm these conclusions³, although a photoelectron study had suggested that the molecular orbitals were ordered such that the loss of an electron on ionisation should have been from an oxygen lone pair orbital rather than from

the nitrogen lone pair orbital as indicated by the mass spectrometric results⁴.

The molecular orbital study presented here was undertaken to ascertain whether any theoretical evidence could be obtained in support of the charge localisation concept for these compounds.

6.2 Amides and Thioamides

6.2.1 Methanamides and Thiomethanamides

The compounds studied in this section were methanamide, thiomethanamide and their N-methylated analogues (see figure 6.1).

The major bond lengths, bond angles and charge distributions calculated at the 3-21G^{*} level of theory are given for the neutral molecules **1** to **6** and the radical cations **1^{•+}** to **6^{•+}** in tables 6.1 to 6.6 respectively. The data for the radical cations **1^{•+}** to **6^{•+}** is for the optimised ion geometries, as mentioned in Chapter 4, the radical cations were also calculated at the same geometry as the neutral molecule and this data is presented in the tables as **1^{•+}** to **6^{•+}**. The neutral molecular geometries calculated in this work are all in good agreement with results from previous calculations⁵⁻⁷, and with gas-phase electron diffraction data^{8,9}.

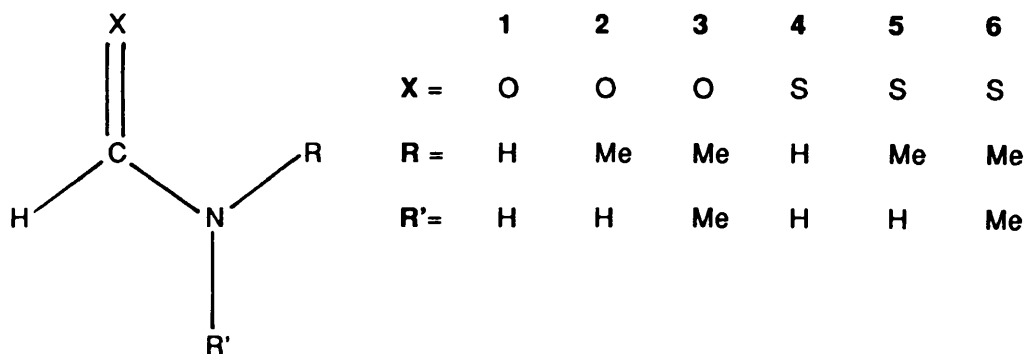


Figure 6.1 Key to the methanamides and thiomethanamides studied.

Table 6.1

3-21G^{*} Ab-Initio molecular orbital results forMethanamide neutral **1** and radical cations **1⁺** and **1'⁺**.

Parameter	1	1⁺	1'⁺
bond lengths / Ångstroms			
C--O	1.212	1.311	1.212
C--N	1.353	1.276	1.353
C--H	1.084	1.075	1.084
N--H	0.995	1.010	0.995
N--H'	0.998	1.008	0.998
bond angles / Degrees			
<HCO	122.43	114.52	122.43
<HCN	112.26	122.16	112.26
<OCN	125.31	123.32	125.31
<CNH	119.39	122.48	119.39
<CNH'	122.00	121.24	122.00
Mulliken atomic charges			
O	-0.60	-0.20	-0.18
C	+0.62	+0.68	+0.66
H	+0.19	+0.42	+0.43
N	-0.92	-0.84	-0.82
H	+0.36	+0.47	+0.46
H'	+0.35	+0.47	+0.45

Table 6.2

3-21G^{*} Ab-Initio molecular orbital results forN-methyl methanamide **2**, and its radical cations **2⁺** and **2²⁺**.

Parameter	2	2⁺	2²⁺
bond lengths / Ångstroms			
C--O	1.215	1.299	1.215
C--N	1.349	1.338	1.349
C--H	1.084	1.069	1.084
N--R	1.464	1.511	1.464
N--H'	0.995	1.015	0.995
bond angles / Degrees			
<HCO	122.59	122.61	122.59
<HCN	113.18	119.28	113.18
<OCN	124.23	118.11	124.23
<CNR	120.26	123.45	120.26
<CNH	120.14	118.48	120.14
Mulliken atomic charges			
O	-0.61	-0.29	-0.31
C	+0.63	+0.54	+0.56
H	+0.19	+0.36	+0.34
N	-0.89	-0.62	-0.59
R	+0.32	+0.54	+0.50
H	+0.36	+0.47	+0.48

Table 6.3

3-21G^{*} Ab-Initio molecular orbital results for N,N'-dimethyl
methanamide **3**, and its radical cations **3⁺** and **3²⁺**.

Parameter	3	3⁺	3²⁺
bond lengths / Ångstroms			
C--O	1.216	1.282	1.216
C--N	1.350	1.357	1.350
C--H	1.084	1.070	1.084
N--R	1.466	1.506	1.466
N--R'	1.457	1.492	1.457
bond angles / Degrees			
<HCO	122.40	122.90	122.40
<HCN	113.18	118.29	113.18
<OCN	124.41	118.81	124.41
<CNR	117.87	120.14	117.87
<CNR'	122.42	121.01	122.42
Mulliken atomic charges			
O	-0.62	-0.32	-0.33
C	+0.65	+0.55	+0.58
H	+0.19	+0.34	+0.31
N	-0.87	-0.60	-0.61
R	+0.33	+0.53	+0.53
R'	+0.33	+0.51	+0.54

Table 6.4

3-21G^{*} Ab-Initio molecular orbital results for
thiomethanamide **4**, and its radical cations **4⁺** and **4²⁺**.

Parameter	4	4⁺	4²⁺
bond lengths / Ångstroms			
C--S	1.639	1.690	1.639
C--N	1.331	1.287	1.331
C--H	1.077	1.078	1.077
N--H	1.000	1.007	1.000
N--H'	0.998	1.007	0.998
bond angles / Degrees			
<HCS	120.30	115.64	120.30
<HCN	113.26	117.29	113.26
<SCN	126.43	127.07	126.43
<CNH	119.71	123.22	119.71
<CNH'	121.98	121.10	121.98
Mulliken atomic charges			
S	-0.20	+0.48	+0.51
C	+0.04	+0.05	+0.02
H	+0.26	+0.38	+0.38
N	-0.86	-0.81	-0.80
H	+0.39	+0.45	+0.44
H'	+0.37	+0.45	+0.45

Table 6.5

3-21G^{*} Ab-Initio molecular orbital results for N-methyl
thiomethanamide **5**, and its radical cations **5⁺** and **5²⁺**.

Parameter	5	5⁺	5²⁺
bond lengths / Ångstroms			
C--S	1.643	1.697	1.643
C--N	1.327	1.281	1.327
C--H	1.077	1.077	1.077
N--R	1.467	1.494	1.467
N--H	0.998	1.007	0.998
bond angles / Degrees			
<HCS	119.79	115.52	119.79
<HCN	113.16	118.11	113.16
<SCN	127.05	126.37	127.05
<CNR	123.32	124.90	123.32
<CNH	118.87	118.40	118.87
Mulliken atomic charges			
S	-0.21	+0.43	+0.47
C	+0.05	+0.06	+0.03
H	+0.25	+0.37	+0.37
N	-0.83	-0.78	-0.77
R	+0.36	+0.47	+0.47
H	+0.37	+0.45	+0.44

Table 6.6

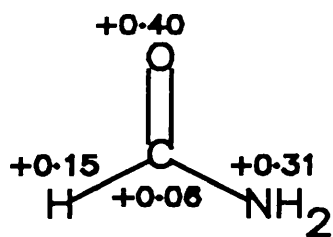
3-21G* Ab-Initio molecular orbital results for N,N-dimethyl
thiomethanamide **6**, and its radical cations **6^{•+}** and **6^{••+}**.

Parameter	6	6^{•+}	6^{••+}
bond lengths / Ångstroms			
C--S	1.648	1.706	1.648
C--N	1.325	1.323	1.325
C--H	1.077	1.073	1.077
N--R	1.471	1.506	1.471
N--R'	1.468	1.499	1.468
bond angles / Degrees			
<HCS	119.23	119.57	119.23
<HCN	113.28	116.04	113.28
<SCN	127.49	124.39	127.49
<CNR	120.62	123.18	120.62
<CNR'	121.90	120.62	121.90
Mulliken atomic charges			
S	-0.23	+0.33	+0.33
C	+0.07	-0.05	-0.05
H	+0.25	+0.34	+0.33
N	-0.81	-0.61	-0.62
R	+0.38	+0.49	+0.52
R'	+0.34	+0.50	+0.52

No data was available on the structures of the radical cations for these compounds so no comparisons of the ion structures obtained were possible. Recently however, Hrusak and co-workers have published some MNDO calculations on substituted carbonyl compounds¹⁰ and their data for some of the amide radical cations is in good agreement with the results reported here. All molecules and radical cations studied in this section were calculated to be planar, within the accuracy of the experimental method and therefore the dihedral angles are not listed. Similarly, all C-H bond lengths and angles in methyl groups were calculated to be close to the expected values for sp³ carbon and these values are also not listed in these tables for reasons of clarity, although all the above mentioned parameters were optimised and planarity was not assumed. The change in atomic charges on going from the neutral molecule to the corresponding radical cation are given in figure 6.2 below, for the methanamides and thiomethanamides. This data is obtained by considering the difference between the atomic charges calculated for the neutral molecules and those calculated for the geometry optimized radical cations. The charge distribution data presented in tables 6.1 to 6.6 emphasizes that there is an uneven distribution of electrons in these molecules before ionisation occurs, since N, O and S all act as electronegative centres. The data presented in the tables gives the actual calculated charge distribution in the neutrals and in the radical cations. The N and O atoms both have net negative charges, even after ionisation, and S is the only heteroatom calculated to become positive. However Figure 6.2 shows where net gain or loss of electrons occurs on formation of the radical cations and thereby indicates whether or not the electron deficiency is localised on particular atoms or groups in the ion. The radical cations have been calculated at two different geometries as indicated above and by the results presented in the tables.

These two geometries correspond to : (i) the same geometry as the neutral molecule, i.e. the structure of the radical cation immediately after ionisation and before any nuclear movement has occurred; and (ii) the optimised geometry for the radical cation, i.e. the structure of the radical cation after allowing for electron redistribution and nuclear movement in order to attain a more stable configuration after ionisation. As may be expected the charge is slightly more localised in the initial radical cation where the electron is removed from the highest occupied

Methanamides



Thiomethanamides

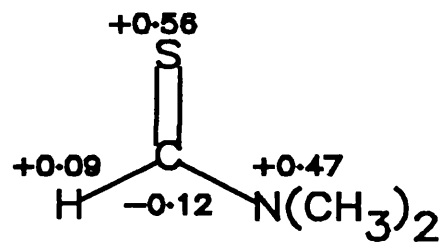
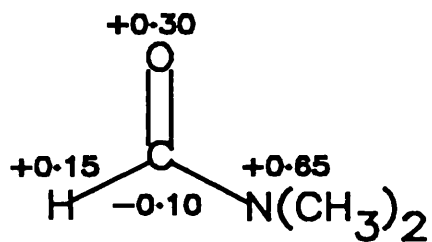
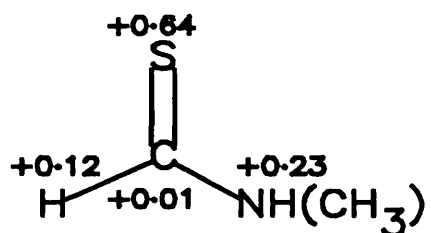
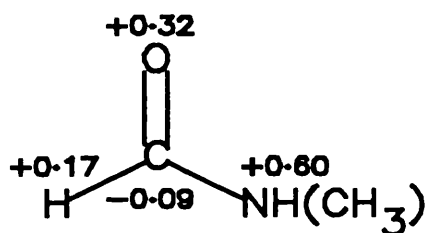
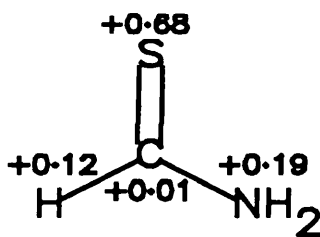


Figure 6.2. Calculated net changes in charge distribution on ionisation for the methanamides and thiomethanamides 1 to 6.

molecular orbital of the neutral molecule. More delocalisation is observed in the optimised radical cation where the electronic structure has been allowed to reorganise itself to minimise the potential energy of the ion, however even allowing for electronic reorganisation the data in Figure 6.2 indicates significant correlation of the change in charge distribution in the amides and thioamides studied with the experimental observations from ionisation energy measurements mentioned above. The theoretical calculations also give the orbital energies for all the calculated molecular orbitals associated with a given structure.

These results have been used to calculate the ionisation energies, IE's, for the two highest occupied molecular orbitals of each structure studied. This data is presented in Table 6.7 and has been calculated using Koopmans' theorem, the values have then been scaled by 0.92 following Brundle et al⁴. Experimental values from photoelectron spectroscopy (PES)^{4,11} and electron impact mass spectrometry (EIMS)³ are provided for the purposes of comparison with the data obtained by calculation and these are presented in table 6.9. The results of these calculations show substantial differences in the site of electron loss associated with the formation of the radical cations of the methanamides and thiomethanamides and provide a somewhat surprising degree of correlation with the previously determined experimental data.

Table 6.7

HOMO's and I.E.'s calculated for the methanamide and thiomethanamide neutral molecules studied.

	HOMO	2-HOMO	E(HOMO)	E(2-HOMO)	I.E.	2-I.E.
1	2A''	10A'	-0.40196	-0.41847	10.06	10.48
2	3A''	13A'	-0.37955	-0.41393	9.50	10.36
3	4A''	16A'	-0.35984	-0.41049	9.01	10.48
4	13A'	3A''	-0.32293	-0.33376	8.09	8.35
5	16A'	4A''	-0.31685	-0.32547	7.93	8.15
6	19A'	5A''	-0.31171	-0.31500	7.80	7.89

All orbital energies are in the atomic units of Hartrees, whilst all ionisation energies (IE's) are reported in electron volts (eV).

In the thioamides, electron loss is largely from a non-bonding molecular orbital associated with a sulphur lone pair of electrons. This is in contrast to the situation in the methanamides where the electron loss is largely associated with a non-bonding orbital which is a combination of the nitrogen lone pair and the carbonyl electrons. The largest change in the charge distributions brought about by methylation occurs for methanamide, where electron loss which previously involved both N and O, becomes largely centred on N after N-methylation. The effect of N,N-dimethylation is a further small increase in the electron loss from N at the expense of that from O. For thiomethanamide, where the electron loss is largely located on S, the effect of N-methylation is barely significant although there is a small increase in the electron loss from N with a corresponding decrease in the loss observed from S. A more significant change occurs with N,N-dimethylation where the electron loss from sulphur is substantially reduced with a corresponding increase in the electron loss from nitrogen. The losses of electronic charge from the above molecules on ionisation is seen to correlate with loss of an electron from the highest occupied molecular orbital (HOMO) calculated for each molecule (see table 6.7). Thus in thiomethanamide the HOMO is calculated to be the 13A' non-bonding orbital which corresponds to a sulphur lone-pair orbital, with an ionisation energy of 8.09 eV. The second highest occupied molecular orbital is calculated to be the 3A'' non-bonding orbital which corresponds to an orbital containing the nitrogen lone-pair and carbonyl π -electrons. This orbital ordering remains the same throughout the thiomethanamide series studied, although the effect of N-methylation is to reduce the energy difference between the two orbitals. In the case of methanamide the HOMO is calculated to be the 2A'' non-bonding orbital corresponding to an orbital containing the nitrogen lone-pair and the carbonyl electrons; whilst the oxygen lone-pair orbital, 10A' in this case, becomes the second highest occupied molecular orbital. Thus the orbital ordering is reversed in the methanamides compared to that calculated for the thiomethanamides. Also the effect of N-methylation is to increase the energy difference between the orbitals throughout the methanamide series studied. These trends are also

Table 6.8

Mulliken Symmetry Symbols.

Symbol	Meaning
A	Symmetrical with respect to a $360^\circ/n$ rotation about an n-fold principle axis.
B	Antisymmetrical with respect to a $360^\circ/n$ rotation about an n-fold principle axis.
E	Doubly degenerate.
T	Triply degenerate.
Subscripts	
1	Symmetrical with respect to a 180° rotation about a C_2 axis perpendicular to the principle axis, or with respect to reflection in a σ_v plane if no such C_2 axis exists.
2	Antisymmetrical with respect to a 180° rotation about a C_2 axis perpendicular to the principle axis, or with respect to reflection in a σ_v plane if no such C_2 axis exists.
g	Symmetrical with respect to inversion.
u	Antisymmetrical with respect to inversion.
Superscripts	
'	Symmetrical with respect to reflection in a σ_h plane.
"	Antisymmetrical with respect to reflection in a σ_h plane.

reflected in the calculated ionisation energies, which show changes of about 0.5 eV for each N-methylation of methanamide, where the methyls are proposed to be stabilizing the charge

site on the nitrogen; but only 0.15 eV for each N-methylation of thiomethanamide, where the methyls are remote from the charge site.

In general, molecular orbitals are described according to their symmetry, this convention has been used throughout this study and table 6.8 shows the Mulliken symmetry symbols with their meanings. The difference in the symmetry of the orbitals as indicated by the superscript ' or " also indicates that the electron loss is occurring from orbitals in different environments and is further evidence for the correct assignment of the orbitals (see table 6.8).

Table 6.9

Comparison of calculated and experimentally determined I.E.'s for the methanamides and thiomethanamides studied.

	Gaussian-82 3-21G* (This work)				Photoelectron Spectroscopy				M.S.
	1-MO	1-IE	2-MO	2-IE	1-MO	1-IE	2-MO	2-IE	IE
1	2A"	10.06	10A'	10.48	10A'	10.32	2A"	10.52	10.50
2	3A"	9.50	13A'	10.36	3A"	9.87	13A'	10.05	10.05
3	4A"	9.01	16A'	10.28	4A"	9.25	16A'	9.77	9.45
4	13A'	8.09	3A"	8.35	--	8.69	--	--	--
5	16A'	7.93	4A"	8.15	--	--	--	--	--
6	19A'	7.80	5A"	7.89	--	8.16	--	--	--

The orbital assignments from PES agree with our calculated assignments with one notable exception. In the case of methanamide the PES assignment gives the HOMO as 10A' and the second highest molecular orbital as 2A" which is a reversal of our calculated ordering. For the N-methylated methanamides the PES assignments agree with our calculated ordering of the MO's, and it has been suggested that the calculated ordering of the MO's would be reversed

so that they agreed with the PES ordering for methanamide if electron correlation was included in the calculations ¹¹. However, the IE differences and the calculated charge distributions support our calculated orbital ordering, and methanamide shows the largest geometry changes on ionisation, which may be consistent with removal of an electron from a delocalized orbital. It should also be pointed out that calculations at the Hartree-Fock level of theory, as is the case with those reported here, may be subject to error where the orbitals are calculated to be close in energy. The calculations for methanamide and thiomethanamide were repeated using Moller-Plesset perturbation theory, terminated at the third order, to account for electron correlation. The results obtained showed the same ordering for the highest occupied molecular orbitals as the previous calculations. The results presented here do not agree with the PES data in this case. It would seem likely that the PES bands have been miss-assigned due to the complexities of the vibrational fine structure. The Mulliken population analysis technique has been criticised for being such an arbitrary method of assigning the electron density between two atoms, to the individual atoms. Whilst this is a valid criticism, it is also true that any other method of dividing up the electron population of the overlap integrals will also be arbitrary to some extent and therefore may not necessarily improve the situation. Other methods for dividing the electron population of the overlap integrals have been proposed but Mulliken analysis is still the most widely used. More specific criticisms of the Mulliken method have been made by Reed et al, whose natural population analysis technique ¹² overcomes many of the problems associated with the Mulliken method and is rapidly becoming more widely used for the calculation of atomic charges. These authors have stated that Mulliken analysis is unsatisfactory in that: (i) it can yield negative values for electron distribution, which clearly has no physical meaning; (ii) it is unduly sensitive to the size of the basis set; and (iii) it gives poor results for highly polar or ionic compounds ¹². With regard to these points it can be stated that in the present study: (i) has not occurred; point (ii) has been investigated by repeating some of the calculations using the 6-31G^{*} basis set. This basis set allows the participation of d-symmetry functions on all heavy atoms and although differences in the calculated total atomic charges were observed (see table 6.10 and 6.11), they did not alter any of the conclusions

reached; and (iii) is not applicable in this particular study. Mulliken analysis is also known to over-emphasize the population of sulphur d-orbitals, however it is anticipated that systematic errors of this type will cancel in a comparison of this kind. The fact that electron correlation has not been used in this study may also introduce some systematic errors which may affect the calculated electron distributions; however, constraints on the amount of computer time available and the need to be able to directly compare all the results obtained precluded the use of electron correlation in all but a few of these calculations. The Gaussian-82 program performs the Mulliken population analysis on the uncorrelated wavefunctions and these results could not therefore be used to show the effect of electron correlation on the calculated charge distribution. In particular it has been criticised for not providing an accurate physical picture of the true ion structure. One of the major criticisms of the charge localisation concept is that the removal of an electron from a delocalised molecular orbital must necessarily lead to a delocalisation of the ionic charge and therefore the whole concept of localised charges is without physical foundation. This is a valid and serious criticism since any electron taking part in a molecular orbital of any sort is no longer under the sole influence of the atom to which it may have belonged in the pure atomic state. The molecular orbital calculation method mixes the atomic orbitals of similar energy on neighbouring atomic centres in the molecule to form the molecular orbitals which describe the molecular bonding and structure. The electrons contributed by individual atoms are of necessity then shared between two or more atomic centres in most cases. It should be emphasised here that all the calculations reported in this study show the charge to be delocalised over the whole molecular or ionic structures as expected, however the site of major change in charge distribution when the molecules are ionised is seen to be substantially different for the methanamides and the thiomethanamides and it is this difference which correlates so well with the experimental data on ionisation measurements as described above. However, due to the undoubted delocalisation of the charge, it is perhaps unrealistic to call this effect charge localisation. Beynon and Williams in their paper on charge localisation in mass spectrometry¹³, recalled that the major factor in fragmentation reactions was likely to be the radical electron site rather than the charge site and

this is an important point in the context of this current work, and the previous attempts to calculate charge distributions and relate them to mass spectrometric fragmentation. The reason this is important is that in all the attempts to calculate charge distributions the ion is presumed to be formed by removal of an electron from the calculated HOMO of the neutral molecule. This implies that the radical electron left is located within the same orbital. If the calculated HOMO is delocalised itself then both the charge density and the unpaired electron density will be shared over several atomic centres, however, if the calculated HOMO is fairly localised, as is the case for the thioamides studied here, then both the charge and the unpaired electron density will also be localised to a greater extent. So for the thioamide calculations reported here and throughout the remainder of this work the calculated HOMO is largely localised around the sulphur atom and therefore the charge and the unpaired electron are also more localised on the sulphur atom. However for the amides the calculated HOMO is delocalised over the nitrogen and the carbonyl group and contains π -electron density from all three atoms, therefore the charge and the unpaired electron density are also going to be delocalised over the same atoms. The calculations reported here do not take any account of *distonic* ions, i.e. ions where the charge and radical sites are separated within the ion, none of the previous work on calculated charge distributions has considered this option for ionic structures either. The whole concept of charge/radical localisation and its possible effects is discussed in more detail in section 6.6, however it is noted here that the radical electron can reduce the activation energy for a fragmentation reaction by reducing the strength of bonds immediately neighbouring the radical site, however no such mechanism exists for a charge site to make a given fragmentation reaction more or less favourable. Indeed neither a radical site or a charge site can be said to cause any fragmentation reaction directly, since all that is required for any reaction to proceed is that the appropriate amount of energy be available. It is therefore more than likely that the correlations with electronic charge being presented here will also correlate with unpaired electron density and that it is the latter which is responsible for the fragmentation reactions observed in the mass spectra. The data presented in tables 6.10 and 6.11 was calculated by taking the geometry obtained at the 3-21G* level of theory and recalculating the

energies and the population analysis at the MP3/6-31G* level of theory. This higher level of theory represents a more complete description of the electronic structure of the molecules and radical cations studied since it is closer to the exact solution of the Schrodinger equation, utilising a larger basis set and electron correlation through Moller-Plesset perturbation theory terminated at third order (see chapter 2 for a full description of these methods). The data in tables 6.10 and 6.11 shows some differences from that presented in tables 6.1 and 6.4, as expected, however the charge distribution has not altered significantly on going to the higher level of theory and the conclusions drawn above are seen to be valid for the calculation carried out using the larger basis set. Although these calculations also included electron correlation, via Moller-Plesset perturbation theory, as mentioned above, this will not have affected the Mulliken population analysis because the population analysis is carried out on the un-correlated wavefunction in the version of the software used. This means that the differences in the charge distributions presented in tables 6.10 and 6.11 from those presented in tables 6.1 and 6.4 are entirely due to the difference in the basis sets used in the calculations and as can be seen these differences are small and do not alter the conclusions reached. Another point to be considered here is that all of the calculations here relate to the ground electronic state of the neutral molecules, and more importantly of the radical cations; i.e. it is assumed that the radical cations formed by electron impact are formed in their electronic ground states. No calculations on excited states were carried out for any of the species studied, however since the two highest occupied molecular orbitals are so close in energy for these compounds it may be possible that some of the molecular radical cations formed from 70eV electron bombardment might be formed in an excited state, this could limit the scope for the interpretation of their mass spectra in terms of the calculated charge distributions. The ionic structures calculated as minimum energy structures reported here may also correspond to local minima on the potential energy surface, whilst some care has been taken to ensure that the structures reported are global energy minima, it is possible that there may be other structures of lower energy. In particular with systems of this size there are a large number of potential structures for the ions and no bridged or "non-classical" structures were considered in this study.

Table 6.10

UMP3/6-31G**/3-21G* Ab-Initio molecular orbital results for
methanamide **1** and its radical cation **1⁺**.

Parameter	1	1⁺
bond lengths / Ångstroms		
C--O	1.212	1.311
C--N	1.353	1.276
C--H	1.084	1.075
N--H	0.998	1.010
N--H'	0.995	1.008
bond angles / Degrees		
<HCO	122.43	114.52
<HCN	112.26	122.16
<OCN	125.31	123.32
<CNH	119.39	122.48
<CNH'	122.00	121.24
Mulliken atomic charges		
O	-0.57	-0.13
C	+0.51	+0.56
H	+0.15	+0.36
N	-0.88	-0.77
H	+0.40	+0.49
H'	+0.39	+0.49

Table 6.11

UMP3/6-31G^{*}//3-21G^{*} Ab-Initio molecular orbital results for
thiomethanamide **4** and its radical cation **4⁺**.

Parameter	4	4⁺
bond lengths / Ångstroms		
C--S	1.639	1.690
C--N	1.331	1.287
C--H	1.077	1.078
N--H	1.000	1.007
N--H'	0.998	1.007
bond angles / Degrees		
<HCS	120.30	115.64
<HCN	113.26	117.29
<SCN	126.43	127.07
<CNH	119.71	123.22
<CNH'	121.98	121.10
Mulliken atomic charges		
S	-0.27	+0.42
C	+0.03	+0.02
H	+0.22	+0.34
N	-0.80	-0.73
H	+0.42	+0.47
H'	+0.40	+0.48

Since it is known that for keto- compounds in particular the radical cation is more stable in its enol form, the tautomeric imide structure of methanamide was studied to check the energy of this form relative to that of the methanamide itself. The calculations were carried out at the 3-21G* level of theory so that comparisons were possible and before the calculations were performed on the methanamide system, the method was checked by calculating the energies of the ethanal/ethenol tautomeric pair to ascertain that the correct energy ordering was obtained. This calculated data is presented in tables 6.12 and 6.13 whilst that for the methanamide/methanimide tautomers is shown in tables 6.1 and 6.14. The ethanal/ethenol system was previously studied by Scharzw and co-workers¹⁴ who found that the ethanal neutral molecule was more stable than the ethenol tautomer by 41 kJ mol⁻¹, whilst the ethenol radical cation was more stable than its ethanal counterpart by some 63 kJ mol⁻¹. This data was obtained by considering the *syn* neutral going to the *anti* radical cation for ethenol. The data calculated in this study gave slightly different energy differences although the conclusions were identical. As shown in table 6.12 the 3-21G* ab-initio calculations reported here gave the ethanal neutral as being 48.18 kJ mol⁻¹ more stable than the neutral ethenol, whilst the ethenol radical cation was calculated to be 36.32 kJ mol⁻¹ more stable than the radical cation for ethanal. The results reported in table 6.13 are then seen to be in reasonable agreement with those reported earlier by Scharzw and co-workers despite the fact that different levels of theory were used and that the calculations reported in this work considered the *anti* neutral of ethenol going to the corresponding *anti* radical cation. This difference in the structures of the neutral ethenol used in the two calculations probably explains a substantial amount of the difference between the reported relative stabilities of the ethenol neutrals and radical cations.

Having established that the calculation method being used here does correctly assign the order of stability of the tautomers in the ethanal/ethenol system, the methanimide tautomer of methanamide was calculated using the same methods. The relative stabilities of the methanamide and methanimide neutrals and radical cations are presented in table 6.16. The data shows that the methanamide neutral is calculated to be 73.7 kJ mol⁻¹ more stable than

Table 6.12

3-21G^{*} Ab-Initio molecular orbital results for
ethanal **7** and its radical cation **7⁺**.

Parameter	7	7⁺
bond lengths / Ångstroms		
C--O	1.208	1.249
C--C ₁	1.507	1.489
C--H	1.087	1.084
C ₁ --H'	1.080	1.079
C ₁ --H'	1.086	1.089
C ₁ --H'	1.086	1.089
bond angles / Degrees		
<HCO	120.91	114.98
<HCC ₁	114.31	121.99
<OCC ₁	124.78	123.02
<CC ₁ H'	109.95	112.49
Mulliken atomic charges		
O	-0.52	-0.11
C	+0.34	+0.36
H	+0.18	+0.43
C ₁	-0.73	-0.74
H'	+0.25	+0.35
H'	+0.23	+0.36
H'	+0.23	+0.36

Table 6.13

3-21G^{*} Ab-Initio molecular orbital results for
ethenol **8** and its radical cation **8⁺**.

Parameter	8	8⁺
bond lengths / Ångstroms		
C--O	1.385	1.284
C--C ₁	1.311	1.400
C--H	1.074	1.074
O--H	0.963	0.979
C ₁ --H'	1.071	1.072
C ₁ --H'	1.070	1.071
bond angles / Degrees		
<HCO	116.38	120.21
<HCC ₁	121.78	121.54
<OCC ₁	121.84	118.25
<CC ₁ H'	120.76	119.36
<CC ₁ H'	120.81	120.10
<COH	112.58	120.88
Mulliken atomic charges		
O	-0.70	-0.58
H	+0.40	+0.52
C	+0.15	+0.33
H	+0.22	+0.37
C ₁	-0.51	-0.34
H'	+0.24	+0.36
H'	+0.22	+0.35

the methanimide neutral and that in contrast to the ethanal/ethenol system the methanamide radical cation is calculated to be 99.27 kJ mol⁻¹ more stable than the radical cation of the methanimide tautomer. Since the energy difference in favour of the methanamide radical cation is substantial, just over 1 eV, the tautomeric forms have not been considered any further, although as mentioned above they may play a role in the 70eV mass spectra due to the range of internal energies which may be present in the radical cations formed by this technique.

Table 6.14

Calculated energy differences between the ethanal and ethenol neutral molecules and their radical cations.

	neutral molecule	radical cation
Ethanal	-152.0552487	-151.7373171
Ethenol	-152.0368999	-151.7511497
Energy difference (this work)	-48.18 kJ mol ⁻¹	+36.32 kJ mol ⁻¹
Energy Difference (Schwarz et al. ¹⁴)	-41 kJ mol ⁻¹	+63 kJ mol ⁻¹

Table 6.15

3-21G^{*} Ab-Initio molecular orbital results for
methanimide tautomer **9** and its radical cation **9⁺**.

Parameter	9	9⁺
bond lengths / Ångstroms		
C--O	1.361	1.294
C--N	1.245	1.269
O--H	0.969	0.976
C--H	1.074	1.075
N--H	1.007	1.008
bond angles / Degrees		
<HCO	109.71	114.73
<HCN	128.22	118.56
<OCN	122.07	126.70
<COH	110.52	121.44
<CNH	116.69	150.76
Mulliken atomic charges		
O	-0.70	-0.62
H	+0.41	+0.50
C	+0.47	+0.72
H	+0.24	+0.41
N	-0.71	-0.52
H	+0.30	+0.51

Table 6.16

Calculated energy differences between the methanamide and methanimide neutral molecules and their radical cations.

	neutral molecule	radical cation
Methanamide	-167.9849000	-167.6899300
Methanimide	-167.9568301	-167.6491229
Energy Difference	-73.70 kJ mol ⁻¹	-99.27 kJ mol ⁻¹

6.2.1.1 Mass Spectrometry.

The 70 eV mass spectra of the methanamides and thiomethanamides are presented in figures 6.3 to 6.5 and are presented in pairs, so that the spectrum of each methanamide is presented with the corresponding thioamide spectrum. All the spectra, in common with other simple aliphatic amides, show the molecular ion (M^+) as base peak and fragmentations which fit those outlined by Gilpin.¹⁵ The spectrum of methanamide, **1** (fig. 6.3a) shows the major fragment peak at m/z 29 to be the product of an α -cleavage reaction from the carbonyl function leaving HCO^+ . The other half of the molecule at m/z 16 is only a weak peak although there is a major fragment at m/z 17, NH_3^+ . This must be the result of a competing re-arrangement reaction, and may explain the weak intensity of the fragment at m/z 16. The only other fragments of any note are peaks at m/z 44, and m/z 43 which correspond to losses of H^- and H_2 respectively. The compositions of all the major fragment peaks for both the amides and the thioamides were confirmed by accurate mass measurement at 7,500 resolution (10% valley definition), as detailed in Chapter 4 (see table 6.17). The spectrum of thiomethanamide, **4** (fig. 6.3b) shows many similar features, although the ion at m/z 17 is noticeably reduced, and the peaks at m/z 18, 28 and 32 are distorted by an air leak in the instrument. The peak at m/z 43 (CH_3CO^+) would appear to be due to the acetone solvent and is discounted in the following discussion. Table 6.17 gives the accurate masses found for the most abundant ion at the fragment mass

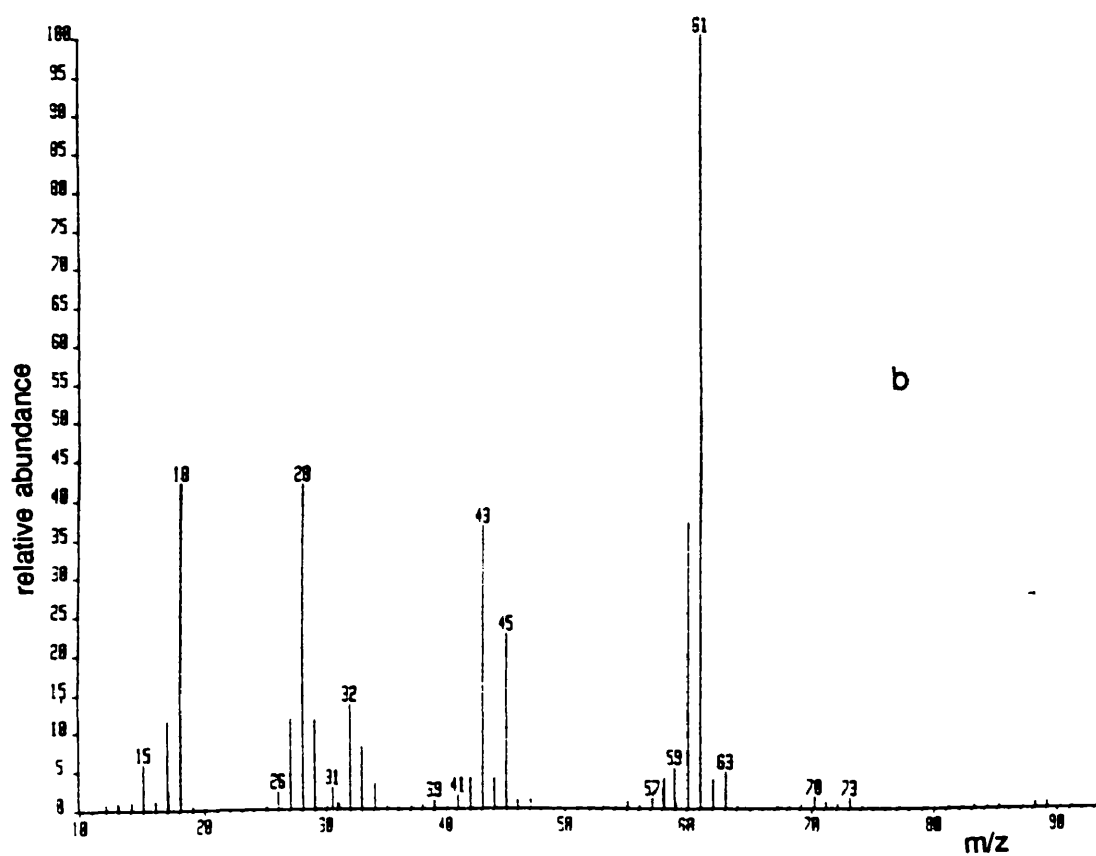
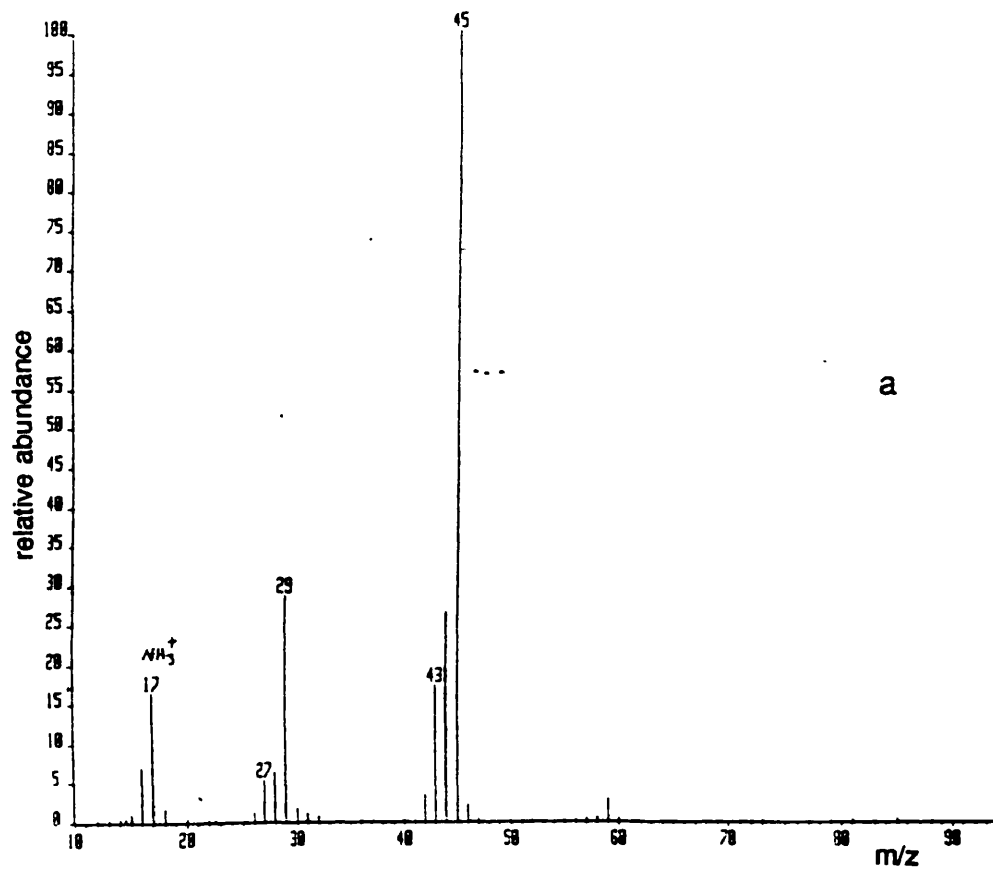


Figure 6.3. 70eV EI mass spectra for (a) methanamide. 1 and (b) thiomethanamide. 4.

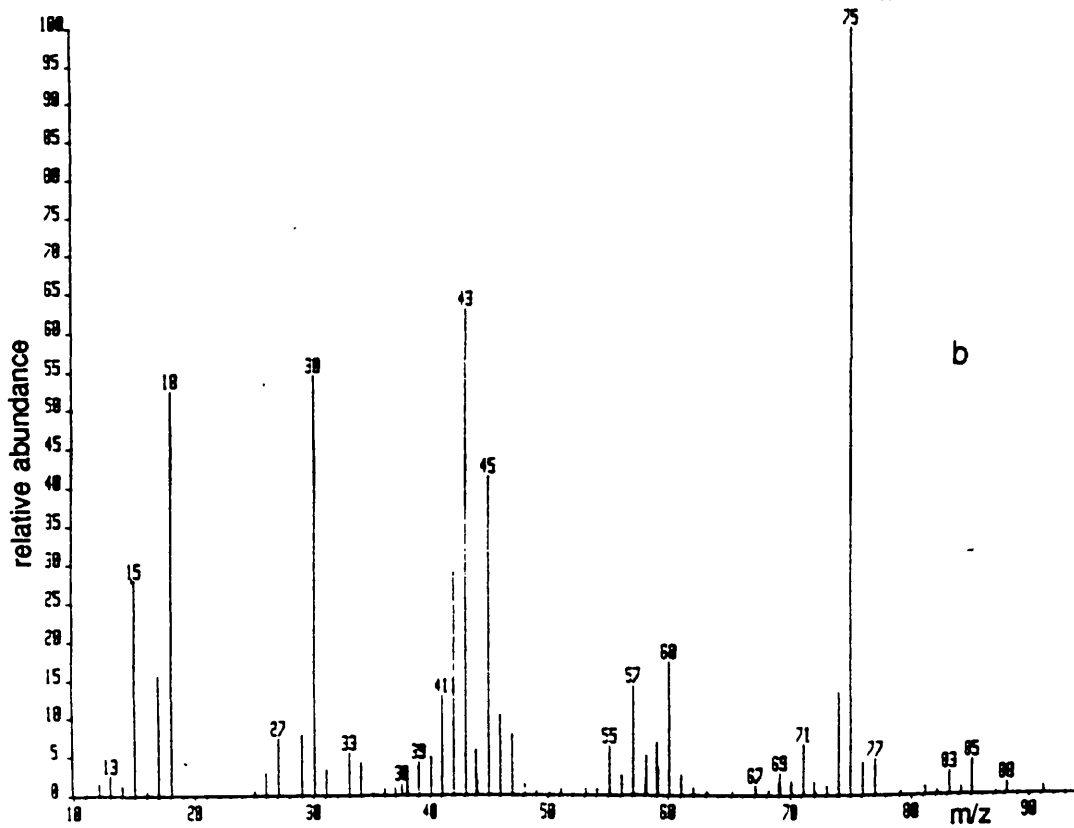
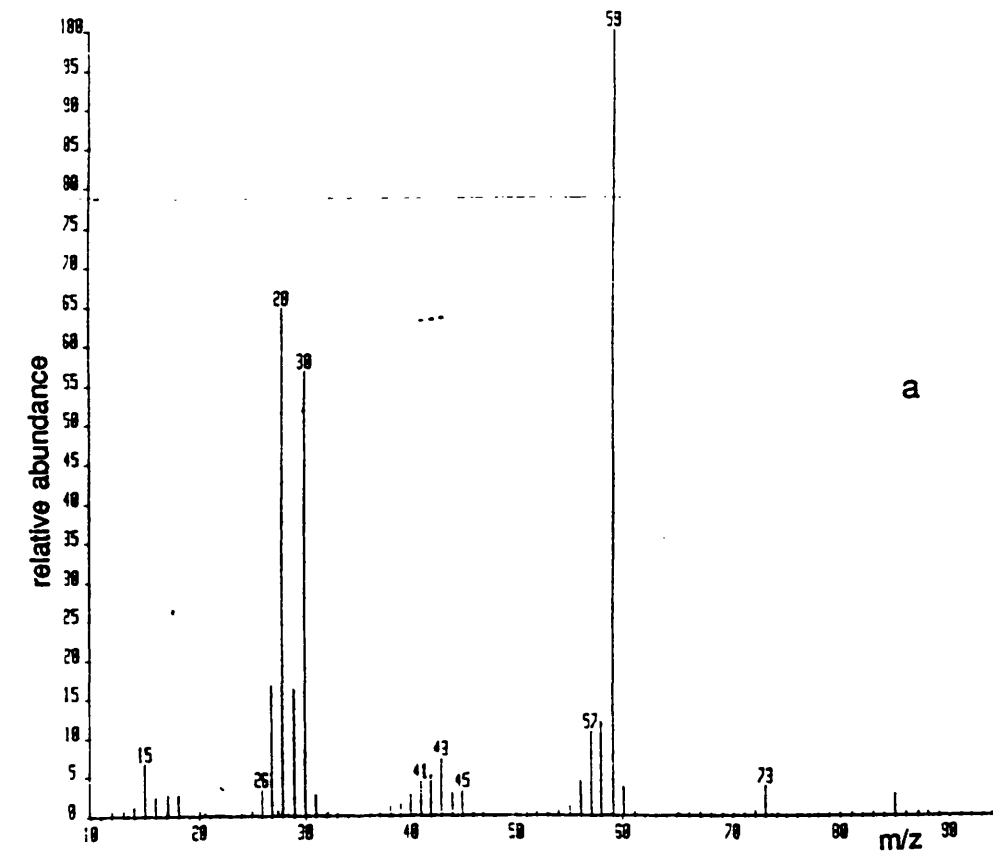


Figure 6.4. 70eV EI mass spectra for (a) N-methylmethanamide, 2 and (b) N-methylthiomethanamide, 5.

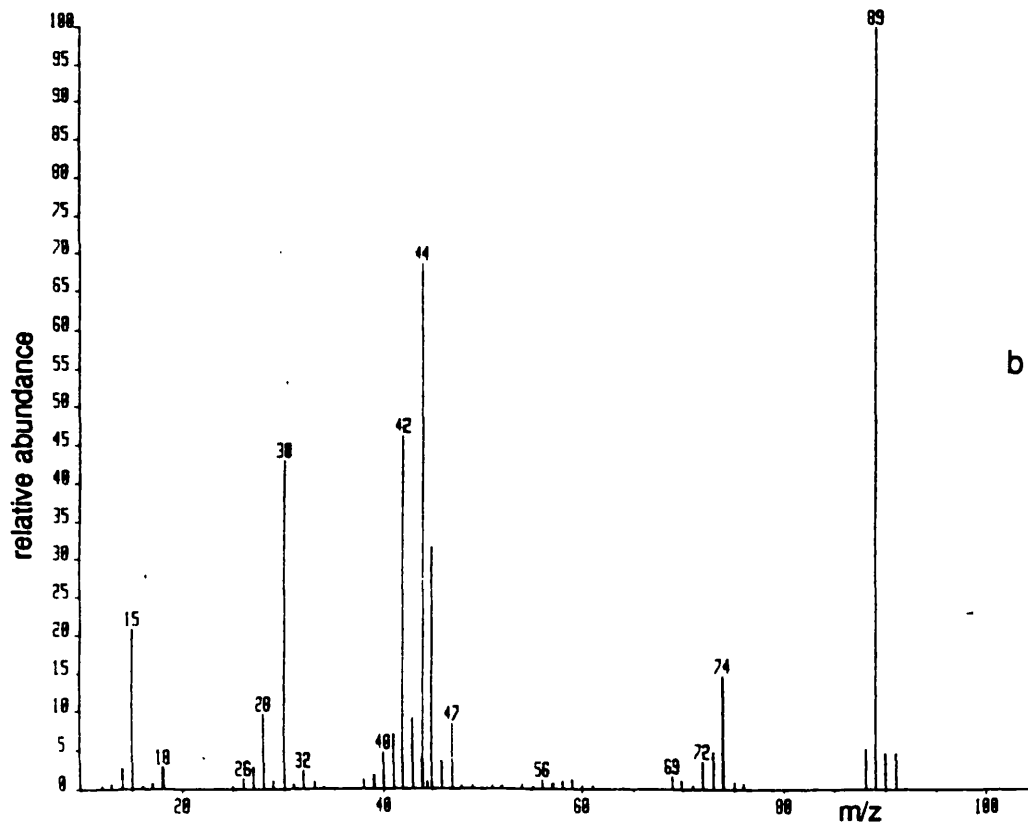
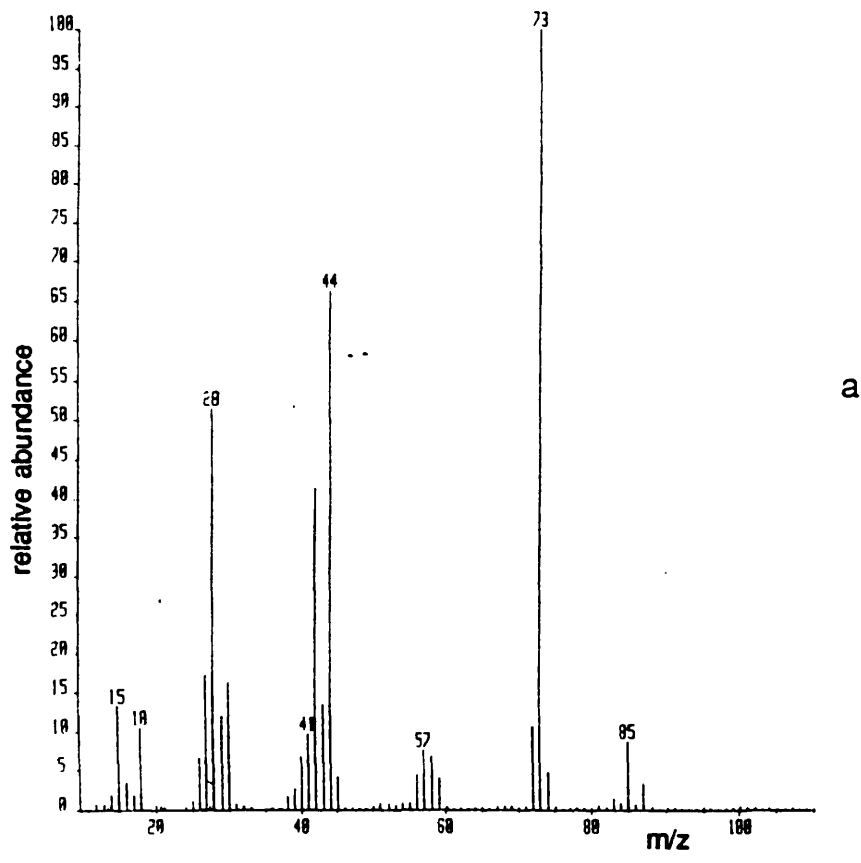


Figure 6.5. 70eV EI mass spectra for, (a) N,N-dimethylmethanamide, **3** and (b) N,N-dimethylthiomethanamide, **6**.

in question, in several cases the peaks shown on the spectra in figs. 6.3-6.5 are multiplets.

The other isobaric masses were often due to background in the mass spectrometer and as such have not been reported.

The accurate masses for all the molecular ions of all the compounds studied were also measured and, in all cases, confirmed the correct molecular formula for the ion.

Table 6.17

Accurate mass measurement data for methanamides and thiomethanamides.

Acc. Mass calculated	Acc. mass measured for compounds 1-6					
	1	2	3	4	5	6
17.02652	17.0265	--	--	--	--	--
27.99500	27.9950	27.9949	27.9949	--	--	--
28.01870	--	28.0187	--	--	--	--
29.00273	29.0027	29.0027	29.0027	--	--	--
30.01053	--	30.0102	--	--	--	--
30.03430	--	30.0343	30.0343	--	30.0343	30.0343
42.03437	--	--	42.0343	--	--	42.0344
43.97207	--	--	--	--	43.9721	43.9719
44.01364	44.0136	44.0136	--	--	--	--
44.05002	--	--	44.0499	--	--	44.0500
44.97988	--	--	--	44.9798	44.9798	44.9799

The rearrangement to form the NH_3^+ ion is common in the ureas, but is not observed in the thioamides. Instead the thioamides all show significant peaks due to loss of SH^- via a different

rearrangement reaction. Otherwise most of the other peaks are produced from α -cleavage reactions from the molecular ions. The range of internal energies of the ions produced by 70eV electron impact is considerable and leads to a plethora of competing and consecutive reactions which may make it difficult to follow any effects due to charge-radical localisation. To attempt to circumvent this problem and to obtain simpler mass spectra on which to work the 8eV mass spectra of the commonly available amides and thioamides were run; this data is presented in table 6.18 below.

Table 6.18

8eV mass spectra for the commonly available methanamides
and thiomethanamides

Methanamide 1		N-methyl methanamide 2		N,N-dimethyl methanamide 3		N,N-dimethyl thiomethanamide 6	
m/z	Rel. Int.	m/z	Rel. Int.	m/z	Rel. Int.	m/z	Rel. Int.
46	2.86	60	3.95	74	5.71	91	5.19
45	100.00	59	100.00	73	100.00	90	4.67
17	21.43	30	2.63	72	0.57	89	100.00
--	--	--	--	44	3.14	74	0.78
--	--	--	--	--	--	45	0.80
--	--	--	--	--	--	44	4.15

As expected the 8eV spectra show many fewer peaks than the comparable 70eV spectra. The lower energy spectra are known to favour fragmentation reactions which have a lower energy requirement and since the ions formed will have a narrower range of internal energies fewer reactions are possible. For methanamide, 1, the only fragment observed is the NH_3^+ ion at m/z 17 which must be produced via a re-arrangement reaction, which are generally accepted as

having lower energy requirements than bond cleavage reactions. The fact that hydrogen transfer to nitrogen occurs has in the past been cited as evidence for the nitrogen atom being the charge bearing site, although this need not be the case. For the N-methyl methanamide, **2**, the only fragment observed is at mass 30, which accurate mass measurement at 70eV gave as predominantly HNCH_3^+ . This may be expected from the charge distribution data which shows a significant increase in the positive charge associated with this fragment (see fig. 6.2), than for the corresponding fragment in methanamide. In the case of N,N-dimethylmethanamide, **3**, the only fragments observed are loss of H \cdot at m/z 72, and the $\text{CH}_3\text{NCH}_3^+$ ion at m/z 44. The formula of the ion at m/z 44 was confirmed by accurate mass measurement at 70eV (see table 6.17) and again this fragment of the molecule is predicted to be the major site of electron loss on ionisation. Significantly no ions at m/z 29 (HCO^+) or m/z 28 (CO^+) are observed in any of the low energy spectra of the methanamides. The spectrum of N,N-dimethylthiomethanamide, **6**, shows three fragment peaks corresponding to $[\text{M}-\text{CH}_3]^+$ at m/z 74, the $\text{CH}_3\text{NCH}_3^+$ ion at m/z 44, and a weak peak at m/z 45 corresponding to the HCS^+ ion. The change in charge distribution for compound **6** shows the gain in positive charge to be almost equally shared between the sulphur and the nitrogen fragment. Although the peak heights are obviously not equal in the mass spectrum we can at least see the sulphur containing fragment in the spectrum, whereas the corresponding oxygen containing fragment was totally absent from the amide spectra. It may also be significant that the ionisation energies of the thioamides are below those of the amides and therefore the thioamide ions may have slightly higher internal energies. Probably the most important argument is the application of the Stevenson/Audier rule, this rule states that the fragment which carries the charge from any reaction, will be the fragment with the lowest ionisation energy. If the effect of sulphur is to reduce the ionisation energy of the thioamides relative to the amides (see table 6.9), then it follows that the ionisation energy of HCS will be lower than that for HCO , if the energy of HCS is reduced to the level where it starts to compete with the CH_3NCH_3 moiety for the charge then both fragments may be seen in the spectrum, as indeed they are. This would perhaps be more clearly demonstrated if the other thiomethanamides had been available for low energy study.

6.2.2 Ethanamides and Thioethanamides

The compounds ethanamide, thioethanamide and their N-methylated analogues were studied and the results are reported in this section (see figure 6.6). The calculations on the ethanamides and thioethanamides were again performed at the 3-21G^{*} level of theory so that direct comparisons can be made with the methanamides and thiomethanamides reported above. The major bond lengths, bond angles and Mulliken atomic charges are reported for the neutral molecules **10** to **15** and the radical cations **10^{•+}** to **15^{•+}** in tables 6.19 to 6.24 respectively.

The radical cations of ethanamide and thioethanamide were also calculated at the same geometry as the neutral molecule and these ions are represented by **10^{•+}** and **13^{•+}** respectively in the tables below.

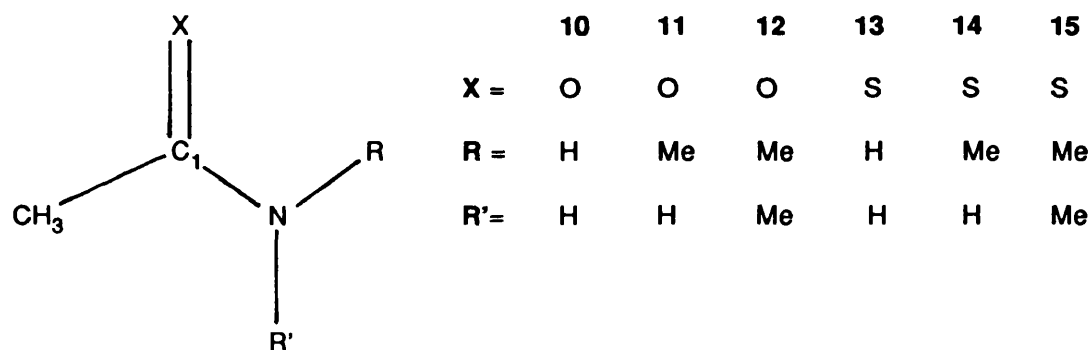


Figure 6.6 Key to the ethanamides and thioethanamides studied.

All species studied were calculated to be planar and therefore dihedral angles have not been reported, the C-H bond lengths and bond angles for the methyl groups were entirely consistent with the expected sp³ carbon values and therefore these are not listed explicitly in the tables below. Although as explained for the case of the methanamides and thiomethanamides reported in 6.3.1 above these parameters were all optimised and planarity was not assumed for any of the structures reported.

Table 6.19

Ab-Initio calculated results for Ethanamide **10**, and its radical cations **10⁺** and **10²⁺**.

Parameter	10	10⁺	10²⁺
bond lengths / Ångstroms			
C ₁ --O	1.215	1.315	1.215
C ₁ --N	1.360	1.285	1.360
C ₁ --C	1.516	1.500	1.516
N--H	0.997	1.008	0.997
N--H'	0.995	1.006	0.995
bond angles / Degrees			
<CC ₁ O	123.44	116.15	123.44
<CC ₁ N	113.84	124.10	113.84
<OC ₁ N	122.72	119.76	122.72
<C ₁ NH	118.76	122.24	118.76
<C ₁ NH'	122.60	121.34	122.60
Mulliken atomic charges			
O	-0.63	-0.24	-0.22
C ₁	+0.82	+0.90	+0.85
CH ₃	+0.03	+0.31	+0.34
N	-0.93	-0.88	-0.84
H	+0.36	+0.45	+0.44
H'	+0.35	+0.46	+0.45

Table 6.20

Ab-Initio calculated results for N-methyl ethanamide **11**,
and it's radical cation **11⁺**

Parameter	11	11⁺
bond lengths / Ångstroms		
C ₁ --O	1.219	1.311
C ₁ --N	1.358	1.336
C ₁ --C	1.517	1.498
N--R	1.461	1.502
N--H'	0.996	1.014
bond angles / Degrees		
<CC ₁ O	123.05	123.10
<CC ₁ N	113.97	120.86
<OC ₁ N	122.98	116.04
<C ₁ NR	121.79	125.35
<C ₁ NH'	119.62	118.08
Mulliken atomic charges		
O	-0.63	-0.31
C ₁	+0.84	+0.75
CH ₃	+0.03	+0.23
N	-0.90	-0.65
R	+0.31	+0.53
H'	+0.35	+0.46

Table 6.21

Ab-Initio calculated results for N,N-dimethyl ethanamide **12**,
and it's radical cation **12⁺**

Parameter	12	12 ⁺
bond lengths / Ångstroms		
C ₁ --O	1.222	1.288
C ₁ --N	1.361	1.366
C ₁ --C	1.518	1.500
N--R	1.465	1.500
N--R'	1.462	1.493
bond angles / Degrees		
<CC ₁ O	121.40	121.16
<CC ₁ N	116.08	122.57
<OC ₁ N	122.53	116.27
<C ₁ NR	118.94	121.51
<C ₁ NR'	123.22	121.06
Mulliken atomic charges		
O	-0.64	-0.34
C ₁	+0.87	+0.76
CH ₃	+0.03	+0.18
N	-0.89	-0.63
R	+0.32	+0.52
R'	+0.31	+0.51

Table 6.22

Ab-Initio calculated results for thioethanamide **13**, and it's radical cations **13^{•+}** and **13^{•+•}**.

Parameter	13	13^{•+}	13^{•+•}
bond lengths / Ångstroms			
C ₁ --S	1.651	1.704	1.651
C ₁ --N	1.335	1.293	1.335
C ₁ --C	1.518	1.513	1.518
N--H	0.999	1.006	0.999
N--H'	0.998	1.007	0.998
bond angles / Degrees			
<CC ₁ S	122.71	117.87	122.71
<CC ₁ N	114.18	119.31	114.18
<SC ₁ N	123.11	122.82	123.11
<C ₁ NH	119.54	123.25	119.54
<C ₁ NH'	122.07	121.05	122.07
Mulliken atomic charges			
S	-0.20	+0.46	+0.49
C ₁	+0.23	+0.24	+0.20
CH ₃	+0.09	+0.26	+0.27
N	-0.87	-0.84	-0.82
H	+0.39	+0.44	+0.43
H'	+0.37	+0.44	+0.44

Table 6.23

Ab-Initio calculated results for N-methyl thioethanamide **14**,
and its radical cation **14⁺**

Parameter	14	14⁺
bond lengths / Ångstroms		
C ₁ --S	1.657	1.712
C ₁ --N	1.333	1.286
C ₁ --C	1.522	1.517
N--R	1.466	1.491
N--H'	1.000	1.008
bond angles / Degrees		
<CC ₁ S	121.16	116.50
<CC ₁ N	113.17	119.20
<SC ₁ N	125.68	124.29
<C ₁ NR	126.03	127.76
<C ₁ NH'	117.77	117.53
Mulliken atomic charges		
S	-0.22	+0.42
C ₁	+0.26	+0.26
CH ₃	+0.07	+0.24
N	-0.85	-0.82
R	+0.37	+0.47
H'	+0.37	+0.43

Table 6.24

Ab-Initio calculated results for N,N-dimethyl thioethanamide

15, and it's radical cation **15⁺**

Parameter	15	15⁺
bond lengths / Ångstroms		
C ₁ --S	1.668	1.737
C ₁ --N	1.335	1.319
C ₁ --C	1.525	1.518
N--R	1.472	1.503
N--R'	1.470	1.500
bond angles / Degrees		
<CC ₁ S	118.21	118.33
<CC ₁ N	116.92	120.56
<SC ₁ N	124.87	121.12
<CN ₁ R	122.78	125.37
<CN ₁ R'	124.97	122.97
Mulliken atomic charges		
S	-0.24	+0.33
C ₁	+0.28	+0.17
CH ₃	+0.08	+0.19
N	-0.82	-0.67
R	+0.36	+0.45
R'	+0.36	+0.49

The data presented in Tables 6.19 to 6.24 shows clear parallels with that presented for the methanamides and thiomethanamides in Tables 6.1 to 6.6 above. This is not too surprising given the similarity of the structures. However, the results show that the same conclusions can be drawn regarding the distribution of the positive charge in the radical cations, and that the effect of the electron donating methyl group is minimal in terms of the HOMO for the molecules. The data has been treated in exactly the same way as for the methanamides above so that direct comparison is possible and Figure 6.7 shows the calculated changes in the net charge distribution produced on ionisation of the ethanamides and thioethanamides studied. These data have again been produced directly from the calculated Mulliken atomic charges presented in the tables above. Mulliken population analysis shows the charge, initially shared between the nitrogen and the oxygen, becoming progressively more localised on the nitrogen with successive N-methylation for the ethanamides; whilst the charge is localised more consistently on the sulphur atom for the thioethanamides.

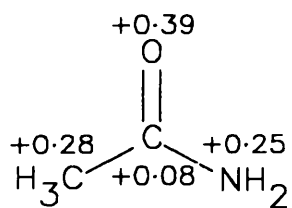
Table 6.25

HOMO's and I.E.'s calculated for the ethanamide and thioethanamide neutral molecules studied.

	HOMO 2-HOMO		E(HOMO)	E(2-HOMO)	I.E.	2-I.E.
10	3A''	13A'	-0.39533	-0.40620	9.90	10.17
11	4A''	16A'	-0.37369	-0.40340	9.36	10.10
12	5A''	19A'	-0.35416	-0.39741	8.87	9.95
13	16A'	4A''	-0.31462	-0.32552	7.87	8.15
14	19A'	5A''	-0.30935	-0.31753	7.75	7.95
15	22A'	6A''	-0.30310	-0.30755	7.59	7.70

Orbital energies are in the atomic units of Hartrees, whilst all ionisation energies (IE's) are given in electron volts (eV).

Ethanamides



Thioethanamides

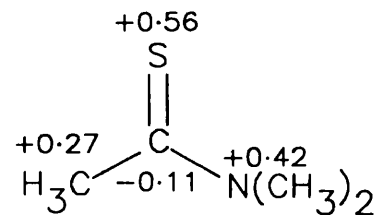
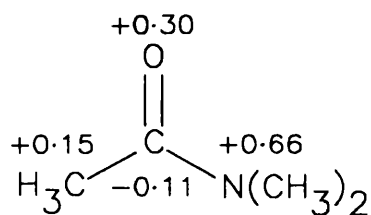
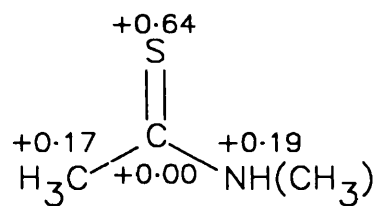
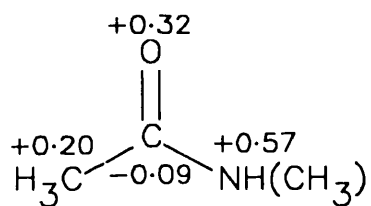
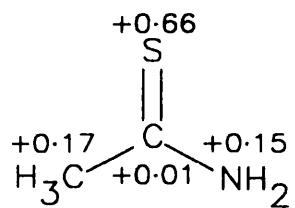


Figure 6.7. Calculated net changes in charge distributions on ionisation for the ethanamides and thioethanamides 10 to 15.

Table 6.26

Comparison of calculated and experimentally determined I.E.'s for the ethanamides and thioethanamides studied.

	Gaussian-82 3-21G [*] (This work)				Photoelectron Spectroscopy				M.S.
	1-MO	1-IE	2-MO	2-IE	1-MO	1-IE	2-MO	2-IE	
10	3A [*]	9.90	13A'	10.17	13A'	9.96	3A [*]	10.32	10.15
11	4A [*]	9.36	16A'	10.10	4A [*]	9.68	16A'	9.85	9.70
12	5A [*]	8.87	19A'	9.95	5A [*]	9.09	19A'	9.43	9.20
13	16A'	7.87	4A [*]	8.15	--	8.36	--	9.01	--
14	19A'	7.73	5A [*]	7.95	--	--	--	--	--
15	22A'	7.59	6A [*]	7.70	--	7.86	--	8.25	--

The ionisation energies reported above have been calculated by using Koopman's Theorem (see Chapter 2), and have been empirically scaled by 0.92.⁴ All values are in electron volts (eV).

The effect of N-methylation on the ionisation energy follows a similar pattern to that observed for the methanamides and thiomethanamides in that the main site of electron loss on ionisation is seen to be shared between O and N initially, but becomes preferentially from N as N-methylation occurs. Again for the thioethanamides the site of electron loss upon ionisation is preferentially from S throughout the series. Also from Table 6.26 it can be seen that the effect of N-methylation is to reduce the ionisation energy of the ethanamides by approx. 0.5eV for each N-methylation. Whereas in the thioethanamides N-methylation causes the ionisation energy to be reduced by approx. 0.15eV each time. The explanation for this is the same as that given for the same effect being observed for the methanamides and thiomethanamides above;

the N-methylation in the amides is occurring at the charge site and thus has a greater effect, whereas in the case of the thioamides the N-methylation is occurring remote from the charge site and therefore the effect is attenuated. The calculated HOMO for the ethanamides was again found to correspond to a delocalised non-bonding orbital containing the nitrogen lone-pair electrons and the carbonyl π -electrons (A''), whilst the second highest occupied molecular orbital (2-HOMO), corresponded to a non-bonding orbital containing an oxygen lone-pair of electrons (A'). In the case of the thioethanamides the ordering of these orbitals was reversed with the calculated HOMO now corresponding to a non-bonding orbital containing sulphur lone-pair electrons, and the 2-HOMO corresponding to the delocalised non-bonding orbital containing the nitrogen lone-pair and carbonyl π -electrons. For the amides the effect of N-methylation is to increase the separation between the highest occupied molecular orbitals, whereas in the case of the thioamides the effect of N-methylation is to bring the two orbitals closer together in energy. This follows from the above comments on the way that the energy of the nitrogen lone-pair containing orbital is affected to a much greater extent by N-methylation than the other orbitals being considered. The two orbitals become very close in energy for the N,N-dimethylthioethanamide and this is reflected in the fact that electron loss on ionisation appears to largely shared between the two sites. When the orbitals become this close in energy, the energy difference between the orbitals is approx. 0.09eV, the accuracy of the Hartree-Fock calculations may be suspect and the correct energy ordering of the molecular orbitals may not be achieved. The orbitals from which the electron is lost upon ionisation are again seen to have different symmetry properties, and in all respects the data for the ethanamides and thioethanamides calculated by ab-initio MO theory is similar to the results obtained for the methanamides and their thio-analogs.

The same comments apply to the ion structures considered here as were made for the methanamides and thiomethanamides, namely that the large number of isomeric forms have not in general been considered, although two tautomeric forms of ethanamide were calculated to compare their energies with that of ethanamide itself. The data for the tautomeric forms of ethanamide are given in tables 6.27 and 6.28 below.

Table 6.27

3-21G^{*} Ab-initio calculated parameters for ethanimide
tautomer 16 and it's radical cation 16⁺

Parameter	16	16 ⁺
bond lengths / Ångstroms		
C ₁ --O	1.366	1.303
C ₁ --N	1.249	1.275
C ₁ --C	1.509	1.505
N--H	1.008	1.006
O--H	0.968	0.975
bond angles / Degrees		
<CC ₁ O	111.29	116.34
<CC ₁ N	129.12	120.95
<OC ₁ N	119.59	122.72
<C ₁ NH	116.57	149.74
<C ₁ OH	109.90	120.26
Mulliken atomic charges		
O	-0.71	-0.64
C ₁	+0.69	+0.91
CH ₃	+0.07	+0.31
N	-0.74	-0.56
H	+0.29	+0.50
H _o	+0.41	+0.48

Table 6.28

3-21G^{*} Ab-initio calculated parameters for ethenolamine
tautomer 17 and it's radical cation 17⁺

Parameter	17	17 ⁺
bond lengths / Ångstroms		
C ₁ --O	1.374	1.312
C ₁ --N	1.362	1.293
C ₁ --C	1.328	1.435
N--H	0.994	1.008
N--H'	0.993	1.004
O--H _o	0.963	0.970
bond angles / Degrees		
<CC ₁ O	124.16	123.20
<CC ₁ N	126.93	121.78
<OC ₁ N	108.91	115.02
<C ₁ NH	118.57	119.40
<C ₁ NH'	121.59	122.99
<C ₁ OH _o	112.54	119.76
Mulliken atomic charges		
O	-0.74	-0.70
C ₁	+0.76	+0.91
CH ₂	-0.18	+0.28
N	-0.96	-0.87
H	+0.36	+0.45
H'	+0.35	+0.44
H _o	+0.41	+0.48

A comparison of the computed Hartree-Fock (HF) energies for the tautomers and ethanamide itself will inform us which is the most stable isomeric form for both the neutral molecule and the radical cation. This data is shown in table 6.29.

Table 6.29

Computed Hartree-Fock energies for ethanamide and its tautomers.

	neutral molecule	radical cation
Ethanamide (10)	-206.8158000	-206.534525
Ethanamide (16)	-206.7852805	-206.4942373
Ethenolamine (17)	-206.7767387	-206.5437188
Energy Difference (10-16)	-0.0305200	-0.040288
Energy Difference (10-17)	-0.0390620	+0.009193
Energy Difference (16-17)	-0.0085420	+0.049481

The above energies are given in Hartrees, an atomic unit of energy, the energy differences have been converted into kJ mol^{-1} in table 6.30 below for ease of comparison.

Table 6.30

Energy differences between ethanamide tautomers in kJ mol^{-1}

Energy Difference (10-16)	-80.138	-105.786
Energy Difference (10-17)	-102.567	+24.138
Energy Difference (16-17)	-22.429	+129.924

The data presented in tables 6.29 and 6.30 indicates that whilst the ethanamide structure is calculated to be the most stable isomeric form for the neutral molecules, being some 80 kJ mol⁻¹ more stable than the ethanimide tautomer and some 102 kJ mol⁻¹ more stable than the ethenolamine tautomer, the situation is different in the radical cation structures. For the radical cations the ethenolamine tautomer is calculated to have the most stable structure being some 24 kJ mol⁻¹ more stable than the ethanamide radical cation structure and some 130 kJ mol⁻¹ more stable than the ethanimide radical cation. This is in keeping with the previous findings by Schwarz et al. and others that where keto-enol tautomerism exists the keto form predominates in the neutral molecules but that the enol form predominates in the radical cations. It is not possible to form an enolamine tautomer for the methanamides or thiomethanamides but the fact that the ethanamides have a more stable tautomeric radical cation structure will complicate the discussion on interpretation of their mass spectra.

The change in charge distribution upon ionisation for the tautomers of ethanamide are shown in figure 6.8 and shows the charge to be delocalised around the whole structure for all three isomers. The effect of the hydroxyl is to reduce the amount of charge lost by the oxygen.

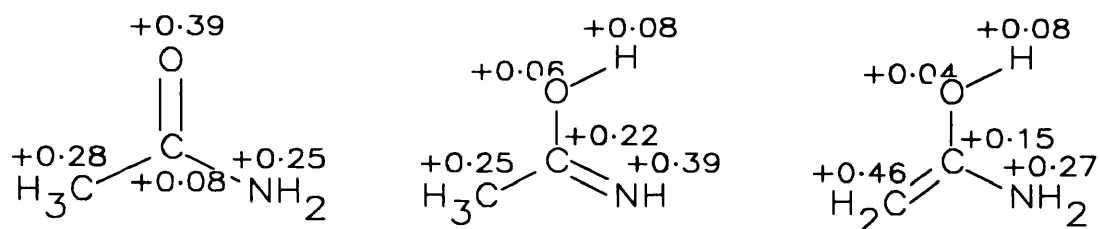


Figure 6.8 Change in charge distribution upon ionisation for the tautomeric forms of ethanamide

As can be seen from figure 6.8 the oxygen of ethanamide gains 0.39 of an electronic charge upon ionisation, whereas in the ethenolamine isomer, the oxygen gains only 0.04 of a charge, and in the ethanimide isomer the oxygen gains only 0.06 of a charge. Table 6.31 shows the energy of the two highest occupied molecular orbitals for the three isomeric structures with the

first two ionisation energies for each isomer.

Table 6.31

Orbital energies and ionisation energies for the ethanamide tautomers.

Compound	HOMO	2-HOMO	E(HOMO)	E(2-HOMO)	I.E.	2-I.E.
10	3A"	13A'	-0.39533	-0.40620	9.90	10.17
16	3A"	13A'	-0.39538	-0.40970	9.90	10.26
17	3A"	2A"	-0.29705	-0.44918	7.44	11.25

The ethenolamine isomer, 17, has a much lower ionisation potential than the other two isomers, and indeed the HOMO contains only $2p_z$ electron density from all four heavy atoms in the molecule. The same electron density is seen in the second highest occupied molecular orbital which has different symmetry properties and is more stable. The HOMO's for the other two isomers contain different electron density including both $2p_y$ and $2p_z$ from the heavy atoms and are again delocalised orbitals. In the thioethanamides the HOMO calculated corresponds to a non-bonding orbital containing sulphur lone-pair electrons, however, only the thioethanamide isomers have been considered, no calculations were performed on the thioethenolamine tautomers so it is unknown at present whether or not the thioamides would also have lower energy tautomeric forms of their radical cations.

6.2.2.1 Mass Spectrometry.

The 70eV mass spectra of the ethanamides and thioethanamides are presented in figures 6.8 to 6.10. They share many features in common with the spectra of the methanamides and their thioanalogs, and again the spectra are dominated by the products from α -cleavage reactions. The thioethanamides all show substantial peaks at $[M-SH]^+$, although the ethanamide spectrum does not show a substantial ion at m/z 17 $[NH_3^+]$ as seen in the spectrum of methanamide.

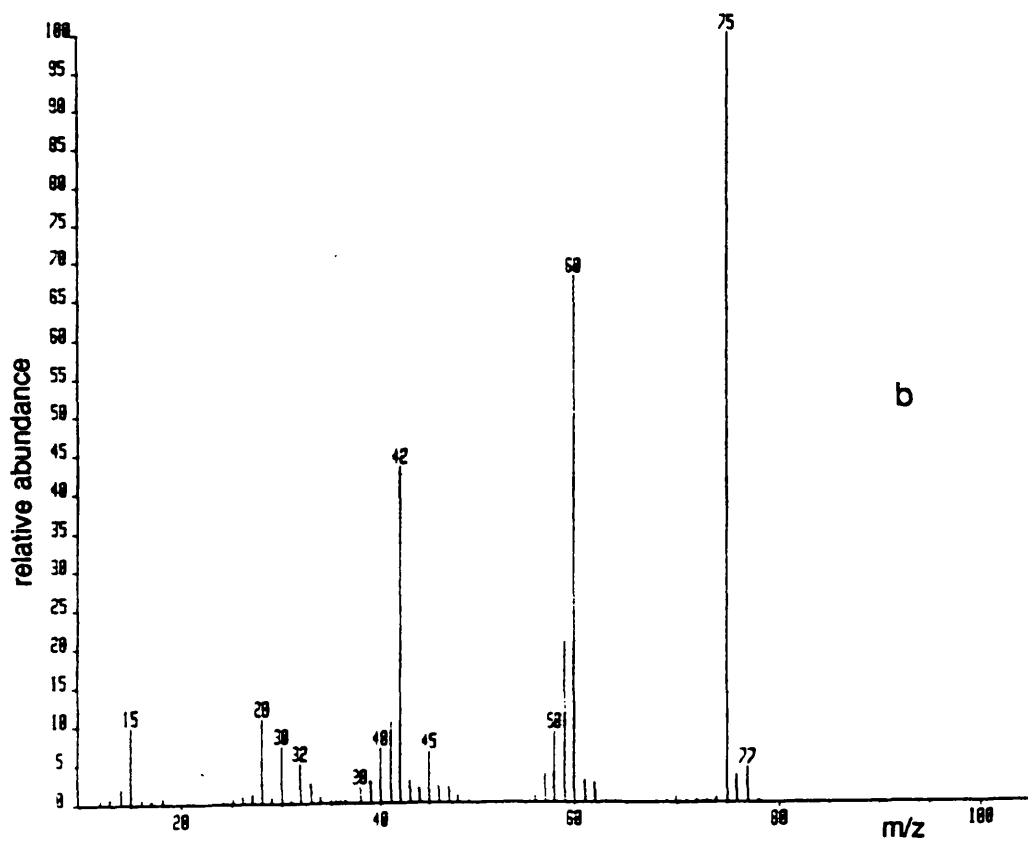
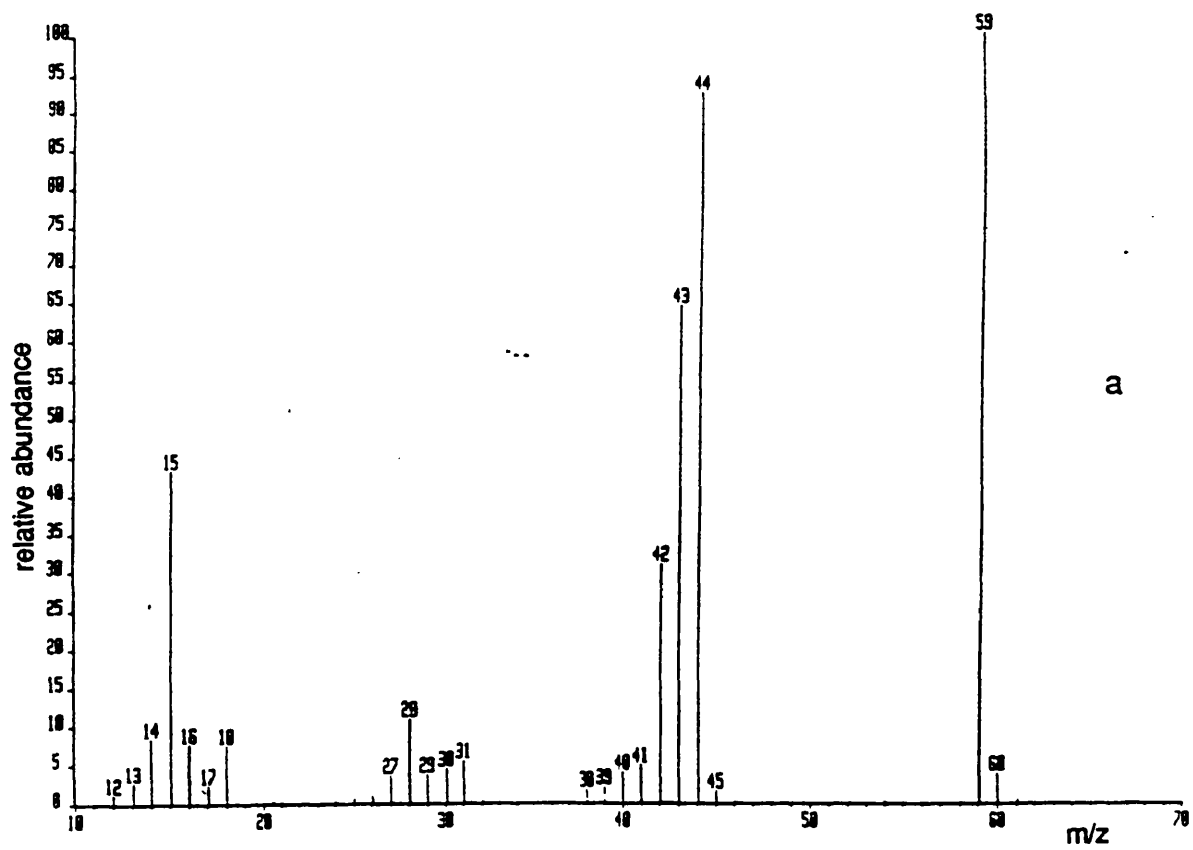


Figure 6.9 70eV mass spectra of (a) ethanamide and (b) thioethanamide

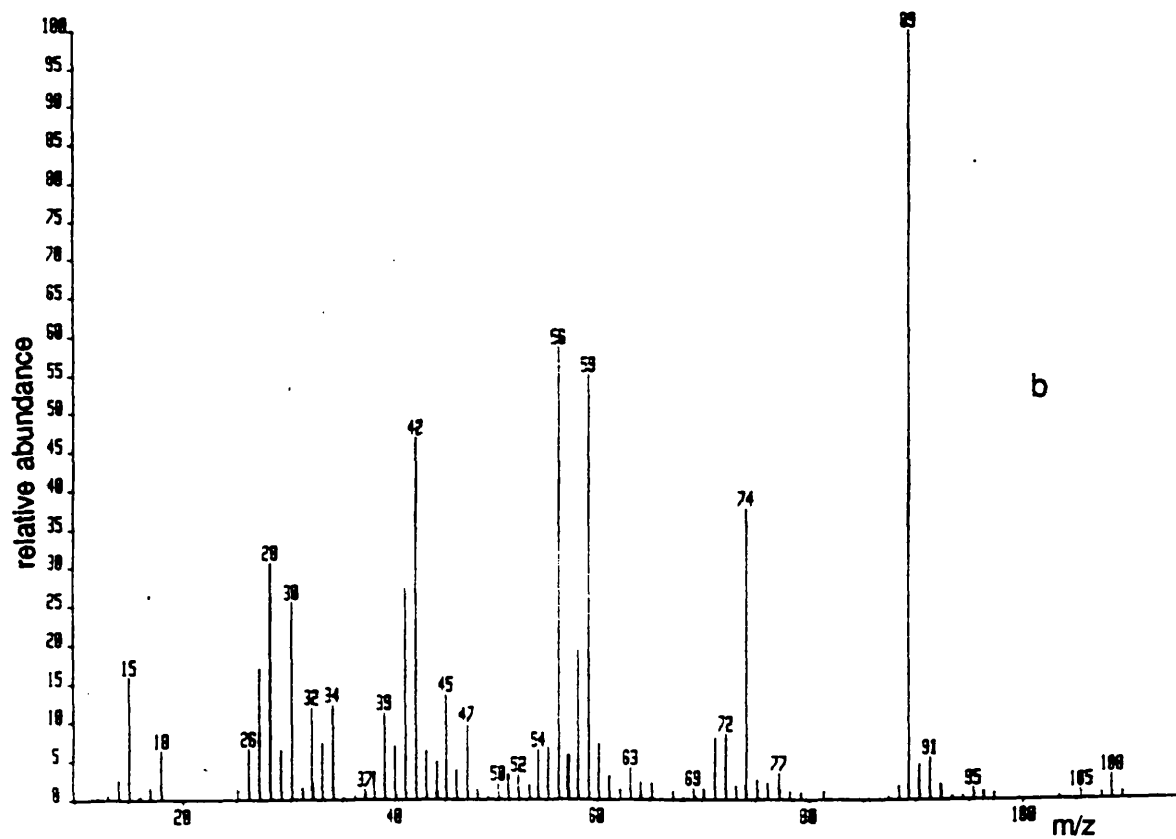
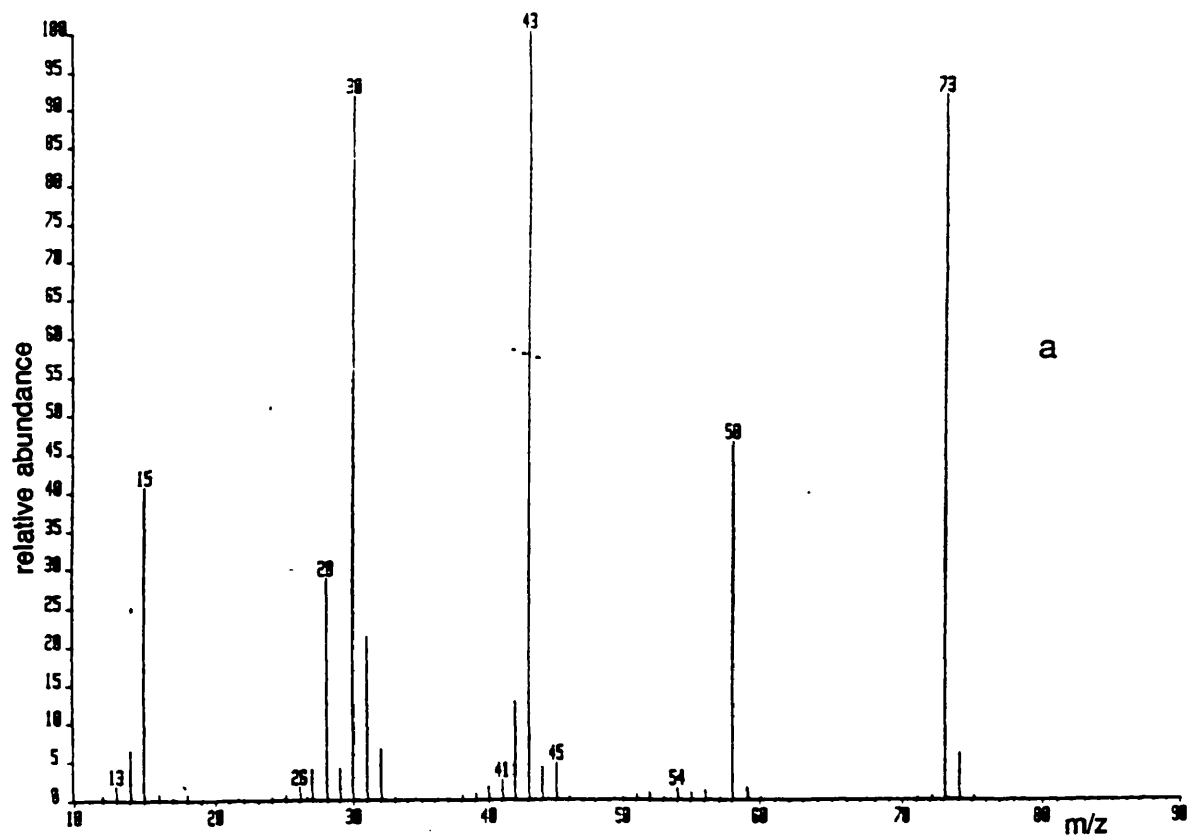


Figure 6.10 70eV mass spectra of (a) N-methylethanamide and (b) N-methylthioethanamide

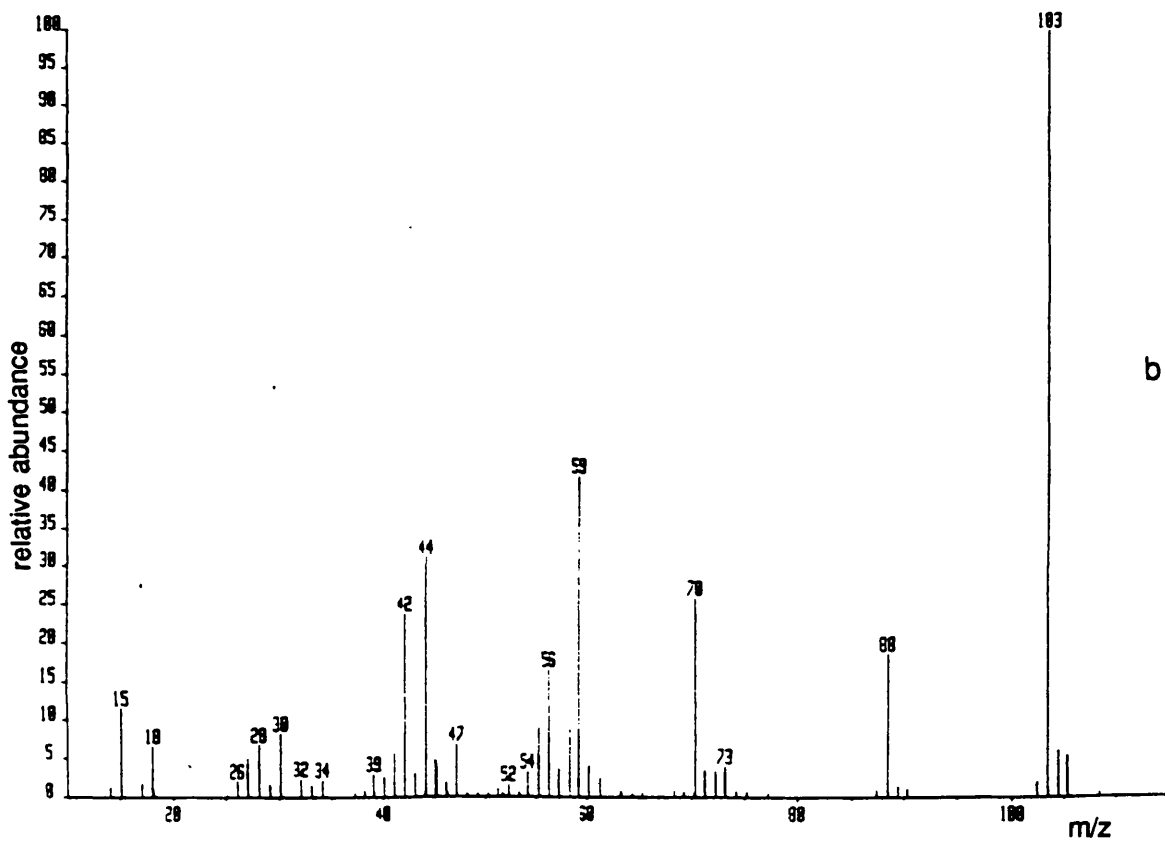
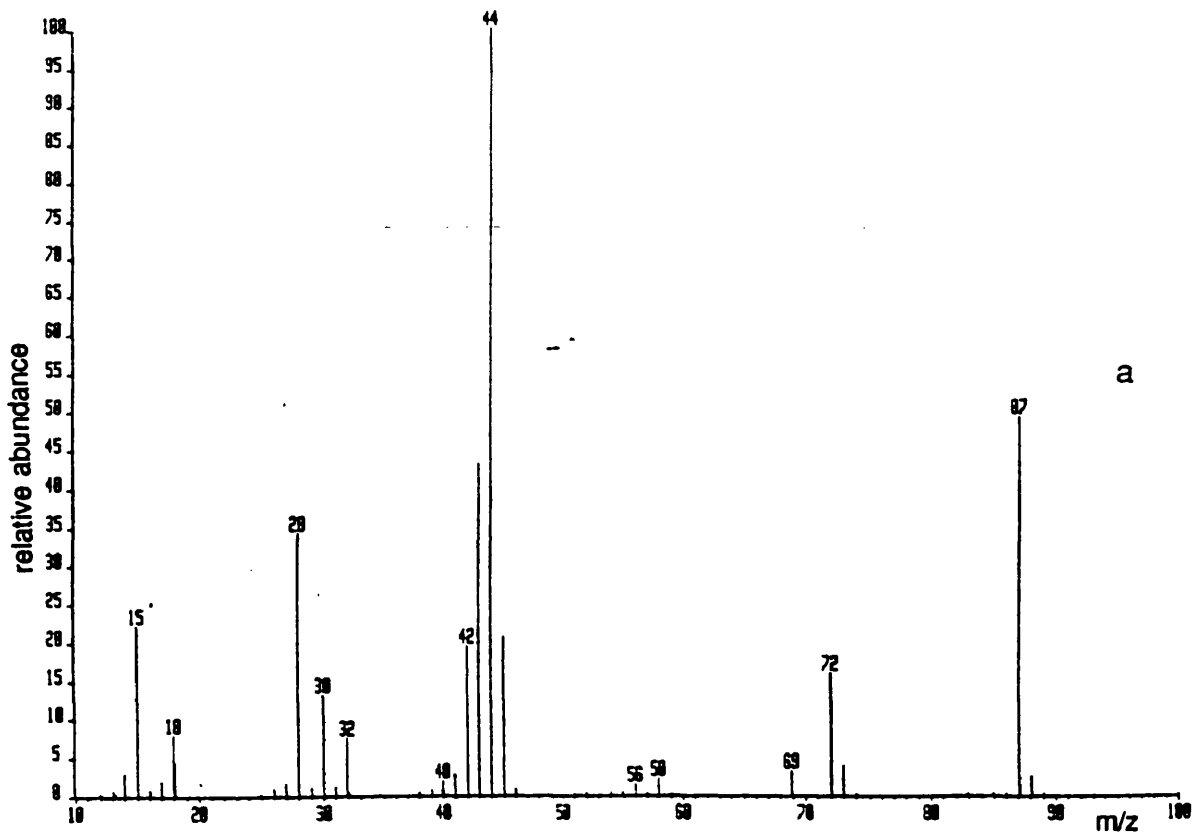


Figure 6.11 70eV mass spectra of (a) N,N-dimethylethanamide and (b) N,N-dimethylthioethanamide

In fact another reaction path is seen for all the ethanamides and their thio analogs, this is the α -cleavage from either the carbonyl (or thio-carbonyl) or the amine functions to lose $\text{CH}_3\cdot$ and give an ion at $[\text{M}-15]^+$. A peak at m/z 15 is also observed in the spectra for all the ethanamides and the thioethanamides studied this peak is due to CH_3^+ . This reaction cannot occur in the methanamide structures and neither of the above peaks is seen in their spectra. The fragmentation reactions of the ethanamides and their thio analogs are summarised in figure 6.12. The same scheme can be applied to the methanamides with the exception of reactions (c) and (d) and the addition of the rearrangement to produce the NH_3^+ ion at m/z 17.

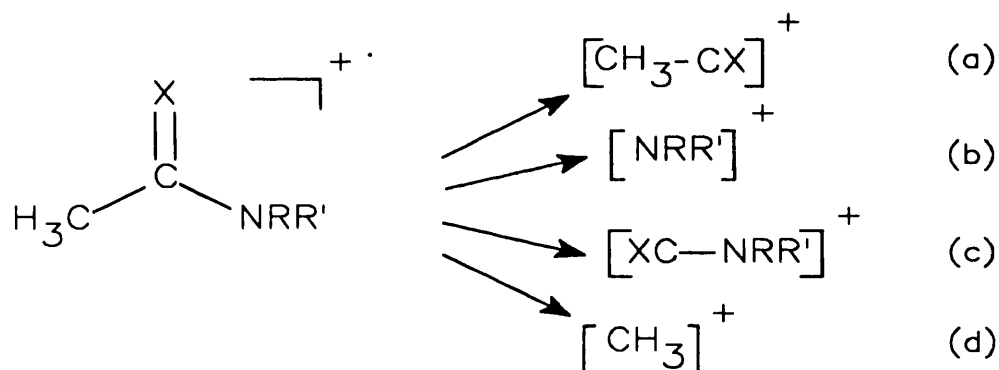


Figure 6.12 Fragmentation scheme for the ethanamides and thioethanamides.

According to this scheme the product distribution from the above reactions may be interpreted in terms of the initial charge distribution in the radical cations, although there are limitations to this approach as have already been discussed. The main problems are that the calculations as reported here only relate to ground state ions whereas 70 eV electron impact will give ions with a wide distribution of internal energies. 70 eV spectra will also show the products of sequential secondary fragmentations and there may well be advantages in studying these reactions at low electron energy and possibly also low source temperatures so that only primary reactions will be observed.¹⁶ It is also necessary to consider the thermochemical aspects of the fragmentation reactions and competition for the charge between the two

fragment species as discussed by Stevenson¹⁷ and Audier¹⁸. The above effects may all mask the charge distribution. With the above points in mind the mass spectra for the commonly available ethanamides and thioethanamides were run using an electron energy of 8eV for ionisation and a source temperature of 200 degrees centigrade, this data is presented in table 6.32 below. The chemical formulae of the major fragment peaks was checked by accurate mass measurement using 70eV electron impact mass spectrometry and by analogy with similar ions produced by the methanamides and their thio analogs as indicated in this table 6.17.

Table 6.32

8eV mass spectra for some of the commonly available ethanamides and thioethanamides

Ethanamide 10		N-methyl ethanamide 11		N,N-dimethyl ethanamide 12		Thioethanamide 13	
m/z	Rel. Int.	m/z	Rel. Int.	m/z	Rel. Int.	m/z	Rel. Int.
60	2.77	74	4.64	88	6.29	77	5.55
59	100.00	73	100.00	87	100.00	76	4.44
44	4.95	58	1.61	72	1.20	75	100.00
43	2.18	45	5.53	45	18.57	60	1.39
42	0.39	43	0.89	44	1.71	59	1.67
--	--	31	3.57	15	0.80	45	0.95
--	--	30	2.50	--	--	42	1.39

Once again the 8eV mass spectra show less fragmentation than the corresponding 70eV spectra, as expected, however in comparison with the methanamides and their thio analogs, more reactions are observed for the ethanamides and thioethanamides.

The 8eV spectrum of ethanamide, **10**, shows fragments due to loss of $\text{CH}_3\cdot$ at m/z 44; and loss of $\text{NH}_2\cdot$ at m/z 43. The ion at m/z 42 is a mixture of two isobaric components one due to ketene $[\text{CH}_2\text{CO}]^+$ which corresponds formally to a loss of ammonia, although it is not known whether this is a single or double step reaction. The larger component of m/z 42 is due to the ion $[\text{CH}_2\text{CNH}_2]^+$, this ion is due to loss of $\text{OH}\cdot$ which is presumed to be lost from the more stable tautomeric ethenolamine radical cation. No ions are observed containing only the amino moiety, in fact the only fragment observed which contains the nitrogen atom is that at m/z 44 which also contains the carbonyl function. The calculated changes in charge distribution on ionisation for ethanamide show that the charge is lost from the oxygen atom and the amine function as well as the methyl group (see fig.6.7). It should also be borne in mind that the molecular orbital data indicates that ethenolamine tautomer is more stable as a radical cation and the change in charge distribution on ionisation for this species shows the electronic charge to increase substantially across the $\text{C}=\text{C}$ double bond, and the nitrogen function with much less change at the oxygen. This tautomer may well account for the loss of $\text{OH}\cdot$ to give rise to the ion observed at m/z 42 as discussed above. The low energy spectrum of N-methylethanamide, **11**, also shows a similar pattern with ions m/z 58 due to loss of $\text{CH}_3\cdot$ and an ion at m/z 45 which corresponds to $[\text{M}-28]^+$, although it is not clear how this ion originates or what its structure may be. The ion at m/z 43 is the acetyl cation CH_3CO^+ formed by cleavage of the C-N bond and the ion at m/z 30 is the HNCH_3^+ ion which is the other fragment from the same cleavage. Both products of the C-N bond cleavage are therefore observed in the spectrum and the nitrogen containing fragment is of greater intensity and also shows the larger gain of positive charge on ionisation. The peak at m/z 31 corresponds to the loss of ketene (CH_2CO) from the molecular ion, leaving the charge on the nitrogen containing fragment again. The low energy spectrum of **11** therefore shows several ions with the charge associated with the nitrogen containing fragments in marked contrast to the low energy spectrum of **10**. This coincides with the calculated changes in charge distribution on ionisation for these compounds where the effect of N-methylation is seen to significantly increase the gain in positive charge on ionisation by the nitrogen containing part of the molecule. The spectrum of N,N-dimethyl

ethanamide obtained using 8eV electron impact shows a peak at m/z 72 which is caused by loss of $\text{CH}_3\cdot$ from the molecular ion; a weaker peak at m/z 15 is also observed which corresponds to the same reaction with charge retention by the methyl group. The largest fragment peak appears to be at m/z 45 and this would appear to be due to loss of ketene from the molecular ion, although it is not known why this fragment should be so large in this spectrum, and it is possible that it is due to an impurity in the mass spectrometer ion source. The other fragment observed is at m/z 44 and is the $\text{CH}_3\text{NCH}_3^+$ ion caused by fission of the C-N bond, according to the change in charge distribution on ionisation this fragment gains about 0.66 of a positive charge. The 8eV spectrum of thioethanamide, **13**, shows ions at m/z 60 due to loss of $\text{CH}_3\cdot$; and at m/z 59 due to loss of $\text{NH}_2\cdot$; both these ions can be viewed as the result of α -cleavage reactions to break the C-C and the C-N bonds respectively. The other ions observed are at m/z 42 which is due to loss of $\text{HS}\cdot$ from the molecular ion, and the ion at m/z 45 which would appear to be due to HCS^+ although it is not known how this ion arises from thioethanamide or its tautomers. As with the spectrum of ethanamide above the only ion in the low energy spectrum of thioethanamide which contains the nitrogen function is the ion at m/z 60, and this ion also contains the thiocarbonyl function. This is much as we might predict when the change in charge distribution on ionisation is considered because the calculations predict the sulphur atom to gain 0.66 of a positive charge on ionisation with only 0.15 being gained by the nitrogen function or the methyl group. A more detailed discussion of the interpretation of both the 70eV and the 8eV mass spectra of all the amides and thioamides studied in terms of charge distribution is given in the next section.

6.2.3 Charge distribution and the interpretation of mass spectra.

All of the amides and thio-amides studied show major peaks due to α -cleavage of the C-N bond in their mass spectra. The ethanamides and thioethanamides also show a further α -cleavage of the C-C bond in their spectra and as outlined in fig.6.12 these reactions may be used to test whether or not the charge distribution data calculated by MO theory can be used to predict the fragmentation patterns in these molecules. As has already been pointed out

above, the charge distributions will also relate to the radical electron density distribution since separation of the charge and the radical sites have not been considered in this work. It is possible to study *distonic* ions by the molecular orbital methods employed in this study but to include the possibilities for this type of ion in this study was not possible due to the limited computer time available. With the data available one approach to using the charge/radical distribution data is to compare the charge/radical distribution calculated for the parts of the amide and thioamide molecules with the intensities of the fragment peaks observed for the same parts of the structures. If we want to compare the charge distributions on the nitrogen with those on the oxygen or sulphur atoms, then we can consider the C-N bond cleavage reaction. This reaction will give two possible products as outlined below for the methanamides and thiomethanamides, and by taking the ratio of the intensity of the two possible ionic fragments and comparing this with the ratio of the charge distributions for the two parts of the structure we can look for a correlation. This data is presented in tables 6.33 and 6.34 below for the 70eV mass spectrometric results.

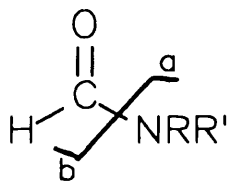


Figure 6.13 C-N bond cleavage for the methanamides.

Generally speaking the mass spectra of all the amides and thioamides studied showed peaks corresponding to both fragments a and b in the above diagram, so it is possible to see whether or not the ratio of the fragment ion intensities correlates with the calculated charge distributions for the two parts of the structure. The data in tables 6.33 and 6.34 shows that there does seem to be a correlation between the calculated charge distributions and the fragment ion intensity

ratios although the relationship would appear to be more complex than this simple treatment allows. This is indicated by the fact that the ion intensity ratio does not increase at the same rate as the charge distribution ratio with N-methylation. This may not be too surprising given the fact that there are competing reaction channels in the 70eV mass spectra and that the product ions being considered may themselves be decomposing further so that their intensities will be distorted from the simple picture provided by the charge distribution data.

Table 6.33

Change in charge distribution on ionisation for the methanamides.

	O	C	H	NRR'
NH ₂ 1	+0.40	+0.06	+0.23	+0.31
HNCH ₃ 2	+0.32	-0.09	+0.17	+0.60
CH ₃ NCH ₃ 3	+0.30	-0.10	+0.15	+0.65

Table 6.34

Fragment ion intensities and charge distribution ratios for the methanamides.

	1	2	3
Int. a (NRR') ⁺	6.86	56.53	66.08
Int. b (HCO) ⁺	28.50	16.09	11.86
Int. ratio a/b	0.26	3.50	5.5
charge ratio NRR'/O	0.78	1.88	2.17
charge ratio NRR'/HCO	0.45	1.50	1.86

As the change in charge distribution on nitrogen increases with increasing N-methylation so the

intensity of the nitrogen containing fragment ions increases. This is far too simple and the ratio of the ions a/b for compound 1 is anomalous. This may be due to the fact that there is a significant ion at m/z 17 in the spectrum of methanamide, due to NH_3^+ and this is almost certainly affecting the intensity of the peak at m/z 16. If we were to include the intensity of m/z 17 by summing the intensities for the peaks at m/z 16 and m/z 17 then the new ion ratio would be 0.81. This considerably improves the correlation with the charge distribution data, however there are other ions which could be taken into account as well such as m/z 28 which can be due to both CO^+ and NCH_2^+ for compounds 2 and 3 but only CO^+ for compound 1.

If we consider the mass spectral data for the methanamides obtained with 8eV electron impact ionisation then the ions at m/z 29 (HCO^+) are not seen in any of the spectra and it is not possible to calculate the ion intensity ratio a/b. The nitrogen containing ions (NRR') are seen to get more intense with increasing N-methylation and this also correlates with the increase in positive charge gained by this part of the molecule on ionisation.

Table 6.35

Fragment ion intensities for 8eV MS of methanamides.

	1	2	3
Int. a (NRR') ⁺	0.00	2.63	3.14
Int. b (HCO^+) ⁺	0.00	0.00	0.00

The same arguments are now applied to the data for the thiomethanamides studied and again the ratios of the ion intensities a and b have been compared with the calculated changes in charge distribution on ionisation with the corresponding parts of the molecular structure. The situation is complicated in the thiomethanamides by another reaction channel which is the formation of the ion $[\text{M-HS}]^+$ which is a substantial peak for compounds 4 and 5, although it is very weak for 6. This reaction is likely to cause a reduction in the observed intensity of the ions at m/z 45 (HCS^+) since these two reaction channels will be competing processes for the molecular ions. There is also the problem of the ion at m/z 17 (NH_3^+) interfering with the

Table 6.36

Change in charge distribution on ionisation for the thiomethanamides.

	S	C	H	NRR'
NH ₂ 4	+0.68	+0.01	+0.12	+0.19
HNCH ₃ 5	+0.64	+0.01	+0.12	+0.23
CH ₃ NCH ₃ 6	+0.56	-0.12	+0.09	+0.47

Table 6.37

Fragment ion intensities and charge distribution ratios
for the thiomethanamides.

	4	5	6
Int. a (NRR') ⁺	1.82	54.34	65.61
Int. b (HCS) ⁺	22.54	43.90	61.47
Int. ratio a/b	0.09	1.24	1.07
charge ratio NRR'/S	0.28	0.36	0.84
charge ratio NRR'/HCS	0.23	0.30	0.89

intensity of m/z 16 for compound 4, although this time the anomaly cannot be truly corrected without also considering the intensity of the $[M-HS]^+$ ions as well. If we take all these ions into account the new ion intensity ratios a/b (corrected) are 0.24, 0.75 and 1.03 for compounds 4, 5 and 6 respectively. If we take the straight a/b intensity ratio the correlation with the charge distribution data is not particularly good, however, once some of the major competing processes are accounted for with the corrected a/b ratios then the correlation looks much better. From this data it would appear that there is a correlation between the fragment ion

intensities observed in the mass spectra for the amides and thioamides and the change in charge distribution within these molecules on ionisation to form their radical cations. This is still a very simplistic approach and there are other competing fragmentations which have not been accounted for however to try to push the consideration of all the competing reactions would rapidly give rise to the situation where all the intensities of the fragment ions containing nitrogen were summed, as were all the fragment ions containing the carbonyl/thiocarbonyl group. The ratio of the summed ion intensities agreed with the charge distribution ratio for the two parts of the structure, this would have very limited predictive power for the interpretation of mass spectra. So far it has been the change in charge distribution on ionisation which has been considered in all the data given above, however, it is the radical cation which dissociates into the products observed in the mass spectrum, and therefore it is more realistic to consider the charge distribution in the radical cation and try to correlate this with the observed fragmentation. The same exercise can be carried out for the ethanamides and their thio analogs which have been included in this study, and this data is presented below.

Table 6.38

Charge distributions for methanamide and thiomethanamide radical cations.

	X = O			X = S		
	1 ⁺	2 ⁺	3 ⁺	4 ⁺	5 ⁺	6 ⁺
X	-0.20	-0.29	-0.32	+0.48	+0.43	+0.33
C	+0.68	+0.54	+0.55	+0.05	+0.06	-0.05
H	+0.42	+0.36	+0.34	+0.38	+0.37	+0.34
N	-0.84	-0.62	-0.60	-0.81	-0.78	-0.61
R	+0.47	+0.54	+0.53	+0.45	+0.47	+0.49
R'	+0.47	+0.47	+0.51	+0.45	+0.45	+0.50

The above data can now be used in a comparison with the fragment ion intensity ratios calculated previously and this data is tabulated below.

Table 6.39

Charge distributions and ion intensity ratios for the methanamides and thiomethanamides.

	1	2	3	4	5	6
ratio a/b	0.25	3.50	5.50	0.09	1.24	1.07
ratio a/b (corr.)	0.81	3.50	5.50	0.24	0.75	1.03
NRR'/X	--	--	--	0.19	0.33	1.15
NRR'/HC	0.11	0.64	0.79	0.10	0.16	0.61

The correlations with the charge distributions calculated for the radical cations are if anything better than those based on the change in charge distribution on ionisation, the only problem is that for the methanamides the oxygen atom is calculated to still carry a negative charge even in the radical cation and this leads to a rather meaningless negative ratio for NRR'/X for these compounds. However the NRR'/HCX data shows that the charge distribution now correlates quite well with the fragment ion intensity ratios, with the largest change in both charge distribution and fragment ion intensity ratio occurring for N-methylmethanamide with a further small increase in both ratios for the N,N-dimethylmethanamide. The largest change in both charge distribution ratio and fragment ion intensity ratio occurs for N,N-dimethyl thiomethanamide; these are also the compounds which in both cases show the largest calculated changes in charge distribution on ionisation. This pattern is also seen when the change in charge distribution data is used although it is less well defined. The radical cations are assumed to have no memory of the charge distribution in the neutral molecule prior to ionisation therefore it is more realistic to consider the charge distribution in the radical cations

in isolation when discussing the mass spectrometric behaviour of these compounds. The assumption that the radical cations can be considered in isolation is reasonable because it can be anticipated that the electronic reorganisation on ionisation will be very rapid in comparison to the ions lifetime; although the nuclear motion will be slower and the radical cation may not have assumed its minimum energy conformation before reaction occurs.

The same arguments as have been discussed for the methanamides can be seen to apply to the ethanamides as well and the data is presented here, although only the radical cation charge distributions are used for comparison with the ion intensity data.

Table 6.40

Charge distributions for ethanamide and thioethanamide radical cations.

	X = O			X = S		
	10 ⁺	11 ⁺	12 ⁺	13 ⁺	14 ⁺	15 ⁺
X	-0.24	-0.31	-0.34	+0.46	+0.42	+0.33
C	+0.90	+0.75	+0.76	+0.24	+0.26	+0.17
CH ₃	+0.31	+0.23	+0.18	+0.26	+0.24	+0.19
N	-0.88	-0.65	-0.63	-0.84	-0.82	-0.67
R	+0.45	+0.53	+0.52	+0.44	+0.47	+0.49
R'	+0.46	+0.46	+0.51	+0.44	+0.43	+0.49

This data will now be used in comparison with the fragment ion intensities and the intensity ratios following the method used above for the methanamides. The situation with the ethanamides is further clouded by an extra competing reaction channel for the molecular ions, namely the C-C bond cleavage reaction to lose CH₃· and form the [M-15]⁺ ion, which contains both the nitrogen atom and the oxygen/sulphur atom.

Table 6.41

Charge distributions and ion intensity ratios for the ethanamides and thioethanamides.

	10	11	12	13	14	15
Int. a	3.75	88.66	56.67	1.00	26.00	31.00
Int. b	53.57	98.97	79.00	22.00	56.00	44.00
ratio a/b	0.07	0.90	0.72	0.05	0.46	0.70
ratio a/b (corr.)	0.06	0.87	0.91	0.13	0.39	0.57
NRR'/X	--	--	--	0.09	0.19	0.94
NRR'/HC	0.03	0.52	0.67	0.04	0.09	0.45

As with the methanamides, the correlation between the charge distribution data and the fragment ion intensity data is seen, although it is not too surprising that two groups of closely similar molecules should show the same effect. It is surprising that such an apparently simple treatment produces such good correlations, especially as no account has been taken of the energies, i.e. heats of formations of the products of the reactions considered. The importance of the ionisation energies of the fragments from a reaction cannot be over emphasised, since, according to Stevenson's Rule, the fragment with the lowest IE is the one that carries the charge and thus is observed in the mass spectrum. If the C-N bond cleavage in methanamide is considered then it can be viewed as a homolytic cleavage to produce to neutral radicals, $\text{HCO}\cdot$ and $\text{NH}_2\cdot$. The ionisation energies of these species have been calculated from molecular orbital data and show that the IE for $\text{HCO}\cdot$ is the lower at 9.34eV with the IE for $\text{NH}_2\cdot$ being 10.66eV. The effect of methylating the nitrogen will be to reduce the ionisation energy and therefore as we pass through the methanamide series 4, 5 and 6 the nitrogen fragment can

increasingly compete for the charge as it's IE drops. It is also better able to stabilise a positive charge as it becomes more highly substituted. The molecular orbital calculations show the nitrogen containing part of the molecule gaining an increasing proportion of the positive charge as substitution increases at the nitrogen. From the IE's of the two fragments of C-N bond fission the HCO^+ ion would be expected to be the more intense peak in the mass spectrum and this is indeed the case for methanamide. These findings are not at odds with the calculated HOMO for methanamide, as shown earlier the calculated HOMO is a delocalised orbital containing the carbonyl π -electrons and the nitrogen lone-pair. Removing an electron from this orbital would lead to a possible delocalisation of the charge over the molecule, as is observed from the calculated charge distribution data. When the C-N bond cleaves the charge goes to the fragment with the lowest IE, in accordance with Stevenson's Rule, which in the case of methanamide is the HCO^+ fragment ion. Methylating the nitrogen brings a big change and the intensity of the nitrogen fragment becomes substantially larger than HCO^+ , the difference becoming even more marked with N,N-dimethylation, so it would appear that methylating the nitrogen reduces the IE of that fragment below the IE of HCO^+ .

Molecular orbital data was not applied to the rearrangement reactions of the amides and thioamides studied due to problems encountered in calculating the minimum energy structures of the transition states for these reactions. Unfortunately this means that the study of the fragmentation processes in relation to the charge distribution data is not as complete as it could be, however, the data obtained has shown interesting correlations between both fragment ion intensities and changes in ionisation energies on N-methylation with the calculated charge distributions for the amides and thioamides studied. These studies on the correlations between the calculated charge distributions and the charge/radical site inferred from ionisation energy measurements and observed fragmentation reactions have been extended by considering the ureas, thioureas and guanidine.

6.3. Ureas, Thioureas and Guanidine.

The first calculations on urea, thiourea and guanidine were performed using the same procedure as for the amides and thioamides discussed above, however beyond these molecules the size of the structures to be studied became a limiting factor in the use of the ab-initio method. The computer and the program could do the work but it was taking too much computer time to do each structure and therefore the semi-empirical package AMPAC was used instead for these compounds. This means that unfortunately the results for the ureas and the thioureas are not able to be directly related to the results for the amides and thioamides presented above.

For these calculations the newer AM1 hamiltonian was used whenever possible with the MNDO hamiltonian being used for all the thio-compounds since AM1 is not parametrised for sulphur. Again full geometry optimisation was carried out for all the neutral molecules and their corresponding radical cations. Interestingly, the calculations did not predict planar structures for all the ureas and thioureas studied despite the same methods being adopted for all the calculations.

First the ab-initio data for urea, thiourea and guanidine is presented and discussed, this is then compared with the semi-empirical calculations on the same compounds and then on the N-methylated series of ureas and thioureas which have been studied. Figures 6.14 and 6.15 show the ureas and thioureas respectively which have been studied in this work.

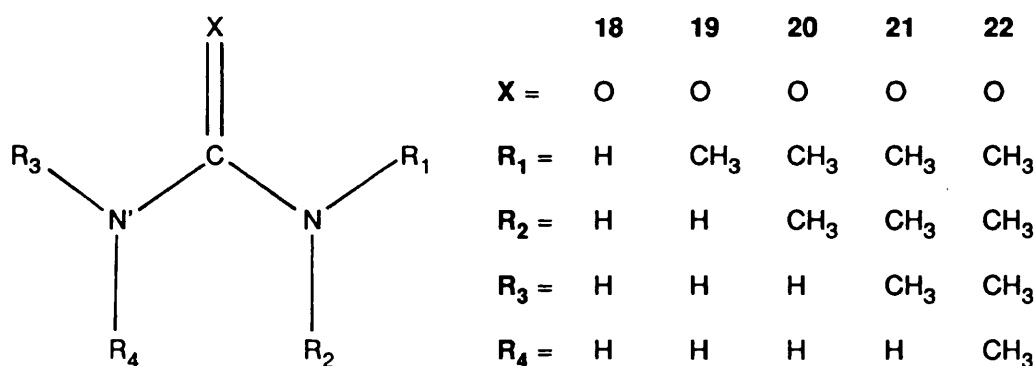


Figure 6.14. Key to the ureas studied.

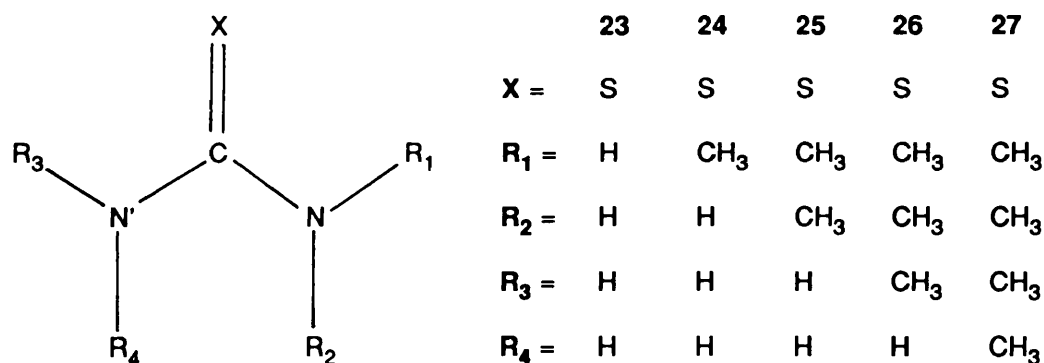


Figure 6.15. Key to the thioureas studied.

The data presented in tables 6.42 to 6.44 details the ab-initio calculated parameters for urea, thiourea and guanidine. The HOMO for urea was calculated to be ($2B_1$) and corresponds to a delocalised orbital consisting of $2p_x$ electrons from all four heavy atoms although the symmetry functions of the electron density were different for the different atoms making the orbital non-bonding. The 2-HOMO was calculated to be ($5B_2$) and corresponds to a delocalised orbital which consists primarily of oxygen lone-pair electrons, with some electron density from the N and C atoms. The symmetry point group for the molecule was C_{2v} as predicted and the molecule was predicted to be planar. The thiourea and guanidine molecules were also predicted to be planar in the ab-initio calculations as are their corresponding radical cations. The $\langle S^2 \rangle$ parameter for the radical cations is predicted to be 0.75 for a pure doublet state, although in practice higher values are usually obtained, values within 10% of the theoretical are considered acceptable. The $\langle S^2 \rangle$ parameter calculated for the urea radical cation was 0.98 and this high value indicates contamination by spin states of higher multiplicity, such as quartets, but having the same symmetry. This problem can be overcome by recalculating the structure using a larger basis set and including electron correlation. The $\langle S^2 \rangle$ parameters for the thiourea and guanidine radical cations were acceptable with values of 0.76. The charge distribution data presented in figure 6.16 indicates that the charge whilst still delocalised around

Table 6.42

Ab-initio calculated results for Urea **18**, and it's radical cation **18⁺**

Parameter	18	18 ⁺
bond lengths / Ångstroms		
N--C	1.365	1.390
C--O	1.220	1.207
C--N'	1.365	1.390
N--R ₁	0.995	1.014
N--R ₂	0.994	1.009
N'--R ₃	0.995	1.014
N'--R ₄	0.994	1.009
bond angles / degrees		
<NCO	122.80	125.04
<NCN'	114.40	109.92
<N'CO	122.80	125.04
<R ₁ NC	117.40	116.81
<R ₂ NC	123.70	125.94
<R ₃ N'C	117.40	116.81
<R ₄ N'C	123.70	125.94
Mulliken atomic charges		
O	-0.67	-0.51
C	+1.15	+1.03
N	-0.95	-0.69
R ₁	+0.37	+0.48
R ₂	+0.34	+0.45
N'	-0.95	-0.69
R ₃	+0.37	+0.48
R ₄	+0.34	+0.45

Table 6.43

Ab-initio results for thiourea **23**, and it's radical cation **23⁺**

Parameter	23	23⁺
bond lengths / Ångstroms		
N--C	1.342	1.312
C--S	1.685	1.747
C--N'	1.342	1.312
N--R ₁	0.996	1.002
N--R ₂	0.998	1.004
N'--R ₃	0.996	1.002
N'--R ₄	0.998	1.004
bond angles / degrees		
<NCS	121.85	119.14
<NCN'	116.30	121.72
<N'CS	121.85	119.14
<R ₁ NC	118.37	122.19
<R ₂ NC	123.03	121.92
<R ₃ N'C	118.37	122.19
<R ₄ N'C	123.03	121.92
Mulliken atomic charges		
S	-0.28	+0.43
C	+0.62	+0.66
N	-0.92	-0.90
R ₁	+0.40	+0.43
R ₂	+0.35	+0.42
N'	-0.92	-0.90
R ₃	+0.40	+0.43
R ₄	+0.35	+0.42

Table 6.44

3-21G^{*} Ab-Initio results for guanidine **28** and its radical cation **28⁺**

Parameter	28	28⁺
bond lengths / Ångstroms		
N--C	1.380	1.311
C--N [*]	1.268	1.416
C--N'	1.371	1.302
N [*] --H	1.009	1.017
N--R ₁ & R ₂	0.994	1.003
N--R ₃ & R ₄	0.993	1.004
bond angles / Degrees		
<NCN [*]	126.84	123.07
<NCN'	113.65	123.89
<N'CN [*]	119.51	113.05
<HN [*] C	115.19	114.62
<R ₁ NC	120.06	121.72
<R ₂ NC	122.17	122.49
<R ₃ N'C	116.89	118.16
<R ₄ N'C	123.48	123.98
Mulliken atomic charges		
N [*]	-0.79	-0.44
H	+0.25	+0.36
C	+1.04	+1.12
N	-0.95	-0.91
R ₁	+0.35	+0.43
R ₂	+0.34	+0.43
N'	-0.94	-0.87
R ₃	+0.37	+0.45
R ₄	+0.33	+0.43

the molecular and ionic structures, is somewhat less delocalised than in the amides and thioamide systems previously discussed. This is particularly true for thiourea where 0.71 of an electronic charge is calculated to be lost from the sulphur atom on ionisation. In contrast the urea molecule shows loss of 0.48 of an electronic charge from each nitrogen atom on ionisation, this is clearly evidence for the original hypothesis that the charge in the urea radical cation was located on nitrogen whereas the charge was located on sulphur in the thiourea radical cations. However it must be emphasised that the results shown in figure 6.16 relate to the change in electronic charge for the atoms on ionisation of the neutral molecule, the charge distribution in the radical cation itself is totally different, as shown in tables 6.42 to 6.44. In the case of guanidine the main site for electron loss on ionisation is from the imine nitrogen showing a change in charge distribution of +0.46 of an electronic charge. However both the amine nitrogen functions also lose some electron density and the electron loss is seen to be spread over the whole structure.

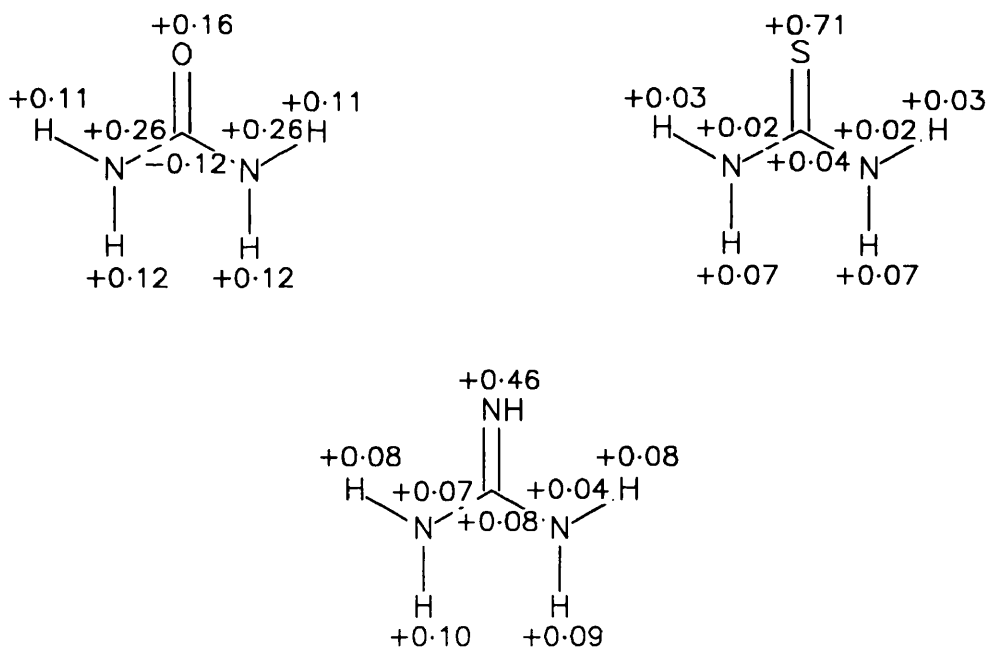


Figure 6.16 Ab-initio calculated changes in charge distribution on ionisation for urea, thiourea and guanidine.

The above calculations have been repeated using semi-empirical molecular orbital methods so that they can be compared to the calculations carried out for the N-methylated ureas and thioureas. The semi-empirical MO data is reported in tables 6.45 to 6.54 in the same format as the ab-initio data reported above. As has already been mentioned above, the semi-empirical (AMPAC) MO calculations did not always predict planar structures for all the neutral molecules studied, this is an unexpected result and may indicate that the structures reported in these cases are not the true global minimum energy structures for the molecules in question; but rather local energy minima on the potential energy surface. However, despite several attempts to minimise the energy of the molecular species starting from different geometries, the same energy minimum resulted. This may be an artifact of the methods used for this part of the study and should not be taken to indicate that these molecules actually are non-planar. These molecules were all prepared and initially energy minimised using the molecular mechanics program CHARMM (see Chapter 4 for details), however it is known that CHARMM has a bias against planar structures. The CHARMM minimised structures were then used as input for the semi-empirical MO program AMPAC (see Chapter 4 for details). Although semi-empirical MO methods have been widely used in calculating charge distributions for both neutral molecules and radical cations in the past; there are potential problems in that the methods will only give accurate descriptions for systems where the bonding situations are within the parametrisation set for the method being used. This may present problems with some of the radical cation structures, particularly where non-classical structures are thought to exist. The major reason for the popularity of the semi-empirical methods is that they require a lot less computer time than the ab-initio methods employed so far in this study, and are consequently cheaper. Ab-initio MO methods were chosen for the bulk of this study because they do not rely on any parametrisation of the method with experimental data and are therefore able to calculate any bonding situation. With the above points in mind care has to be taken with the data presented below and was not prudent to take the analysis too far when doubts exist over the validity of the calculated structures. Despite these shortcomings, the data has proved useful in studying the effect of N-methylation on ionisation energy for the ureas and thioureas.

Table 6.45

Semi-empirical (AMPAC) results for Urea **18a** and it's radical cation **18a⁺**

Parameter	18a	18a ⁺
bond lengths / Ångstroms		
N--C	1.403	1.349
C--O	1.256	1.350
C--N'	1.403	1.349
N--R ₁	0.994	1.005
N--R ₂	0.991	1.000
N'--R ₃	0.994	1.005
N'--R ₄	0.991	1.000
bond angles / degrees		
<NCO	119.96	116.68
<NCN'	120.09	126.71
<N'CO	119.96	116.61
<R ₁ NC	114.03	118.84
<R ₂ NC	118.58	122.84
<R ₃ N'C	114.03	118.81
<R ₄ N'C	118.57	122.83
Mulliken atomic charges		
O	-0.40	-0.01
C	+0.35	+0.32
N	-0.40	-0.25
R ₁	+0.22	+0.31
R ₂	+0.20	+0.29
N'	-0.40	-0.25
R ₃	+0.22	+0.31
R ₄	+0.20	+0.29

Table 6.46

Semi-empirical (AMPAC) results for N-methyl urea **19** and it's radical cation **19⁺**

Parameter	19	19 ⁺
bond lengths / Ångstroms		
N--C	1.411	1.493
C--O	1.255	1.241
C--N'	1.404	1.356
N--R ₁	1.434	1.388
N--R ₂	0.996	1.007
N'--R ₃	0.994	1.001
N'--R ₄	0.991	0.992
bond angles / degrees		
<NCO	121.26	114.67
<NCN'	119.36	118.57
<N'CO	119.38	126.76
<R ₁ NC	118.03	119.92
<R ₂ NC	116.69	120.21
<R ₃ N'C	114.01	116.89
<R ₄ N'C	118.75	124.14
Mulliken atomic charges		
O	-0.39	-0.27
C	+0.35	+0.36
N	-0.35	-0.09
R ₁	+0.17	+0.51
R ₂	+0.20	+0.27
N'	-0.40	-0.35
R ₃	+0.22	+0.30
R ₄	+0.20	+0.27

Table 6.47

AMPAC results for N,N-dimethylurea **20** and its radical cation **20⁺**

Parameter	20	20⁺
bond lengths / Ångstroms		
N--C	1.417	1.501
C--O	1.256	1.239
C--N'	1.400	1.360
N--R ₁	1.437	1.419
N--R ₂	1.441	1.414
N'--R ₃	0.990	0.991
N'--R ₄	0.994	1.000
bond angles / degrees		
<NCO	120.62	114.86
<NCN'	120.54	119.36
<N'CO	118.84	125.78
<R ₁ NC	119.44	121.50
<R ₂ NC	116.71	116.62
<R ₃ N'C	114.34	116.85
<R ₄ N'C	119.41	124.03
Mulliken atomic charges		
O	-0.40	-0.26
C	+0.36	+0.36
N	-0.31	-0.05
R ₁	+0.15	+0.36
R ₂	+0.18	+0.41
N'	-0.40	-0.37
R ₃	+0.22	+0.26
R ₄	+0.20	+0.30

Table 6.48

AMPAC results for tri-methylurea **21** and it's radical cation **21⁺**

Parameter	21	21 ⁺
bond lengths / Ångstroms		
N--C	1.409	1.515
C--O	1.256	1.238
C--N'	1.405	1.359
N-R ₁	1.436	1.412
N--R ₂	1.431	1.416
N'--R ₃	1.431	1.449
N'--R ₄	0.993	0.996
bond angles / degrees		
<NCO	119.95	113.54
<NCN'	119.72	117.73
<N'CO	120.33	128.73
<R ₁ NC	118.65	117.24
<R ₂ NC	123.57	118.95
<R ₃ N'C	119.20	120.06
<R ₄ N'C	118.66	121.72
Mulliken atomic charges		
O	-0.40	-0.26
C	+0.39	+0.36
N	-0.34	-0.07
R ₁	+0.15	+0.21
R ₂	+0.19	+0.35
N'	-0.37	-0.32
R ₃	+0.18	+0.28
R ₄	+0.21	+0.26

Table 6.49

AMPAC results for tetra-methylurea **22** and it's radical cation **22⁺**

Parameter	22	22 ⁺
bond lengths / Ångstroms		
N--C	1.419	1.410
C--O	1.256	1.250
C--N'	1.418	1.423
N--R ₁	1.439	1.445
N--R ₂	1.443	1.424
N'--R ₃	1.438	1.440
N'--R ₄	1.443	1.421
bond angles / degrees		
<NCO	119.60	118.79
<NCN'	120.79	123.55
<N'CO	119.61	117.65
<R ₁ NC	115.74	114.81
<R ₂ NC	119.94	125.88
<R ₃ N'C	115.86	114.88
<R ₄ N'C	120.10	125.65
Mulliken atomic charges		
O	-0.39	-0.31
C	+0.37	+0.32
N	-0.31	-0.15
R ₁	+0.15	+0.34
R ₂	+0.17	+0.29
N'	-0.31	-0.13
R ₃	+0.16	+0.34
R ₄	+0.17	+0.29

Table 6.50

Semi-empirical (AMPAC) results for thiourea **23a** and its radical cation **23a⁺**

Parameter	23a	23a ⁺
bond lengths / Ångstroms		
N--C	1.406	1.347
C--S	1.579	1.700
C--N'	1.405	1.347
N--R ₁	1.004	1.006
N--R ₂	1.005	1.007
N'--R ₃	1.004	1.007
N'--R ₄	1.005	1.008
bond angles / degrees		
<NCS	122.63	120.36
<NCN'	114.75	119.95
<N'CS	122.62	119.69
<R ₁ NC	116.77	124.27
<R ₂ NC	113.60	120.96
<R ₃ N'C	116.81	124.53
<R ₄ N'C	113.63	121.35
Mulliken atomic charges		
S	-0.17	+0.36
C	+0.12	+0.19
N	-0.29	-0.26
R ₁	+0.15	+0.24
R ₂	+0.16	+0.25
N'	-0.29	-0.27
R ₃	+0.15	+0.24
R ₄	+0.16	+0.25

Table 6.51

AMPAC results for N-methyl thiourea **24** and it's radical cation **24⁺**

Parameter	24	24⁺
bond lengths / Ångstroms		
N--C	1.397	1.353
C--S	1.582	1.693
C--N'	1.411	1.353
N--R ₁	1.463	1.487
N--R ₂	1.005	1.011
N'--R ₃	1.005	1.006
N'--R ₄	1.004	1.005
bond angles / Degrees		
<NCS	124.27	122.09
<NCN'	114.14	119.44
<N'CS	121.59	118.47
<R ₁ NC	122.94	126.35
<R ₂ NC	124.20	119.22
<R ₃ N'C	113.25	120.84
<R ₄ N'C	116.69	124.04
Mulliken atomic charges		
S	-0.20	+0.35
C	+0.16	+0.18
N	-0.36	-0.29
R ₁	+0.22	+0.33
R ₂	+0.17	+0.23
N'	-0.29	-0.28
R ₃	+0.16	+0.25
R ₄	+0.14	+0.24

Table 6.52

AMPAC results for N,N-dimethyl thiourea **25** and it's radical cation **25⁺**

Parameter	25	25 ⁺
bond lengths / Ångstroms		
N--C	1.402	1.365
C--S	1.584	1.681
C--N'	1.411	1.356
N--R ₁	1.473	1.493
N--R ₂	1.470	1.490
N'--R ₃	1.006	1.004
N'--R ₄	1.004	1.002
bond angles / Degrees		
<NCS	123.90	121.54
<NCN'	115.59	121.72
<N'CS	120.51	116.74
<R ₁ NC	118.92	119.18
<R ₂ NC	122.56	123.38
<R ₃ N'C	112.82	120.97
<R ₄ N'C	116.45	124.84
Mulliken atomic charges		
S	-0.21	+0.36
C	+0.18	+0.19
N	-0.42	-0.34
R ₁	+0.22	+0.30
R ₂	+0.21	+0.30
N'	-0.29	-0.29
R ₃	+0.16	+0.24
R ₄	+0.14	+0.24

Table 6.53

AMPAC results for tri-methyl thiourea **26** and its radical cation **26⁺**

Parameter	26	26 ⁺
bond lengths / Ångstroms		
N--C	1.406	1.363
C--S	1.593	1.681
C--N'	1.389	1.358
N--R ₁	1.475	1.491
N--R ₂	1.466	1.492
N'--R ₃	1.461	1.481
N'--R ₄	0.998	1.006
bond angles / Degrees		
<NCS	122.02	118.90
<NCN'	117.26	120.00
<N'CS	120.72	121.11
<R ₁ NC	117.96	121.01
<R ₂ NC	124.49	122.20
<R ₃ N'C	124.57	123.49
<R ₄ N'C	121.19	118.97
Mulliken atomic charges		
S	-0.26	+0.36
C	+0.25	+0.18
N	-0.43	-0.34
R ₁	+0.23	+0.30
R ₂	+0.20	+0.28
N'	-0.40	-0.31
R ₃	+0.23	+0.31
R ₄	+0.18	+0.23

Table 6.54

AMPAC results for tetra-methyl thiourea **27** and it's radical cation **27⁺**

Parameter	27	27 ⁺
bond lengths / Ångstroms		
N--C	1.442	1.369
C--S	1.580	1.690
C--N'	1.393	1.362
N--R ₁	1.472	1.494
N--R ₂	1.471	1.491
N'--R ₃	1.474	1.495
N'--R ₄	1.472	1.492
bond angles / Degrees		
<NCS	122.97	118.04
<NCN'	113.63	123.03
<N'CS	123.41	118.93
<R ₁ NC	115.88	120.03
<R ₂ NC	115.57	124.39
<R ₃ N'C	118.80	119.48
<R ₄ N'C	123.69	125.24
Mulliken atomic charges		
S	-0.18	+0.32
C	+0.20	+0.19
N	-0.43	-0.36
R ₁	+0.18	+0.30
R ₂	+0.18	+0.29
N'	-0.39	-0.33
R ₃	+0.22	+0.30
R ₄	+0.22	+0.30

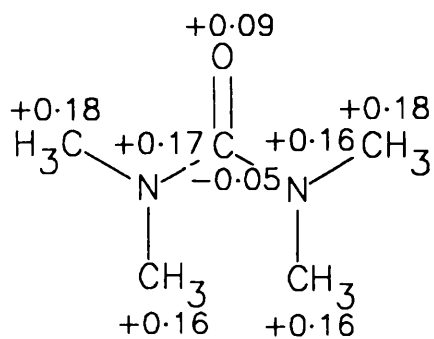
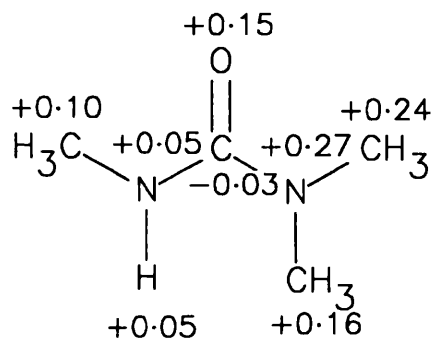
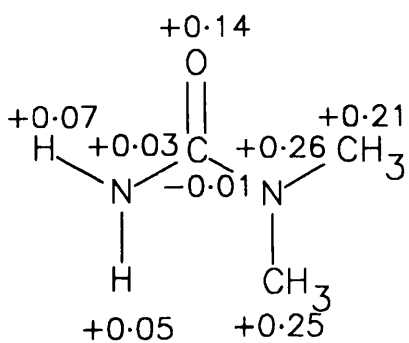
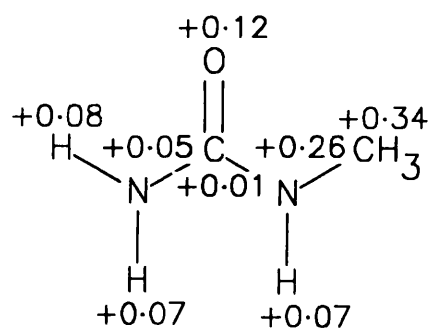
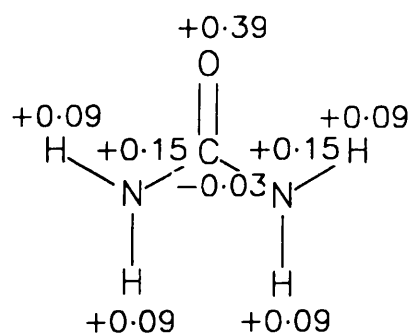


Figure 6.17 AMPAC calculated change in charge distribution on ionisation for the ureas.

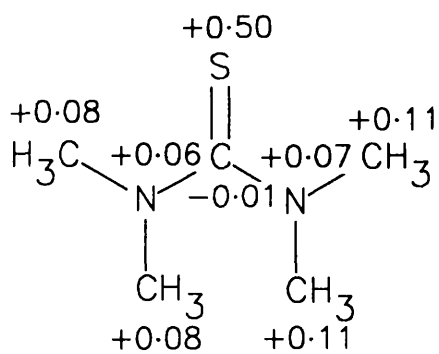
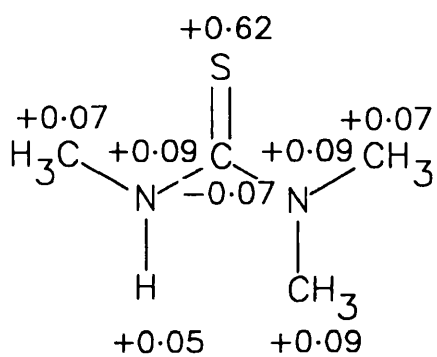
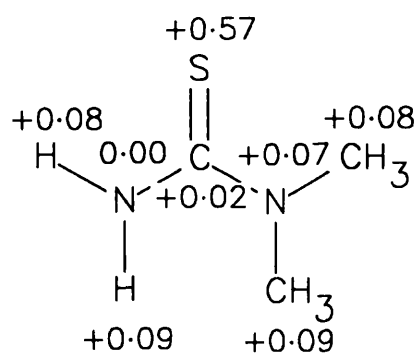
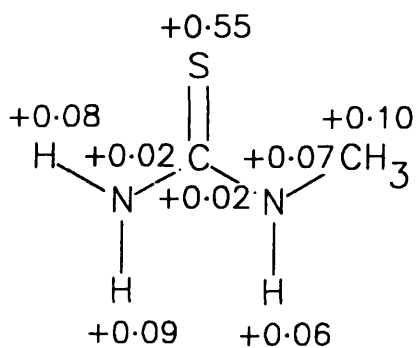
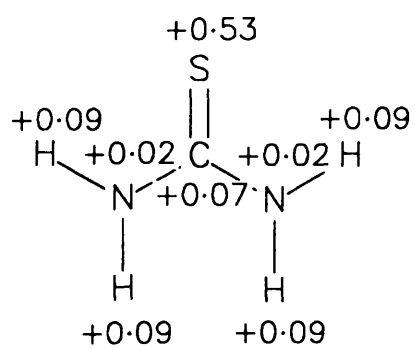


Figure 6.18 AMPAC calculated change in charge distribution on ionisation for the thioureas.

The data presented above for the ureas and thioureas closely parallels that presented above for the amides and thioamides using ab-initio MO calculations. The semi-empirical MO calculations again show the sulphur atom gains most in positive charge on ionisation of the thioureas, whereas the charge is shared almost equally between the oxygen and the two nitrogens for urea. The effect of N-methylation is once again to increase the amount of positive charge associated with the nitrogen moieties, this increase is substantial in the ureas but is much less significant in the thioureas. This is analogous to the results for the amides and thioamides above. A similar pattern emerges for the calculated HOMO's for the ureas and thioureas, the major difference being that the HOMO in the case of the ureas is a delocalised orbital comprising carbonyl π -electrons and lone pair electrons from both nitrogen atoms. This may explain why the change in charge distribution on ionisation shows the positive charge evenly shared by both nitrogen atoms for urea and tetramethyl-urea. The HOMO for the thioureas is again calculated to be an orbital containing the sulphur lone pair electrons.

The calculated HOMO's for the neutral molecules have again been used to calculate the IE's of the compounds using Koopman's theorem and the results have been empirically scaled by 0.92 as discussed above for the amides and thioamides. This IE data is presented in table 6.55 along with data obtained by mass spectrometry^{2,3,19} for comparison. The data shows that the calculated ionisation energies are reasonably comparable to those measured by EI/MS, although they tend to be slightly higher than the measured data. This is not too surprising in view of the doubts about the calculated structures not all representing global energy minima on the potential energy surface. The data clearly shows the greater effect that N-methylation has on the ionisation energies for the ureas in comparison with that for the thioureas. This can be rationalised by same arguments as have already been used in the case of the amides and thioamides discussed above; namely that the effect of N-methylation on the ionisation energies of the ureas is greater because this is a primary effect. The substitution is taking place directly at the proposed charge site, whereas the effect of N-methylation on the ionisation energies of the thioureas is lesser because this is a secondary effect with the substitution occurring remote from the proposed charge site. The data is not as clear cut as that for the amides and

thioamides, although this is also true for the EI/MS data so that the effect of N-methylation is not simply additive for these compounds.

Table 6.55

Ionisation Energies of the ureas and thioureas studied.

Substitution	AMPAC MO calculated IE's /eV		EI/MS measured IE's /eV	
	Urea	Thiourea	Urea	Thiourea
Unsubstituted	9.77	8.38	10.27	8.50
N-Methyl	9.31	8.24	9.73	8.29
N,N-Dimethyl	8.92	8.22	9.10	8.34
N,N'-Dimethyl	-	-	9.42	8.17
Trimethyl	8.73	7.94	8.94	7.93
Tetramethyl	8.72	8.23	8.74	7.95

The effect of N-methylation on the HOMO's of the ureas is to increase the energy separation of the two highest orbitals as is also observed for the amides, in the case of the thioureas, the effect of N-methylation is to decrease the energy separation of the two highest orbitals as was seen for the thioamides. In this respect the data for the amides and thioamides is completely analogous to that for the ureas and thioureas reported above. The data reported here for the ureas and thioureas also shows that the charge in the radical cations is delocalised over the ionic structures, despite this there is also some support for the representation of the molecular ions given in figure 6.19. These representations are those put forward by Maccoll and co-workers on the basis of the ionisation energy measurements reported above. The calculated data reported here shows these representations not to be unreasonable notwithstanding the fact that the charge is certainly delocalised over the ionic structures. This is

particularly true for the N-methylated compounds, where most charge is lost from the substituted nitrogen on ionisation for the ureas, but most charge is still lost from the sulphur atom on ionisation of the thioureas.

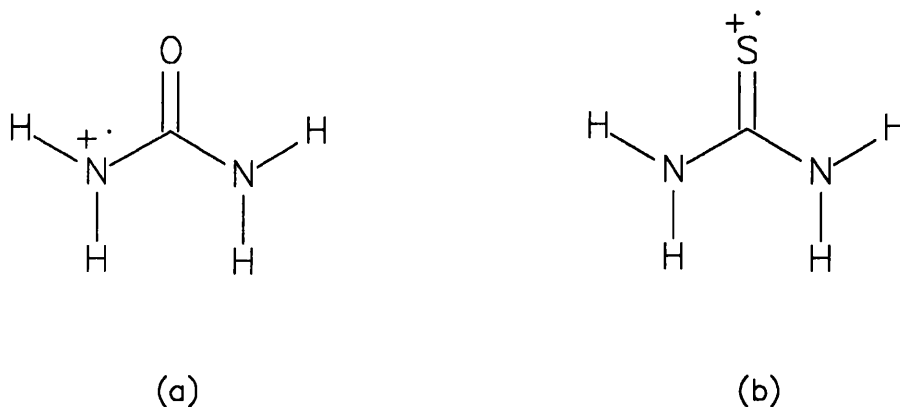


Figure 6.19 Representations of M^+ for (a) urea and (b) thiourea.

6.3.1 Charge distribution and mass spectrometry.

The fragmentation of the ureas and thioureas in relation to the experimentally predicted charge site was the subject of a series of papers during the 1970's by Baldwin and co-workers.²⁰⁻²³ The data presented in these papers was used to conclude that the molecular ion representations given above in figure 6.19 were the most likely situations to be found in the ground state molecular ions. These conclusions were derived from the observed differences in fragmentation for the different classes of molecule as well as the changes in ionisation energy on methylation, which has been discussed above. The fragmentation of the ureas was shown to proceed via four major reactions (see Chapter 5) which together with the molecular ion accounted for about 70% of the total ion current observed.²⁰ For the purposes of this work the rearrangement reactions will be ignored, since to use the charge distribution data effectively some knowledge of the charge distribution in the transition state is required. As has already been explained in the discussion for the amides and thioamides, this data was not obtained in this study due to the excessive demand on computer time required to calculate all the transition states for all the

molecules studied. The main reaction considered will again be the cleavage of the central C-N bond, which can be regarded as an α -cleavage reaction. The previous study on the fragmentation of the ureas used the ratio of the ion products from this cleavage, namely $A^+/[M-A]^+$ to study the possible charge location in the molecular ion. This approach has been followed in this work and the charge distribution ratios for the same cleavage products has been calculated for comparison with the ion intensity data previously reported.

In table 6.56 the recorded intensity ratios for the product ions $A^+/[M-A]^+$ are shown along with the calculated charge distribution ratios for the same ion products. The charge distribution ratios have been determined from the calculated charge distributions for the radical cations of the ureas studied by summing the appropriate atomic charges presented in tables 6.45 to 6.49. The charge distributions which have been used in this treatment are those calculated for the radical cations themselves and not the data for the change in charge distribution on ionisation, since it is the radical cation which is fragmenting to produce the observed products.

Table 6.56

Observed ion intensity ratios and calculated charge distribution ratios $A^+/[M-A]^+$ for the ureas.

	NH ₂ CO		MeNHCO		Me ₂ NCO	
	Rel. Int. ratio	Charge Dist. ratio	Rel. Int. ratio	Charge Dist. ratio	Rel. Int. ratio	Charge Dist. ratio
NH ₂	0.30	0.54	0.50	0.27	0.30	0.22
MeNH	3.10	2.33	2.00	-	0.35	0.28
Me ₂ N	7.20	2.57	5.00	2.13	0.30	0.92

Despite the simplistic nature of the treatment some correlation is observed between the observed fragment ion ratios and the calculated charge distributions for the putative fragments in the molecular radical cation. It is almost certainly not worth trying to extend the analysis

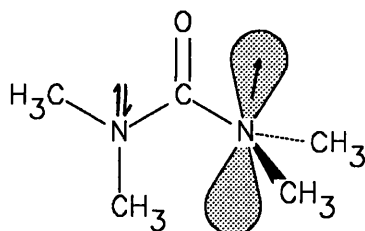
beyond the treatment given above, particularly since the use of the observed ion intensity ratios measured at the detector has been shown to be an unreliable indicator of the concentration of those ions in the source of the mass spectrometer.²⁴ This is mainly due to the fact that the kinetics of the reactions have been ignored and the rate constants have been shown to vary with the accelerating voltage used in the instrument. The above data has also taken no account of competing or consecutive reaction channels which may distort the observed ion intensity ratios. In general the data reflects the increasing stability of the ions formed so that the series; $\text{Me}_2\text{N}^+ > \text{MeN}^+\text{H} > \text{N}^+\text{H}_2$ and $\text{Me}_2\text{N}^+\text{CO} > \text{MeN}^+\text{HCO} > \text{N}^+\text{H}_2\text{CO}$ can readily be deduced.

6.4 The tetra-methylurea radical cation.

During the period 1986 to 1987 there was considerable debate in the literature about the structure of the tetra-methylurea (TMU) radical cation and its stability. The debate centred around the observation that the e.s.r. spectrum of a dilute solution of TMU in CFCl_3 at 77K and after exposure to γ -rays from ^{60}Co appeared to be identical to the esr spectrum for $\cdot\text{NMe}_2$ radicals generated by other means. These observations suggested to Symons that the parent TMU radical cations underwent a unimolecular breakdown as shown below.²⁵



However this scheme raised strong objections from Qin et al., who favoured an 'orthogonal' structure where the TMU radical cation had become deconjugated (see below),²⁶ on chemical grounds.



The above reaction scheme is of course observed in the mass spectrum of TMU and the

original authors soon responded that the new interpretation whilst reasonable was not compelling and that the breakdown scheme previously presented was still possible, with the deconjugated structure existing as a transition state on the way to the central C-N cleavage. This required that the deconjugated structure be accessible but not necessarily the lowest energy structure. However Qin et al. seemed to be convinced that they had correctly interpreted their data so Symons et al. performed further experiments using ^{13}C labelled TMU, with the labelled atom being the carbonyl carbon. In this compound the $\text{Me}_2\text{N}^\bullet$ radicals would not show any significant ^{13}C hyperfine coupling. The results were definitive and seemed to establish beyond all doubt that the deconjugated structure (shown above) was correct since ^{13}C splittings were observed on all signals in the esr spectrum. The results agreed with those expected for the deconjugated structure and ruled out the fragmentation reaction at 77K.²⁷ This was interpreted as evidence for the novel concept that deconjugation can occur in a π -system on electron loss. At about the same time the whole concept of stabilisation via π -delocalisation was called into question as a broad generalisation in a much wider context.²⁸ The reason this discussion has been included here is that the calculations carried out for this thesis included TMU both as a neutral molecule and a radical cation, so as a matter of interest the calculated results were compared with the esr conclusions.

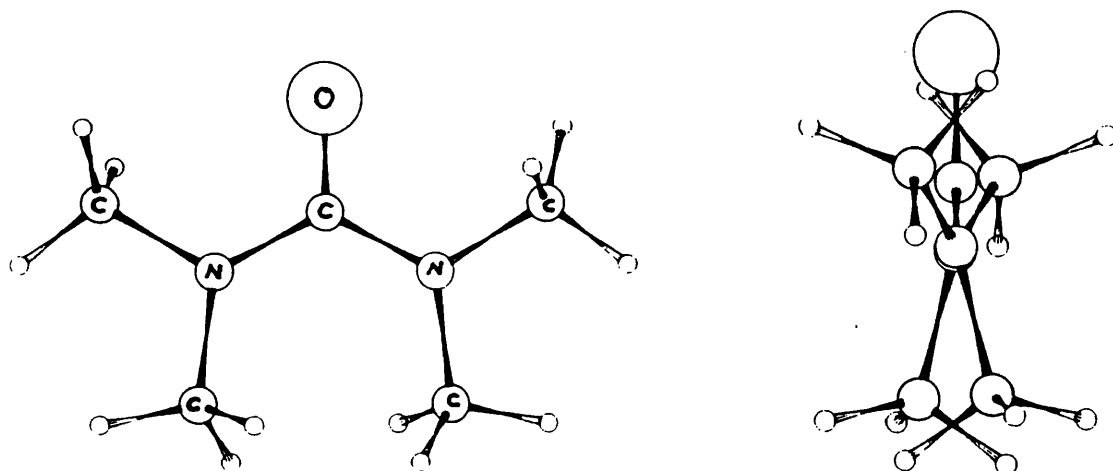


Figure 6.20 AMPAC calculated structures for the radical cation of TMU.

Despite starting from planar conformations, the calculations predict non-planar structures for both the neutral molecule and the radical cation of TMU. The loss of planarity seemed to be due to a steric interaction between the methyl substituents on the nitrogen atoms. Interestingly the calculations predict that the conjugation between the N-lone pairs and the carbonyl π -electrons has been lost for both N atoms (see figure 6.19), and the orthogonal structure found by esr is not the structure found in these calculations.

Unfortunately it is not possible to say too much about this because there is no guarantee that the structures calculated are true global minimum energy structures. It is possible that the calculated structures reported above are local minima on the potential energy surface, this problem was addressed by explicitly calculating the 'orthogonal' structure using the AM1 hamiltonian with full geometry optimisation. The results were disappointing in that the fully optimised structure obtained was identical, within the accuracy of the experimental method, to the structure obtained when the planar geometry was used as the starting point. This does not rule out the possibility of an 'orthogonal' structure since the starting geometry for the calculation performed here may not have been good enough for the program to have located the required 'orthogonal' energy minimum. The major fragmentation observed in the 70eV mass spectrum of tetra-methyl urea is the C-N bond cleavage reaction as discussed above, and this might be expected if the 'orthogonal' structure predicted by the esr experiments were correct, in that the conjugation between the carbonyl- π electrons and the nitrogen lone-pair would have been broken for one of the C-N bonds. The calculations reported here do not provide any evidence for such an orthogonal structure for the tetramethyl urea radical cation but these calculations are certainly not exhaustive and cannot rule out the possible existence of such a structure. The only compound where an orthogonal structure was considered was urea itself and in all cases no stable structure could be found, although a higher energy minimum was found for a structure of urea with both NMe₂ groups rotated through 90 degrees relative to the more stable planar conformation.

6.5 Conclusions.

The work presented here describes an investigation into the correlation of calculated charge distributions, in both neutral molecules and their corresponding radical cations, with the fragmentation of those radical cations observed in a mass spectrometer. It is common within mass spectrometry to rationalise fragmentation reactions by first assigning a specific structure to the molecular radical cation. This is generally accomplished by assuming that a low energy electron, such as a non-bonding electron, from a "lone-pair", on a hetero atom will be lost on ionisation such that the heteroatom is written as carrying both the charge and the radical electron. This charge localisation concept, first introduced by McLafferty, has enjoyed much popularity in that it allows electrons "book-keeping" to be carried out and can rationalise fragmentation reactions by treating them analogously to other organic reactions.

Previous studies of this type have been discussed in chapter 5 and have utilised a range of calculation methods and have arrived at a number of different points of view concerning the utility of the approach.

The amides and their thio-analogues were chosen as the subjects for this study because of the existing mass spectrometric evidence that the two classes were ionised from different orbitals. This was the conclusion of Maccoll and co-workers from a detailed study of the effect of N-methylation on the ionisation potentials of these classes of compound. The results presented in this work clearly show the ab-initio calculations performed are able to accurately reflect these results and the calculated ionisation potentials are in excellent agreement with those measured from mass spectrometry and photoelectron spectroscopy. It is not too surprising that, given the sophistication of the current computational programs, they are able to accurately reflect chemical trends such as occur on N-methylation. The calculated data in this study reinforces the previous conclusions that the amides and thioamides are indeed ionised from different orbitals. This is indicated by the fact that the radical cations have different electronic states and the HOMO's are of different symmetries, however the charge distribution data for the radical cation alone would not support the concept of charge localisation as concluded from the mass

spectrometric work. The effect of N-methylation on the energies of the HOMO's and therefore on the ionisation energies of the molecules is also calculated to very closely follow the patterns observed from the mass spectrometric measurements. The effect of N-methylation on the ionisation energy is greatest in the amides and ureas where the substitution is occurring in close proximity to the ionised orbital. In the thioamides and thioureas the effect of N-methylation on the ionisation energy is much less significant, and this can be regarded as being due to the substitution occurring at a site remote from the ionised orbital in these compounds. These conclusions are also supported by the geometric changes which the compounds undergo on ionisation, the bond length and bond angle changes are not unexpected for electron loss from the calculated highest occupied molecular orbitals. In fact if we ignore charge localisation, the calculated data is in extremely good agreement with the experimental data from mass spectrometry. The results clearly show that in the molecular radical cations the charge is not localised on any one heteroatom, this result is also not surprising since the highest occupied molecular orbitals (HOMO's) are not generally localised on one specific atom either. Therefore any electron loss from the HOMO will be from a delocalised molecular orbital and will thus give rise to a delocalised charge. This is a consequence of the molecular orbital method, which takes atomic orbitals and combines them with other atomic orbitals of similar energy to form multi-centre molecular orbitals. This is generally true for all the compounds studied in this work. Significant differences in the charge distributions of the amides and their thio-analogues are seen, for example, the sulphur atom is the only heteroatom in all the molecules studied which is ever calculated to become positively charged.

The calculated charge distributions show major differences however when the change in charge distribution upon ionisation is considered. The change in charge distribution on ionisation is calculated by taking the difference between the charge distributions calculated for the neutral molecule and its corresponding radical cation. Here the thio-analogues show substantial loss of electron density from the sulphur atom, this is consistent with the HOMO being calculated to be a sulphur "lone-pair" orbital. The amides show loss of electron density from both the amide oxygen and nitrogen atoms, this is consistent with the HOMO being calculated to be a

largely delocalised orbital comprising the nitrogen "lone-pair" and the carbonyl π -electrons. The fact that the charge in the molecular radical cations is delocalised in both the amides and the thioamides raises the issue of what, if any, is the physical significance of the charge localisation concept. The calculated changes in charge distributions upon ionisation show good correlation with a charge localisation picture, albeit that the charge is never calculated to be completely localised on any one atom. This is again a direct consequence of the molecular orbital methods used. The reason why the change in charge distribution on ionisation shows such a good correlation is not known at present, after all it is the radical cation which undergoes fragmentation and the charge distribution in the radical cation shows the charge to be substantially delocalised. The QET theory of mass spectrometric fragmentation rests on the assumption that the internal energy acquired on ionisation is totally randomised prior to fragmentation occurring. It is known that many carbocations undergo rearrangements prior to fragmentation and given that the speed of electron motions within molecules and ions is orders of magnitude faster than nuclear motion, it would be expected that electron reorganisation should also be complete before fragmentation takes place. This would indicate that there should be no memory of the ions previous structure or charge distribution to influence the reactions. This study also includes some calculations on radical cations having the same geometrical structure as the parent neutral molecule, these calculations do show marginally less delocalisation of charge around the whole molecular structure as would be expected, however the charge is certainly not localised even in this case.

The attempt to correlate the calculated charge distributions with the observed mass spectra for the compounds studied again provided some interesting data but no clear conclusions can be drawn without a more detailed study being carried out. Some correlation between fragment ion intensities and charge distributions was observed both for the radical cations themselves and for the change in charge distribution on ionisation. Unfortunately due to the complexity and time consuming nature of these calculations many isomeric possibilities were excluded from this study as were all *distonic* ion structures. To include all possible structures for the number of molecules studied here was not practicable. This means that the observed fragment ions are

assumed to have all been produced by the one parent structure, this is not very realistic, particularly in the case of the 70eV spectra, where the spread of internal energies would allow re-arrangements to occur and other ion structures are well within reach given 1-2 eV of internal energy. The secondary fragmentation reactions have also not been considered in any detail here, and therefore this can only be regarded as a very simple treatment of the results from the available data.

These are not the only difficulties or shortcomings with a study of this type. The validity of the Mulliken population analysis has already been discussed in previous chapters, but the point remains that it is an arbitrary technique for calculating atomic charges from the overlap orbitals whose electrons are shared by more than one atomic centre. Other methods for dividing the electron population up into discrete atomic contributions exist and some are known to produce more reliable figures than the Mulliken analysis in some instances. These newer methods are now becoming more widely available although most commercial programs are still supplied with the Mulliken analysis as standard.

The amides were studied for a variety of reasons, not least because of the existing experimental data as mentioned above, but also because by understanding the electronic structure of the amides and their thio-analogues and how that structure affects the fragmentation chemistry of these compounds it was hoped that much would be learned which could be applied to studies on larger amide linked peptide and protein systems. This may still be possible but many more detailed calculations are required before many firm conclusions can be drawn from this work. It is somewhat surprising that a method which totally ignores the kinetics of fragmentation reactions can provide any correlation with the observed peak intensities in the mass spectra, accounting for these secondary fragmentations still assumes that all fragmentation reactions are occurring in the ion source, this is in fact not a bad assumption, since metastable ions typically account for only 1-2% of the total ion current recorded in a mass spectrum.

The correlations obtained, between the calculated charge distributions and the observed fragment ion ratios indicate that further work in this area may be justified but it is likely that only

access to large scale computing facilities and large amounts of computer time will allow any significant progress to be made. On the basis of the results presented here little physical significance can be attached to the charge localisation approach to fragmentation reactions. However, the interesting correlations which were observed mean that the concept should not be dismissed out of hand, it still provides a useful tool which will undoubtedly continue to be used until a better model takes its place.

6.6 References.

1. J.S. Binkley, R.A. Whiteside, K. Raghavachari, R. Seeger, D.J. DeFrees, H.B. Schlegel, M.J. Frisch, J.A. Pople and L.R. Kahn, GAUSSIAN82 Release A, Carnegie-Mellon University, Pittsburgh, (1982).
2. M.A. Baldwin, A. Kirkien-Konasiewicz, A.G. Loudon, A. Maccoll and D. Smith, *Chem. Commun.*, 574 (1966).
3. M.A. Baldwin, A.G. Loudon, K.S. Webb and P.C. Cardnell, *Org. Mass Spectrom.*, **12**, 279 (1977).
4. C.R. Brundle, D.W. Turner, M.B. Robin and H. Basch, *Chem. Phys. Letts.*, **3**, 292 (1969).
5. T. Ottersen, *Acta Chem. Scand. A*, **29**, 939 (1975).
6. J.A. Defina and P.R. Andrews, *Int. J. Quant. Chem.*, **18**, 797 (1980).
7. L. Radom and N.V. Riggs, *Aust. J. Chem.*, **35**, 1071 (1982).
8. M. Kitano and K. Kutchitsu, *Bull. Chem. Soc. Japan*, **47**, 67 (1974).
9. M. Kitano and K. Kutchitsu, *Bull. Chem. Soc. Japan*, **47**, 631 (1974).
10. J. Hrusak and M. Tkaczyk, *Org. Mass Spectrom.*, **25**, 214 (1990).
11. G.W. Mines and H.W. Thompson, *Spectrochim. Acta*, **31A**, 137 (1975).
12. A.E. Reed, R.B. Weinstock and F. Weinhold, *J. Chem. Phys.*, **83**, 735 (1985).
13. D.H. Williams and J.H. Beynon, *Org. Mass Spectrom.*, **11**, 103 (1976).
14. H. Schwarz, *Advances in Mass Spectrom.*, Part A, Ed. J.F.J. Todd, p13, Wiley (1986), and references within.
15. J. A. Gilpin, *Analytical Chemistry*, **31**, 935-9 (1959).
16. A. Maccoll, *Org. Mass Spectrom.*, **15**, 109 (1983).
17. D.P. Stevenson, *Disc. Faraday Soc.*, **10**, 35 (1951).
18. H.E. Audier, *Org. Mass Spectrom.*, **2**, 283 (1969).
19. M.A. Baldwin, A. Maccoll, A. Kirkien-Konasiewicz and B. Saville, *Chem. and Ind.*, 286 (1966).

20. M.A. Baldwin, A. Kirkien-Konasiewicz, A.G. Loudon, A. Maccoll and D. Smith, *J. Chem. Soc. (B)*, 34 (1968).
21. M.A. Baldwin, A.M. Kirkien, A.G. Loudon and A. Maccoll, *Org. Mass Spectrom.*, 4, 81-88 (1970).
22. M.A. Baldwin, P.C. Cardnell, A.G. Loudon, A. Maccoll and K.S. Webb, *Advances in Mass Spectrom.*, Vol.5, The Institute of Petroleum (1970).
23. M.A. Baldwin, A.G. Loudon, A. Maccoll and K.S. Webb, *Org. Mass Spectrom.*, 11, 1181 (1976).
24. I. Howe and D.H. Williams, *J. Chem. Soc. (B)*, 1213 (1968).
25. M.C.R. Symons, *J. Chem. Soc. Chem. Commun.*, 866 (1987).
26. X-Z. Qin, T.C. Pentecost, J.T. Wang and F. Williams, *J. Chem. Soc. Chem. Commun.*, 450 (1987).
27. C.J. Rhodes, I.D. Podmore and M.C.R. Symons, *J. Chem. Soc. Chem. Commun.*, 1638 (1987).
28. S.S. Shaik, P.C. Hiberty, J-M. Lefour and G. Ohanessian, *J. Amer. Chem. Soc.*, 109, 363 (1987).

Appendix I Publications as author or co-author.

1. Fast atom bombardment using a commercial field ionization/field desorption source. M.A. Baldwin, D.M. Carter and K.J. Welham, *Org. Mass Spectrom.*, 18, 176, (1983).
2. An inexpensive micro-computer based signal averaging system. M.A. Baldwin, D.M. Carter and K.J. Welham, Proceedings of the 13th meeting of the British Mass Spectrometry Society, Warwick 1983, p34.
3. A study of the metal binding ability of small peptide analogues of Gramicidin A by FAB/MS. M.A. Baldwin and K.J. Welham, Proceedings of the 14th meeting of the British Mass Spectrometry Society, Edinburgh 1984, p114.
4. Quantitative aspects of metal ion complexation studied by FAB mass spectrometry. M.A. Baldwin and K.J. Welham, *Advances in Mass Spectrometry*, (Ed. J.F.J. Todd), Wiley, Part B, 1585-1586, (1986).
5. $[M + 18]^+$ peaks in FAB/MS using thioglycerol matrix. M.A. Baldwin and K.J. Welham, *Org. Mass Spectrom.*, 21, 235- 236, (1986).
6. Crown ethers are non-covalent blocking groups which also catalyse peptide synthesis. P. Mascagni, C.B. Hyde, M.A. Charalambous and K.J. Welham, *J. Chem. Soc. Perkin Trans. 2.*, 323-327, (1987).
7. Charge localisation by molecular orbital calculations. 1. Urea and Thiourea. M.A. Baldwin and K.J. Welham, *Rapid Commun. in Mass Spectrom.*, 1, 13-15, (1987).
8. Identification of chiral isomers by FAB/MS. M.A. Baldwin, S.A. Howell, K.J. Welham and F.J. Winkler, Proceedings of the 16th meeting of the British Mass Spectrometry Society, York 1987, p32.
9. A kinetic study of the binding of the neurotoxin acrylamide to glutathione by FAB/MS. M.A. Baldwin, K.K. Dhaliwal, M.E. Harrison, S.A. Howell and K.J. Welham, Proceedings of the 16th meeting of the British Mass Spectrometry Society, York 1987, p29.

10. Charge localisation by molecular orbital calculations for formamides and thioformamides. M.A. Baldwin and K.J. Welham, Proceedings of the 16th meeting of the British Mass Spectrometry Society, York 1987, p178.
11. Identification of chiral isomers by FAB/MS : dialkyl tartrates. M.A. Baldwin, S.A. Howell, K.J. Welham and F.J. Winkler, *Biomed. Environ. Mass Spectrom.*, 16(1-12), 357-360, (1988).
12. Charge localisation by molecular orbital calculations. 2. Formamide, Thioformamide and N-methylated analogues. M.A. Baldwin and K.J. Welham, *Org. Mass Spectrom.*, 23, 425-428, (1988).
13. Hydride abstraction in fast atom bombardment. M.A. Baldwin, K.J. Welham, I. Toth and W.A. Gibbons, *Org. Mass Spectrom.*, 23, 697-699, (1988).
14. Charge localisation and mass spectrometry of some amides and thioamides. M.A. Baldwin and K.J. Welham, *Advances in Mass Spectrometry*, vol. 11B, (Ed. P. Longevaille), Heyden, London, 1989, pp 1636-7.
15. $[M - H]^+$ versus $[M + H]^+$ in fast atom bombardment : the mechanistic significance. M.A. Baldwin, S.A. Howell and K.J. Welham, *Advances in Mass Spectrometry*, vol. 11B, (Ed. P. Longevaille), Heyden, London, 1989, pp 466-7.
16. $[M-H]^+$ pseudomolecular ion formation in the FAB spectra of glucose derivatives. M.A. Baldwin, S.A. Howell, K.J. Welham, P.M. Collins and A. McKinnon, Proceedings of the 17th Meeting of the British Mass Spectrometry Society, Nottingham, 1989, pp 209-11.
17. Rapid identification of secondary products in plant cell tissue cultures by TSP HPLC/MS and other mass spectral methods. S. Abdulrahman, K.J. Welham, M.E. Harrison, M.A. Baldwin, J.D. Phillipson and M.F. Roberts, Proceedings of the 17th Meeting of the British Mass Spectrometry Society, Nottingham, 1989, pp 228-31.
18. Tandem mass spectrometric techniques and their use in differentiating between isomeric ion structures. T. Madden, K.J. Welham, M.A. Baldwin and M. Abebe, Proceedings of the 17th Meeting of the British Mass Spectrometry Society, Nottingham, 1989, pp 166-8.

19. Identification of the NH₂-terminal blocking group of rat mammary gland acyl fatty acid synthetase-thioesterase II. A.R. Slabas, A.A. Aitken, S.A. Howell, K.J. Welham and C.M. Sidebottom, *Biochem. Soc. Trans.*, 17, 886-887, (1989).
20. The use of crown ethers in peptide chemistry. Part 2. Syntheses of dipeptide complexes with the cyclic polyether 18-crown-6 and their derivatisation with DMSO. C.B. Hyde, K.J. Welham and P. Mascagni, *J. Chem. Soc. Perkin Trans. 2.*, 2011-2015, (1989).
21. High Energy CID of Peptides: Is Immonium ion formation affected by Competition between Amino Acids?, T. Madden, K.J. Welham and M.A. Baldwin, Proceedings of the 38th ASMS Conference on Mass Spectrometry and Allied Topics, Tucson, Arizona, 1990, pp .
22. TSP/MS Analysis of Opium alkaloids and their metabolites. S. Abdulrahman, M.E. Harrison, K.J. Welham, M.F. Roberts, J.D. Phillipson and M.A. Baldwin, Proceedings of the 18th Meeting of the British Mass Spectrometry Society, London, 1990, pp 154-7.
23. Revision of the Primary Structure of Plastocyanin from *Scenedesmus Obliquus* algae by Electrospray and FAB/MS. S.A. Howell, K.J. Welham, A. Aitken, R.P. Ambler, B.N. Green and M.A. Baldwin, Proceedings of the 18th Meeting of the British Mass Spectrometry Society, London, 1990, pp 158-161.
24. Factors controlling Immonium Ion Intensities in the High Energy CID of Peptides. T. Madden, K.J. Welham and M.A. Baldwin, Proceedings of the 18th Meeting of the British Mass Spectrometry Society, London, 1990, pp 162-5.
25. Assaying S-Adenyl-L-Methionine and S-Adenyl-L-Homocysteine in blood and other biological fluids by HPLC and TSP/MS. M.P. Hamedani, K.J. Welham and W.A. Gibbons, Proceedings of the 18th Meeting of the British Mass Spectrometry Society, London, 1990, pp 166-9.
26. High-performance liquid chromatographic-mass spectrometric assay of high-value compounds for pharmaceutical use from plant cell tissue culture: *Cinchona* alkaloids. S. Abdulrahman, K.J. Welham, M.E. Harrison, M.A. Baldwin, J.D. Phillipson and M.F. Roberts, *J. Chromat. Biomed. Appl.*, 562, 713-721, (1991).

27. An HPLC/MS assay for SAM and SAH in blood and other biological fluids. M.P. Hamedani, K.J. Welham and W.A. Gibbons, Proceedings of the 3rd Iranian Pharmaceutical Congress, Ahwaz, Iran, 1991.
28. Factors controlling Immonium Ion Intensities in the High Energy Collision Induced Decomposition Spectra of Peptides. T. Madden, K.J. Welham and M.A. Baldwin, *Org. Mass Spectrom.*, **26**, 443-446, (1991).
29. Lipidic Peptides IV. Penicillin and Cephalosporin amide conjugates with Lipidic Amino acids and their Oligomers. I. Toth, R.A. Hughes, P. Ward, W.A. Gibbons and K.J. Welham, *Int. J. Pharmaceutics*, **73**, 259, (1991).
30. HPLC/MS assays for S-Adenyl-L-Methionine and its metabolites in biological fluids and tissues. M.P. Hamedani, P. Slegel, M.E. Harrison, W.A. Gibbons and K.J. Welham, *Advances in Mass Spectrometry*, Vol 12B, (in press).
31. Electrospray Mass Spectrometric evidence for the existence of Covalent Acyl Enzyme Intermediates. D.S. Ashton, C.C. Beddell, D.J. Cooper, B.N. Green, R.W.A. Oliver and K.J. Welham, *FEBS Letters*, (in press).